

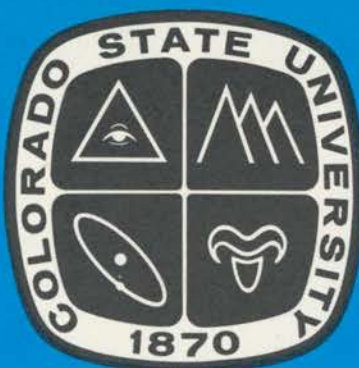
QC852
C6
no. 421
ATSL

LIBRARIES
JAN 22 1988
COLORADO STATE UNIVERSITY

Anisotropy of Reflected Solar Radiation From Fields of Finite Clouds FIRE Series No. 4

by Timothy L. Alberta and Stephen K. Cox

Funding Agency: National Aeronautics & Space Administration



Atmospheric Science
PAPER NO.
421

DEPARTMENT OF ATMOSPHERIC SCIENCE
COLORADO STATE UNIVERSITY
FORT COLLINS, COLORADO

**ANISOTROPY OF REFLECTED SOLAR RADIATION
FROM FIELDS OF FINITE CLOUDS**

FIRE Series No. 4

by
Timothy L. Alberta
and
Stephen K. Cox

Department of Atmospheric Science
Colorado State University
Fort Collins, CO 80523

November, 1987

Atmospheric Science Paper No. 421

ABSTRACT

ANISOTROPY IN REFLECTED SOLAR RADIATION FROM FIELDS OF FINITE CLOUDS

Anisotropy of reflected solar radiation from simulated cloud fields is examined using a laboratory device known as the Cloud Field Optical Simulator (CFOS). Reflectance data from 20 cloud fields, each composed of a different random distribution of simulated clouds covering 30% of the target area, were collected.

One hundred sixty-nine detector locations, each representing a different local zenith and azimuth angle, describe a hemispherical solid angle encompassing the cloud field. Radiances measured at these detector locations were numerically integrated, and locations were found where irradiances determined by assuming isotropy underestimated and overestimated the numerically integrated irradiances. Overestimates were found exclusively at large local zenith angles while the detector measured backscattered radiation. Underestimates were found primarily while the detector measured forward scattered radiation. Results of this comparison are presented in the form of frequency distributions, which also show increasing anisotropy with increasing incident zenith angle.

Seven different incident zenith angles were analyzed for variations in reflected irradiance arising from different cloud field geometries. Results show irradiance differences as great as 107% at small incident zenith angles. Variations in irradiances were shown to be smaller at larger incident zenith angles. Also indicated are increased irradiance values at larger incident zenith angles.

Fourier series analysis was performed on selected portions of the data set to examine the azimuthal dependence of irradiances. It was found that the number of terms required to

QC852
.C6
no. 421
ATSL

produce an accurate representation of the intensity field at a specific local zenith angle was highly dependent on the number of azimuthal measurements available. The importance of both amplitude functions involved in the Fourier series calculations were also examined. Results indicate the increased importance of the sine term when assuming azimuthal dependence.

ACKNOWLEDGEMENTS

I would like to extend my appreciation to Dr. Graeme Stephens and Dr. Steven Ackerman, for their helpful suggestions and assistance which were invaluable during the period in which this research was completed, Christopher Johnson-Pasqua for his expertise with electronic problems encountered during the data collection period, Melissa Tucker and Susan Lini for their assistance during the preparation of this manuscript, and Dr. John Locker, for taking the time to serve on my graduate committee. Special thanks are extended to the following people, for their understanding, support, and encouragement during the period of this research: Josephine H. Alberta, John A. Alberta, Sr., John A. Alberta, Jr., Ted L. Alberta, Jami M. Alberta, Clara E. Ries, and Wendy K. Willard. This research was funded by the National Aeronautics and Space Administration Grant NAG 1-554 and the National Science Foundation grant ATM-8521214.

CONTENTS

ABSTRACT	ii
ACKNOWLEDGEMENTS	iv
TABLE OF CONTENTS	v
LIST OF FIGURES	vii
LIST OF TABLES	ix
1 INTRODUCTION	1
1.1 Satellite measurements	2
1.2 Aircraft measurements	2
1.3 Computer models	3
1.4 Laboratory measurements	4
2 LABORATORY APPARATUS	7
2.1 The light source	7
2.2 Cloud field assembly	7
2.3 Data display/collection system	9
3 GEOMETRY, DEFINITIONS, AND THEORY	12
3.1 Definition of angles	12
3.2 Theory	15
3.2.1 Isotropic and measured irradiances	16
4 EXPERIMENTAL DATA COLLECTION	21
4.1 The cloud fields	21
4.2 The source zenith angles	23
4.3 Scans and scan sets	23
4.4 Calibration	26
4.4.1 System calibration	26
4.4.2 Continuous calibration	28
4.5 Data collection products	29
4.6 Data processing	30
5 RESULTS	34
5.1 Irradiance variations comparing different cloud fields	34
5.2 Errors based on isotropic assumption	38
5.3 Location of maximum and minimum anisotropy	45
5.3.1 Determination of maximum anisotropy	49

5.3.2 Determination of minimum anisotropy	57
5.4 Determination of ideal cloud field sample size	60
6 CONCLUSIONS	64
REFERENCES	68
A Fourier Series Analysis	70
A.1 Introduction	70
A.2 Fourier theory	71
A.3 Analysis	75
A.4 Conclusions	83
B Randomly oriented cloud fields used in study	107
C Relative irradiances as a function of Θ_0 for 20 cloud fields	113
D Locations of anisotropic reflectance factors for each case study	115

LIST OF FIGURES

2.1 A schematic drawing of the Cloud Field Optical Simulator (CFOS). From Davis <i>et al.</i> (1983)	8
2.2 The relative spectral responses of the detectors used in the CFOS with and without optical filters. From Davis <i>et al.</i> (1983).	10
2.3 Schematic diagram of the photodiode/operational amplifier circuit	11
 3.1 Geometry of the CFOS cloud field. η is the photodiode nadir angle, α is the photodiode angle, β is the detector arc angle, and ϕ is the photodiode azimuth angle	12
3.2 Reference photodiode and detector arc azimuth angles.	14
3.3 Geometry of the source zenith angle Θ_0	17
3.4 Graphical representation of the grid used for numerical calculation of irradiances (equation 3.9).	18
 4.1 Cloud pattern of field number one.	22
4.2 Cloud grid on field.	23
4.3 Schematic outline of experimental procedure.	25
 5.1 Mean relative irradiances vs. Θ_0 for all 20 fields.	35
5.2 Same as 5.1, except field number 1 is depicted instead of mean values for the entire data set.	37
5.3 Same as 5.1, except field number 10 is depicted instead of mean values for the entire data set.	37
5.4 Frequency distribution of anisotropic reflectance factors for entire data set.	39
5.5 Same as 5.4, except showing Γ values for a source zenith angle of $\Theta_0 = -60^\circ, \Phi = \Phi_0 + 180^\circ$	42
5.6 Same as 5.4, except showing Γ values for a source zenith angle of $\Theta_0 = -40^\circ, \Phi = \Phi_0 + 180^\circ$	42
5.7 Same as 5.4, except showing Γ values for a source zenith angle of $\Theta_0 = -20^\circ, \Phi = \Phi_0 + 180^\circ$	43
5.8 Same as 5.4, except showing Γ values for a source zenith angle of $\Theta_0 = 0^\circ$	43
5.9 Same as 5.4, except showing Γ values for a source zenith angle of $\Theta_0 = -20^\circ, \Phi = \Phi_0$	44
5.10 Same as 5.4, except showing Γ values for a source zenith angle of $\Theta_0 = -40^\circ, \Phi = \Phi_0$	44
5.11 Same as 5.4, except showing Γ values for a source zenith angle of $\Theta_0 = -60^\circ, \Phi = \Phi_0$	45
5.12 Local zenith angles on 3-d histogram grid.	47
5.13 Same as 5.12, with azimuth angles depicted. Angles are referenced clockwise from the "north"	47

5.14	3-d histogram representing frequency and location of photodiode measurements which result in anisotropic reflectance factors indicated. This figure shows locations of all values of $\Gamma < -40\%$ in the data set	48
5.15	Same as 5.14, except showing locations of anisotropic reflectance factors of $-20\% \leq \Gamma < 0\%$	50
5.16	Same as 5.14, except showing locations of anisotropic reflectance factors of $\Gamma > 60\%$	50
5.17	Similar to 5.14, except showing locations of anisotropic reflectance factors of $\Gamma < -40\%$, at $\Theta_0 = -60^\circ, \Phi = \Phi_0 + 180^\circ$	51
5.18	Similar to 5.14, except showing locations of anisotropic reflectance factors of $\Gamma > 60\%$, at $\Theta_0 = -60^\circ, \Phi = \Phi_0 + 180^\circ$	51
5.19	Similar to 5.14, except showing locations of anisotropic reflectance factors of $\Gamma < -40\%$, at $\Theta_0 = 0^\circ$	52
5.20	Similar to 5.14, except showing locations of anisotropic reflectance factors of $\Gamma > 60\%$, at $\Theta_0 = 0^\circ$	52
5.21	Similar to 5.14, except showing locations of anisotropic reflectance factors of $40\% \leq \Gamma < 60\%$, at $\Theta_0 = -20^\circ, \Phi = \Phi_0$	53
5.22	Similar to 5.14, except showing locations of anisotropic reflectance factors of $\Gamma < -40\%$, at $\Theta_0 = -60^\circ, \Phi = \Phi_0$	54
5.23	Similar to 5.14, except showing locations of anisotropic reflectance factors of $\Gamma > 60\%$, at $\Theta_0 = -60^\circ, \Phi = \Phi_0$	54
5.24	The reflection of an infinitesimally thick beam of radiation from a point located one inch from the top of the cloud.	56
5.25	Similar to 5.14, except showing locations of anisotropic reflectance factors of $-5\% \leq \Gamma \leq 5\%$, at $\Theta_0 = 0^\circ$	57
5.26	Similar to 5.14, except showing locations of anisotropic reflectance factors of $-5\% \leq \Gamma \leq 5\%$, at $\Theta_0 = -20^\circ, \Phi = \Phi_0$	58
5.27	Similar to 5.14, except showing locations of anisotropic reflectance factors of $-5\% \leq \Gamma \leq 5\%$, at $\Theta_0 = -40^\circ, \Phi = \Phi_0$	58
5.28	Similar to 5.14, except showing locations of anisotropic reflectance factors of $-10\% \leq \Gamma \leq 10\%$, at $\Theta_0 = -60^\circ, \Phi = \Phi_0$	59
5.29	Similar to 5.14, except showing locations of anisotropic reflectance factors of $-10\% \leq \Gamma \leq 10\%$, at $\Theta_0 = -60^\circ, \Phi = \Phi_0 + 180^\circ$	59
A.1	Magnitudes of amplitude functions as a function of m for case number one.	79
A.2	Similar to A.1, except case number two is shown.	80
A.3	Same as A.2, except case number three is shown.	80
A.4	Λ as a function of m . Λ is calculated using equation (A.26). Plotted on a linear scale, for case number one.	82
A.5	Same as A.4, for case number two.	82

LIST OF TABLES

3.1	Photodiode angles (in degrees)	13
3.2	Detector arc angles (in degrees)	13
3.3	Nadir angles (in degrees)	15
3.4	Azimuth angles (in degrees)	16
4.1	Mean irradiance values for all scenes (in mV)	30
4.2	Irradiance ranges for all scenes (in mV)	31
4.3	Ranges of variation for all scenes	32
5.1	Statistical comparisons of irradiances among the 20 cloud fields analyzed. All values are in mV.	38
5.2	Anisotropic reflectance factor statistical information. Mean and modal values are in mV. The median, modal range, and cumulative distribution functions are expressed as ranges of Γ where these values are found.	40
5.3	Anisotropic reflectance factor cumulative distribution functions.	41
5.4	Confidence levels using 20 cloud field samples.	61
5.5	Optimized sample sizes for irradiances. All ranges of means are plus/minus.	61
5.6	Optimized sample sizes for backscattered radiances. All ranges of means are plus/minus.	61
5.7	Optimized sample sizes for forward scattered radiances. All ranges of means are plus/minus.	62
A.1	Cases selected for Fourier analysis.	76
A.2	Fourier analysis results from case number one (all values are in mV).	77
A.3	Amplitude functions (in mV) for cases 1-4.	85
A.4	Amplitude functions (in mV) for cases 5-8.	86
A.5	Amplitude functions (in mV) for cases 9-12.	87
A.6	Amplitude functions (in mV) for cases 13-16.	88
A.7	Summed intensities for case number 1 (in mV).	89
A.8	Summed intensities for case number 2 (in mV).	90
A.9	Summed intensities for case number 3 (in mV).	91
A.10	Summed intensities for case number 4 (in mV).	92
A.11	Summed intensities for case number 5 (in mV).	93
A.12	Summed intensities for case number 6 (in mV).	94
A.13	Summed intensities for case number 7 (in mV).	95
A.14	Summed intensities for case number 8 (in mV).	96
A.15	Summed intensities for case number 9 (in mV).	97
A.16	Summed intensities for case number 10 (in mV).	98
A.17	Summed intensities for case number 11 (in mV).	99
A.18	Summed intensities for case number 12 (in mV).	100

A.19 Summed intensities for case number 13 (in mV).	101
A.20 Summed intensities for case number 14 (in mV).	102
A.21 Summed intensities for case number 15 (in mV).	103
A.22 Summed intensities for case number 16 (in mV).	104
A.23 Λ values as a function of m for cases 1–8.	105
A.24 Λ values as a function of m for cases 9–16.	106

Chapter 1

INTRODUCTION

The accurate interpretation of the nature of clouds is an extremely important factor in the study of the earth's radiation budget. As this paper will show, the measurement of cloud effects upon radiation is a process complicated by many different problems which are difficult to resolve. A general circulation model obviously needs to accurately represent these cloud effects to be of value to the scientist and to society. In light of recent developments concerning man-induced climatic changes, it is becoming more and more imperative that these models contain parameterizations which faithfully describe cloud effects on climate. Only if these cloud effects are correctly described can the models provide accurate information concerning climatic change.

An important subset of these cloud effects is reflected radiation. This paper is concerned with properties of reflected radiation only and does not consider factors such as absorption and transmission. Reflected radiation is important in the general circulation context, particularly when considering both the amount of radiation incident upon the earth's surface and the radiation budget at the top of the atmosphere. These factors are of prime importance if one is to expect an accurate radiation budget.

Methods of collection of cloud reflectance characteristics fall into four categories: satellite measurements, aircraft measurements, computer models, and laboratory measurements. Each of these methods has been employed in the attempt to obtain a better understanding of the nature of cloud radiative characteristics. Unfortunately, all of these methods also pose problems which are difficult to resolve satisfactorily.

1.1 Satellite measurements

Since the introduction of the satellite into meteorology, atmospheric scientists have attempted to utilize the satellite to determine an adequate parameterization scheme which describes the reflective properties of clouds. Ruff *et al.* (1968) used Tiros IV radiometer measurements to study the angular distribution of reflected solar radiation from clouds. As many authors, Stowe *et al.* (1980) and Ruff *et al.* (1968) among others, have found, anisotropy increases with increasing solar zenith angle. Stowe *et al.* (1980) studied the anisotropy problem, finding areas of maximum and minimum anisotropy as a function of solar azimuth angle for several scene types including high ice clouds. Numerous other authors have studied cloud reflectance characteristics, usually reaching the same conclusion. To obtain a reflectance pattern for a certain cloud field, a satellite typically collects one radiance measurement of a cloud field, and uses this measurement along with inferred cloud field characteristics to determine the irradiance of the entire field. The nature of the satellite radiometers is such that the satellite senses only that part of the radiation reflected from the cloud field which is directed toward the satellite. This causes problems due to the anisotropic nature of cloud fields. One radiance measurement is usually not sufficient to obtain an accurate value for the reflected irradiance of the field especially when considering increased zenith angles and complex geometries of clouds.

Another problem inherent in satellite measurements is the inability to accurately compare the geometry of cloud fields having similar characteristics. Extraneous variables which introduce undesirable noise into the data set are constantly present. If, for example, a satellite measures reflected radiances while passing over a certain cloud field, the possibility of this measurement being taken again under the same cloud and surface conditions is remote. Thus, the accuracy of the measurement can not be assessed in a statistical fashion.

1.2 Aircraft measurements

Numerous studies involving aircraft and balloon measurements to study reflective properties of clouds have also been documented. Bartman (1968) used balloon mounted

radiometers to measure cloud reflectances. The balloon was able to make accurate radiance measurements at a specific zenith angle, but the measurements were lacking in azimuthal dependence. Brennan and Bandeen (1970) used a high altitude research aircraft to demonstrate the dependence of reflection upon solar zenith, detector zenith, and azimuth angles. Davis and Cox (1982) used aircraft to obtain radiance measurements with a multidetector instrument from which a set of bi-directional reflectance models were presented. The results of all of these studies also indicate increasing anisotropy with increasing solar zenith angles.

The obvious problem with aircraft measurements lies in the inability of the aircraft to make a static measurement of a cloud field. As the aircraft flies around the cloud or cloud field, the field is constantly changing. While this may not pose a problem for examining microphysical characteristics of the cloud, an accurate depiction of the reflectance characteristics of the cloud field on the general circulation scale may be impossible.

1.3 Computer models

Computer models usually handle radiative transfer problems quite well. Computers are better equipped to handle differences in reflection due to geometry. However, as the geometry becomes more and more complex, the model becomes more expensive as well as time consuming to run. The modeler must also be concerned with the problem of finite vs. semi-infinite clouds. Aida (1977) used the Monte Carlo method with cuboidal clouds to determine if a cloud can be considered semi-infinite for modeling purposes. The results of that study indicated a cloud could be considered infinite only if its horizontal extent was greater than five times that of its vertical extent. Other studies, notably Busygin *et al.* (1973) and McKee and Cox (1974), also found significant differences between horizontally finite and semi-infinite cloud models. Davies (1978), Davies (1984), Welch and Wielicki (1984), and Welch *et al.* (1980) have all indicated the importance of cloud geometry in reflection calculations. These studies point to the same conclusion. Without expending huge amounts of computer time, a computer is not able to accurately handle situations occurring in nature.

1.4 Laboratory measurements

A partial solution to these problems can be found in the area of laboratory simulation of cloud fields, and the static measurement of reflectance properties of simulated clouds. Although satellite and aircraft measurements are able to measure actual solar radiances, laboratory simulation can provide the scientist with a good deal of information regarding the relative interactions of clouds among cloud fields. A laboratory investigation has been carried out by Margolis *et al.* (1972), who studied absorption spectra and diffuse reflectivity with a plane parallel cloudy atmosphere. Kuenning *et al.* (1978) used a laboratory model to determine individual interactions among cloud elements. Their findings indicate separations between cubic clouds of greater than 2.5 cloud diameters could be treated as non-interacting clouds, but at distances closer than 2.5 diameters geometric interactions must be considered. McKee *et al.* (1983) compared Monte Carlo calculations with aircraft measurements and laboratory measurements, representing clouds by means of synthetic cotton. The results obtained from using synthetic materials to study reflectance properties of clouds agreed well with theoretical results, giving confidence to the use of synthetic materials in studying radiative properties of clouds.

An advantage of laboratory models over computer models is the absence of the finite vs. semi-infinite cloud problem. The laboratory is obviously equipped to handle finite cloud cases with greater ease than is a computer model. However, problems also exist within the laboratory setting. The synthetic material used to represent the clouds does not simulate scattering within the cloud according to classical Mie theory. However, Davis *et al.* (1983) suggests, "...recent studies have shown that cloud shape may dominate microphysical scattering as the most important factor affecting the radiance pattern (of optically thick clouds)." In order to use this assumption to the advantage of the laboratory experimenter, the simulated clouds must be optically thick. Thin cirroform clouds are not able to be represented by means of a laboratory simulation using the apparatus described in the following chapter. Another concern inherent in the laboratory apparatus used in this study is the black body spectrum of the source and the spectral response of the photodiodes, which are used to measure the reflected radiation. A 5700°K black

body radiator, simulating the sun's black body spectrum, would be ideal coupled with photodiodes which measure intensity of reflected uv or visible radiation. However, this problem may be inconsequential when using synthetic material such as styrofoam to simulate clouds. Davis *et al.* (1983) suggest the importance of the spectral nature of the incident radiation is determined by the microphysical characteristics of the cloud (scattering properties at a certain wavelength λ are determined only as a function of $\frac{\lambda}{r}$ where r is the radius of the droplet). Since the simulated clouds used in this study exhibit microphysical characteristics unlike those of real clouds, a light source which yields the same spectral response as that of the sun would not necessarily result in greater experimental accuracy.

It is the purpose of this paper to make use of a laboratory method to study reflectance patterns of 20 different finite cloud fields which are all similar except for the patterns created by individual simulated cloud elements in the cloud field. As will be shown, each of these simulated cloud fields effectively represents 30% fractional cloud cover. From this point forward, the simulated clouds in this study will be referred to as clouds unless otherwise noted. This study attempts to answer the following questions:

- i) What degree of variation may be expected in reflected irradiances of cloud fields of similar size which differ only by the geometric relationships within the cloud field?
- ii) What types of errors may be expected when calculating irradiances of cloud fields assuming isotropy?
- iii) Do these errors depend upon the solar zenith angle?
- iv) Is there an ideal source-cloud-detector geometry where these errors will be a minimum?

The latter three questions have all been at least partially answered by authors cited above. Avaste and Vaynikko (1974) found that, "satisfactory results can be obtained for the mean radiation fluxes and influxes in broken clouds by knowing only the degree of cover." If this is the case, the 20 cloud fields in this study should exhibit similar

irradiances. Most of the literature referenced above point to the opposite conclusion. That is, cloud field irradiances depend on a number of variables including cloud cover and the contributions to anisotropy resulting from cloud field geometry. The results of this study, which will be shown later in the text, show factors other than the amount of cloud cover are indeed important in this determination.

Appendix A of this paper will address the calculation of reflected intensity by means of a Fourier analysis. As will be shown, the reflected intensities and upward irradiances can be represented by a Fourier series. This section will also show the importance of the anisotropic nature of cloud reflectance properties and will attempt to provide a better understanding of this process and its relation to the problem of cloud reflectance measurements.

Throughout this experiment, isotropy is not assumed, since the laboratory environment makes possible the use of azimuthal reflectance differences as well as zenith angle differences, in the calculation of total upward irradiances. The assumption of isotropy will be considered only when studying differences between anisotropic and isotropic assumptions.

Chapter 2

LABORATORY APPARATUS

The system used to collect data is called a Cloud Field Optical Simulator (CFOS). A complete description of the CFOS apparatus can be found in Davis *et al.* (1983). However, the main components of CFOS will be described in this chapter. The CFOS is composed of three primary parts: the light source, the cloud field assembly, and the data display/collection system. This system is able to collect cloud reflectance data from optically thick, simulated clouds which can be situated in any type of source-cloud geometry desired. The nature of the detector arc system (to be explained later in this chapter) allows a complete canvassing of the cloud field by the arc, enabling the experimenter to collect bi-directional reflectance data which represents the reflectance pattern of the entire cloud field. Thus, zenith and azimuthal dependence can be accurately portrayed by this system.

2.1 The light source

The light source is composed of five G.E. par 56 lamps which provide a nearly plane-parallel beam of light upon the target. The light is reflected by a large mirror to allow the beam to diverge to a cross sectional size large enough to cover the cloud field. The cloud field and the light source are placed behind circular apertures to assure nearly plane-parallel light.

2.2 Cloud field assembly

Figure 2.1 is a depiction of the CFOS apparatus. The cloud field consists of a vertically standing circular base approximately 38 inches in radius, a detector arc which houses 15 photodiode detectors, and a mechanical drive system which serves two purposes. First,

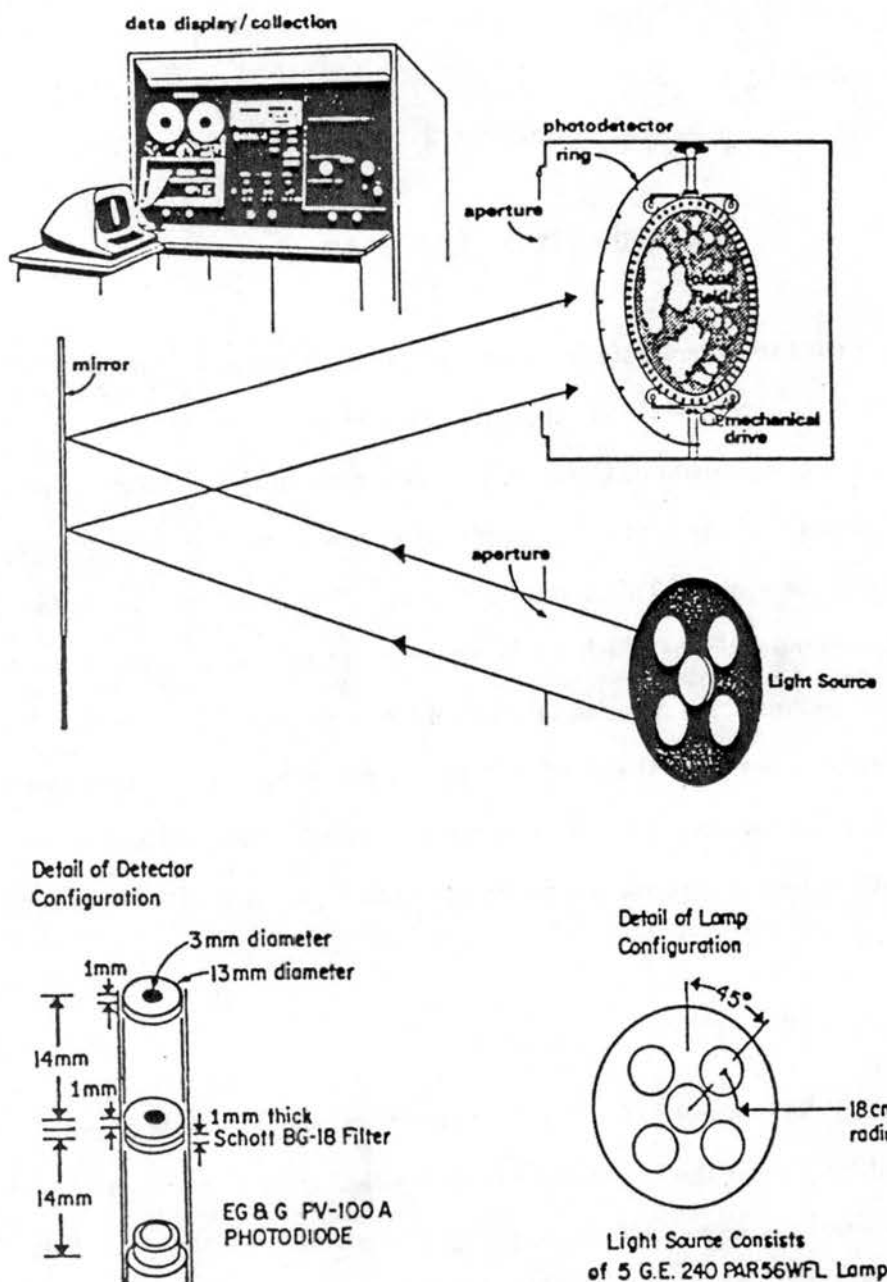


Figure 2.1: A schematic drawing of the Cloud Field Optical Simulator (CFOS) designed to simulate the interaction of visible solar radiation with optically thick clouds. From Davis *et al.* (1983).

the drive system allows the cloud field to be situated in any geometric position desired with respect to the light source, allowing the observer to choose a solar zenith angle which corresponds to any location on earth at any time of the day or year. The field can also be rotated azimuthally to observe changes in reflectance characteristics due to this rotation. Secondly, the drive system allows the detector arc to canvass the cloud field, allowing a complete sampling of the cloud field. The detector arc is comprised of a metal ring containing 15 photodiode detectors. These detectors are placed in 10° increments about the ring, beginning in the center of the ring and continuing outward in both directions from the central point. This array of diodes further compliments the system's ability to cover the entire field with reflectance measurements. Data obtained from the outermost diode on each side (70° from the center of the detector arc) were ignored. The fields of view subtended by these two diodes included, to a fairly large extent, areas outside the cloud field. Although data collected by these diodes was consistent with data collected by the other 13 diodes, the data collected by these two diodes did not complement the reflection pattern enough to merit their inclusion within the data set. From this point forward, the text will refer to the 13 diodes actually used in the data processing scheme.

The photodiodes convert the intensity of radiation incident upon the diode to a current which can be measured. Each diode is covered by a collimator can which effectively reduces the diode's field of view to a 7.5° half-angle when the diode is at nadir. The elliptical field viewed by the diode, which is a circle at nadir, changes as the position of the diode changes about the cloud field. The collimator can also houses a filter which limits the spectral response of the diode to the visible spectrum. Figure 2.1 shows a cutaway view of a diode, and figure 2.2 shows the relative spectral response of a filtered and non-filtered diode. This filtration models the diode's spectral response to that of the human eye, so changes in reflectance seen by the observer are faithfully recorded.

2.3 Data display/collection system

The data display/collection system serves two purposes. First, this system contains the controls of the mechanical drive systems which are used to change the geometry of

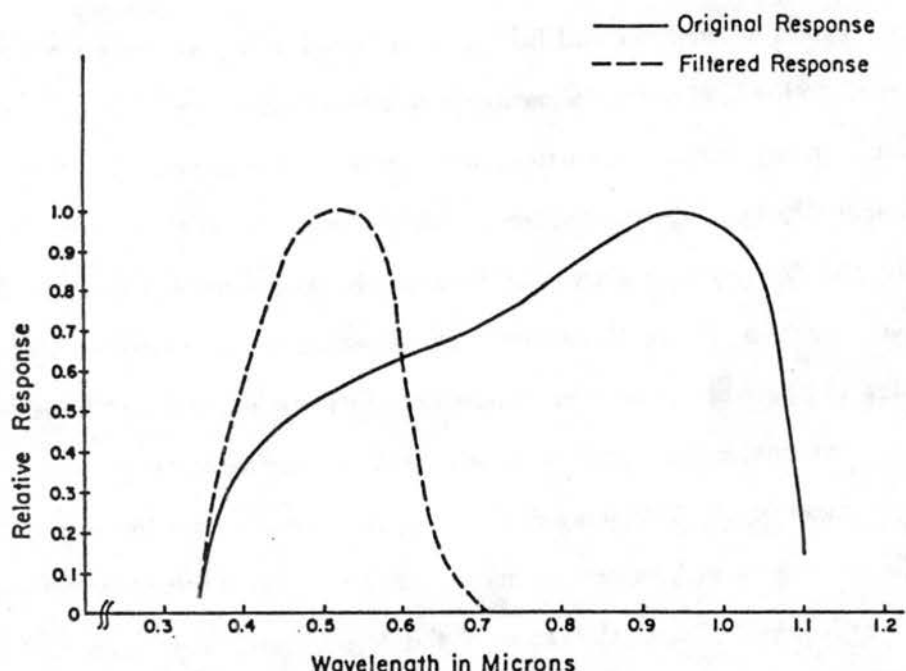


Figure 2.2: The relative spectral responses of the detectors used in the CFOS with and without optical filters. From Davis *et al.* (1983).

the field in accordance with the experimentor's purpose. Three separate motors control the detector arc rotation, the source zenith angle (the source zenith angle changes by rotating the cloud field about its vertical axis) and the azimuthal rotation of the cloud field. The azimuthal rotation is changed by rotating the field about an axis perpendicular to the cloud field. Azimuthal rotation was not used in this experiment. Azimuth angles discussed in this text are angles relating the azimuth angle of the photodiodes with respect to the cloud field.

The data display/collection system also contains the computer equipment necessary to record the data collected onto disk for processing and the equipment necessary to display current collected by the photodiodes. The current passes through an operational amplifier circuit which amplifies the initial signal into a current which can be easily measured, and through an analog to digital converter to display and record digital signals. Figure 2.3 is a schematic diagram of the photodiode/operational amplifier circuit. Each of the 15 photodiodes produce a current which is channeled through 15 operational amplifiers before it is displayed. The display board receives digital signals which are linearly proportional to the intensity of radiation received by each of the photodiodes. Digital signals are also

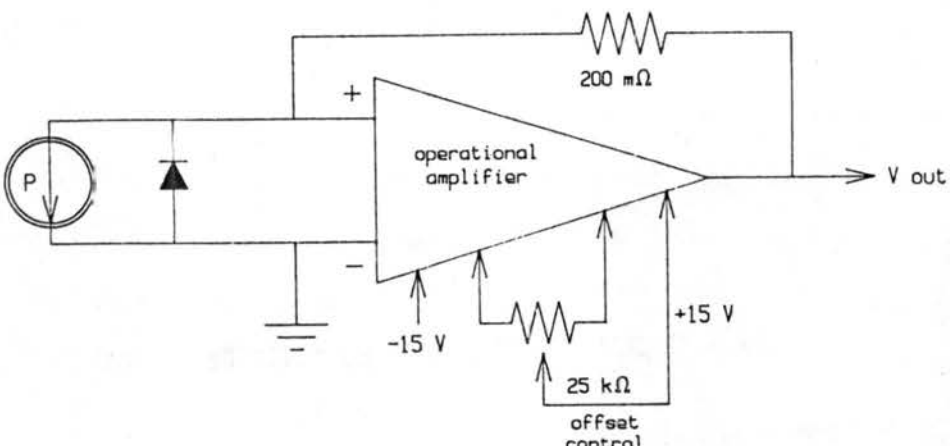


Figure 2.3: Schematic diagram of the photodiode/operational amplifier circuit. The photodiode detector is shown at left. The offset control, used to modify the output current, is used only in the initial set-up of the photodiode system. Differences in output voltages between photodiodes due to the offset control are considered during calibration procedures. The offset control is not changed throughout the experiment.

sent to the display board which provide information regarding source zenith, cloud field azimuth, and detector arc angles. Signals are also sent to an *Apple II* microcomputer. The microcomputer displays these signals, represented by voltages, and stores these onto floppy disk. The analog to digital conversion is partially responsible for slight variations in collected voltages and the display of angles used in the data collection process. This difference is considered in the calibration process, which is described in chapter four. Data processing is accomplished by an *Apple III* microcomputer which is separate from the CFOS laboratory. The display board exhibits instantaneous voltages, while the *Apple II* microcomputer receives approximately two signals per second from each photodiode. The photoelectric detectors housed in each of the drive motors send signals to the display board and to the microcomputer in a similar manner. The software used to collect this data allows for any number of signals to be averaged and displayed or stored. In this experiment, 30 voltages were averaged for each photodiode measurement to provide an accurate sampling of the scene. The processing software, although extensive in its present form, is continuously updated to meet the needs of the experiment in progress. The data is user-friendly in that any type of processing program desired will successfully read the raw data file. This processing software is discussed in further detail in chapter four.

Chapter 3

GEOMETRY, DEFINITIONS, AND THEORY

3.1 Definition of angles

Figure 3.1 shows the geometry of the CFOS cloud field. The field is shown in a horizontal position so the vertical or north-south axis runs from the upper left to the lower right of the figure. The vertical axis is analogous to the vertical axis of rotation of

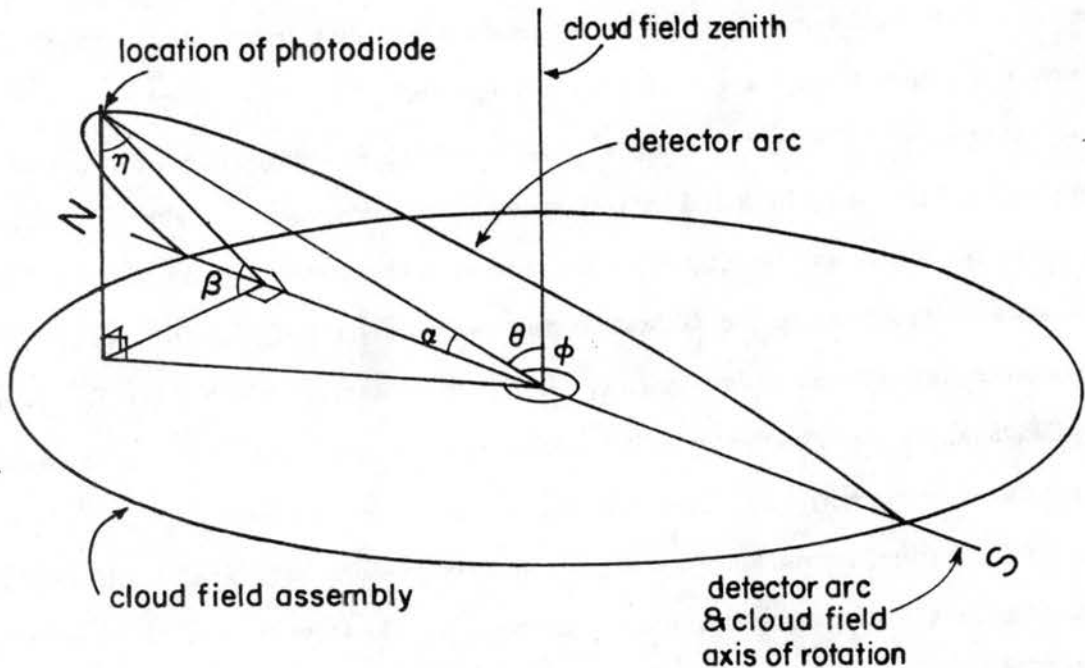


Figure 3.1: Geometry of the CFOS cloud field. η is the photodiode nadir angle which is analogous to the local zenith angle θ . α represents the photodiode angle, β is the detector arc angle, and ϕ is the azimuth angle of the photodiode with respect to the cloud field. The detector arc scans over the field about the detector arc axis of rotation.

the cloud field and detector arc. To understand the final products of the data collection process, it is necessary to first understand the angles used in the irradiance calculations. Two angles are provided by the system. The photodiode angle, α , is the angle between

the position of the photodiode in question on the detector ring and the vertical axis of the field. The photodiode angles are fixed for each photodiode since the photodiodes do not move on the detector ring. The detector arc angle, β , is defined as the angle determined by the position of the detector ring with respect to the horizontal plane of the field. Table 3.1 lists the photodiode angles referenced to the cloud field zenith and Table 3.2 lists the detector arc angles used in this study.

Table 3.1: Photodiode angles (in degrees)

Diode:	1	2	3	4	5	6	7	8	9	10	11	12	13
ϕ_r													$\phi_0 + 135^\circ$
α :	60	50	40	30	20	10	0	10	20	30	40	50	60

Table 3.2: Detector arc angles (in degrees)

Scan:	1	2	3	4	5	6	7	8	9	10	11	12	13
ϕ_r													$\phi_0 + 180^\circ$
β :	60	50	40	30	20	10	0	10	20	30	40	50	60

The photodiode and detector angles are referenced azimuthally to differentiate photodiode and detector arc positions which are symmetric about the zenith of the cloud field. Figure 3.2 shows these reference azimuth angles. The detector arc in the cloud field's western hemisphere corresponds to a reference azimuth angle of $\phi_r = \phi_0$, and in the eastern hemisphere, to $\phi_r = \phi_0 + 180^\circ$. The photodiode angles correspond to $\phi_r = \phi_0 + 90^\circ$ and $\phi_r = \phi_0 + 135^\circ$ in the northern and southern parts of the hemisphere, respectively. Since α is referenced to the vertical, or north-south axis and β is referenced to the horizontal, or east-west axis of the cloud field, the reference azimuth, ϕ_r , differs from the actual azimuth of the photodiode at position j, k . The notations j and k refer to the scan and photodiode numbers respectively. These notations are used later in the text to refer to the scan and photodiode positions. The nadir angle, η , and the azimuth angle, ϕ , are both functions of the photodiode angle and detector arc angle. The nadir angle is given by:

$$\eta = \cos^{-1}(\sin \alpha \sin \beta) \quad (3.1)$$

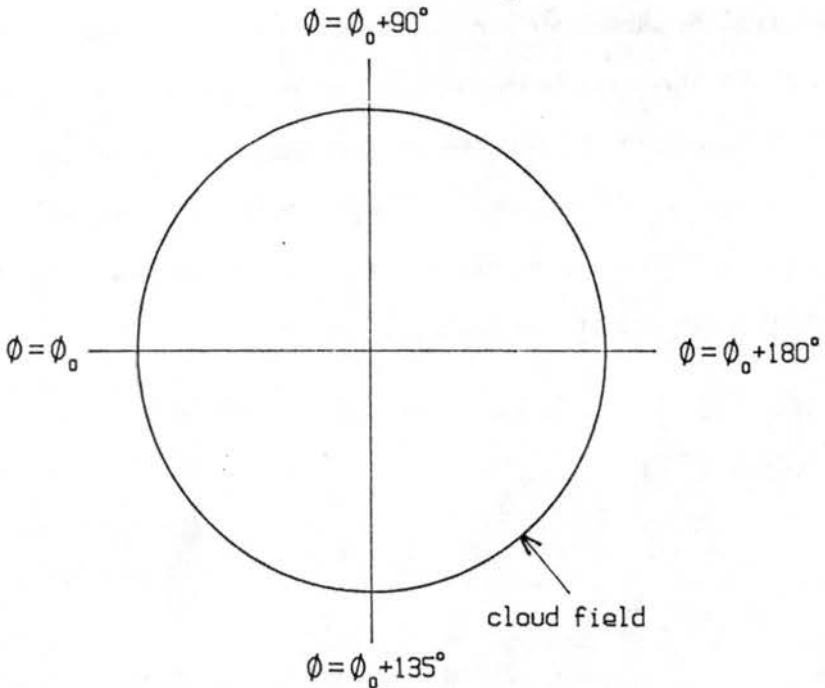


Figure 3.2: Reference photodiode and detector arc azimuth angles. The vertical axis in this figure corresponds to the north-south axis, or the photodiode axis. The horizontal, or east-west axis, corresponds to the detector arc axis.

and the azimuth angle:

$$\phi = \cos^{-1} \left(\frac{\cos \alpha}{\sin \eta} \right). \quad (3.2)$$

The azimuth angle is modified so it is referenced clockwise from the top of the cloud field assembly, so ϕ is related to ϕ_0 by $\phi = 0^\circ \equiv \phi_0 + 90^\circ$. Tables 3.3 and 3.4 list the nadir and azimuth angles respectively for each photodiode angle and detector arc angle pair.

Care must be taken to differentiate the source zenith angle from the local zenith angle or simply, zenith angle. The source zenith angle, Θ_0 , shown in figure 3.3, is the angle of incident radiation upon the cloud field. The source zenith angle is always negative, since it represents radiation which is in a downward direction relative to the cloud field. For reference purposes, the source in the “western” portion of the hemisphere is denoted by a source zenith angle of $\Theta_0, \Phi = \Phi_0$, and in the “eastern” portion of the hemisphere, by $\Theta_0, \Phi = \Phi_0 + 180^\circ$, where Φ_0 is an arbitrary source azimuth angle. The eastern, or “morning” source zenith angles are symmetric with the western, or afternoon source zenith angles about $\Theta_0 = 0^\circ$. The source zenith angle does not change during a scene measurement. The local zenith angle θ however, changes throughout the scene measurement. θ

Table 3.3: Nadir angles (in degrees)

Diode:	1	2	3	4	5	6	7	8	9	10	11	12	13
Scan													
1	76	71	68	64	62	61	60	61	62	64	68	71	76
2	71	65	61	56	53	51	50	51	53	56	61	65	71
3	68	61	54	49	44	41	40	41	44	49	54	61	68
4	64	56	49	41	36	32	30	32	36	41	49	56	64
5	62	53	44	36	28	22	20	22	28	36	44	53	62
6	61	51	41	32	22	14	10	14	22	32	41	51	61
7	60	50	40	30	20	10	0	10	20	30	40	50	60
8	61	51	41	32	22	14	10	14	22	32	41	51	61
9	62	53	44	36	28	22	20	22	28	36	44	53	62
10	64	56	49	41	36	32	30	32	36	41	49	56	64
11	68	61	54	49	44	41	40	41	44	49	54	61	68
12	71	65	61	56	53	51	50	51	53	56	61	65	71
13	76	71	68	64	62	61	60	61	62	64	68	71	76

is analogous to the nadir angle of the photodiode. This relationship can be seen in figure 3.1. The source zenith angle is defined by the experimentator, while the local zenith angle is a function of the photodiode's position with respect to the cloud field. Obviously, the local zenith angle is different for each photodiode, and changes for each photodiode as the detector arc is swept across the cloud field.

3.2 Theory

All equations used in this study are derived from the governing equation relating irradiance, or intensity, to the radiance values collected experimentally and to the geometry of the photodiode which collects the radiance. Note the voltages measured by the photodiodes are analogous to radiances reflected by real clouds. The basic equation for monochromatic irradiance is given as

$$F_\lambda = \int_{\Omega} I_\lambda \cos \theta d\Omega \quad (3.3)$$

where I_λ is the monochromatic radiance measured by the photodiode and $d\Omega$ is the differential solid angle represented by the photodiode. This solid angle is given by

$$d\Omega = \sin \theta d\theta d\phi \quad (3.4)$$

Table 3.4: Azimuth angles (in degrees)

Diode:	1	2	3	4	5	6	7	8	9	10	11	12	13
Scan													
1	333	324	314	304	293	281	270	258	247	236	226	216	207
2	336	327	317	307	296	283	270	257	245	233	222	213	204
3	340	332	323	312	300	285	270	254	241	228	218	209	201
4	344	337	329	319	306	289	270	250	234	221	211	203	196
5	349	344	338	329	317	297	270	243	223	211	202	196	191
6	354	352	348	343	335	316	270	225	206	197	192	189	186
7	0	0	0	0	0	0	0	180	180	180	180	180	180
8	6	8	11	17	26	45	90	135	155	163	168	172	174
9	11	16	22	30	43	62	90	117	137	150	158	164	169
10	16	23	31	41	54	70	90	109	126	139	149	157	164
11	21	28	37	48	61	74	90	105	120	132	143	152	160
12	24	33	42	53	65	77	90	103	115	127	138	147	156
13	26	36	46	56	67	78	90	101	113	124	134	144	154

where θ and ϕ have been defined as the local zenith angle and the azimuth angle, respectively. (From Liou, 1980.)

3.2.1 Isotropic and measured irradiances

In polar coordinates, the monochromatic irradiance can be written as

$$F_\lambda = \int_0^{2\pi} \int_0^{\frac{\pi}{2}} I_\lambda(\theta, \phi) \cos \theta \sin \theta d\theta d\phi. \quad (3.5)$$

Due to the spectral independence of the radiances collected in this study, (3.5) becomes

$$F = \int_0^{2\pi} \int_0^{\frac{\pi}{2}} I(\theta, \phi) \cos \theta \sin \theta d\theta d\phi. \quad (3.6)$$

Equation (3.6) represents the governing equation for irradiance calculation. Assuming angular independence of I , equation (3.6) can be integrated to yield

$$F_i = I \int_0^{2\pi} \frac{\sin^2(\frac{\pi}{2})}{2} d\phi \equiv \pi I. \quad (3.7)$$

Equation (3.7) defines the isotropic irradiance, which is denoted by the subscript i .

The azimuthally dependent case requires a numerical solution of (3.6) which is given by

$$F_m = \sum_{a=1}^{A=12} \sum_{b=1}^{B=18} I(\theta_b, \phi_a) \cos \bar{\theta}_b \sin \bar{\theta}_b \Delta\theta \Delta\phi. \quad (3.8)$$

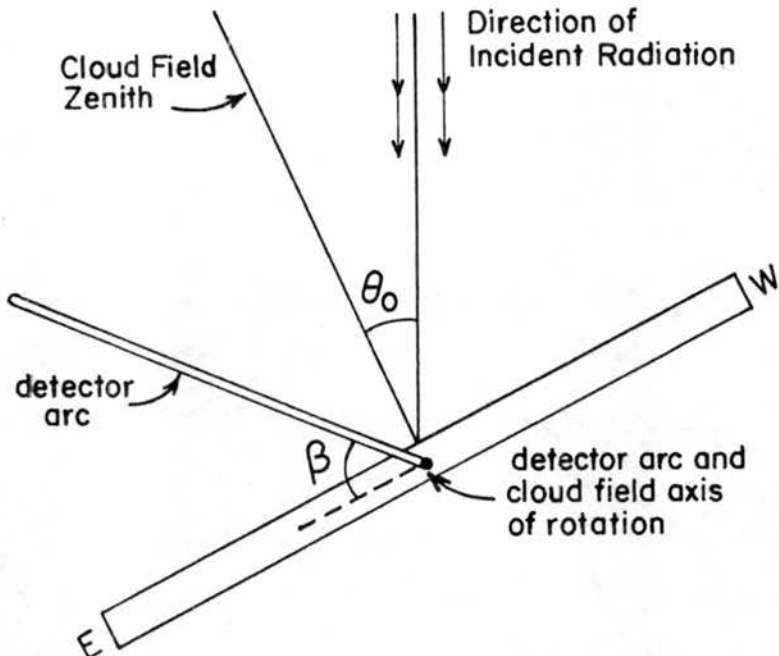


Figure 3.3: Geometry of the source zenith angle Θ_0 . Θ_0 is fixed during a scan set while β changes. The field is shown as an observer would see it while looking down onto the top of the field. In this depiction, the light source is in the western portion of the “sky”, so the source zenith angle would be denoted as $\Theta_0, \Phi = \Phi_0$.

Equation (3.8) represents the calculated azimuthally dependent upward irradiance, or simply, measured irradiance, denoted by the subscript m . Numerical calculation requires the cloud field to be divided into separate grid sections. Each of these grid sections is summed resulting in a total upward irradiance. Figure 3.4 is a graphical representation of the grid created for this purpose. The field is shown as an observer would see it while looking down onto the field at nadir. The field was divided into 18 sections representing zenith angles ranging from 0° to 90° , or from 0 to $\frac{\pi}{2}$ radians. $\Delta\theta$ is therefore 5° . Data were not collected for the $b = 17$ and $b = 18$ zenith angle sections, resulting in a summation from 0° to 80° , as can be seen in equation (3.9) given as

$$F_m = \sum_{a=1}^{A=12} \sum_{b=1}^{B=16} I(\theta_b, \phi_a) \cos \bar{\theta}_b \sin \bar{\theta}_b \Delta\theta \Delta\phi. \quad (3.9)$$

Values collected for zenith angles greater than 80° were not considered accurate due to the large elliptical fields viewed by photodiodes at these angles. Azimuthally, the field was divided into $m = 12$ sections, resulting in a $\Delta\phi$ of 30° or $\frac{\pi}{6}$ radians. $\bar{\theta}$ for all

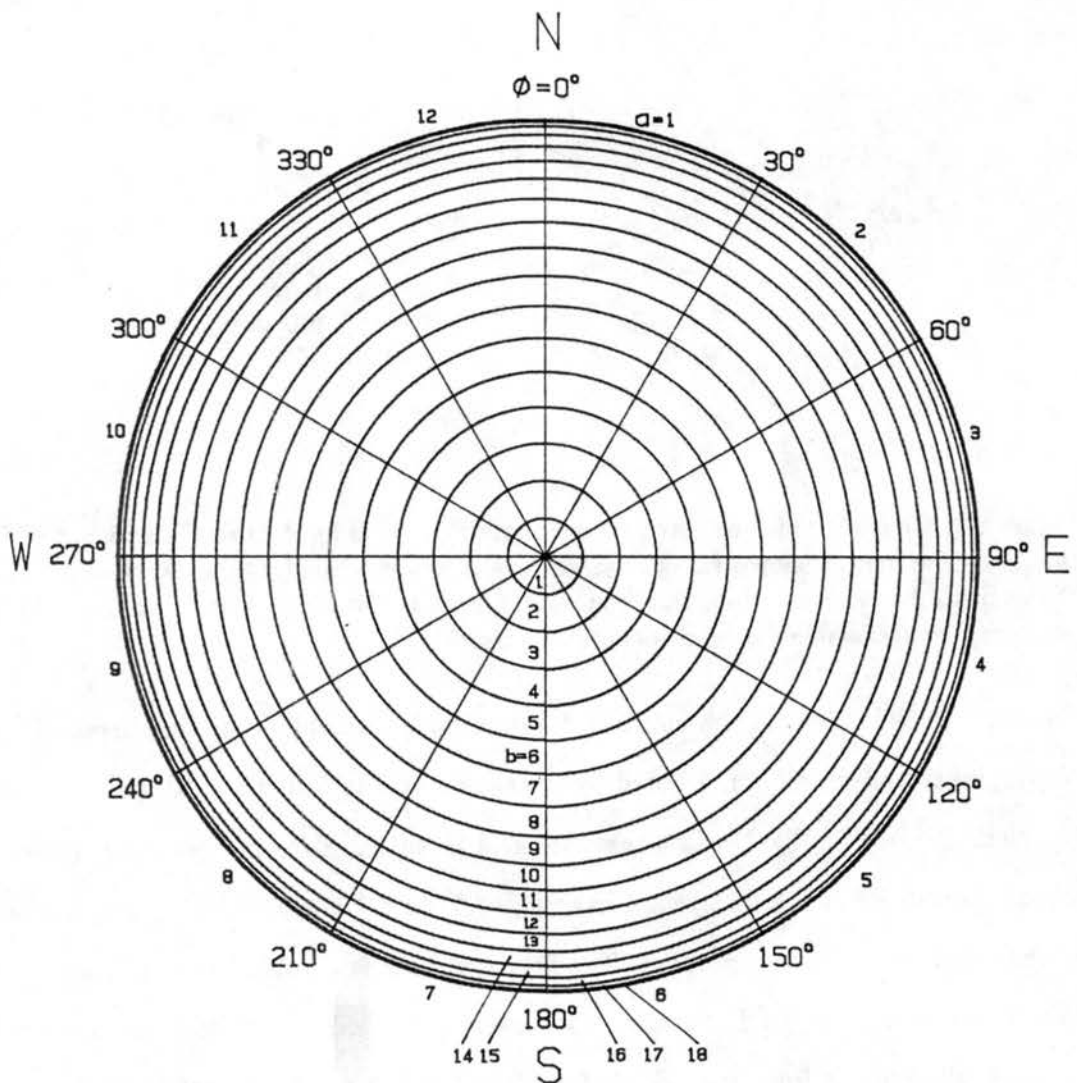


Figure 3.4: Graphical representation of the grid used for numerical calculation of irradiances (equation 3.9). This scene is depicted as an observer positioned directly above would see it when looking down onto the target. The circular rings represent an entire hemisphere, with the top of the hemisphere located in the center of the figure. Numbers within the rings ($b = 1$ to $b = 18$) represent local zenith angles, and numbers located outside the furthermost circle ($a = 1$ to $a = 12$) denote azimuth angles. Local zenith angles increase as the distance from the center of the field increases.

cases is simply $\frac{(\theta_i + \theta_{i+1})}{2}$. Photodiodes occupied most of these grid sections at one point in the scan set measurement. A grid section which contains more than one photodiode measurement resulted in an average radiance for that section. A small number of grid sections contained no observational data. Values for these sections were interpolated using the four sections immediately adjacent to the section not containing data. The total upward flux, or irradiance, was calculated by summing each grid section using equation (3.9). Of course, for comparisons to be accurate, F_i must be integrated between 0 and $\frac{4\pi}{9}$ radians. Equation (3.7) will therefore become

$$F_i = I \int_0^{2\pi} \frac{\sin^2(\frac{4\pi}{9})}{2} d\phi \equiv 0.97\pi I. \quad (3.10)$$

The contribution to the irradiance for zenith angles greater than 80° is only 3% that of the total irradiance when assuming isotropy. Since this study is concerned only with comparisons between measured and isotropic irradiances, accurate results can be obtained as long as both F_i and F_m are integrated (or summed) between the same two angles.

The anisotropic reflectance factor, Γ , is defined as the difference between the measured and the isotropic irradiance divided by the measured irradiance:

$$\Gamma = 100 \times \left(\frac{.97\pi I(\theta) - \sum_0^{2\pi} \sum_0^{\frac{4\pi}{9}} I(\theta, \phi) \cos \bar{\theta} \sin \bar{\theta} \Delta \theta \Delta \phi}{\sum_0^{2\pi} \sum_0^{\frac{4\pi}{9}} I(\theta, \phi) \cos \bar{\theta} \sin \bar{\theta} \Delta \theta \Delta \phi} \right), \quad (3.11)$$

or

$$\Gamma = 100 \times \left(\frac{F_i - F_m}{F_m} \right). \quad (3.12)$$

An isotropic irradiance which is exactly equal to the measured irradiance of the cloud field will result in anisotropic reflection function of zero. An underestimation of F_i ($F_i < F_m$) will result in a negative Γ while an overestimation ($F_i > F_m$) results in a positive value of Γ . Results of these calculations are shown graphically in chapter five.

Differences between these values of measured and isotropic irradiances are one of the main concerns of this study. Γ calculations can be used to show where anisotropic errors are at a maximum or minimum. Γ will be used to assess differences arising from both the source zenith angle Θ_0 and the local zenith angle θ .

As touched upon in the introduction, this study also examines factors other than those associated with the anisotropic reflectance factor Γ . Simple statistical analysis is utilized to assess reflectance variations due to differences in cloud field geometry between the 20 cloud fields. This analysis is explained in further detail in chapter four.

The Fourier series analysis in azimuth is of a somewhat different nature than the theory discussed above. It deals primarily with intensities collected at several azimuth angles situated along a specific local zenith angle. This analysis is covered in detail in appendix A.

Chapter 4

EXPERIMENTAL DATA COLLECTION

The primary goal of the data collection process is to obtain data from which the reflectance properties of 20 simulated cloud fields may be assessed. The outline of the experimental process is given first, followed by an explanation of each of the procedures. The first step of the process is to select the 20 different cloud fields mentioned previously. For each field, seven different source zenith angles were measured. Each source zenith angle is defined as a scene. A total of 140 scenes comprise this portion of the data set (20 fields x 7 scenes per field). Four scan sets of the exact same scene were taken for each of these source zenith angles to ensure the repeatability and validity of the scene measurement.

4.1 The cloud fields

A rectangular grid 56 inches vertically by 40 inches horizontally was mapped onto the cloud field. This grid was separated into four inch squares, so the completed grid contains 14 vertical and 10 horizontal squares. All simulated clouds had similar shapes, with cylindrical bases, and sculpted hemispherical tops. The cloud bases were approximately four inches in diameter with a height of approximately four inches. The simulated clouds are composed of ordinary white styrofoam. This type of material has been found to display reflectance characteristics similar to Monte Carlo modeled results (Davis *et al.* (1983)). Fifty-three clouds were arranged randomly on each cloud field. The total area of the simulated cloud bases covers approximately 30% of the grid area. These characteristics comply with the results of Plank (1969) who found both the 30% cover and the 1:1 height-base ratio common among Florida cumulus populations. The 20 simulated cloud fields differed only by the geometric relationships of the simulated clouds with respect

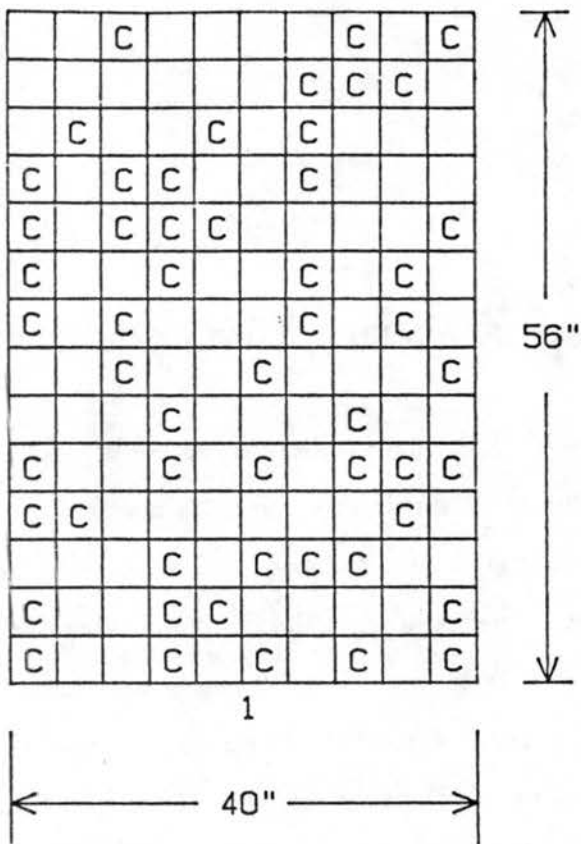


Figure 4.1: Cloud pattern of field number one. Grid squares containing clouds are denoted by "C". Appendix B contains diagrams of cloud patterns for all 20 fields.

to one another. The random fields were generated by a simple computer routine which chose 53 random coordinates upon which simulated clouds were placed. Appendix B contains diagrams which represent the cloud fields for each of the 20 cases. Figure 4.1 is a representation of the cloud pattern of field number one.

The reason for the 20 different fields is twofold. First, the use of 20 random fields all consisting of 30% cover creates a statistical sample resulting in mean irradiance values which approximate the mean irradiance of an infinite population of cloud fields with similar fractional cloud cover reasonably well. The statistical validity of this statement is covered in further detail in chapter five. Secondly, a portion of this study is to determine the reflectance characteristics differences, if any, of the cloud fields by virtue of these geometric relationships between individual simulated cloud elements. Figure 4.2 depicts the grid placed upon the field.

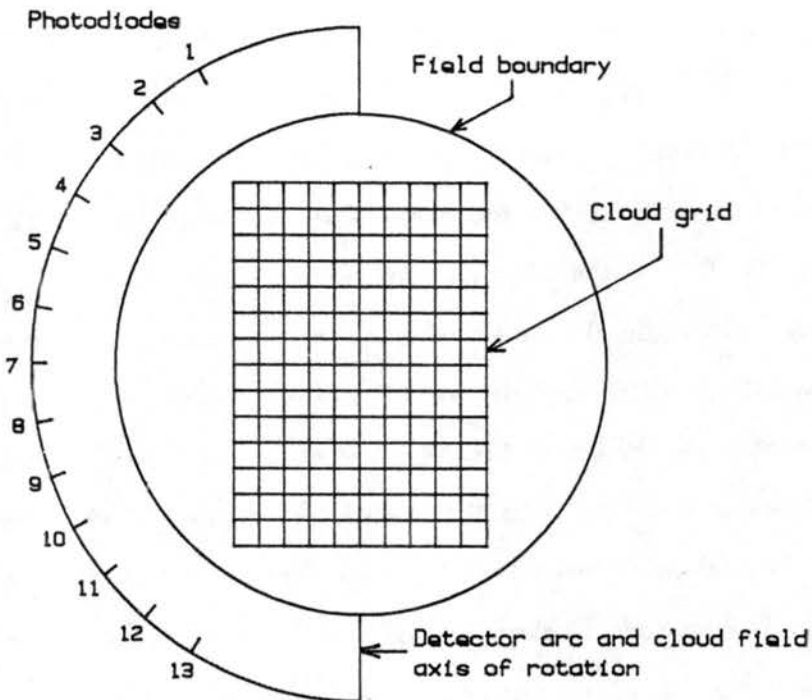


Figure 4.2: Cloud grid on field. Photodiodes located on detector arc are numbered 1-13.

4.2 The source zenith angles

As mentioned previously, data were collected for seven different source zenith angles, or scenes, per cloud field. The angles chosen were from $\Theta_0 = -60^\circ, \Phi = \Phi_0$ to $\Theta_0 = -60^\circ, \Phi = \Phi_0 + 180^\circ$ in 20° increments. A source zenith angle of $\Theta_0 = 0^\circ$ would correspond to local noon if the field was located at the equator during the vernal or autumnal equinoxes. These particular source zenith angles were chosen to provide a representative view of reflectance throughout one "day".

4.3 Scans and scan sets

Each source zenith angle in each cloud field was scanned four different times to ensure the repeatability of the scene. A scan set is defined as one of these scans. Hence, a scene is comprised of four scan sets.

A scan set is comprised of 13 scans. These scans describe the movement of the detector arc across the field. The detector arc begins its scan set at a detector arc angle

of $+60^\circ$, $\phi_r = \phi_0$ relative to the cloud field and records data at 10° increments to an angle of $+60^\circ$, $\phi_r = \phi_0 + 180^\circ$. The reference azimuth ϕ_r is defined in the previous chapter.

A scan is defined as one of these scan set increments. Each scan results in the recording of 18 values. Thirteen of these values are the reflected radiances measured by the 13 diodes. Three of the values recorded represent the geometry of the scene: the first is the source zenith angle, Θ_0 ; the second is the angle of the detector with respect to a source zenith angle of 0° (This angle is modified in the processing software so it is referenced with respect to the position of the cloud field at Θ_0); and the third value is the azimuth angle of the cloud field with respect to the source zenith angle, which was not used in this study. The final two values recorded are the dark current voltage and the light source intensity. The dark current diode is used in the calibration procedures described below. The light source diode is mounted on a fixed, non-rotating platform above the cloud field and is directed toward the incident light. This diode is used to account for fluctuations in the incident light intensity. The data processing software monitors changes in the light source intensity and adjusts the reflected radiances accordingly. Figure 4.3 is a schematic outline of the experimental procedure.

Each of the 18 values collected during one scan represent an average intensity. During one scan, each diode collects 30 measurements over a period of approximately 15 seconds to provide an accurate sampling of several instantaneous measurements. These measurements are then averaged before they are stored onto floppy disk. This is another advantage of a laboratory procedure over satellite and aircraft measurements. Taking all measurements into account, the data set of the reflected intensity measurements alone contains well over two million values.

In addition to the reflected intensity data collected, two data files were recorded before each scene measurement for use in the calibration procedures discussed in the next section. One of these files is the dark current voltage update file, and the other is a file containing relative sensitivities of each diode.

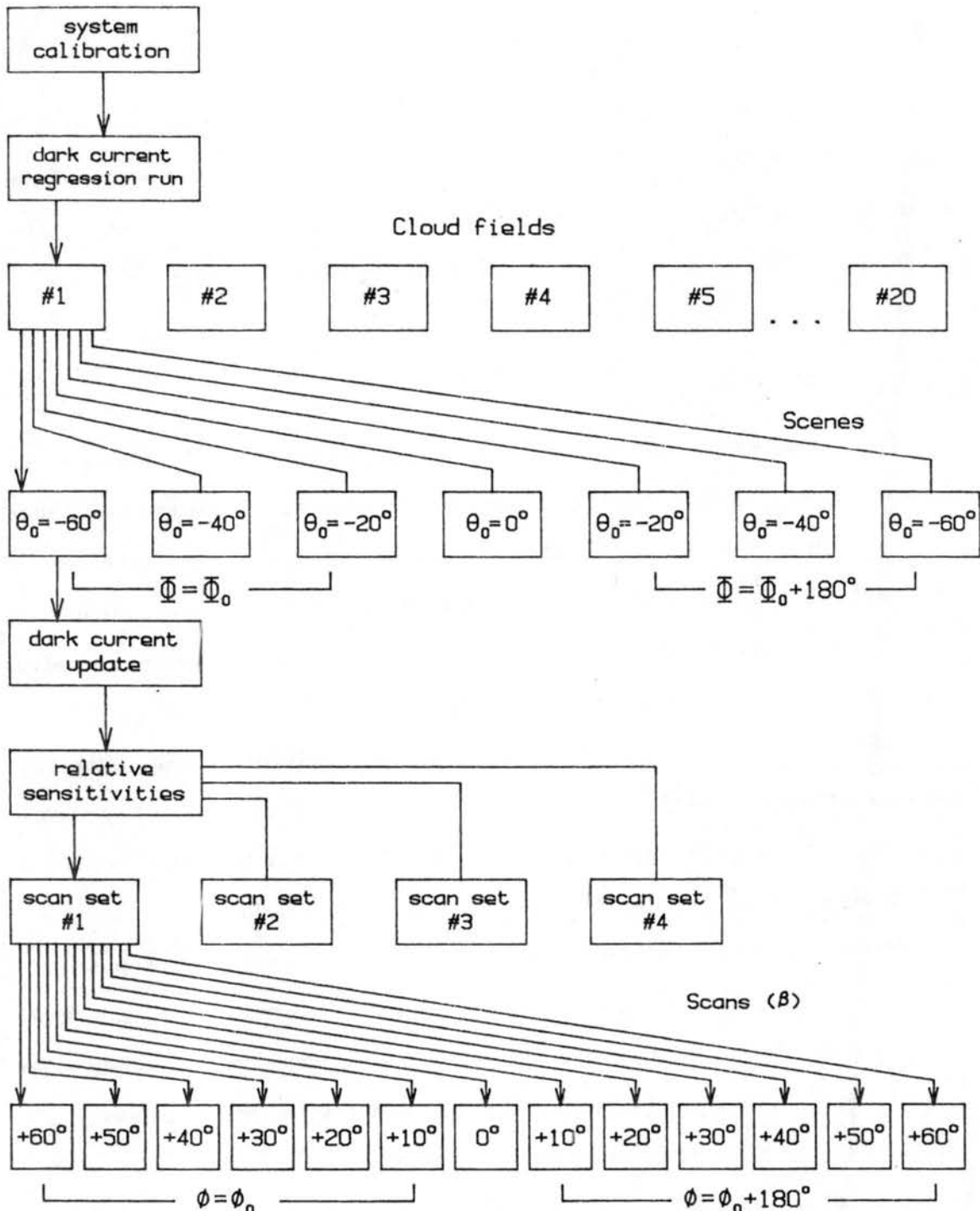


Figure 4.3: Schematic outline of experimental procedure. System calibration and initial dark current regression run are completed before data collection begins. Lines show progression of procedure. For each cloud field, seven different scenes are analyzed. Dark current updates and relative sensitivity updates are measured prior to each scene measurement. For each scene, four scan sets are measured. For each scan set, 13 scans are measured each at a different detector angle β . Lines with arrows show the step by step procedure for field number one, $\Theta_0 = -60^\circ$, $\Phi = \Phi_0$, scan set number one.

4.4 Calibration

The calibration procedures used in this study can be separated into two sections: system calibration and continuous calibration. System calibration involves procedures which must be undertaken before any data collection has begun. Continuous calibration primarily updates system calibration procedures taking into account any changes in the system as the experiment progresses.

4.4.1 System calibration

The primary goal of system calibration is to prepare the CFOS for the collection of accurate data. This procedure takes place at the beginning of the experiment before any data collection has begun. Although the system calibration procedures are extremely important in obtaining accurate final products of data collection, the detailed explanation of these procedures does not provide any added information helpful to the interpretation of the data; therefore, the explanation of this procedure will be brief.

The first step in the system calibration procedure involves alignment of the light source. The source platform is moved in a manner such that it is visually symmetric with the cloud field. This is a trivial procedure, which results in greater accuracy in accomplishing the next two steps of the system calibration procedure.

Step two is the determination of the true zero zenith angle. Since the source zenith angle is found using analog equipment which is translated into digital format, an analog to digital converter is utilized. This converter can stray from producing the accurate values of source zenith angles over a long period of time, so a calibration becomes necessary. The symmetry of the light source is important to this procedure which is the primary reason it is accomplished early in the calibration procedure. The determination of the zero source zenith angle is accomplished by placing a single photodiode near the geometric center of the cloud field. This photodiode is different from the photodiodes mentioned previously in that the diode is portable and is placed directly upon the cloud field facing the light source. It therefore measures incident radiation rather than reflected radiation which is measured by photodiodes located on the detector arc. The field is initially rotated so

the source zenith is offset from zero in one direction. The field is then rotated through the zero zenith and beyond. Throughout this fairly continuous operation, the photodiode is monitored for changes in intensity registered by the diode. Since the intensity of the source upon the field is dependent upon the cosine of the source zenith angle, the diode registers a maximum when the source zenith angle is zero. The difference between true zero and zero displayed on the CFOS monitors is then programmed into the processing software.

The next step in the calibration procedure involves the adjustment of one or more of the source lamps so the source produces a spatially homogeneous incident radiation field upon the cloud field. This is accomplished by measuring the incident radiation upon the cloud field at several different locations on the field. The voltage anomalies are noted and the positions of the lamps are adjusted to compensate. Note that the illumination produced by the individual lamps overlap significantly, so these two steps must be repeated until a spatially homogeneous field is produced, i.e. voltages are similar regardless of the position of the monitoring photodiode within the field. The field in this study is spatially homogeneous to within 2% precision. This means that of the 21 locations upon which the portable photodiode was placed, the range of the voltages registered by the diode at these locations divided by the mean voltage registered by these diodes collectively is less than 2%. Once this procedure is accomplished, the true zero source zenith angle must be reset due to changes in the source lamp directions. These two steps are repeated until there is no change in either the true zero measurement or the spatial homogeneity procedure.

The last two system calibration steps involve the alignment of the photodiodes so their fields of view are centered on the field, and the centering of the detector arc so the detector angles are accurate. The photodiodes are aligned by placing a small penlight over each photodiode collimator can which illuminates a portion of the cloud field. The photodiodes are adjusted so the illumination is centered on the center of the cloud field. The centering of the detector arc is accomplished by noting the shadow produced by the light source and the detector arc which falls upon the cloud field at a source zenith angle of $\Theta_0 = 0^\circ$. The difference between the detector arc nadir and the displayed detector arc angle is then programmed into the processing software.

4.4.2 Continuous calibration

The signal produced by the photodiodes are fed into an operational amplifier circuit. Figure 2.1 shows the photodiode/operational amplifier circuit. Due to the nature of this amplification, the photodiodes produce a significant dark current signal which is always present. This dark current is extremely temperature sensitive, so it is imperative that it is monitored closely throughout the experiment and compensated for when needed. This is the purpose of the dark current diode mentioned previously. The first data file collected is one which monitors this signal for a long period of time, at least for a few hours. This file is utilized by a program which provides linear regression coefficients which are constantly updated throughout the experiment. Dark current updates were performed at the beginning of each scene measurement. These updates notify the system of any temperature-induced or other changes in dark current voltage during the experiment. The program which processes the software utilizes these coefficients to eliminate any contribution to the reflected intensity by the dark current voltage.

The second continuous calibration procedure is one which adjusts for the relative sensitivities of the diodes with respect to each other. The sensitivities of each photodiode are somewhat different, and are somewhat temperature dependent. After current dark current updates are collected, an isotropic reflector is placed upon the field. The isotropic reflector used in this experiment is a circular object approximately 44 inches in diameter composed of polyurethane foam. Ordinary polyurethane foam has been proven to provide a nearly isotropic surface upon which to obtain these sensitivities (Davis *et al.* (1983)). A file is then collected from which each diode's sensitivity is determined. The processing software then normalizes these sensitivities to a single diode's sensitivities, and utilizes these values during subsequent normalization procedures.

The final continuous calibration procedure involves monitoring of light source intensity. Since the line voltage which supplies the light source is not constant in time, and the source lamps do undergo some aging, the intensity of the light upon the field will not be constant. While these changes are not apparent to the human eye, they must be dealt with to achieve accurate final results. The light source is monitored by the light source diode

mentioned previously. Light source intensities are recorded each time a scan is recorded and the observed intensity values are scaled appropriately in the processing software. This procedure is accomplished for each scan set only, so an additional normalization must be undertaken when any scan set comparison is done. Chapter five notes this modification when discussing results of the experiment.

4.5 Data collection products

The end results of this data collection procedure are 560 files each containing 169 radiance measurements (13 photodiodes, 13 detector angles per file). The radiances in these raw data files are modified by considering dark current calibration coefficients, relative sensitivities of the 13 photodiodes, and variation in light source intensity. Specific details concerning the processing of these radiances are discussed below. Since each scene measurement includes 4 scan sets of the scene, this results in 140 files with different scene information (20 fields x 7 scenes per field). All irradiance results in chapter five are comprised of the averages of the four scan sets in each scene. Tables 4.1, 4.2, and 4.3 contain statistical information, including mean irradiances, ranges, and ranges of variation for each scene. Mean measured irradiances are found by averaging the four measured irradiances calculated in each scan set. Ranges of variation are defined as the range of irradiances divided by the mean irradiance. All values in these tables have been normalized to the mean light source intensity of the entire data set, but not to the power density differences due to the decrease of incident radiation intensity as Θ_0 increases. Field number 11 shows higher irradiance values than the other fields (see table 4.1). Since all fields are normalized, it is assumed these higher values are the result of the geometry of field number 11, although the geometry of this field is not markedly different from that of other fields studied. In all cases, the differences between measured irradiances for each scan set in a scene is small, usually less than 5% (see table 4.3). Similar irradiances within each scan set provide a high confidence level when studying differences in irradiances arising from geometric effects. Measured radiances were numerically integrated for each of the 560 files and were integrated assuming isotropy for each of the 169 radiance values in each of these files. Anisotropic reflectance factors were then calculated for the entire data set.

Table 4.1: Mean irradiance values for all scenes (in mV)

$\Theta_0:$	-60°	-40°	-20°	0°	-20°	-40°	-60°
$\Phi:$	Φ_0				$\Phi_0 + 180^\circ$		
Field							
1	4914	5305	5936	5582	6422	5915	5160
2	7552	9412	10347	9893	9799	9675	8181
3	3787	5107	4841	5179	4801	4996	4233
4	7982	9106	10082	10272	9619	9395	7841
5	8156	9722	10376	9652	9205	9160	8182
6	7051	8500	8452	8125	7771	8067	6646
7	4892	5953	5984	6039	6360	6025	5239
8	6386	5888	6615	5986	6429	6691	5916
9	5310	5809	6757	6128	6694	7082	5806
10	8707	10060	9822	9765	9817	9780	8408
11	9611	12307	13360	13149	13507	12490	9353
12	7698	9017	9002	9143	9290	9371	7989
13	6909	7969	8329	8283	8701	8494	6842
14	5636	7447	7960	7759	7489	7027	6444
15	6193	7212	7708	7086	6921	7065	6386
16	7293	7971	8263	7865	8277	8130	7412
17	7891	8712	9877	9384	9557	9411	7620
18	4839	5766	5768	6089	5772	6010	4613
19	6279	7539	8248	8225	8189	8010	6600
20	6934	8254	8778	8914	8397	8819	7068

4.6 Data processing

Three factors must be considered when processing the raw data file: the dark current, relative sensitivities of each photodiode, and variations in light source intensity. After these factors are taken into account, the end product becomes intensities, or radiances, which are analyzed using equations introduced in chapter three.

The first file written to floppy disk contains hundreds of scans which were collected with no incident light. This is the initial dark current file. From this file, simple linear regression was used to calculate a slope and an offset from the slope for each photodiode. The slope is given by

$$m = \frac{N \sum_{n=1}^N xy - \sum_{n=1}^N x \sum_{n=1}^N y}{\sum_{n=1}^N x^2 - (\sum_{n=1}^N x)^2} \quad (4.1)$$

where N is the number of scans recorded for each photodiode in the file, x is the reference diode value, and y is the value of the diode being considered. The offset value of the diode

Table 4.2: Irradiance ranges for all scenes (in mV)

$\Theta_0:$	-60°	-40°	-20°	0°	-20°	-40°	-60°
$\Phi:$	Φ_0				$\Phi_0 + 180^\circ$		
Field							
1	582	550	596	173	165	321	239
2	142	160	150	175	109	261	165
3	96	90	196	240	255	94	194
4	185	89	379	77	141	139	150
5	215	64	172	63	75	173	43
6	111	225	168	111	44	83	243
7	147	116	199	210	256	98	120
8	249	110	251	167	34	179	230
9	167	170	166	166	92	769	400
10	63	78	279	37	141	113	350
11	244	99	85	291	79	181	86
12	141	101	97	239	75	104	236
13	151	241	300	105	52	237	212
14	118	346	236	324	80	69	94
15	106	118	154	163	66	141	75
16	410	55	212	87	283	210	377
17	303	69	215	154	190	259	266
18	217	44	209	47	89	60	211
19	178	65	30	284	102	101	163
20	440	112	141	344	153	111	332

from the slope is

$$O_1 = \bar{y} - m\bar{x}. \quad (4.2)$$

This results in a slope and offset calculated for each of the 13 photodiodes and provides the user with an idea of the variability of each photodiode with reference to the dark current diode variability. Since the dark current values of the 13 photodiodes cannot be measured when collecting a data file with the light source illuminating the field, the linear regression analysis provides a means to predict the dark current which is inherently present within the raw radiance measurements. The actual dark current is constantly monitored using a single photodiode, which is masked off so that no incident or reflected radiation is detected. This initial dark current file is used by all 560 data files. However, the offset values are updated each time a scene is changed using

$$O_2 = O_1 - \left[\sum_{n=1}^N (mx_n + O_{1,n} - y_n) \right]. \quad (4.3)$$

Table 4.3: Ranges of variation for all scenes

$\Theta_0:$	-60°	-40°	-20°	0°	-20°	-40°	-60°
$\Phi:$	Φ_0				$\Phi_0 + 180^\circ$		
Field							
1	.119	.104	.100	.031	.026	.054	.046
2	.019	.017	.015	.018	.011	.027	.020
3	.025	.018	.040	.046	.053	.019	.046
4	.023	.010	.038	.007	.015	.015	.019
5	.026	.007	.017	.006	.008	.019	.005
6	.016	.026	.020	.014	.006	.010	.037
7	.030	.019	.033	.035	.040	.016	.023
8	.039	.019	.038	.028	.005	.027	.039
9	.031	.029	.025	.027	.014	.109	.069
10	.007	.008	.028	.004	.014	.012	.042
11	.025	.008	.006	.022	.006	.014	.009
12	.018	.011	.011	.026	.008	.011	.030
13	.022	.030	.036	.013	.006	.028	.031
14	.021	.047	.030	.042	.011	.010	.015
15	.017	.016	.020	.023	.010	.020	.012
16	.056	.007	.026	.011	.034	.026	.051
17	.038	.008	.022	.016	.020	.028	.035
18	.045	.008	.036	.008	.015	.010	.046
19	.028	.009	.004	.034	.012	.013	.025
20	.063	.014	.016	.039	.018	.013	.047

This new offset value, which represents changes in the dark current established by the dark current file calculations due to environmental temperature differences, is subtracted from the radiances in the raw data set. The method described above accurately predicts dark currents for each of the 13 data collecting photodiodes. Although there is no exact method of determining actual dark current differences within a data scan, correlation coefficients between the dark current diode and the collecting diode differences were between .972 and .994, depending on the photodiode being considered. Thus, a high confidence level is possible when determining these predicted dark currents.

The photodiode detectors are not identical. Each photodiode measures a slightly different intensity when subjected to the same amount of radiation incident upon the photodiode. This is in part due to the manufacturing of the diodes, and the amplification involved in processing the signal created by the photodiode. These differences must be considered if precise radiance values are to be determined. The calculation involved in

computing the relative sensitivity of each photodiode is a simple normalization. To obtain these sensitivities, the isotropic reflecting surface was placed on the field before each scene measurement with the light source on so each photodiode received a similar amount of reflected radiation. Assuming isotropy within this reflector, the photodiodes should show similar radiances since the field has already been tested for spatial homogeneity of the incident beam of radiation. A file was created for each scene containing several scans of isotropic radiances collected by each of the 13 photodiodes. After subtracting the dark current from each photodiode in each scan, the scans were averaged for each photodiode. The relative sensitivities were calculated by dividing the radiances measured by each diode by the radiance measured by one specified photodiode. If for example, the radiance measured by diode number two divided by the radiance collected by diode number eight (the reference diode) is .9, the final processing will divide the radiance (measured by diode number two) by .9. Assuming an isotropic reflector, this calculation compensates for any differences in the sensitivities of the diodes.

The normalization of the collected radiances within each scan set concludes with the light source normalization. The light source monitor values are recorded during each scan, and radiances are adjusted in a manner similar to that of the relative sensitivity normalization, using the first light source measured (scan number one) as a reference. The radiances are normalized further with respect to one mean light source so comparisons between different fields can be made. Comparisons between different scenes in the same field can be made after using a correction factor relating the decrease of incident radiation due to an increased source zenith angle to reflected irradiances. This completes the continuous calibration procedure. The results of these calibration procedures are radiances which can be used in further processing for analysis of the cloud field.

Chapter 5

RESULTS

As stated in the introduction, the goal of this paper was to answer several different questions concerning the nature of cloud reflectance properties. This chapter discusses these questions. Each section of this chapter will discuss a different area of study. The first section is concerned with the variations in measured irradiances among the 20 different cloud fields. The second section compares irradiances which have been integrated assuming isotropy with irradiances which have been numerically integrated assuming azimuthal and zenith angle dependence. Section 5.2 will also discuss results derived from different source zenith angles. Section 5.3 is an attempt to interpret radiance variations within the solid angle encompassing the cloud field, thus determining where errors due to isotropic assumption are to be found.

5.1 Irradiance variations comparing different cloud fields

This experiment is ideally suited to finding differences in irradiances arising from the geometries of cloud elements within the cloud field. Data from all 20 fields were collected in the same manner. The same background was present throughout the experiment and, unlike real cloud fields, all cloud fields in this experiment were independent of time. The only difference among the various cloud fields was the organization of the individual clouds within the field. These differences can be noted by referring to Appendix B, which shows the cloud patterns of all 20 fields. Differences in irradiances arising from the different cloud field geometries are shown in this section.

One irradiance was calculated for each scan set and normalized with respect to light source voltage differences during the scene measurements. As explained in Chapter 4, each of the four irradiances in a scene were then normalized with respect to the average

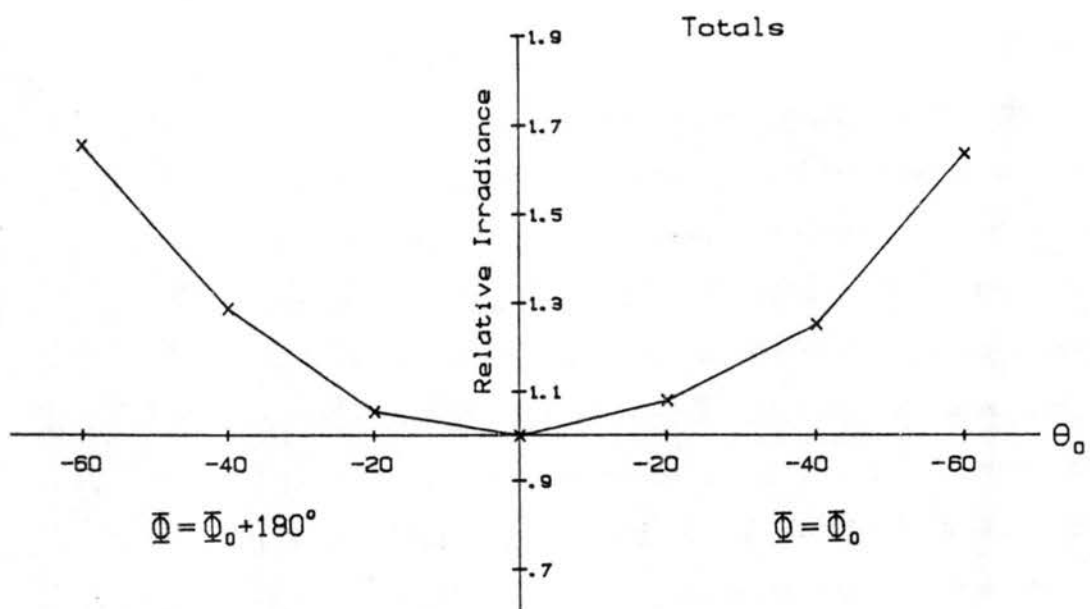


Figure 5.1: Mean relative irradiances vs. Θ_0 for all 20 fields. Irradiances are normalized to the irradiance value for $\Theta_0 = 0^\circ$, and to the decrease of light source power density due to increasing source zenith angles.

light source voltage of the four scan sets. The irradiances of the four scan sets in each scene were then averaged to produce one mean irradiance value and one mean light source voltage for each scene. As shown in table 4.3, the differences in these averaged irradiances produced ranges of variation generally less than 0.05 (5%).

The final normalization procedure involves adjusting irradiances calculated for all $\Theta_0 \neq 0^\circ$ for power density differences (amount of incident radiation per unit area) arising from different source zenith angles. As Θ_0 increases, the irradiance upon the cloud field decreases. Theoretically, for a plane parallel homogeneous cloud field, the incident power density decreases by a factor of $\cos \Theta_0$. The CFOS system shows a similar decrease in incident light source intensity as Θ_0 increases. All reflected irradiances were multiplied by $\cos \Theta_0$ for all source zenith angles.

Figure 5.1 is a plot comparing the relative irradiances (relative to $\Theta_0 = 0^\circ$) as a function of Θ_0 for the average irradiances of the 20 cloud fields. Theoretically, a plot of this type depicting an isotropic field would be comprised of a straight line along the abscissa if the incident source intensity decreases were considered. These plots therefore

show the differences arising from cloud geometry. Relative irradiances are found by simply dividing the irradiance measured at Θ_0 by the irradiance measured at $\Theta_0 = 0^\circ$. The abscissa represents source zenith angles and the ordinate represents the relative irradiances found at that source zenith angle. Figure 5.1 is representative of most cloud fields in the data set. One can see that the relative irradiances increase with increasing source zenith angles, with the $\Theta_0 = -60^\circ$ cases showing the greatest increase. Welch *et al.* (1980) report increased reflectances (reflected radiation divided by incident radiation) with increasing source zenith angles when modeling single clouds with variable microphysical characteristics within the cloud. The cloud used by Welch *et al.* (1980) is comparable to cloud fields used in this study, since both the single cloud and the cloud fields contain "holes" from which limited reflectance is observed. As the source zenith angle increases, the possibility of a photon being reflected increases, since the photon is less likely to encounter a cloud-free hole within the cloud field. Although a significant difference exists between reflectance and irradiance, comparisons may be made between these two studies when source zenith angle irradiance differences are considered since irradiances measured at all source zenith angles were normalized to one light source value. Figures 5.2 and 5.3 are relative irradiances of cloud fields 1 and 10 respectively. These are shown as a visual means to compare different cloud fields with one another. Field number one is shown because it represents the greatest deviation from other fields in this study. Irradiances for $\Theta_0 = -20^\circ, \Phi = \Phi_0$, $\Theta_0 = -20^\circ, \Phi = \Phi_0 + 180^\circ$, and $\Theta_0 = -40^\circ, \Phi = \Phi_0$ are less than the irradiance measured at $\Theta_0 = 0^\circ$. Most fields in this study show plots which are similar to figures 5.1 and 5.3. Relative irradiances of all 20 fields can be found in tabular form in appendix C. Table 5.1 is a compilation of pertinent statistical data for the 20 fields. Statistical results were calculated for each source zenith angle. This table depicts irradiances which have been adjusted for both light source intensity differences and for the decrease in incident radiation as Θ_0 increases. σ_{n-1} is the standard deviation of the 20 fields sampled at each source zenith angle, found using

$$\sigma_{n-1} = \sqrt{\frac{\sum_{n=1}^{20} (X_n - \bar{X})^2}{n - 1}}. \quad (5.1)$$

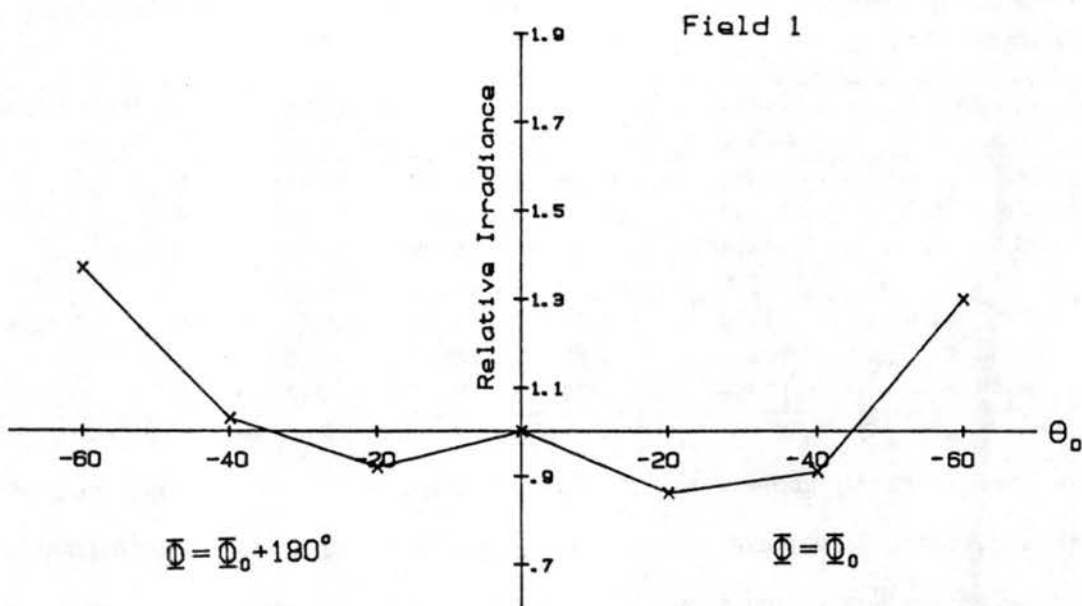


Figure 5.2: Same as 5.1, except field number 1 is depicted instead of mean values for the entire data set.

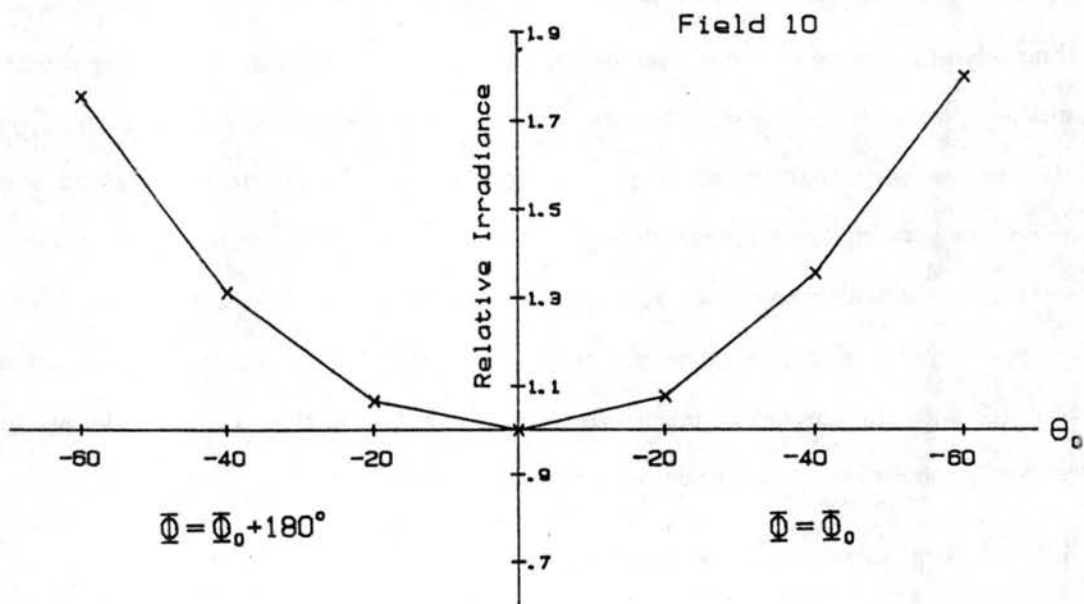


Figure 5.3: Same as 5.1, except field number 10 is depicted instead of mean values for the entire data set.

Table 5.1: Statistical comparisons of irradiances among the 20 cloud fields analyzed. All values are in mV.

Θ_0	Φ	Mean irradiance	Maximum irradiance	Minimum irradiance	σ_{n-1}	Range	Range/mean
-60°	Φ_0	13594	18706	8467	2721	10240	0.75
-40°	Φ_0	10548	16304	6522	2314	9783	0.93
-20°	Φ_0	8674	14374	5109	2062	9265	1.07
0°		8126	13149	5179	1984	7970	0.98
-20°	$\Phi_0 + 180^\circ$	8859	14217	5151	2154	9066	1.02
-40°	$\Phi_0 + 180^\circ$	10251	16065	6667	2426	9398	0.92
-60°	$\Phi_0 + 180^\circ$	13359	19222	7573	2943	11649	0.87

σ_{n-1} increases as Θ_0 increases, a result of increased irradiance with increasing source zenith angles. A better depiction of the variations among cloud fields are the ranges of irradiances for each Θ_0 , which are quite large. The range of variation (range of irradiances divided by the mean irradiance) is as high as 1.07 (107%) in the $\Theta_0 = -20^\circ$, $\Phi = \Phi_0$ case. The means are simply the average irradiances of the 20 fields at the source zenith angle noted. Also noted in this table are the distribution of ranges. The range of variation increases as Θ_0 approaches zero, then decreases somewhat at $\Theta_0 = 0^\circ$. This result leads to the conclusion that more variation may be present in reflected irradiance due to geometry at smaller source zenith angles. This observation concurs with the work of Busygin *et al.* (1973) who found that the effect of cloud geometry on the albedo of the cloud is most conspicuous at smaller solar zenith angles. By considering the range of irradiances for a certain source zenith angle, we gain insight into the amount of variation which can be expected due to the geometric cloud interactions within the cloud fields. This is not to be confused with the amount of anisotropy at smaller zenith angles. These results are based on geometric differences of measured irradiances only.

5.2 Errors based on isotropic assumption

This section investigated the differences between measured irradiances and isotropic irradiances assuming an isotropic cloud field. The anisotropic reflectance factor, Γ , is useful in assessing these errors. Stowe *et al.* (1980) used an anisotropic reflectance factor similar to the one used in this study. However, an important difference is noted between Γ

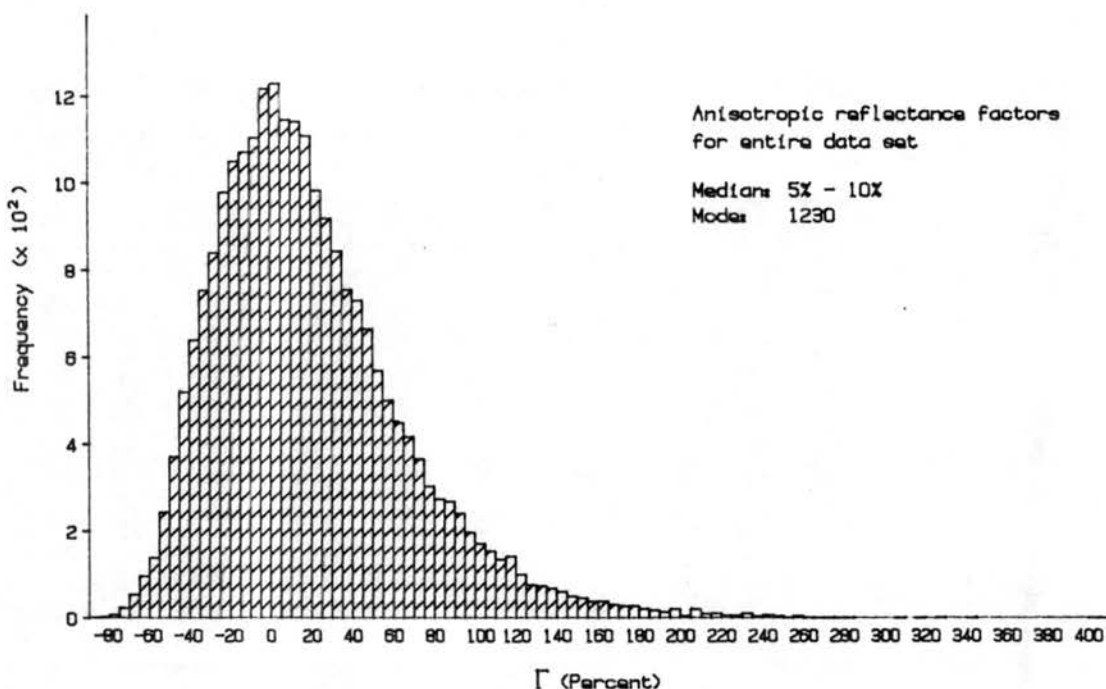


Figure 5.4: Frequency distribution of anisotropic reflectance factors for entire data set. This plot represents the frequency of photodiodes which measure radiances integrated to yield the value of Γ indicated. Γ is defined by equation (3.12). Statistical parameters associated with this histogram are found in tables 5.2 and 5.3.

and the anisotropic reflectance factor used in the study done by Stowe *et al.* (1980). While the anisotropic reflectance factor used by Stowe *et al.* (1980) divides the isotropic assumed irradiance by the measured irradiance, Γ in this study is calculated using equation (3.12). The result is multiplied by 100 to express the answers in percentages.

A useful representation of Γ is a histogram plot of frequency of occurrence as a function of Γ for each different source zenith angle. Figure 5.4 is a representation of anisotropic reflectance factors considering the entire data set. The ordinate represents the frequency of photodiode measurements which exhibit the anisotropic reflectance factor noted on the abscissa. The entire data set is a compilation of all seven source zenith angles. For each source zenith angle, 3380 photodiode radiances were measured (20 fields \times 169 averaged radiances per scan set). The result for the data set is a skewed gamma distribution which shows most of the Γ values between -40% and 60%. A negative value indicates underestimation of the measured irradiance by the isotropic irradiance, while a positive value of Γ is an overestimation. Figure 5.4 has a median which lies in the 5% - 10%

Table 5.2: Anisotropic reflectance factor statistical information. Mean and modal values are in mV. The median, modal range, and cumulative distribution functions are expressed as ranges of Γ where these values are found.

Θ_0	Φ	Mean	Median	Mode	Modal range	20% CDF	80% CDF
-60°	Φ_0	58	-10 - -5	214	-35 - -30	-40 - -35	40 - 45
-40°	Φ_0	50	5 - 10	186	-5 - 0	-20 - -15	55 - 60
-20°	Φ_0	56	15 - 20	225	0 - 5	-10 - -5	55 - 60
0°		58	15 - 20	250	15 - 20	-10 - -5	45 - 50
-20°	$\Phi_0 + 180^\circ$	54	15 - 20	215	0 - 5	-10 - -5	50 - 55
-40°	$\Phi_0 + 180^\circ$	48	15 - 20	188	-5 - 0	-20 - -15	55 - 60
-60°	$\Phi_0 + 180^\circ$	54	-10 - -5	189	-35 - -30	-35 - -30	45 - 50
All		296	5 - 10	1230	0 - 5	-20 - -15	50 - 55

range, and modal value of 1230 mV, which is located between 5% and 10%. Of the total number of radiances, approximately 40% would underestimate the total upward irradiance using the isotropic assumption, and approximately 60% would produce an overestimate. It is interesting to note that underestimates do not fall below -80%, while overestimates are as great as 400%. These overestimates will be shown to occur in the backscattering direction of the incident light source. This contrasts with the work of Stowe *et al.* (1980), who found that for large solar zenith angles, Γ could be overestimated by as much as 800% when the detector views toward the forward scattering direction. The results of that study however, were based on measurements of high ice clouds. Histograms representing frequencies of Γ values for each source zenith angle are shown in figures 5.5 - 5.11. These histograms show the same type of distribution found in figure 5.4. Tables 5.2 and 5.3 are comprised of statistical information associated with anisotropic reflectance factors. The last row in table 5.2 consists of all values of Γ measured. The two columns on the right side show the 20% and 80% cumulative distribution function locations as a measure of the width of the distribution. It is clear from these columns that the distributions widen as Θ_0 increases. Table 5.3 shows the entire range of cumulative distribution functions.

Referring to table 5.2, it is noted that as the source zenith angle approaches 0°, the mode approaches the zero Γ . In other words, as the source zenith angle decreases, the differences between isotropic and measured irradiances decrease. The modes, which represent the greatest frequency of occurrence, are more negative as Θ_0 increases or decreases from

Table 5.3: Anisotropic reflectance factor cumulative distribution functions.

$\Theta_0:$	-60°	-40°	-20°	0°	-20°	-40°	-60°	All
$\Phi:$	Φ_0				$\Phi_0 + 180^\circ$			
Γ Range								
-75% - -70%	0	0	0	0	0	0	1	0
-70% - -65%	1	0	0	0	0	0	1	0
-65% - -60%	2	0	0	0	0	1	3	1
-60% - -55%	3	1	0	0	0	1	4	1
-55% - -50%	6	1	0	0	1	2	7	2
-50% - -45%	10	2	1	0	1	3	10	4
-45% - -40%	15	4	1	1	2	5	15	6
-40% - -35%	20	8	3	2	4	7	20	9
-35% - -30%	26	11	4	3	6	9	25	12
-30% - -25%	32	15	7	5	8	13	30	16
-25% - -20%	38	19	10	7	11	17	36	20
-20% - -15%	43	24	14	11	15	21	40	24
-15% - -10%	48	29	18	15	19	25	46	29
-10% - -5%	53	34	22	20	25	30	49	33
-5% - 0%	57	40	28	26	31	36	53	39
0% - 5%	60	45	34	32	37	40	57	44
5% - 10%	64	50	40	39	43	44	61	49
10% - 15%	67	54	46	46	49	49	65	53
15% - 20%	69	58	52	53	54	54	68	58
20% - 25%	72	62	56	59	59	58	70	62
25% - 30%	74	65	61	65	63	62	73	66
30% - 35%	77	68	65	70	67	66	75	70
35% - 40%	79	72	69	74	71	69	77	73
40% - 45%	82	74	72	78	74	72	80	76
45% - 50%	83	77	76	81	78	75	82	79
50% - 55%	85	79	79	84	80	78	84	81
55% - 60%	87	82	81	86	82	80	85	83
60% - 65%	89	83	84	88	84	82	87	85
65% - 70%	90	86	85	90	86	84	88	87
70% - 75%	91	87	87	92	88	85	90	89
75% - 80%	92	88	89	93	90	87	91	90
80% - 85%	93	89	90	94	91	88	92	91
85% - 90%	94	90	92	95	92	89	93	92
90% - 95%	95	91	93	96	93	90	94	93
95% - 100%	96	92	94	96	94	91	95	94
100% - 105%	96	93	95	97	95	92	95	95
105% - 110%	97	94	95	97	96	93	96	95
110% - 115%	97	95	96	97	96	94	96	96
115% - 120%	98	95	96	98	97	95	97	97
120% - 125%	98	96	97	98	97	96	97	97
125% - 130%	98	96	97	98	98	96	98	97
130% - 135%	99	96	97	99	98	96	98	98

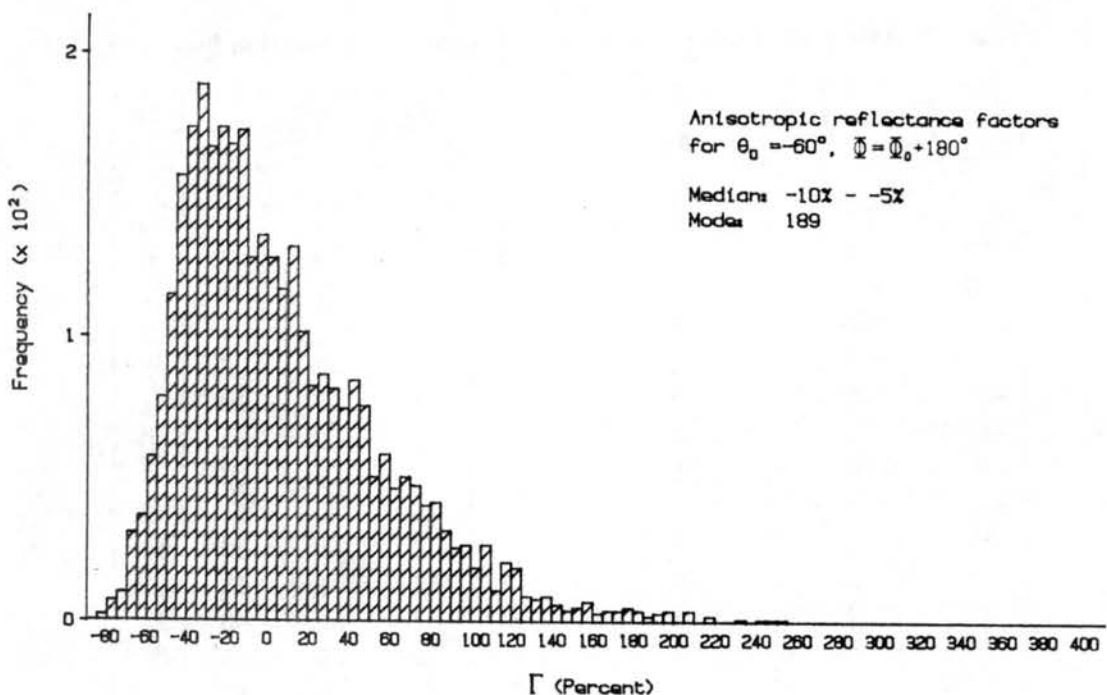


Figure 5.5: Same as 5.4, except showing Γ values for a source zenith angle of $\Theta_0 = -60^\circ, \bar{\Phi} = \Phi_0 + 180^\circ$.

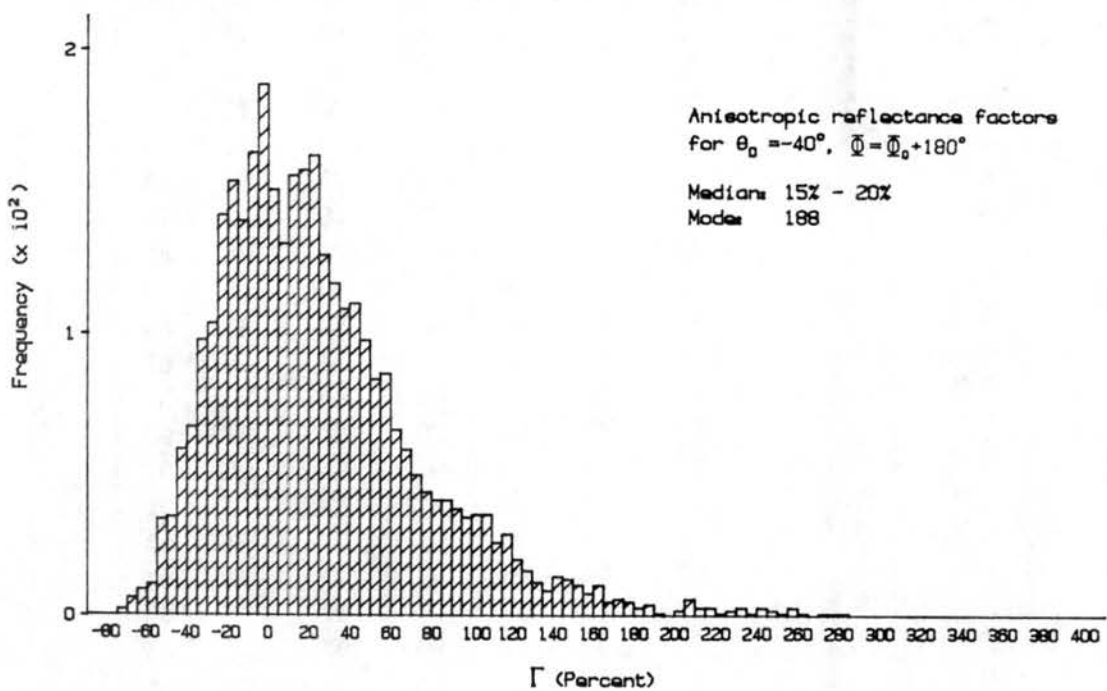


Figure 5.6: Same as 5.4, except showing Γ values for a source zenith angle of $\Theta_0 = -40^\circ, \bar{\Phi} = \Phi_0 + 180^\circ$.

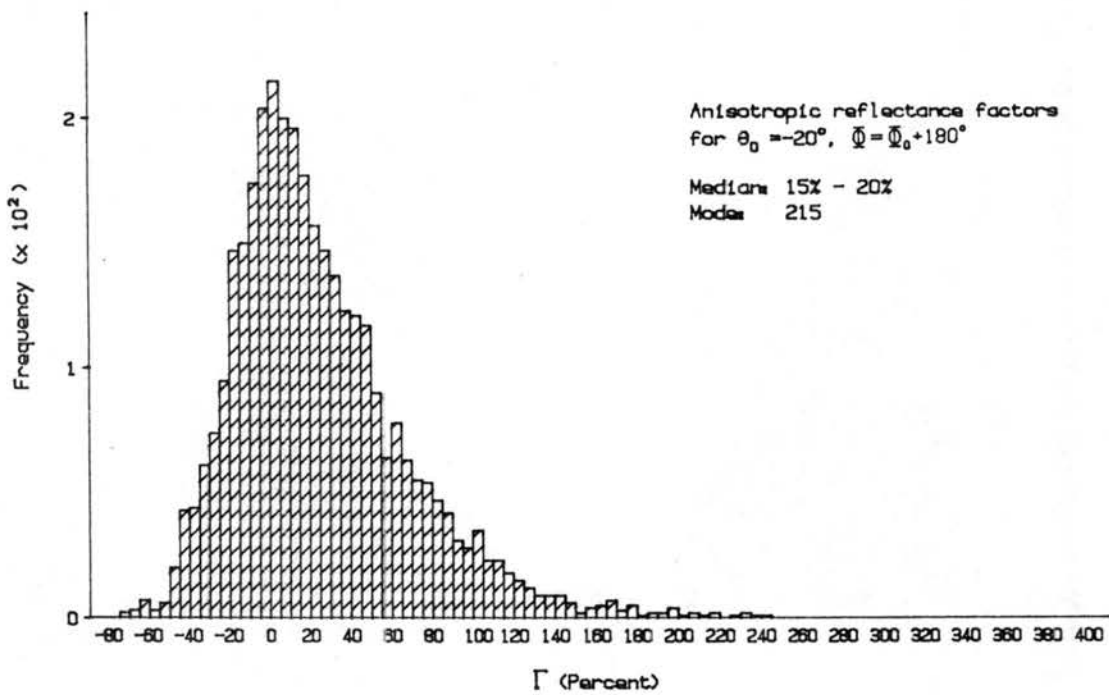


Figure 5.7: Same as 5.4, except showing Γ values for a source zenith angle of $\Theta_0 = -20^\circ$, $\Phi = \Phi_0 + 180^\circ$.

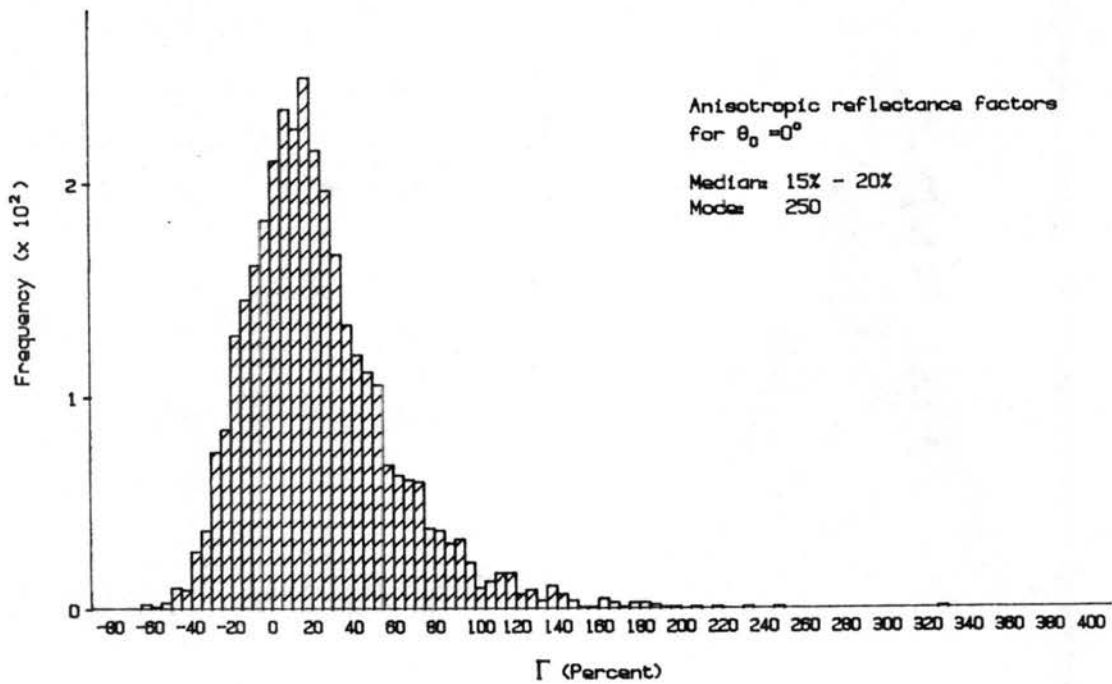


Figure 5.8: Same as 5.4, except showing Γ values for a source zenith angle of $\Theta_0 = 0^\circ$.

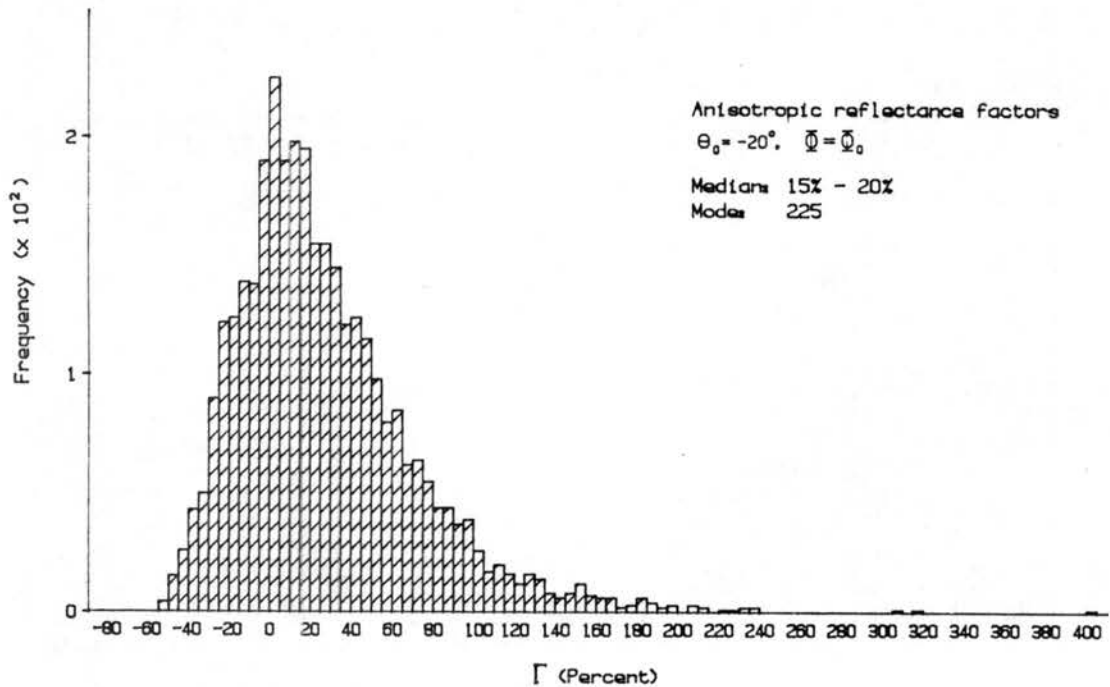


Figure 5.9: Same as 5.4, except showing Γ values for a source zenith angle of $\Theta_0 = -20^\circ, \Phi = \Phi_0$.

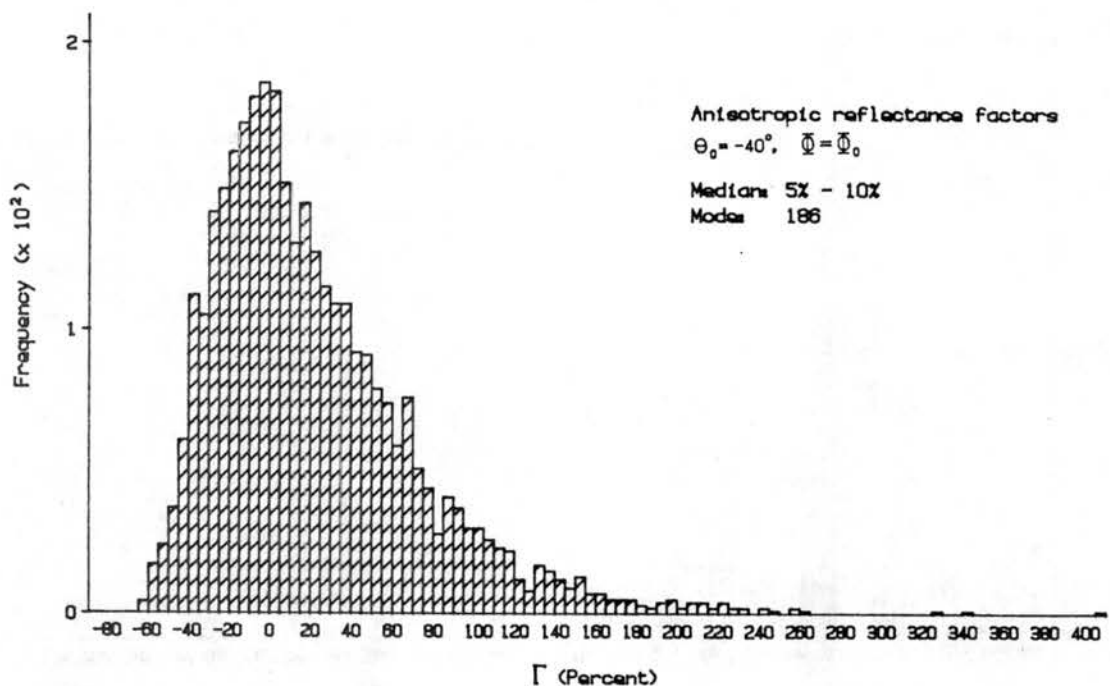


Figure 5.10: Same as 5.4, except showing Γ values for a source zenith angle of $\Theta_0 = -40^\circ, \Phi = \Phi_0$.

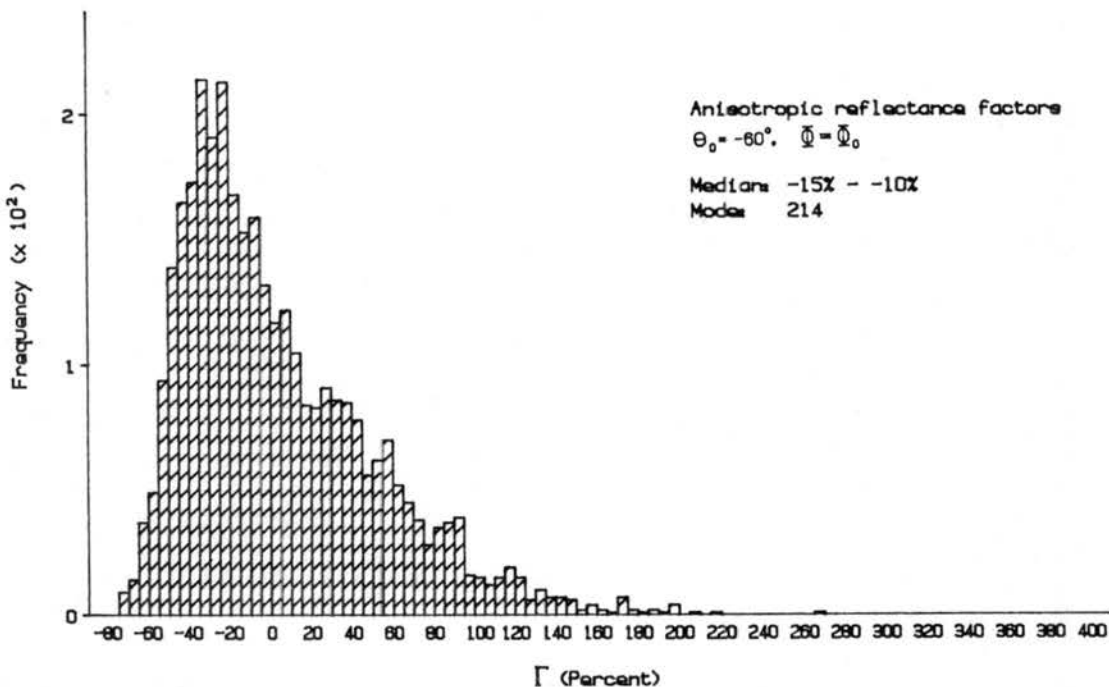


Figure 5.11: Same as 5.4, except showing Γ values for a source zenith angle of $\Theta_0 = -60^\circ, \Phi = \Phi_0$.

$\Theta_0 = 0^\circ$. The $\Theta_0 = 0^\circ$ case actually shows positive values of Γ , indicating a progression from underestimation to overestimation of F_m as Θ_0 decreases. This is consistent with the results of several studies (Stowe *et al.*, Ruff *et al.*, Davis and Cox (1982), and Brennan and Bandeen (1970)), all of which determined increasing anisotropy with increasing Θ_0 . For larger source zenith angles, the median value also shifts to the left on the histograms, suggesting a tendency toward underestimation of the reflected irradiance at large source zenith angles.

5.3 Location of maximum and minimum anisotropy

Although the results mentioned in section 5.2 show frequency distributions of the anisotropic reflectance factors, there is no indication of the position of the local zenith angle θ where these factors exist. It would be helpful to know where Γ is a minimum, since a minimum value of this quantity indicates an isotropic irradiance which approximates the measured irradiance well. It can be seen in figures 5.5 – 5.11, that minimum anisotropic reflectance factors do exist. The purpose of this section is to determine if a local zenith

angle exists where these anisotropic reflectance factors are consistently low. This section will also examine locations of maximum values of Γ .

Figure 5.12 is a diagrammatical representation of each photodiode's local zenith angle with respect to the cloud field as the detector arc sweeps over the field. Figure 5.13 is a similar representation of each photodiode's azimuth angles. Each row of squares slanting diagonally upward to the right represents one photodiode location. The squares are numbered from diode number $k = 1$ to $k = 13$. Columns, which slant upward to the left, represent the detector arc's position over the cloud field. The first column represents the 13 photodiode measurements during scan number one, etc. Scans are numbered from $j = 1$ to $j = 13$. The detector arc axis is a line beginning at the center of the lower right side of the figure (in the center of the $j = 7$ square) and extending upward and to the left, parallel to the lines which denote the detector scans. Of course, since these plots are representations of photodiode positions, the actual position of the detector arc would be above these fields. The numbers inside the boxes of figures 5.12 and 5.13 represent the local zenith angle and azimuth angle, respectively, of the corresponding photodiode at the corresponding detector angle. Consider the $j = 1, k = 1$ square. The photodiode taking radiance measurements here is located at $\theta = 76^\circ, \phi = 333^\circ$.

Analysis of anisotropic reflectance factors is divided into seven primary groups, each representing a different range of Γ values, for each source zenith angle and for the entire data set, which includes all seven source zenith angles. The ranges analyzed are as follows: $\Gamma < -40\%$, $-40\% \leq \Gamma < -20\%$, $-20\% \leq \Gamma < 0\%$, $0\% \leq \Gamma < 20\%$, $20\% \leq \Gamma < 40\%$, $40\% \leq \Gamma < 60\%$, and $\Gamma > 60\%$. Supplemental analysis was done using $-5\% \leq \Gamma \leq 5\%$ and $-10\% \leq \Gamma \leq 10\%$.

The histograms shown in this section may look somewhat confusing, but are actually fairly simple to read. Figure 5.14 is a plot representing the entire data set at $\Gamma < -40\%$. Since $\Gamma < 0\%$, this plot therefore shows the locations of diodes which collect radiances which, when integrated (assuming isotropy) using equation (3.10), result in irradiances which underestimate the measured irradiance of the field of which that diode measurement was a part. The vertical axis, numbered one to five, represents the frequencies of

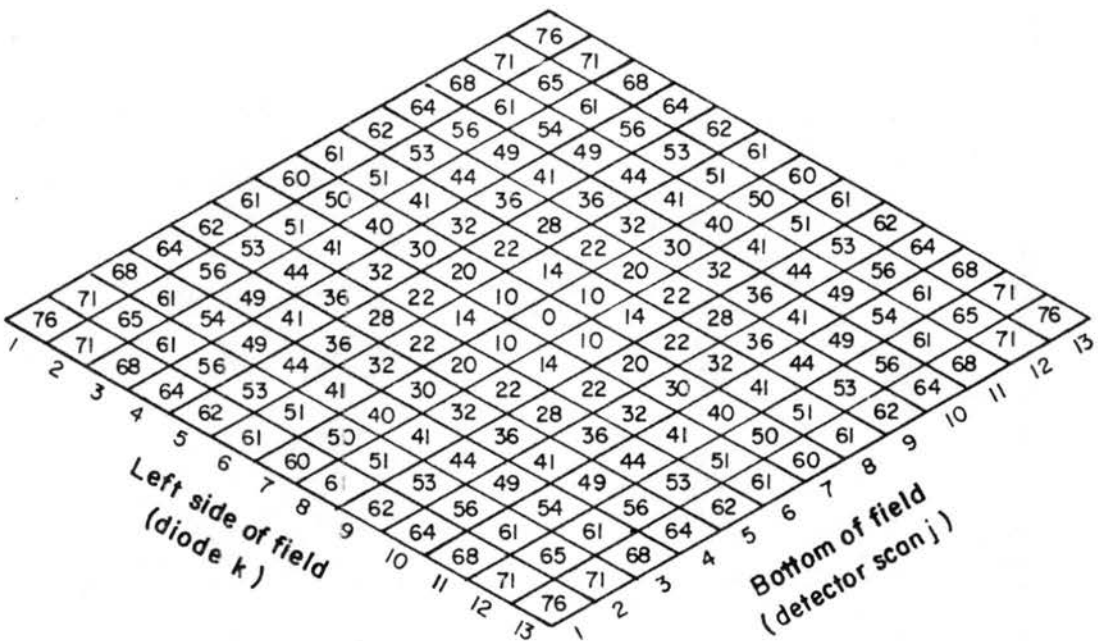


Figure 5.12: Local zenith angles on 3-d histogram grid. Coordinates labeled 1–13 on left side of plot represent diode numbers (k) and numbers on the right side denote detector arc scan number (j).

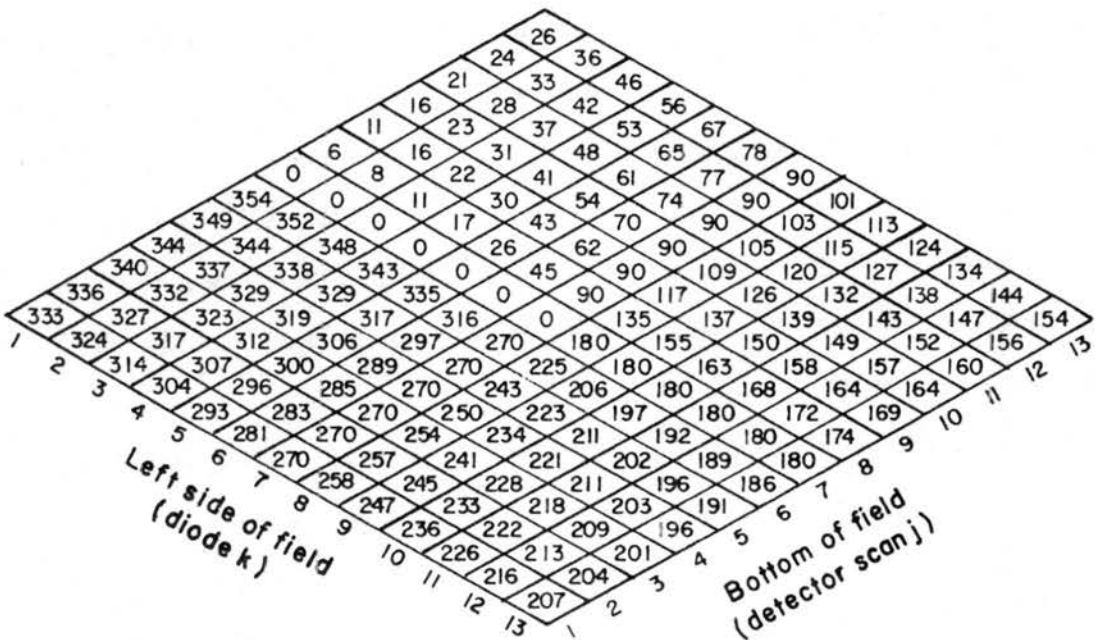


Figure 5.13: Same as 5.12, with azimuth angles depicted. Angles are referenced clockwise from the “north”.

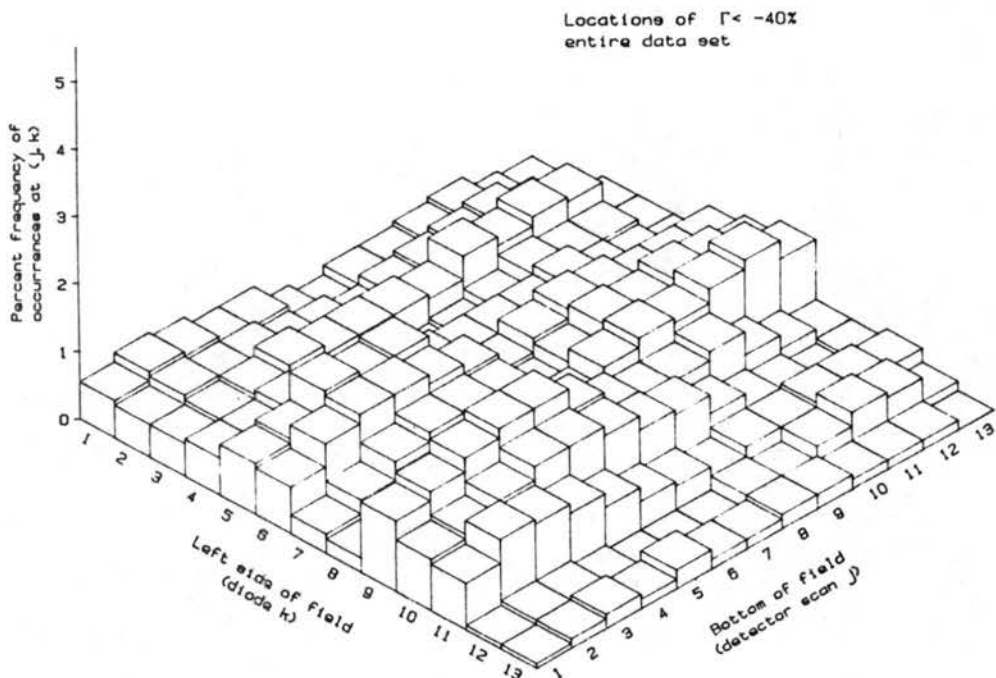


Figure 5.14: 3-d histogram representing frequency and location of photodiode measurements which result in anisotropic reflectance factors indicated. This figure shows locations of all values of $\Gamma < -40\%$ in the data set.

occurrence expressed in percentages. All plots are scaled similarly so comparisons may be made between plots. As an example, note that the bar located at the coordinates $j = 1$, $k = 1$ displays a value of $\sim .5\%$. This indicates that $\sim .5\%$ of all diode values in the data set integrated to yield irradiances which are less than -40% that of the measured irradiance were measured when photodiode number one ($k = 1$) was at detector scan number one ($\beta = 60^\circ$; $j = 1$). Furthermore, referring back to figure 5.12, the local zenith angle at that location is $\theta = 76^\circ$. It should be clear that summation of all bars in each plot will result in a value of 100%.

Figure 5.14 shows underestimates which have Γ values of $< -40\%$ occur throughout the field. There is some indication that the greatest underestimates occur less frequently at large local zenith angles, but in general, these underestimates occur in a fairly uniform distribution throughout the scan set. Figure 5.15 shows smaller underestimates ($-20\% \leq \Gamma < 0\%$), still using the entire data set. These smaller underestimates are shown to occur with the greatest frequencies near the center of the field at small local zenith angles. Although this case is more clear cut than the $\Gamma < -40\%$ entire data set case, the latter

two figures contrast sharply with figure 5.16, which shows locations of Γ values which are greater than 60%. This figure clearly shows that overestimates of large magnitudes occur at large local zenith angles. Referring to figure 5.12, one can see that most large overestimates occur when $\theta > 50^\circ$.

Care must be taken when attempting to make further conclusions concerning figures representing the entire data set. This data set includes source zenith angles which are symmetric about $\Theta_0 = 0^\circ$, and many effects which may be present when individual source zenith angles are considered tend to cancel out when the entire data set is considered. Further study requires the data set to be broken into plots which show features of each source zenith angle. Although the figures shown in this section are representative of the entire study, appendix D lists the complete set of anisotropic reflectance factor locations in tabular form.

5.3.1 Determination of maximum anisotropy

Figures 5.17 and 5.18 show underestimates and overestimates of the isotropic irradiances respectively for a source zenith angles of $\Theta_0 = -60^\circ, \Phi = \Phi_0 + 180^\circ$. Since a negative source zenith angle corresponds to morning hours when the sun is in the east (upper right in the figures) it is evident from figure 5.17 that large underestimates ($\Gamma < -40\%$) occur when the photodiodes are measuring forward scattering. Azimuthally, the greatest frequencies of underestimates are very close to 180° from the direction of the source radiation. Large overestimates (figure 5.18) occur predominately when the diodes are measuring backscattered radiation. Plots showing similar underestimates and overestimates for the $\Theta_0 = -40^\circ, \Phi = \Phi_0 + 180^\circ$ and $\Theta_0 = -20^\circ, \Phi = \Phi_0 + 180^\circ$ cases (not shown) show similar characteristics, with slightly suppressed results probably due to the decreasing source zenith angle. Figure 5.19 shows large underestimates ($\Gamma < -40\%$) at $\Theta_0 = 0^\circ$. Large underestimates are shown most frequently at smaller local zenith angles ($\theta < 40^\circ$ in many cases). Large overestimates ($\Gamma > 60\%$) seen in figure 5.20 for $\Theta_0 = 0^\circ$ occur again at large local zenith angles (usually $\theta > 60^\circ$). Note the overestimates occur at all four corners of the grid which contrasts with figure 5.18, in which the overestimates are all on the right side of the grid. This difference is due to the source zenith angle differences in the two

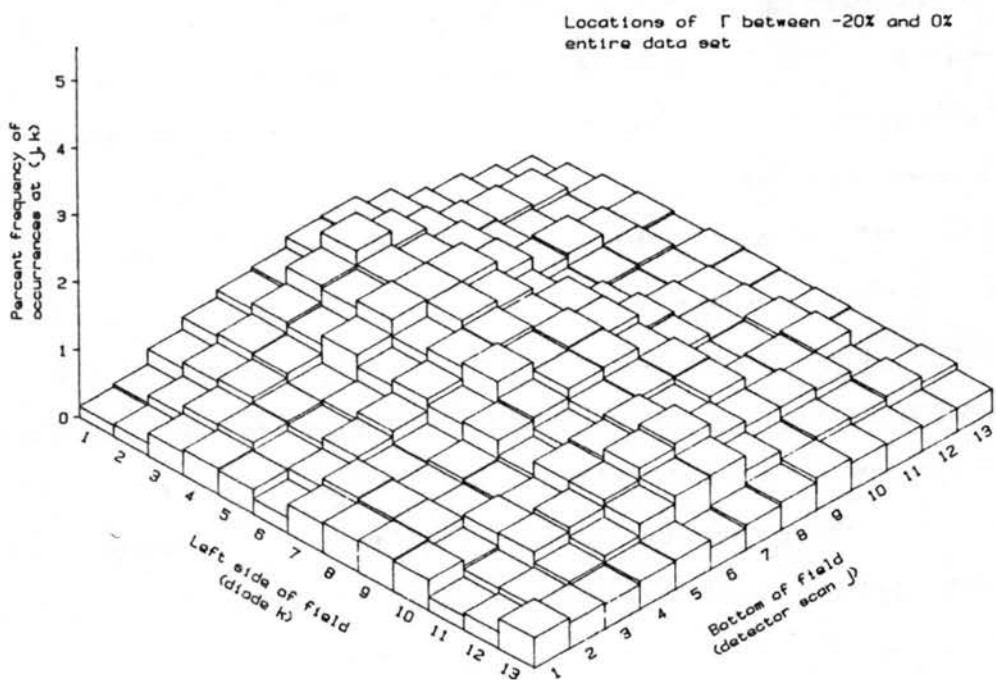


Figure 5.15: Same as 5.14, except showing locations of anisotropic reflectance factors of $-20\% \leq \Gamma < 0\%$.

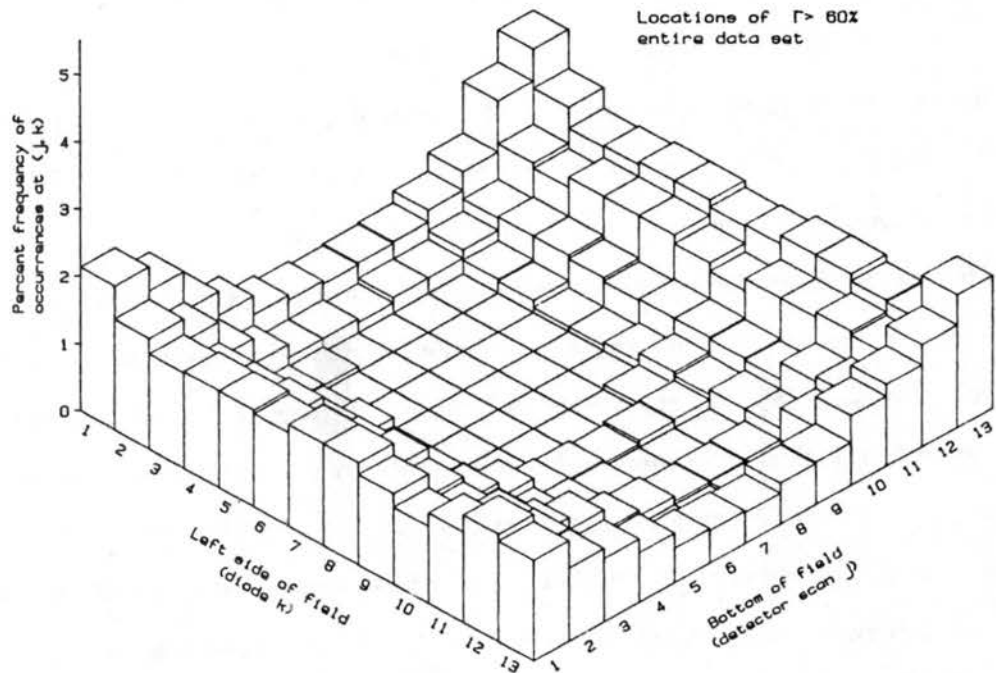


Figure 5.16: Same as 5.14, except showing locations of anisotropic reflectance factors of $\Gamma > 60\%$.

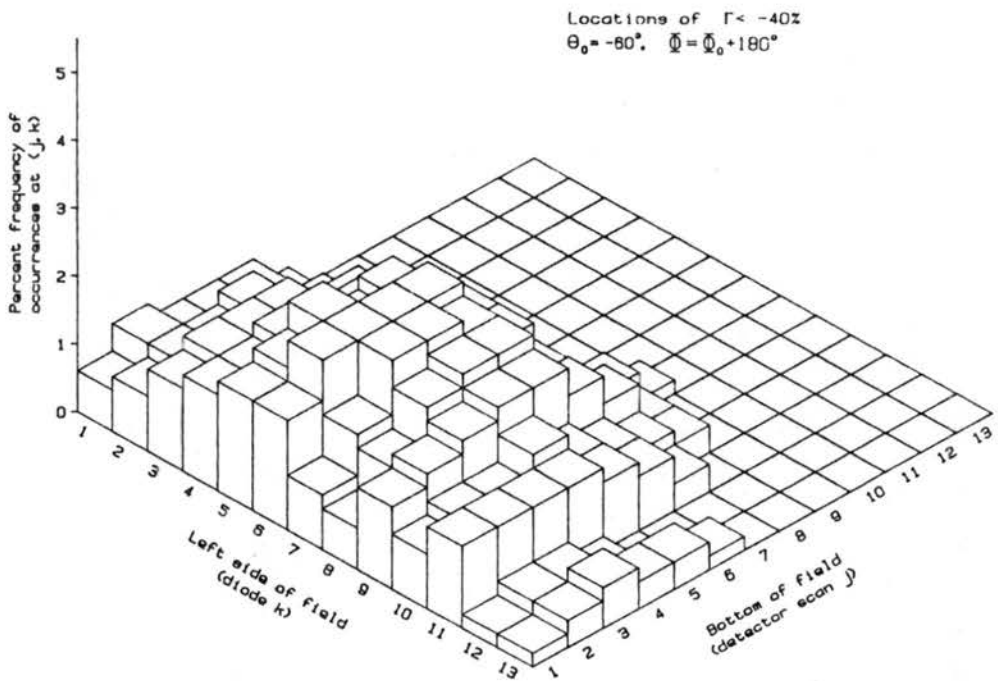


Figure 5.17: Similar to 5.14, except showing locations of anisotropic reflectance factors of $\Gamma < -40\%$, at $\Theta_0 = -60^\circ$, $\Phi = \Phi_0 + 180^\circ$.

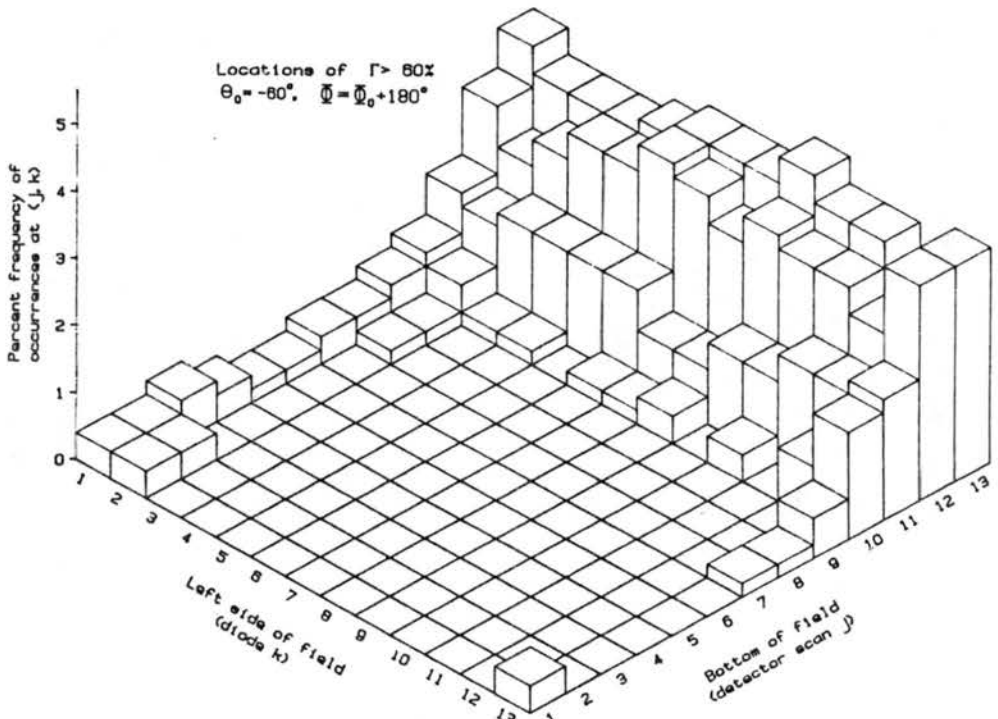


Figure 5.18: Similar to 5.14, except showing locations of anisotropic reflectance factors of $\Gamma > 60\%$, at $\Theta_0 = -60^\circ$, $\Phi = \Phi_0 + 180^\circ$.

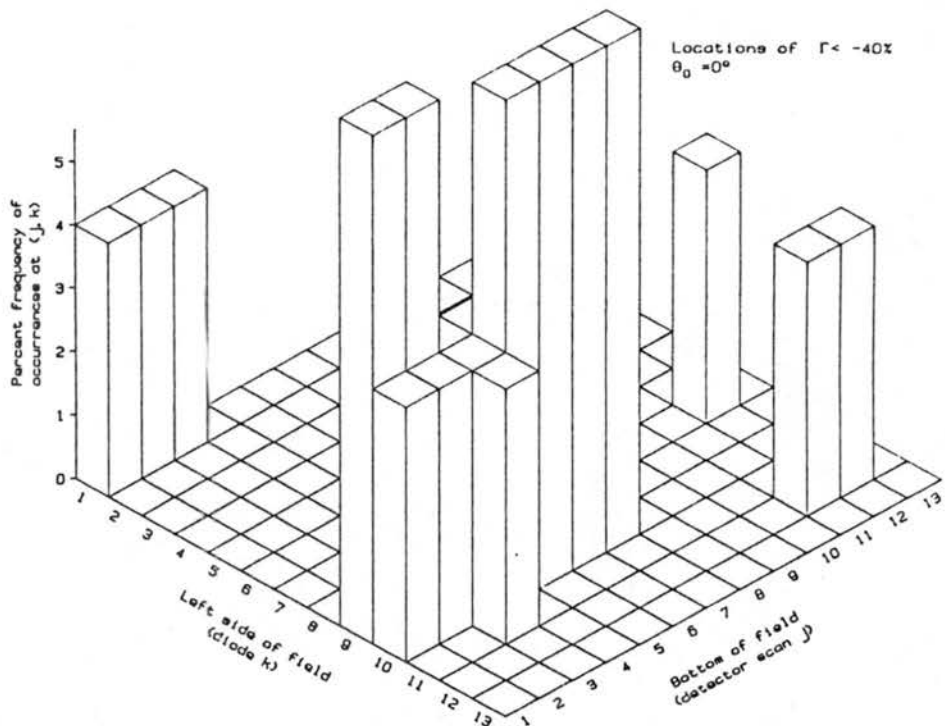


Figure 5.19: Similar to 5.14, except showing locations of anisotropic reflectance factors of $\Gamma < -40\%$, at $\Theta_0 = 0^\circ$.

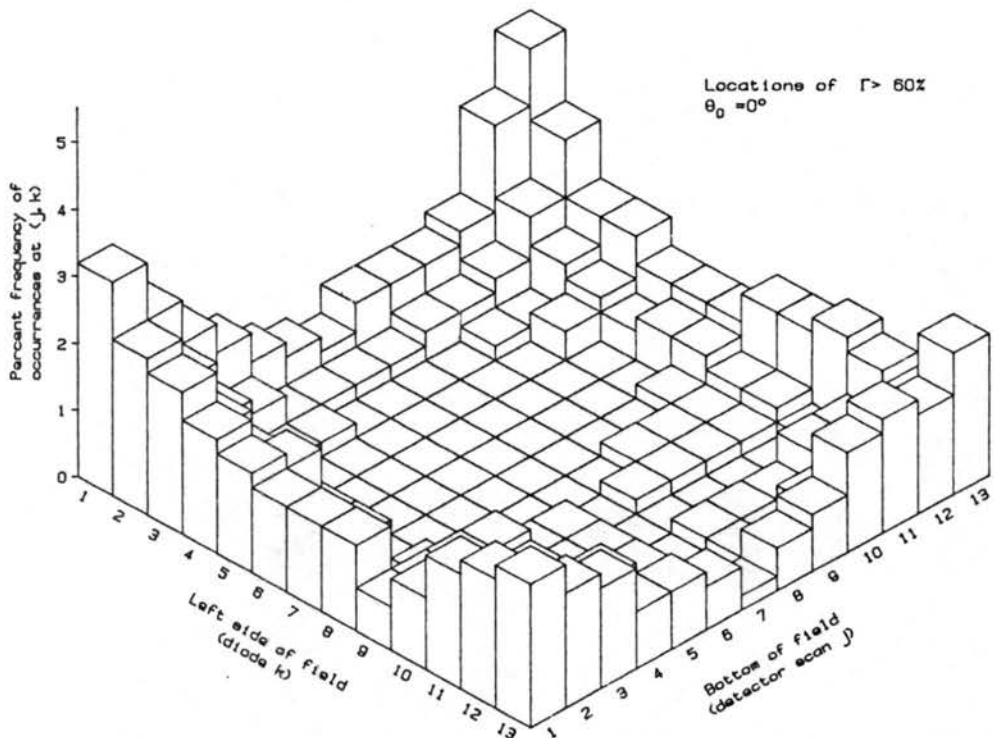


Figure 5.20: Similar to 5.14, except showing locations of anisotropic reflectance factors of $\Gamma > 60\%$, at $\Theta_0 = 0^\circ$.

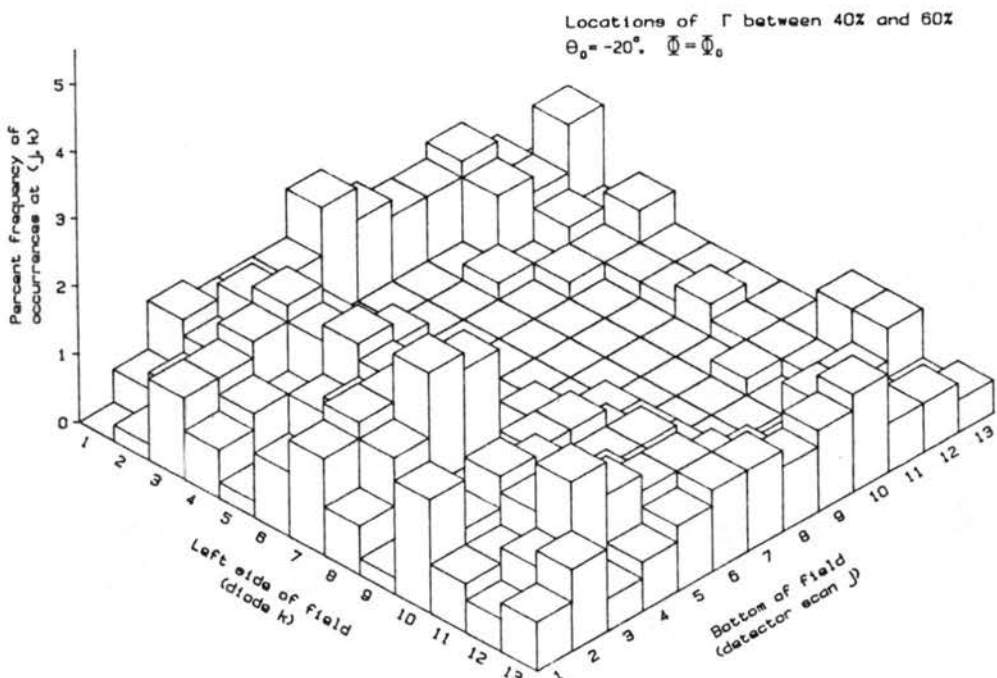


Figure 5.21: Similar to 5.14, except showing locations of anisotropic reflectance factors of $40\% \leq \Gamma < 60\%$, at $\Theta_0 = -20^\circ$, $\Phi = \Phi_0$.

cases. Forward scattering is obviously not present in the same context of the definition of forward scattering at $\Theta_0 = 0^\circ$ and backscattering should be azimuthally homogeneous for plane parallel cloud fields. Azimuthal differences at $\Theta_0 = 0^\circ$ are a function of the geometry of the cloud fields only. Since all 20 fields are included in these plots, no azimuthal differences are resolved. The greater frequencies present on the corners are at local zenith angles of $\theta = 76^\circ$, the largest local zenith angle on the grid. Overestimates of $\Gamma > 60\%$ were not found in the center of the field at all, while large underestimates ($\Gamma < -40\%$), although not as discernible as the overestimates, seem to be concentrated in the center of the field. Figure 5.21 shows smaller overestimates ($40\% \leq \Gamma < 60\%$) for $\Theta_0 = -20^\circ, \Phi = \Phi_0$. Backscattering is again recognized as an important factor in these overestimates, but are not as clear as with larger source zenith angles. Note that backscattering is shown on the left side of the grids when the source zenith angle is referenced as $\Theta_0, \Phi = \Phi_0$ and on the right side of the grid in the previous cases when the source zenith is referenced as $\Theta_0, \Phi = \Phi_0 + 180^\circ$. Figures 5.22 and 5.23 (large underestimates and large overestimates for $\Theta_0 = -60^\circ, \Phi = \Phi_0$) show the same characteristics as similar Γ values for $\Theta_0 = -60^\circ, \Phi = \Phi_0 + 180^\circ$, but they are on opposite sides of the grid. When studying

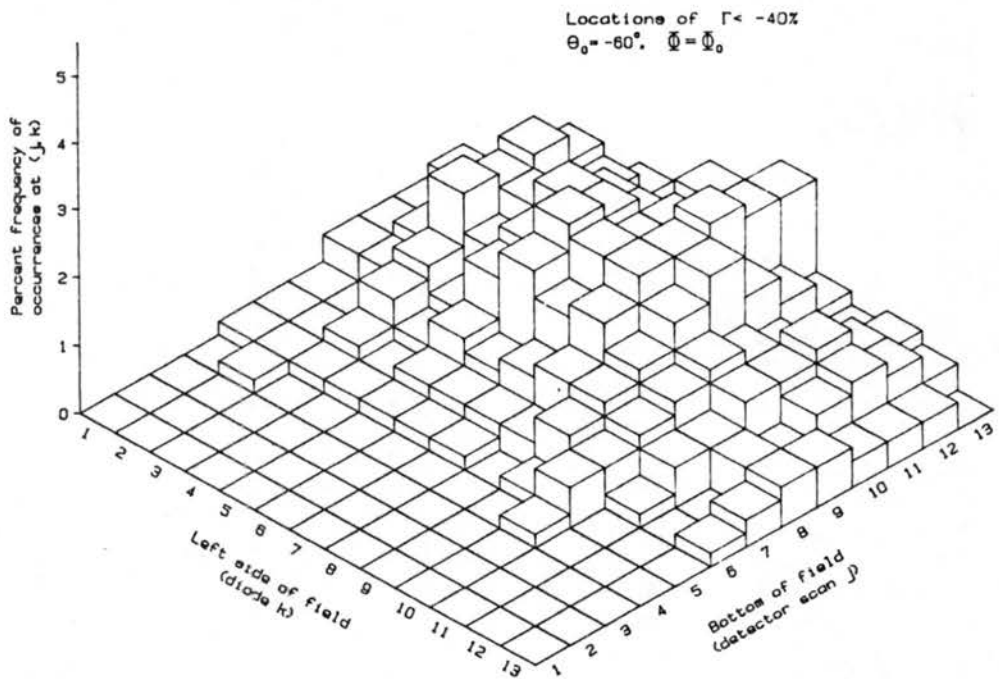


Figure 5.22: Similar to 5.14, except showing locations of anisotropic reflectance factors of $\Gamma < -40\%$, at $\Theta_0 = -60^\circ$, $\Phi = \Phi_0$.

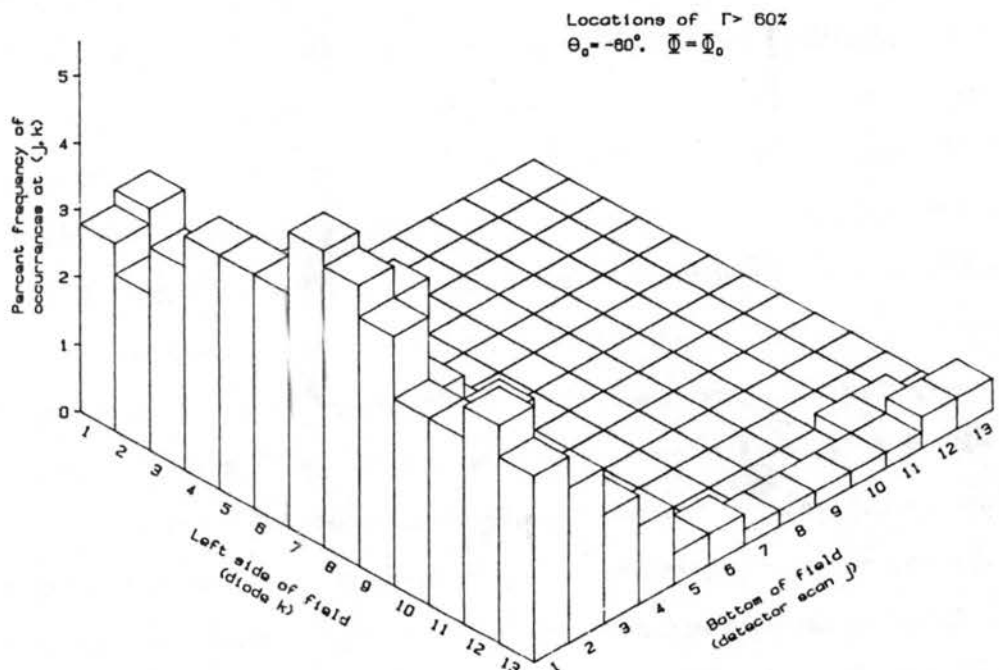


Figure 5.23: Similar to 5.14, except showing locations of anisotropic reflectance factors of $\Gamma > 60\%$, at $\Theta_0 = -60^\circ$, $\Phi = \Phi_0$.

the entire data set, the symmetry of these plots tend to cancel each other out. All plots which depict $\Gamma > 60\%$ (not all shown) show these overestimates occur exclusively at large local zenith angles ($\theta > 60^\circ$).

Some conclusions may be drawn concerning maximum anisotropic reflectance patterns. Smaller values of backscattered irradiances are a primary factor in the underestimation of irradiance calculations. In this data set, these effects are important for all source zenith angles with the exception of $\Theta_0 = 0^\circ$. Underestimates seem to occur more often when the azimuth of the photodiode is 180° from the direction of the incoming radiation. Conversely, overestimates of the measured irradiances are found almost exclusively when photodiodes are measuring backscattered radiation at large local zenith angles. Two factors are responsible for this behavior; first, within a plane-parallel incident beam of radiation, and a nearly non-absorbing, non-transmitting cloud, much of the incident radiation will be reflected by the hemispheric tops of the cloud at an angle of reflection which depends upon the point at which the incident radiation touches the cloud. Referring to figure 5.24, assuming a specular reflector and utilizing simple spherical geometry, a beam of radiation infinitesimally thick reaching the cloud one inch (horizontally) from the top of the cloud will be reflected at an angle which is 60° from the incident path. This reflected radiation would be measured by a detector which is at a local zenith angle of 60° if $\Theta_0 = 0^\circ$. The surface area of the hemisphere and a hemispherical segment are given as: $S_h = 2\pi R^2$ and $S_s = 2\pi Rh$ respectively, where R is the radius of the hemisphere (2 inches) and h is the height of the segment. h is simply $\sqrt{3}$, as shown in the figure. Solving for the surface areas of both the hemisphere and the segment below the 60° reflection point, it is readily apparent that almost $\frac{7}{8}$ of the photons reaching the cloud tops are reflected at angles of 60° or greater. Thus, radiances will be greater at larger zenith angles. The second factor is evident for measurements when $\Theta_0 \neq 0^\circ$. The cylindrical sides of the clouds will reflect radiation in a manner similar to the above discussion. However, the radiation scattered in the forward direction is likely to be intercepted by another cloud in its path which will reflect the photon in the direction of incoming radiation, rather than in the forward scattering direction. Therefore, larger radiances may be expected when

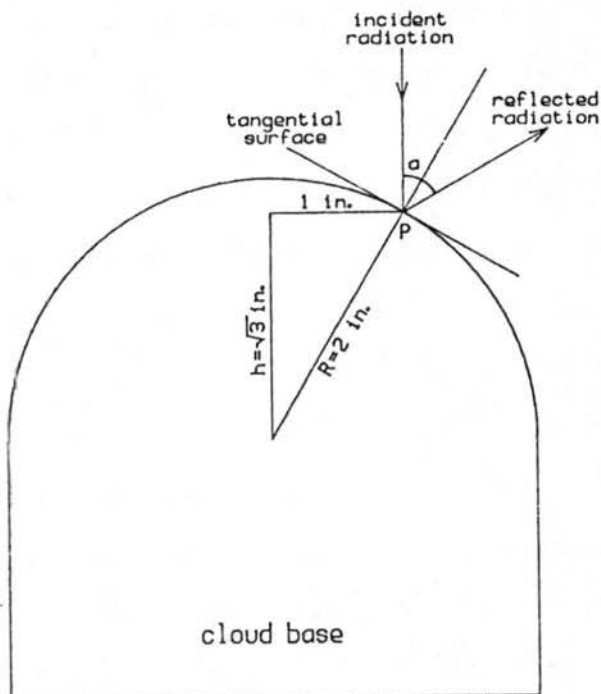


Figure 5.24: The reflection of an infinitesimally thick beam of radiation from a point located one inch from the top of the cloud. The angle of reflection, a , is simply twice the angle the incident beam of radiation makes with the normal to the tangential surface of the cloud at point P . h is the height of the hemispherical segment, and R is the radius of the hemisphere.

the detector is measuring backscattered radiation, and smaller values when the detector measures forward scattering. The simulated clouds in this study have neither perfect specular reflection nor perfect hemispherical tops, but exhibit both of these assumptions sufficiently for qualitative proof.

Overestimates exhibit a somewhat clearer pattern than do underestimates. While overestimates are found primarily at large local zenith angles and rarely found at local zenith angles less than 60° , underestimates are found at all zenith angles in which photodiodes measure forward scattered radiation. Overestimates are found in a large range of azimuth angles (approximately $\pm 70^\circ$ from the principal plane of incoming radiation) almost equally for all source zenith angles. This is not apparent in figure 5.20 ($\Theta_0 = 0^\circ$, but azimuthal uniformity is implied by considering the local zenith angles which correspond to the grid squares located on the perimeter of the grid. Local zenith angles are smaller in the centers of the four sides (see figure 5.12), so radiances shown will be less than radiances in the corners of the grid.

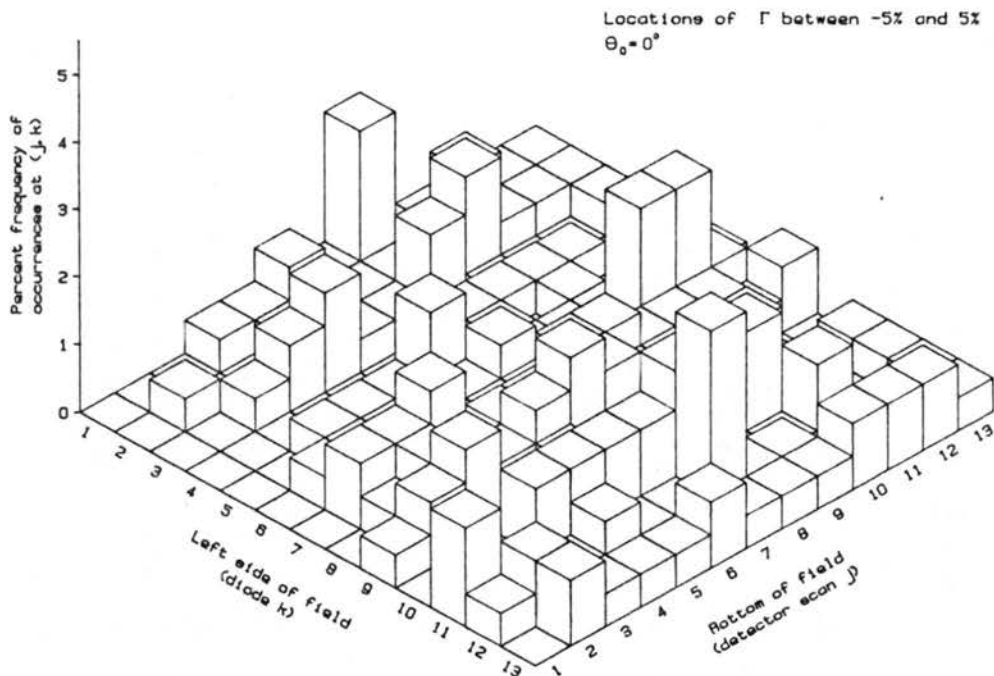


Figure 5.25: Similar to 5.14, except showing locations of anisotropic reflectance factors of $-5\% \leq \Gamma \leq 5\%$, at $\Theta_0 = 0^\circ$.

5.3.2 Determination of minimum anisotropy

The previous section utilized large overestimates and underestimates of the measured irradiances to determine locations of maximum and minimum anisotropy. To determine possible areas of minimum anisotropy, plots which show locations of small values of Γ are used. Figures 5.25 – 5.29 show locations of anisotropic reflectance factors between -5% and 5% and between -10% and 10% . These values correspond to radiances collected by photodiodes which, when integrated, produce irradiances very close to irradiances calculated by using equation (3.9). These figures do not show patterns as obvious as cases showing maximum anisotropy. Patterns become more uniform as Θ_0 approaches 0° . At $\Theta_0 = 0^\circ$ (figure 5.25) small anisotropic reflectance factors are distributed almost evenly about the field. As Θ_0 increases (figures 5.26, 5.27, and 5.28) minimum values of Γ are found with a slightly greater frequency at smaller zenith angles. However, referring to figure 5.28, at local zenith angles near 0° , no minimum values of Γ are found. This can be seen in greater clarity in figure 5.29, which represents small values of Γ at $\Theta_0 = -60^\circ, \Phi = \Phi_0 + 180^\circ$. Once again, similar but opposite characteristics are shown for

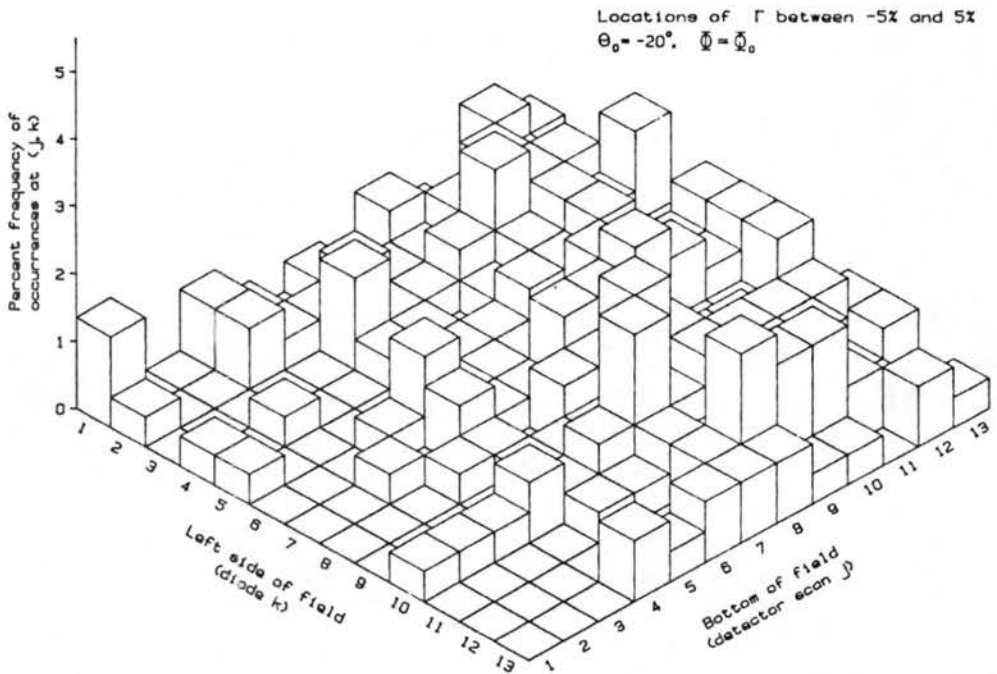


Figure 5.26: Similar to 5.14, except showing locations of anisotropic reflectance factors of $-5\% \leq \Gamma \leq 5\%$, at $\Theta_0 = -20^\circ$, $\Phi = \Phi_0$.

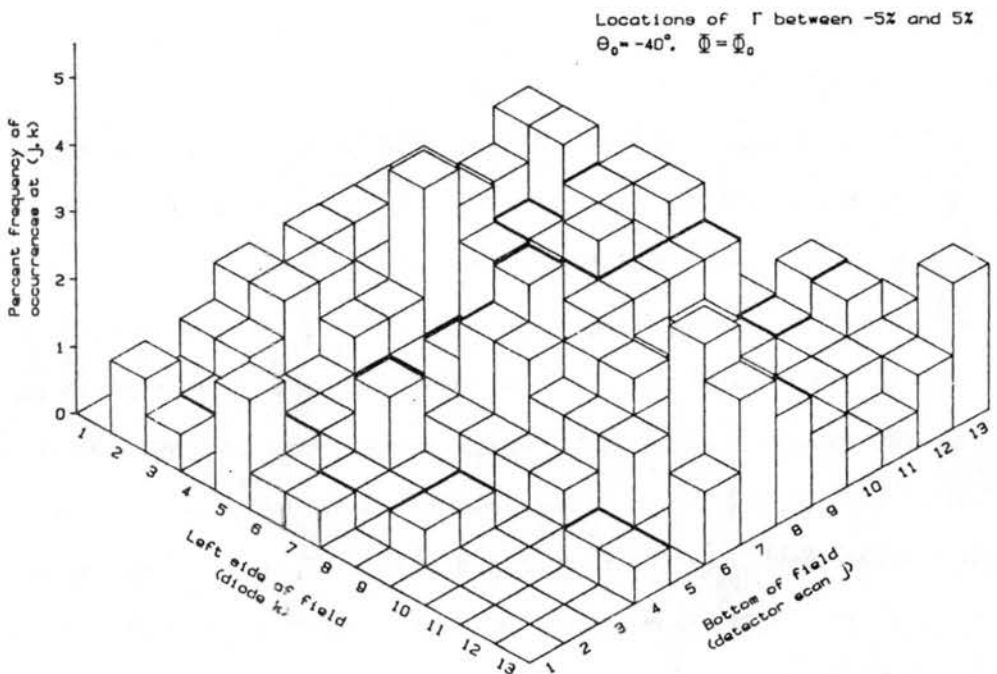


Figure 5.27: Similar to 5.14, except showing locations of anisotropic reflectance factors of $-5\% \leq \Gamma \leq 5\%$, at $\Theta_0 = -40^\circ$, $\Phi = \Phi_0$.

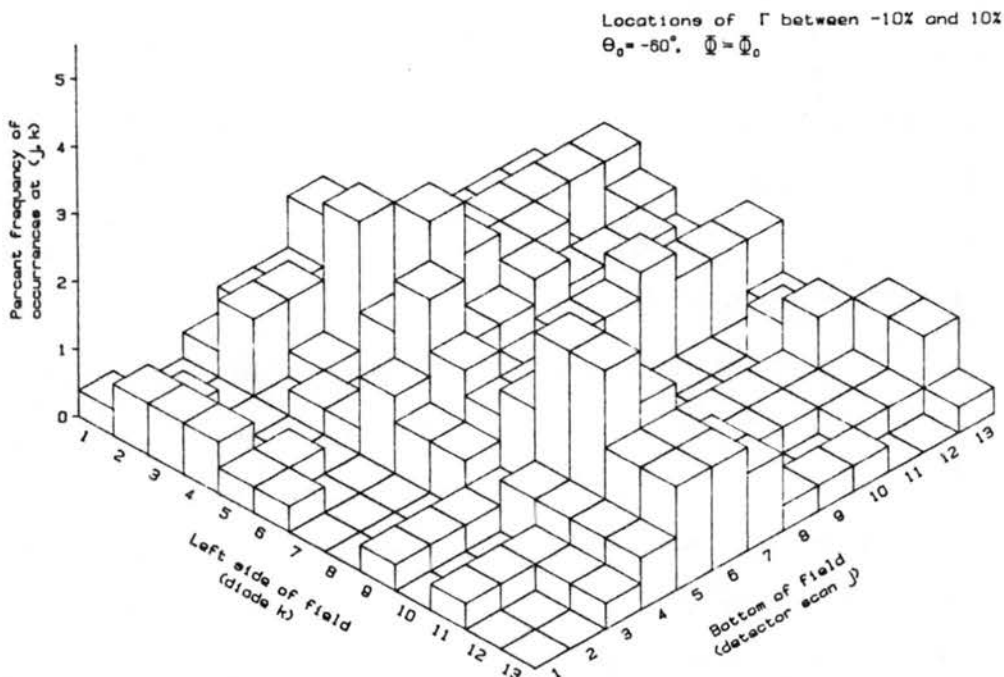


Figure 5.28: Similar to 5.14, except showing locations of anisotropic reflectance factors of $-10\% \leq \Gamma \leq 10\%$, at $\Theta_0 = -60^\circ$, $\Phi = \Phi_0$.

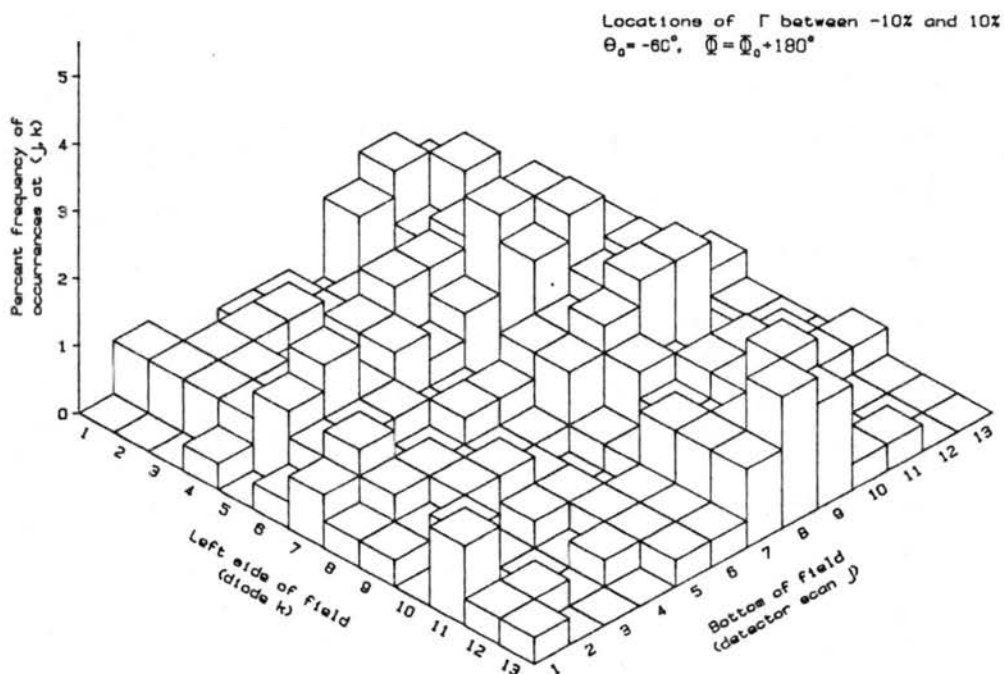


Figure 5.29: Similar to 5.14, except showing locations of anisotropic reflectance factors of $-10\% \leq \Gamma \leq 10\%$, at $\Theta_0 = -60^\circ$, $\Phi = \Phi_0 + 180^\circ$.

these symmetric source zenith angles. Azimuthally, minimum values for Γ are shown on the backscattering side of the incoming radiation at small local zenith angles (maximum frequencies occur at $\theta \approx 20^\circ\text{--}30^\circ$) and in the forward scattering direction at large local zenith angles ($\theta \approx 50^\circ\text{--}65^\circ$). The actual percentage of frequencies is small (rarely over 5% in one location) but groups of locations exhibiting frequencies larger than locations around them give confidence to the analysis of these plots.

According to the results of this study, if one were to attempt to determine an irradiance arising from only one radiance measurement, the worst detector location would obviously be at large local zenith angles in either the backscattering direction or the forward scattering direction. Although anisotropy is greater at larger source zenith angles, the greatest confidence would be achieved at larger source zenith angles, where the pattern of minimum anisotropy is more defined than at small source zenith angles. The best detector location would be in a backscattering direction at local zenith angles approximately between 20° and 30° .

5.4 Determination of ideal cloud field sample size

Cloud fields consisting of 30% fractional cloud cover with randomly distributed clouds within each field may be considered an infinite population, since the geometric possibilities within each field are infinite. A statistical analysis was performed to determine the validity of a limited sample of only 20 randomly oriented cloud fields. Confidence levels were found by calculating the means and standard deviations of the 20 irradiances for each source zenith angle studied (see table 5.1). These results (presented in tables 5.4 – 5.7) demonstrated confidence levels of 91% to 96%, depending upon the source zenith angle considered, that population mean values would be within $\pm 10\%$ of the sample means found in this study. The first table shows these confidence levels, while the latter three tables represent the ideal number of cloud fields which are necessary to achieve the confidence levels shown. One can immediately see a large increase in the sample size is needed when attempting to obtain sample means which would be within $\pm 5\%$ of the population means at every confidence level considered. It was also determined that a 90% confidence level

Table 5.4: Confidence levels using 20 cloud field samples.

		Irradiances		Radiances			
Range of mean:		±10%	±5%	±10%	±5%	±10%	±5%
Θ_0	Φ			backscattered		forward scattered	
-60°	Φ_0	96	70	87	57	85	54
-40°	Φ_0	94	66	87	57	84	53
-20°	Φ_0	91	62	82	51	84	53
0°		91	61				
-20°	$\Phi_0 + 180^\circ$	91	62	90	60	75	44
-40°	$\Phi_0 + 180^\circ$	92	63	91	62	77	46
-60°	$\Phi_0 + 180^\circ$	94	66	92	63	84	53

Table 5.5: Optimized sample sizes for irradiances. All ranges of means are plus/minus.

level:		99%		98%		95%		90%		80%	
range of mean:		10%	5%	10%	5%	10%	5%	10%	5%	10%	5%
Θ_0	Φ										
-60°	Φ_0	34	133	27	105	19	72	13	49	9	30
-40°	Φ_0	41	159	33	126	23	86	16	59	10	35
-20°	Φ_0	48	187	38	147	26	101	18	69	11	41
0°		50	197	40	155	28	106	19	73	12	44
-20°	$\Phi_0 + 180^\circ$	50	195	40	154	27	105	19	72	12	43
-40°	$\Phi_0 + 180^\circ$	47	185	38	146	26	100	18	68	11	41
-60°	$\Phi_0 + 180^\circ$	41	160	33	127	23	87	16	60	10	36

Table 5.6: Optimized sample sizes for backscattered radiances. All ranges of means are plus/minus.

level:		99%		98%		95%		90%		80%	
range of mean:		10%	5%	10%	5%	10%	5%	10%	5%	10%	5%
Θ_0	Φ										
-60°	Φ_0	61	240	49	190	33	129	23	89	14	53
-40°	Φ_0	62	242	49	191	34	130	23	89	14	53
-20°	Φ_0	81	320	64	252	44	172	31	118	19	70
0°											
-20°	$\Phi_0 + 180^\circ$	54	211	43	167	30	114	21	78	13	47
-40°	$\Phi_0 + 180^\circ$	49	192	39	151	27	103	19	71	12	42
-60°	$\Phi_0 + 180^\circ$	46	180	37	142	25	97	18	67	11	40

Table 5.7: Optimized sample sizes for forward scattered radiances. All ranges of means are plus/minus.

level:		99%		98%		95%		90%		80%	
range of mean:		10%	5%	10%	5%	10%	5%	10%	5%	10%	5%
Θ_0	Φ										
-60°	Φ_0	69	271	55	214	38	146	26	100	16	60
-40°	Φ_0	73	288	58	227	40	155	28	106	17	63
-20°	Φ_0	72	283	57	223	39	152	27	104	17	62
0°											
-20°	$\Phi_0 + 180^\circ$	109	433	86	341	59	232	41	159	25	94
-40°	$\Phi_0 + 180^\circ$	101	398	80	314	55	214	38	146	23	87
-60°	$\Phi_0 + 180^\circ$	72	283	57	223	39	152	27	104	17	62

of sample mean values within $\pm 5\%$ of the population means could be obtained by using 49 – 73 randomly oriented cloud fields, again depending upon the source zenith angle. As shown in table 5.4, the use of twenty fields results in confidence levels of only 61% – 70% that these sample means are within $\pm 5\%$ of mean irradiances of the entire population. Comparisons among source zenith angles show these confidence levels tend to decrease to as Θ_0 decreases.

Confidence levels were also determined for backscattering and forward scattering radiances. Two blocks of radiances, from both the backscattering and forward scattering directions, were analyzed. These blocks consisted of photodiode locations of $j = 2 - 5, k = 5 - 9$ and $j = 9 - 12, k = 5 - 9$ for each scene (see figures 5.12 and 5.13 for the respective zenith and azimuth angle ranges considered). The twenty radiances located within each of these solid angles were averaged to provide a representative radiance in each scene. Results of these calculations are also shown in tables 5.4, 5.6, and 5.7. These show that in general, a lower confidence level is found for radiances than for irradiances. Confidence levels for forward scattered radiances are markedly less than for backscattered radiation. This of course implies that an increase of the sample size, or number of fields, is needed to achieve results which are associated with greater confidence levels. As with the irradiances, confidence levels decrease as Θ_0 decreases.

The importance of these observations are obvious. The use of a large number of cloud fields which differ only by virtue of the geometry of individual cloud elements within the

field is necessary if one is to accurately parameterize these fields in a climate model. This poses problems for the satellite meteorologist who is unable to obtain such measurements. The use of a greater number of fields than were used in this study could widen or narrow the irradiance and radiance distributions, leading to irradiance differences among cloud fields which may be greater than or less than the values shown in this text. The distributions of anisotropic reflectance factors may also change. These statistical results indicate that further study of this problem is warranted.

Chapter 6

CONCLUSIONS

Reflected radiances from twenty simulated broken cumulus cloud fields, each with a fractional cloud cover of 30%, were examined. The variation of patterns of individual cloud elements within these fields resulted in large differences in reflected irradiances. Three important conclusions may be drawn from this part of the study:

1. As the source zenith angle increases, reflected irradiance increases, probably due to the increase of effective cloud cover as a result of increasing source zenith angles;
2. Geometric differences in cloud fields account for greater irradiance variations at smaller source zenith angles. This study found differences as great as 107% at small zenith angles.
3. Approximately sixty randomly structured cloud fields would be required to accurately predict irradiance variations in which the experimenter could be 90% confident that the irradiance of the sample mean would be within $\pm 5\%$ of the mean irradiance of an infinite population of cloud fields which consist of 30% fractional cloud cover.

Anisotropy in the reflected radiation field was studied to determine minimum and maximum anisotropy. Radiances were numerically integrated using 169 radiances per scene measurement, each measured at a different local zenith and azimuth angle. Collectively, the locations of these measurements (detector locations) describe a hemispherical solid angle which encompasses the entire cloud field. Each of radiances were also integrated assuming isotropy. The anisotropic reflectance factor (Γ) was introduced (equation (3.12)) to examine differences between isotropic and numerically integrated, or measured

irradiances. An isotropic irradiance which is exactly equal to the measured irradiance would produce an anisotropic reflectance factor equal to zero. Underestimates of the measured irradiance (F_m) occur when $\Gamma < 0$, which corresponds to an isotropic irradiance which is less than the measured irradiance for the field in consideration. Overestimates occur when $\Gamma > 0$. Maximum anisotropy is defined as magnitudes of Γ which are greater than 40%. Minimum anisotropy is defined as isotropic irradiances which approximate the measured irradiance well. For an isotropic irradiance to exhibit minimum anisotropy, Γ values must be near zero.

Frequency distributions of the anisotropic reflectance factors demonstrate an inverse relationship between Θ_0 and modal value ranges of Γ (the Γ range where the modal value lies). As Θ_0 increases, modal ranges for Γ decrease, showing overestimates of F_m by 15% - 20% at $\Theta_0 = 0^\circ$, and underestimates of F_m by 30% - 35% at $\Theta_0 = -60^\circ$, $\Phi = \Phi_0$ and $\Theta_0 = -60^\circ$, $\Phi = \Phi_0 + 180^\circ$. Cumulative distribution functions show a widening of the distribution as Θ_0 increases. These results indicate increasing anisotropy as Θ_0 increases.

Detector locations of maximum and minimum anisotropy were examined. Large overestimates of F_m (corresponding to high positive values of Γ) were consistently found at large local zenith angles, regardless of the source zenith angle. Overestimates of F_m were almost always found when the photodiode detectors were measuring backscattered radiation (when $\Theta \neq 0^\circ$). Underestimates (corresponding to low negative values of Γ) were found while the detector measured forward scattered radiation and were most prevalent at larger source zenith angles. The factors responsible for this behavior are related to the geometry of the individual clouds, and are explained in further detail in chapter five.

Minimum anisotropy was found at detector locations located throughout the solid angle with no clear concentration at small source zenith angles. At large source zenith angles, specific local zenith and azimuth angles were evident where $\Gamma \approx 0\%$. Minimum anisotropy was somewhat more evident at $\theta \approx 20^\circ - 40^\circ$ when the detector measured backscattered radiation.

Statistically, the greatest chance of obtaining accurate reflected irradiance estimates from a single radiance measurement would be to utilize smaller local zenith angles at

large source zenith angles. Here, there is a definite location of minimum anisotropy. Azimuthally, a smaller degree of anisotropy is found in the near-backscattering direction. Overestimates are isolated at larger local zenith angles, and underestimates are concentrated in the forward scattering direction at larger local zenith angles when Θ_0 was large.

Fourier series analysis was performed on selected cases within the data set. This analysis examined the azimuthal dependence of isolated intensity fields within the solid angle described by the detector arc rotation about the field. Results indicate the relative importance of the sine term in the Fourier series after one repetition of the series. After the first repetition, the sine terms are of the same order of magnitude as the cosine terms in most of the cases (see tables A.3 – A.6 in appendix A). Results also suggest that the number of terms needed to accurately describe reflected intensity at a certain local zenith angle is dependent upon the azimuthal resolution of the field. A greater number of azimuthal measurements result in increased accuracy when determining the reflected intensity of the field at a specific local zenith angle. Accurate intensities were calculated using a small number of Fourier terms with azimuthal resolution as low as 45° . Errors as low as 10% were found after only three repetitions of the series in all cases studied. Minimum errors were found when $m = \frac{P}{2}$, where m represents the term of the series and P is the number of azimuth angles used to calculate the intensity.

Suggestions for further study of the geometric dependence of clouds on irradiance calculations could include the use of a greater statistical database than the 20 fields used in this study. Statistical studies showed that confidence levels about the mean were approximately 93% for a mean value within $\pm 10\%$ of the sample mean. A population sample of approximately 60 cloud fields increase the confidence level to approximately 90% for mean values within $\pm 5\%$ of the mean. These statistical results also demonstrated the inadequacy of using an irradiance determined by using a single cloud field consisting of a specific fractional cloud cover. A greater number of cloud fields may also yield results which allow a better determination of locations of minimum anisotropy than do the results of this study. Different optically thick, simulated cloud fields could produce interesting results. The use of a different fractional cloud cover is suggested, to attempt to determine

the dependence of the results presented in this paper on fractional cloud cover. Different size clouds, and clouds with different shapes may also provide insight into the dependence of cloud geometry on accurate irradiance calculations. As shown in Chapter 5, a large amount of radiation detected at large local zenith angles was due to the shape of the simulated cloud tops used in this study. Fourier series analysis was considered only briefly in this study, but the potential for further study in this area was realized.

This study yields quantitative information on the degree of variation which may be expected due to the complex geometries of a cloud field. It is essential for computer models which predict future climates to have the ability to consider these factors in their results. Without the accurate parameterizations of reflection, of solar radiation by realistic cloud fields, the ability to justify predicted climate results are highly questionable.

REFERENCES

- Aida, M., 1977: Scattering of solar radiation as a function of cloud dimension and orientation. *J. Quant. Spectrosc. Radiat. Transfer.*, **17**, 303-310.
- Avaste, O.A., and G.M. Vaynikko, 1974: Solar radiation transfer in broken clouds. *Izv. Atmos. Oceanic Phys.*, **10**, 1054-1061.
- Bartman, F.L., 1968: Earth reflectance patterns measured by radiometer on high altitude balloon flights. Tech. Report 05863-13-T, University of Michigan, NASA contract No. NASr-54(03), 15 pp.
- Brennan, B., and W.R. Bandeen, 1970: Anisotropic reflectance characteristics of natural earth surfaces. *Appl. Opt.*, **9**, 405-412.
- Busyggin, V.P., N.A. Yeustratov and Ye.M. Feygel'son, 1973: Optical properties of cumulus and radiant fluxes for cumulus cloud cover. *Izv. Atmos. Oceanic Phys.*, **9**, 1142 - 1151.
- Davis, J.M., and S.K. Cox, 1982: Reflected solar radiances from regional scale scenes. *J. Appl. Meteor.*, **21**, 1698-1712.
- Davis, J.M., S.K. Cox and T.B. McKee, 1983: Design and verification of a cloud field optical simulator. *J. Appl. Meteor.*, **22**, 947-958.
- Davies, R., 1978: The effects of finite cloud geometry on the three dimensional transfer of solar irradiance in clouds. *J. Atmos. Sci.*, **35**, 1712-1725.
- Davies, R., 1984: Reflected solar radiances from broken cloud scenes and the interpretation of scanner measurements. *J. Geophys. Res.*, **89**, 1259-1266.
- Green, R.N., 1980: The effect of directional radiation models on the interpretation of earth radiation budget measurements. *J. Atmos. Sci.*, **37**, 2298-2313.
- King, M.D., 1983: Number of terms required in the fourier expansion of the reflection function for optically thick atmospheres. *J. Quant. Spectrosc. Radiat. Transfer*, **30**, 143-161.
- Kreyszig, D., 1983: Advanced Engineering Mathematics. New York, John Wiley and Sons, 988 pp.

- Kuenning, J.A., T.B. McKee and S.K. Cox, 1978: A laboratory investigation of radiative transfer in cloud fields. *Atmos. Sci. Pap.* No. 286, Colorado State University, 55 pp.
- Liou, K.-N., 1980: An Introduction to Atmospheric Radiation. New York, Academic Press, 392 pp.
- Margolis, J.S., D.J. McCleese, and G.E. Hunt, 1972: Laboratory simulation of diffuse reflectivity from a cloudy atmosphere. *Appl. Opt.*, **11**, 1212-1216.
- McKee, T.B., and S.K. Cox, 1974: Scattering of visible radiation by finite clouds. *J. Atmos. Sci.*, **31**, 1885-1892.
- McKee, T.B., M. DeMaria, J.A. Kuenning and S.K. Cox, 1983: Comparison of Monte Carlo calculations with observations of light scattering in finite clouds. *J. Atmos. Sci.*, **40**, 1016-1023.
- McKee T.B., and J.T. Klehr, 1978: Effects of cloud shape on scattered solar radiation. *Mon. Wea. Rev.*, **106**, 399-404.
- Neter, J., W. Wasserman and G.A. Whitmore, 1982: Applied Statistics. 2nd ed. Boston, Allyn and Bacon, Inc. 773 pp.
- Ohring, G., and P. Clapp, 1979: The effect of changes in cloud amount on the net radiation at the top of the atmosphere. *J. Atmos. Sci.*, **37**, 447-454.
- Plank, V.G., 1969: The size distribution of cumulus clouds in representative Florida Populations. *J. Appl. Meteor.*, **8**, 46-67.
- Ruff, I., R. Koffler, S. Fritz, J.S. Winston and P.K. Rao, 1968: Angular distribution of solar radiation reflected from clouds as determined from TIROS IV radiometer measurements. *J. Atmos. Sci.*, **25**, 323-332.
- Spiegel, M.R., 1961: Theory and Problems of Statistics. New York, Schaum Publishing Co. 359 pp.
- Stephens, G.L., 1987: Radiative transfer through randomly fluctuating optical media: I General solution. Submitted to *J. Atmos. Sci.*.
- Stowe, L.L., H. Jacobowitz and V.R. Taylor, 1980: Reflectance characteristics of earth and cloud surfaces as measured by the ERB scanning channels on the Nimbus 7 satellite. *Proc. Int. Radiation Symp.*, Ft. Collins, Amer. Meteor. Soc., 124-127.
- Welch, R.M., S.K. Cox and J.M. Davis, 1980: *Solar Radiation and Clouds*. *Meteor. Monog.*, No. 39, Amer. Meteor. Soc., 96pp.
- Welch, R.M. and B.A. Wielicki, 1984: Stratocumulus cloud field reflected fluxes: the effect of cloud shape. *J. Atmos. Sci.*, **41**, 3085-3103.

Appendix A

FOURIER SERIES ANALYSIS

A.1 Introduction

Fourier series analysis has been a helpful tool in the study of theoretical radiative transfer. Stephens (1987) presented a method which utilizes Fourier analysis in azimuth to study radiative transfer through anisotropically scattering media. King (1983) applied Fourier analysis to two different radiative transfer models in the attempt to determine the number of Fourier series terms required to accurately describe reflection functions for optically thick atmospheres. The results of this study demonstrated a strong dependence on the incident and local zenith angle, as well as on details of the phase function.

The Fourier analysis used in this study is based on parts of the same data set analyzed in chapter five. The analysis in this study is somewhat different than previous studies in that a laboratory model is utilized to produce the data subject to the Fourier analysis. Although the analysis can be used to determine irradiances of the cloud fields used here, the emphasis is placed on specific radiances and their relationships with radiances which lie along the same azimuth circle, at a specific zenith angle θ . Of the 540 files created during the experimental procedure, only certain parts of 14 files were analyzed in this manner. From each of the 14 files, one local zenith angle was selected from which a number of azimuthal diode collections were present. Referring to figure 3.3, one complete circle around the grid represents one local zenith angle ring. All measurements which were inside this ring were analyzed. The specific local zenith angle ring differed with each scan set analyzed. With the exception of one scan set, only one zenith angle was selected. The scan set of exception included three different local zenith angle rings. The basis for the choice of eight of these scan sets (including the scan set with three local zenith angle

rings) was the relative contribution to the total irradiance of the field. Each of these rings were comprised of a number of radiances which, when averaged about the circle and integrated with respect to zenith angle, produced a number which was within .1% of the measured irradiance of the entire field. The reason for this selection is arbitrary, since irradiances are not the focus of this portion of the study. The remaining scan sets were selected because they produced large differences between the averaged/isotropic irradiance and the measured irradiance of the entire field. These were selected to possibly provide some insight to possible differences between the two different types of cases. Upon further investigation, it was noted that differences do not exist, except when considering the total irradiances of the fields. As stated before, this analysis is concerned with intensities at a limited number of specific zenith angles within each scan set. Therefore, no conclusions will be made concerning the total irradiances. The only advantage of using a zenith angle which accurately represents the total irradiance is the inferences which can be made if one is use Fourier analysis to study a cloud field while considering the complete solid angle which describes the field.

A.2 Fourier theory

Any continuous function which is periodic (with period p) can be expressed in terms of a Fourier series. In this case, the function is reflected intensity at a specific local zenith angle θ . Continuity is implied when considering the overlapping fields of view of adjacent photodiodes. The period is simply one azimuthal revolution about the center of the field which is 2π radians, or 360° . The periodicity of this method is obvious. The radiance collected at azimuth n for example, is the same radiance at $n + 2\pi$. It will be shown that the intensities along these 2π radians are important factors within the series analysis. The Fourier series takes the form of

$$f(x) = \sum_{m=0}^{\infty} (a_m \cos mx + b_m \sin mx) \quad (A.1)$$

where all variables are generalized, to be replaced with the proper variables later. $f(x)$ represents $I_{f,\theta_i}(\phi)$ which is the reflected intensity (or contribution to the total irradiance

F) at zenith angle θ_i . The variable m represents the term of the series being considered. The $m = 0$ case is of special interest and will be discussed in detail below. The x variables will be replaced by ϕ , since this series is analyzed azimuthally. For now, noting that for $m = 0$, the sine term in equation (A.1) equals zero and (A.1) can be rewritten as

$$f(x) = a_0 + \sum_{m=1}^{\infty} (a_m \cos mx + b_m \sin mx). \quad (\text{A.2})$$

The coefficients a_0 , a_m , and b_m represent amplitude functions which are functions of radiances along the local zenith ring. These functions are found using the following derivations, adapted from Kreyszig (1983). First, determination of a_0 involves integrating both sides of (A.2) from zero to 2π (the period of the function) which gives

$$\int_0^{2\pi} f(x) dx = \int_0^{2\pi} \left[a_0 + \sum_{m=1}^{\infty} (a_m \cos mx + b_m \sin mx) \right] dx. \quad (\text{A.3})$$

This can be shown to be equivalent to

$$\int_0^{2\pi} f(x) dx = a_0 \int_0^{2\pi} dx + \sum_{m=1}^{\infty} \left(a_m \int_0^{2\pi} \cos mx dx + b_m \int_0^{2\pi} \sin mx dx \right). \quad (\text{A.4})$$

Integrating the right side of (A.4), it can be readily seen that the first term equals $2\pi a_0$, while the rest of the right side equals zero. a_0 is therefore:

$$a_0 = \frac{1}{2\pi} \int_0^{2\pi} f(x) dx. \quad (\text{A.5})$$

To determine a_m , equation (A.2) is first multiplied by $\cos nx$ where n is any fixed positive integer, and then integrated over the period of the function:

$$\int_0^{2\pi} f(x) \cos nx dx = \int_0^{2\pi} \left[a_0 + \sum_{m=1}^{\infty} (a_m \cos mx + b_m \sin mx) \right] \cos nx dx. \quad (\text{A.6})$$

Integrating term by term, the right side of (A.6) becomes

$$a_0 \int_0^{2\pi} \cos nx dx + \sum_{m=1}^{\infty} \left[a_m \int_0^{2\pi} \cos mx \cos nx dx + b_m \int_0^{2\pi} \sin mx \cos nx dx \right]. \quad (\text{A.7})$$

The first integral is zero. By using the trigonometric identities

$$\cos x \cos y = \frac{1}{2} [\cos(x+y) + \cos(x-y)] \quad (\text{A.8})$$

and

$$\sin x \cos y = \frac{1}{2} [\sin(x+y) + \sin(x-y)] \quad (\text{A.9})$$

for the second and third terms of (A.7) respectively, we obtain

$$a_m \int_0^{2\pi} \cos mx \cos nx dx = a_m \left[\frac{1}{2} \int_0^{2\pi} \cos(m+n)x dx + \frac{1}{2} \int_0^{2\pi} \cos(m-n)x dx \right] \quad (\text{A.10})$$

and

$$b_m \int_0^{2\pi} \sin mx \cos nx dx = b_m \left[\frac{1}{2} \int_0^{2\pi} \sin(m+n)x dx + \frac{1}{2} \int_0^{2\pi} \sin(m-n)x dx \right]. \quad (\text{A.11})$$

Integration of the four terms on the right of equations (A.10) and (A.11) yields zero, except for the second term on the right of (A.10) which equals π when $m = n$. Solving for a_m gives

$$a_m = \frac{1}{\pi} \int_0^{2\pi} f(x) \cos mx dx \text{ for } m = 1, 2, 3, \dots \quad (\text{A.12})$$

Determination of b_m involves multiplying (A.2) by $\sin nx$ where n is again any fixed positive integer, and integrated from 0 to 2π :

$$\int_0^{2\pi} f(x) \sin nx dx = \int_0^{2\pi} \left[a_0 + \sum_{m=1}^{\infty} (a_m \cos mx + b_m \sin mx) \right] \sin nx dx. \quad (\text{A.13})$$

After term by term integration, the right side of (A.13) becomes

$$a_0 \int_0^{2\pi} \sin nx dx + \sum_{m=1}^{\infty} \left[a_m \int_0^{2\pi} \cos mx \sin nx dx + b_m \int_0^{2\pi} \sin mx \sin nx dx \right]. \quad (\text{A.14})$$

Integration of the first and second term of (A.14) yields zero (the second term equals zero for $m = 1, 2, 3, \dots$). Using the trig identity

$$\sin x \sin y = \frac{1}{2} [\cos(x-y) + \cos(x+y)] \quad (\text{A.15})$$

for the third term, we obtain

$$b_m \int_0^{2\pi} \sin mx \sin nx dx = b_m \left[\frac{1}{2} \int_0^{2\pi} \cos(m-n)x dx - \frac{1}{2} \int_0^{2\pi} \cos(m+n)x dx \right]. \quad (\text{A.16})$$

The last term of (A.16) equals zero, and the first term on the right side of (A.16) is zero when $m \neq n$ and π when $m = n$. b_m is therefore

$$b_m = \frac{1}{\pi} \int_0^{2\pi} f(x) \sin mx dx \text{ for } m = 1, 2, 3, \dots \quad (\text{A.17})$$

Equations (A.5), (A.12), and (A.17) are the amplitude functions of the Fourier series. Substituting the previously defined variables in for x , $f(x)$, a_0 , a_m , and b_m , (A.1) can be rewritten as

$$I_{f,\theta_i}(\phi) = I_{m=0,c,\theta_i} + \sum_{m=1}^{\infty} (I_{mc,\theta_i} \cos m\phi + I_{ms,\theta_i} \sin m\phi) \quad (\text{A.18})$$

where $I_{f,\theta_i}(\phi)$ has been defined as the reflected intensity of the local zenith angle ring θ_i , ϕ_i is the azimuth angle of the reflected radiation, referenced from the azimuth of the incident radiation, $I_{m=0,c,\theta_i}$ is the amplitude function for the $m = 0$ case, I_{mc,θ_i} is the amplitude function which corresponds to the cosine term of (A.2) or (A.17), and I_{ms,θ_i} is the amplitude function corresponding to the sine term of (A.2) or (A.17). Making the appropriate substitutions into equations (A.5), (A.12), and (A.17), the amplitude functions are

$$I_{m=0,c,\theta_i} = \frac{1}{2\pi} \int_0^{2\pi} I_{f,\theta_i}(\phi) d\phi, \quad (\text{A.19})$$

$$I_{mc,\theta_i} = \frac{1}{\pi} \int_0^{2\pi} I_{f,\theta_i}(\phi) \cos m\phi d\phi \text{ for } m = 1, 2, 3, \dots, \quad (\text{A.20})$$

and

$$I_{ms,\theta_i} = \frac{1}{\pi} \int_0^{2\pi} I_{f,\theta_i}(\phi) \sin m\phi d\phi \text{ for } m = 1, 2, 3, \dots \quad (\text{A.21})$$

Introducing the Kronecker delta function, δ_m , where

$$\delta_m = \begin{cases} 1, & \text{if } m = 0 \\ 0, & \text{otherwise} \end{cases}$$

(A.19) and (A.20) can be combined to yield

$$I_{mc,\theta_i} = \frac{1}{(1 + \delta_m)\pi} \int_0^{2\pi} I_{f,\theta_i}(\phi) \cos m\phi d\phi \text{ for } m = 0, 1, 2, \dots \quad (\text{A.22})$$

The combination of these functions enable (A.18) to be written as

$$I_{f,\theta_i}(\phi) = \sum_{m=0}^{\infty} (I_{mc,\theta_i} \cos m\phi + I_{ms,\theta_i} \sin m\phi). \quad (\text{A.23})$$

Equations (A.21), (A.22), and (A.23) are the governing equations in this analysis. Since isotropy is not assumed, these equations must be solved numerically. Equation (A.23) is already in numerical form, and equations (A.21) and (A.22) become

$$I_{mc,\theta_i} = \frac{1}{(1 + \delta_m)\pi} \left[\sum_{m=0}^P V_n \cos m\bar{\phi}\Delta\phi \right] \text{ for } m = 0, 1, 2, \dots \quad (\text{A.24})$$

and

$$I_{ms,\theta_i} = \frac{1}{\pi} \left[\sum_{m=0}^P V_n \sin m\bar{\phi}\Delta\phi \right] \text{ for } m = 0, 1, 2, \dots \quad (\text{A.25})$$

where V represents the voltage collected by the photodiode at azimuth ϕ_n and P represents the number of azimuth angles considered.

A.3 Analysis

The purpose of this analysis is twofold. First, within the theoretical study of radiative transfer, it is common practice to neglect the sine term of equation (A.2), since symmetry in ϕ is often assumed (Stephens, 1987). It can easily be shown that equation (A.2) reduces to zero under this assumption, resulting in a zero for the sine term. Since the data set used in this study allows anisotropy, it is possible to determine the importance of the sine term. Secondly, the results of this analysis will show convergence of this series with the measured intensities using a specific number of repetitions of the series. Using appropriate data, an intensity averaged around an azimuth circle at a specified zenith angle (corresponding to the $m = 0$ case) may be analyzed with the Fourier series to determine the number of repetitions which lead to convergence.

The data set was scanned to find instances where an intensity averaged azimuthally around a zenith angle θ_i could be integrated to equal the measured flux F_m to within .1%. The voltages collected by photodiodes located within $\pm 5^\circ$ of θ_i were then used to calculate I_{mc} and I_{ms} for each m . Since the resolution of the grid used to calculate I_m was ten degrees, the accuracy of I_f will be similar. Table A.1 shows pertinent data for each case. The second column of this table is the source zenith angle, and the third is the local zenith angle. The fourth column shows the number of photodiode measurements which were located on the local zenith angle ring (each of these measurements is at a different azimuth angle). The fifth column in this table is the reflected intensity (in millivolts) found by averaging all photodiode measurements along the zenith angle ring, and the sixth column represents the measured intensities along these rings. These values are also

Table A.1: Cases selected for Fourier analysis.

Case	Θ_0	Φ	θ	ϕ 's used	I_i (mV)	I_c (mV)
1	-60°	$\Phi_0 + 180^\circ$	40°	24	1969	1986
2	-40°	$\Phi_0 + 180^\circ$	50°	40	2438	2462
3	-20°	$\Phi_0 + 180^\circ$	51°	40	2877	2882
4	-20°	$\Phi_0 + 180^\circ$	40°	24	2872	2882
5	-20°	$\Phi_0 + 180^\circ$	28°	16	2858	2882
6	0°		36°	24	2585	2563
7	-20°	Φ_0	50°	40	1906	1888
8	-40°	Φ_0	51°	40	2480	2501
9	-60°	Φ_0	41°	24	2387	2415
10	-60°	$\Phi_0 + 180^\circ$	36°	24	2295	2418
11	-40°	$\Phi_0 + 180^\circ$	49°	38	1632	1736
12	-20°	$\Phi_0 + 180^\circ$	32°	24	2780	4133
13	0°		51°	40	1834	1820
14	-20°	Φ_0	41°	24	1440	1660
15	-40°	Φ_0	36°	24	1411	1825
16	-60°	Φ_0	49°	38	1424	1386

expressed in millivolts. The number of repetitions of this series for each case performed depended upon the number of azimuth angles used, resulting in values for I_{mc} and I_{ms} for each m which were used to calculate $I_{f,m}$ for each m .

Referring to equations (A.21), (A.22), and (A.23), one can see that the amplitude functions I_{mc} and I_{ms} are functions of the azimuth angle of the measurement location. Azimuthal dependence is therefore incorporated into equation (A.23). According to results from the files analyzed here, the number of photodiode measurements along a zenith angle circle determine the number of terms needed in the series. The number of useful terms of the series depend on the number of azimuth angles where measurements are taken along the zenith angle ring. A cyclic nature in the series was found when calculating intensities at all local zenith angles represented in this part of the study. This can be shown in table A.2, which shows an example of values of I_{mc} and I_{ms} for the first case studied, as well as selected intensity data. The fourth and sixth columns in this table show Fourier intensities for each m , at two different azimuth angles ($\phi = 0^\circ$ and $\phi = 90^\circ$). These intensities are summed in columns five and seven. This appendix contains summed Fourier intensities for eight azimuth angles per case as well as the actual measured intensities for each case. The first values noted in table A.2 are those of the $m = 0$ terms. The value for I_{mc} represents

Table A.2: Fourier analysis results from case number one (all values are in mV).

m	I_{mc}	I_{ms}	$I_{f,\phi=0^\circ}$	$\sum I_{f,\phi=0^\circ}$	$I_{f,\phi=90^\circ}$	$\sum I_{f,\phi=90^\circ}$
0	1969	0	1969	1969	1969	1969
1	-1360	145	-1360	609	145	2114
2	181	-65	181	790	-181	1932
3	11	-22	11	801	22	1954
4	-159	-8	-159	642	-159	1795
5	68	-84	68	710	-84	1711
6	-110	-7	-110	600	110	1822
7	58	-61	58	658	61	1883
8	-9	11	-9	649	-9	1873
9	17	-33	17	666	-33	1840
10	62	30	62	728	-62	1778
11	-45	-14	-45	683	14	1792
12	73	0	73	756	73	1864
13	-45	14	-45	711	14	1878
14	62	-30	62	773	-62	1816
15	17	33	17	790	-33	1783
16	-9	-11	-9	781	-9	1773
17	58	61	58	839	61	1835
18	-110	7	-110	729	110	1945
19	68	84	68	797	-84	1861
20	-159	8	-159	638	-159	1702
21	11	22	11	649	22	1724
22	181	65	181	831	-182	1543
23	-1360	-145	-1360	-530	145	1687
24	3938	0	3938	3408	3938	5625
25	-1360	145	-1360	2048	145	5770
26	181	-65	181	2229	-181	5589
27	11	-22	11	2240	22	5611
28	-159	-8	-159	2081	-159	5452
29	68	-84	68	2149	-84	5368
30	-110	-7	-110	2039	110	5478
31	58	-61	58	2097	61	5539
32	-9	11	-9	2088	-9	5530
33	17	-33	17	2105	-33	5497
34	62	30	62	2167	-62	5435
35	-45	-14	-45	2122	14	5449
36	73	0	73	2195	73	5522
37	-45	14	-45	2150	14	5536
38	62	-30	62	2212	-62	5474
39	17	33	17	2229	-33	5441
40	-9	-11	-9	2220	-9	5432
41	58	61	58	2278	61	5493
42	-110	7	-110	2168	110	5603
43	68	84	68	2236	84	5687

the average of all of the intensities which lie along the local zenith angle circle. I_{ms} is equal to zero, since $\sin(0^\circ) = 0$. The cyclic nature of the I_{mc} and I_{ms} terms can be seen by noting these values for $m = 0$ to $m = 23$. Aside from the $m = 24$ value, each value for I_{mc} and I_{ms} for $m = 24$ to $m = 47$ are identical to values for $m = 0$ to $m = 23$ (Values for $m = 43 - m = 47$ are not shown). The discrepancy in the $m = 24$ case is due to the δ function mentioned previously. Note that $I_{m=24,c}$ is twice that of $I_{m=0,c}$. The Kronecker δ function is 1 when $m = 0$, and 0 otherwise, resulting in a division by two instead of one when $m = 0$. This does not factor into the calculation of I_{ms} , since the δ function is absent. Also of interest in this table are the separations between small intensity values prior to and larger values beyond the point of symmetry. The measured intensity for case number one at $\phi = 0^\circ$ is 719 mV, and 1828 mV at $\phi = 90^\circ$. Once the point of symmetry is passed, values become highly inaccurate, although prior to the point of symmetry, reflected intensity values are very close to the actual measured value.

Table A.2 clearly demonstrates the need for a finite, known number of terms in which to carry out for useful results when using the Fourier series to analyze cloud fields of the type in this study. Inspection of I_{ms} between $m = 1$ and $m = 23$ shows the symmetry of these terms which effectively cancel out. However, the symmetric I_{mc} terms are additive. If the series were to be carried out to $m = P$ terms, where P is the number of azimuth angles included in calculation of the amplitude functions, the I_{ms} terms are not important.

Figure A.1 is a graphical representation of the magnitudes of the I_{mc} and I_{ms} terms as a function of m , for case number one. Values are plotted on a log scale, so the sign of each plotted value is given, and zeros are noted when $I_{ms} = 0$. Most values for I_{mc} and I_{ms} are one to two orders of magnitude lower than $I_{m=0,c}$. However, I_{mc} and I_{ms} for $m > 1$ are of the same order of magnitude. Thus, although the magnitudes of these amplitude functions ($m > 1$) are small, according to the results in this study I_{ms} is as important as I_{mc} for $m > 1$. $I_{m=1,c}$ is of the same order of magnitude as $I_{m=0,c}$. Plots for other cases considered (see figures A.2 and A.3) also demonstrate the importance of $I_{m=1,c}$. The $I_{m=1,c}$ term is the major factor involved in adjustment of the averaged intensity to the intensity present at azimuth angle ϕ . Obviously, an intensity field with

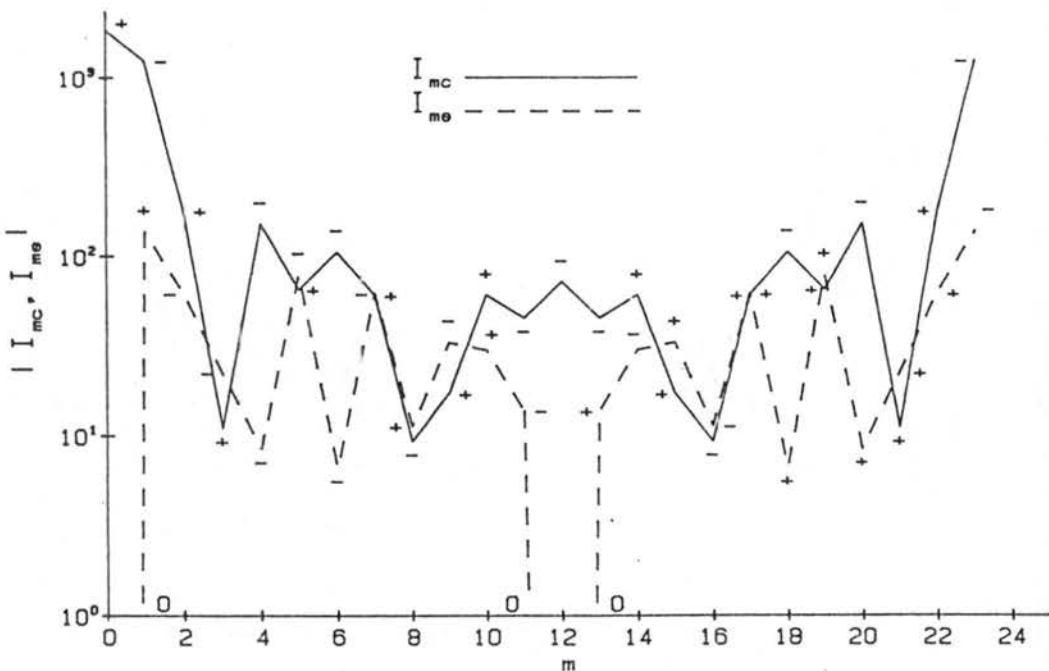


Figure A.1: Magnitudes of amplitude functions as a function of m for case number one. The solid line denotes $|I_{mc}|$, and $|I_{ms}|$ is denoted by the dashed line. Positive and negative values are noted and arrows on the $|I_{ms}|$ line show values of $I_{ms} = 0$. The plot is symmetric about $m = 12$. Twenty-four azimuth angles were used in this case. $\Theta_0 = -60^\circ$, $\Phi = \Phi_0$, and $\theta = 40^\circ$. Plotted on a log scale.

only one azimuthal radiance value cannot provide accurate information concerning any other azimuthal intensity desired. As the number of azimuth measurements increase, calculations of the intensity field at different azimuth angles becomes more accurate. The symmetry of these functions is also apparent in figure A.1, with the point of symmetry drawn on the plot. The point of symmetry is $m = 12$, and this case involved measurements of 24 azimuth angles. Values to the right of the point of symmetry were ignored in figures A.2 and A.3. The reason for this will become clear in the following paragraph.

Figures A.2 and A.3 are designed to demonstrate the relative contribution of the sine term in equation (A.23). Both I_{mc} and I_{ms} are plotted as a function of m for each case illustrated. Amplitude functions for case one and case two are shown. These figures are similar to figure A.1, with one exception. Figures A.2 and A.3 do not show values beyond the point of symmetry as does figure A.1. However, the symmetry is present in all cases studied. Values for amplitude functions for all cases studied are found in tabular form at the end of this appendix.

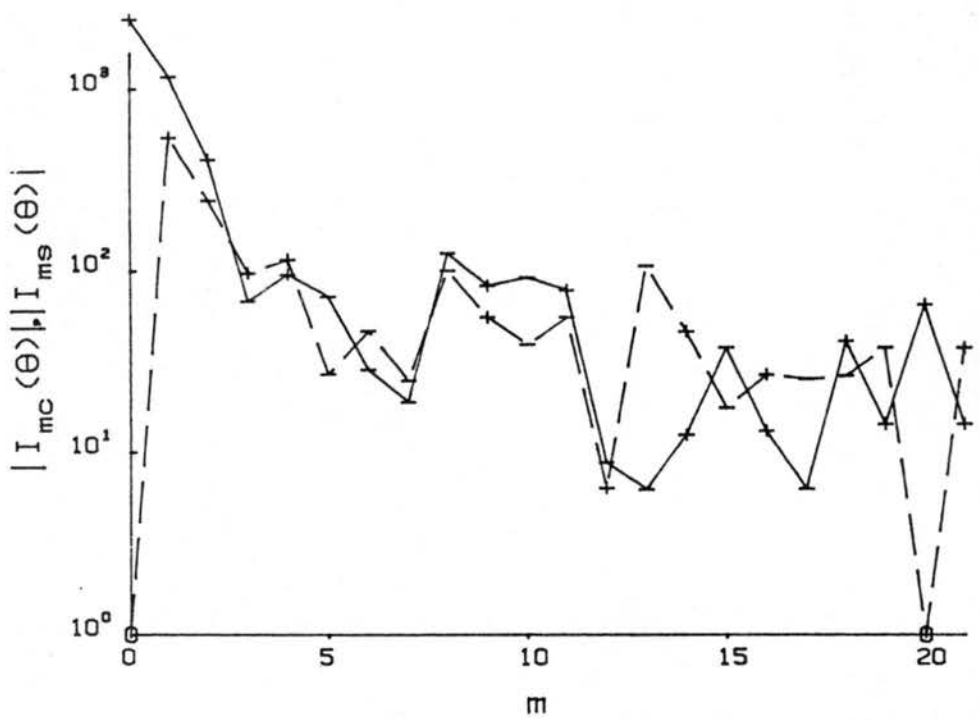


Figure A.2: Similar to A.1, except case number two is shown. $P/2$ repetitions of the Fourier series are shown here, where P is the number of azimuth angles used (40).

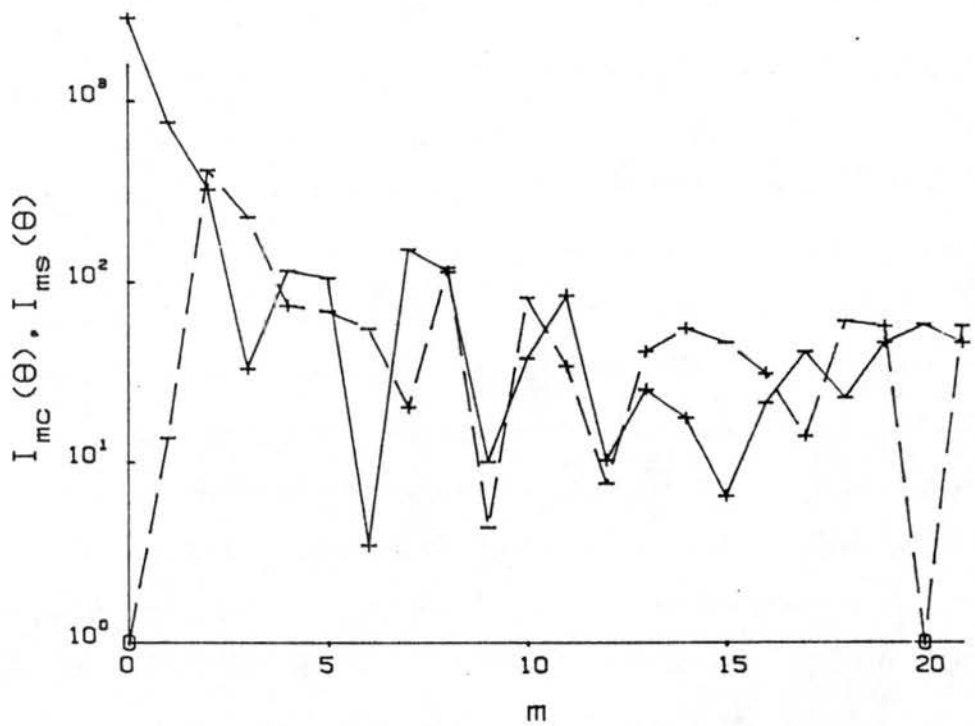


Figure A.3: Same as A.2, except case number three is shown. Forty azimuth angles were used in this case also.

The final analysis in this section involves the comparison of Fourier-calculated intensities with measured intensities. An error function, Λ , is defined as

$$\Lambda(\theta) = \frac{1}{N} \sum_{n=1}^N \left(\frac{I_{f,m,n} - V_n}{V_n} \right) \text{ for } m = 1, 2, 3, \dots \quad (\text{A.26})$$

where $I_{f,m,n}$ is the reflected intensity calculated using the Fourier series for each m , V is the reflected intensity measured by the laboratory system at the same azimuth angle, and N is the number of azimuth angles used in this calculation. Eight azimuth angles were used in this portion of the study, from 0° to 315° in increments of 45° . Cases 11 and 16 were not analyzed with this error function, since all azimuth angles used were not found in the data set for these cases. The error function represents the average error found around the local zenith angle ring when comparing to measured data.

Figures A.4 and A.5 show Λ plotted as a function of m for cases number one and two respectively. One can see from these plots that largest errors occur when only one term of the series is carried out. The values of the error function for $m = 0$ represents the difference between average reflected intensities measured and calculated using the Fourier series. The value shown for the $m = 0$ case demonstrates the differences one could find by using only one azimuth angle to calculate intensities. As table A.1 shows, the number of azimuth angles available for use in cases 1 and 2 are 24 and 40 respectively. There is a substantial error possibility when considering fewer azimuth angles. This is substantiated by data from the remaining cases which are not shown. This appendix contains error functions in tabular form for all cases (tables A.23 and A.24).

These tables also show the importance of the $m = 1$ term of the series. In most cases, the greatest reduction in error occurs with the $m = 1$ term. Errors decrease to values less than 10% after two or three repetitions for all cases in this study, although further repetitions of the series lead to smaller errors. This function is also symmetric about $m = \frac{P}{2}$. The errors begin to increase after the $m = \frac{P}{2}$ term, where P is the total number of azimuth angles used to calculate the amplitude functions I_{mc} and I_{ms} .

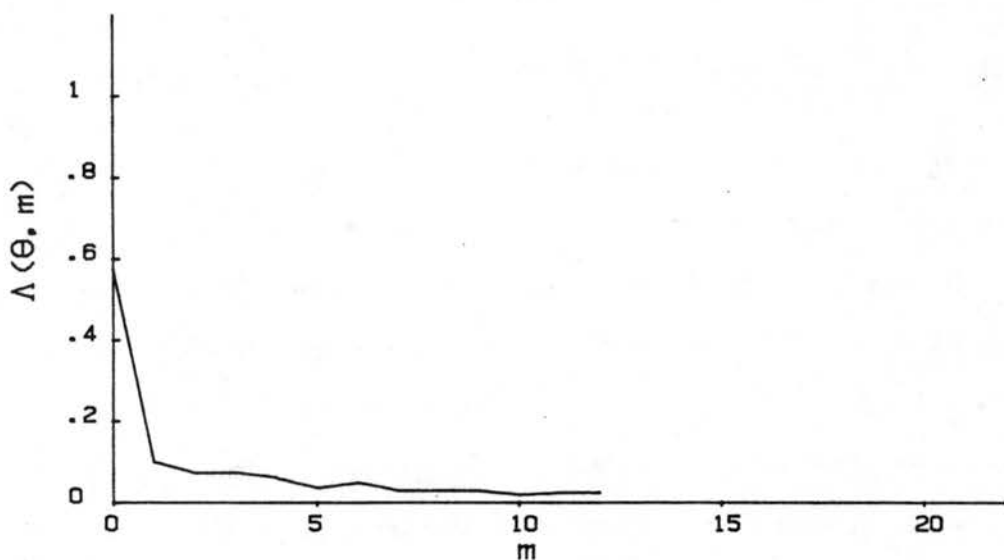


Figure A.4: Λ as a function of m . Λ is calculated using equation (A.26). Plotted on a linear scale, for case number one.

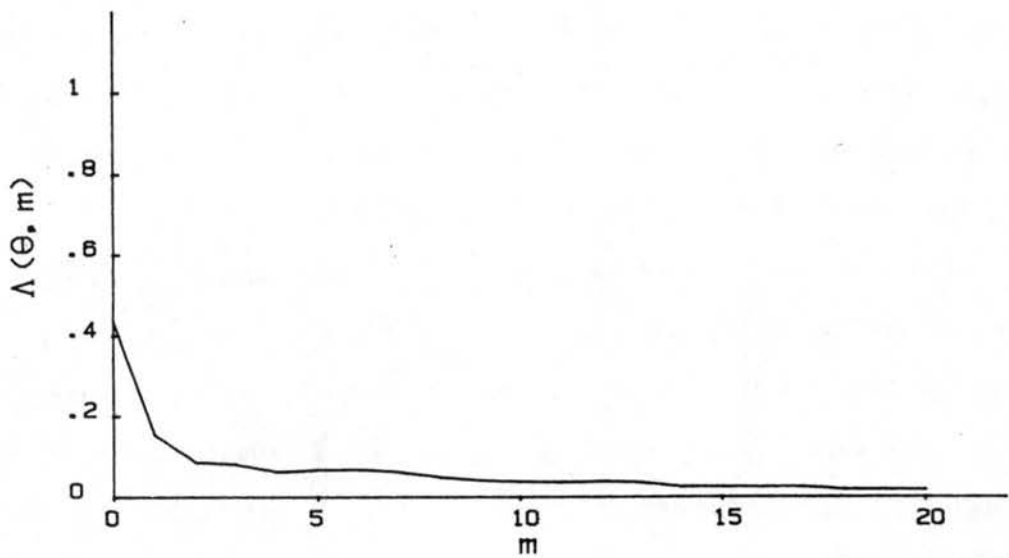


Figure A.5: Same as A.4, for case number two.

A.4 Conclusions

Fourier analysis was utilized in this chapter to study reflected radiation in the laboratory setting. Amplitude functions were analyzed as a function of the number of terms used in the Fourier series. This analysis shows the relative importance of the $m = 0$ and $m = 1$ terms of the series. The importance of the sine term in equation (A.18) is shown. According to the results of this study, this term is as important as the cosine term for terms $m > 0$. Both the I_{mc} and I_{ms} terms for $m > 1$ are usually an order of magnitude lower than I_{mc} and I_{ms} calculated for $m = 0$ and $m = 1$.

The error function Λ , was introduced as a comparison between measured intensities and those calculated using the Fourier series. This function shows significant decrease in Λ occurs for a small numbers of terms considered when eight azimuth angles are used. Further study is suggested to compare this function for one case with a different number of azimuth angles used. One may expect to find an important azimuthal dependence within this context. With an increasing number of azimuth angles used, the number of Fourier terms needed for accurate results should decrease. This is evident on plots of Λ vs. m shown here. Due to the requirements for selection of the first ten cases, the error found for $m = 0$ when all azimuths are considered is zero. Reduction to eight terms results in the errors shown.

A summary of the results of this Fourier series analysis is found in the following three sets of tables. Tables A.3 – A.6 are amplitude values calculated for each m , for all cases. Four cases are shown per page. Tables A.7 – A.22 are summed intensities for each azimuth angle studied. Finally, tables A.23 and A.24 are Λ values calculated for each case as a function of m . Cases 11 and 16 are left blank due to the absence of comparable azimuth angles measured in the laboratory. Values are shown for each repetition of the series considered for each case. All values are in millivolts.

The data set collected during this experiment would be a useful tool in a complete Fourier analysis. Reflected irradiances could be studied in detail using a greater number of case studies than are present in this analysis. The results of this analysis demonstrate the importance of the inclusion of azimuthal dependence when considering reflected intensity

fields. Zenith angle dependence was not considered in this study. However, the importance of both the source and local zenith angle should not be neglected.

Table A.3: Amplitude functions (in mV) for cases 1-4.

m	case 1		case 2		case 3		case 4	
	I_{mc}	I_{ms}	I_{mc}	I_{ms}	I_{mc}	I_{ms}	I_{mc}	I_{ms}
0	1969	0	2438	0	2877	0	2872	0
1	-1360	145	-1178	542	-766	-14	-712	-205
2	181	-65	409	-244	327	-415	129	-251
3	11	-22	-68	97	33	-230	-121	-80
4	-159	-8	96	115	-116	75	32	-66
5	68	-83	-73	-27	-106	-69	-55	-23
6	-110	-7	-29	-47	3	-56	-57	-103
7	58	-61	-19	-25	-151	20	93	-16
8	-9	11	-125	-100	115	-120	88	-10
9	17	-33	83	56	-10	-4	-15	14
10	62	30	-92	-39	-37	-82	9	60
11	-45	-14	79	-56	85	34	14	22
12	73	0	-9	6	10	-8	-139	0
13	-45	14	-6	-106	25	41	14	-22
14	62	-30	13	47	18	55	9	-60
15	17	33	-38	-18	6	-46	-15	-14
16	-9	-11	13	27	-21	31	88	10
17	58	61	-6	-25	-41	14	93	16
18	-110	7	41	-27	-23	-61	-57	103
19	68	83	14	-38	46	57	-55	23
20	-159	8	65	0	-58	0	32	66
21	11	22	14	38	46	-57	-121	80
22	181	65	41	27	-23	61	129	251
23	-1360	-145	-6	25	-41	-14	-712	205
24			13	-27	-21	-31		
25			-38	18	6	46		
26			13	-47	18	-55		
27			-6	106	25	-41		
28			-9	-6	10	8		
29			79	56	85	-34		
30			-92	39	-37	82		
31			83	-56	-10	4		
32			-125	100	115	120		
33			-19	25	-151	-20		
34			-29	47	3	56		
35			-73	27	-106	69		
36			96	-115	-116	-75		
37			-68	-97	33	230		
38			409	244	327	415		
39			-1178	-542	-766	14		

Table A.4: Amplitude functions (in mV) for cases 5-8.

m	case 5		case 6		case 7		case 8	
	I_{mc}	I_{ms}	I_{mc}	I_{ms}	I_{mc}	I_{ms}	I_{mc}	I_{ms}
0	2858	0	2585	0	1906	0	2480	0
1	-567	-108	63	2	680	29	580	517
2	-72	-162	44	-41	384	-403	334	-360
3	-195	-182	-186	-8	30	-43	116	61
4	212	-93	-69	-136	72	-219	38	32
5	-62	-12	-87	28	-20	23	56	-78
6	26	25	-19	-85	-96	-53	-18	-62
7	122	39	-21	-67	22	-3	-48	-34
8	-178	0	-45	-29	-116	17	-128	-12
9	122	-39	26	17	-3	13	-91	49
10	26	-25	55	6	-32	36	-129	-5
11	-62	12	43	-48	-14	-26	-57	-59
12	212	93	19	0	55	24	-36	-40
13	-195	182	43	48	34	-24	11	-107
14	-72	162	55	-6	9	26	14	-7
15	-567	108	26	-17	-4	10	8	-15
16		-45	29	39	-16	13	6	
17		-21	67	7	-9	-1	4	
18		-19	85	25	-41	52	-28	
19		-87	-28	-33	-15	40	-10	
20		-69	136	-78	0	92	0	
21		-186	8	-33	158	40	10	
22		44	41	25	41	52	28	
23		63	-2	7	9	-1	-4	
24				39	16	13	-6	
25				-4	-10	8	15	
26				9	-26	14	7	
27				34	24	11	107	
28				55	-24	-36	40	
29				-14	26	-57	59	
30				-32	-36	-129	5	
31				-3	-13	-91	-49	
32				-116	-17	-128	12	
33				22	3	-48	34	
34				-96	53	-18	62	
35				-20	-23	56	78	
36				72	219	38	-32	
37				30	43	116	-61	
38				384	403	334	360	
39				680	-29	58	7	

Table A.5: Amplitude functions (in mV) for cases 9-12.

m	case 9		case 10		case 11		case 12	
	I_{mc}	I_{ms}	I_{mc}	I_{ms}	I_{mc}	I_{ms}	I_{mc}	I_{ms}
0	2387	0	2295	0	1632	0	2780	0
1	1110	-4	-1182	177	-406	183	-564	-99
2	166	-175	71	37	58	-51	-257	247
3	-83	-5	-63	-68	66	-12	-140	-447
4	-99	-30	-187	61	212	-97	218	62
5	-74	-36	-13	-173	-107	37	-102	-1
6	-61	-45	-47	38	2	-84	79	-25
7	-68	-44	-29	-54	23	83	47	209
8	-4	-28	-8	3	-24	-65	-169	-84
9	-17	-37	12	-57	42	53	51	30
10	29	-2	27	-13	-8	53	-65	-67
11	56	-16	49	35	16	-104	19	-53
12	40	0	-4	0	-26	9	51	0
13	56	16	49	-35	10	7	19	53
14	29	2	27	13	19	-52	-65	67
15	-17	37	12	57	-24	38	51	-30
16	-4	28	-8	-3	-47	-19	-169	84
17	-68	44	-29	54	49	-6	47	-209
18	-61	45	-47	-38	-58	27	79	25
19	-74	36	-13	173	-0	49	-102	1
20	-99	30	-187	-61	58	27	218	-62
21	-83	5	-63	68	-49	-6	-140	447
22	166	175	71	-37	47	-19	-257	-247
23	1110	4	-1182	-177	24	38	-564	99
24					-20	-52		
25					-10	7		
26					26	9		
27					-16	-104		
28					8	53		
29					-42	53		
30					24	-65		
31					-23	83		
32					-2	-84		
33					107	37		
34					-212	-97		
35					-66	-12		
36					-57	-51		
37					406	182		

Table A.6: Amplitude functions (in mV) for cases 13-16.

m	case 13		case 14		case 15		case 16	
	I_{mc}	I_{ms}	I_{mc}	I_{ms}	I_{mc}	I_{ms}	I_{mc}	I_{ms}
0	1834	0	1440	0	1411	0	1424	0
1	88	40	795	-113	706	-170	1042	126
2	410	-459	246	27	181	-69	240	184
3	-47	-45	64	-1	-116	-19	151	-69
4	81	-238	187	-12	21	-48	123	79
5	29	51	21	154	17	98	39	154
6	-75	-59	80	29	51	-12	148	36
7	23	15	-22	176	52	7	125	139
8	-119	27	-40	9	58	4	93	69
9	39	-4	-2	48	12	62	24	133
10	26	50	-84	-2	-40	8	-92	101
11	19	-7	-16	-16	-44	-33	-102	-26
12	54	25	-82	0	-47	0	-43	-70
13	10	-14	-16	16	-44	33	40	-52
14	18	15	-84	2	-40	-8	-35	-20
15	15	-7	-2	-48	12	-62	-8	8
16	19	-15	-40	-9	58	-4	-81	0
17	-13	-12	-22	-176	52	-7	-8	-25
18	-3	-39	80	-29	51	12	-1	6
19	-36	-4	21	-154	17	-98	-0	0
20	-59	0	187	12	21	48	1	6
21	-36	4	64	1	-116	19	8	-25
22	-3	39	246	-27	181	69	81	0
23	-13	12	795	113	706	170	8	8
24	19	15					35	-20
25	15	7					-40	-52
26	18	-15					43	-70
27	10	14					101	-26
28	54	-25					92	102
29	19	7					-24	134
30	26	-50					-93	69
31	39	4					-125	139
32	-119	-27					-148	36
33	23	-15					-39	154
34	-75	59					-123	79
35	29	-51					-151	-69
36	81	238					-240	184
37	-47	45					-1042	126
38	410	459						
39	88	-40						

Table A.7: Summed intensities for case number 1 (in mV).

$\phi =$	0°	45°	90°	135°	180°	225°	270°	315°
m								
0	1969	1969	1969	1969	1969	1969	1969	1969
1	609	1110	2114	3033	3329	2828	1824	905
2	790	1045	1933	3098	3510	2763	1643	970
3	801	1022	1955	3090	3499	2786	1621	978
4	642	1181	1796	3249	3340	2945	1462	1137
5	710	1192	1713	3356	3272	2934	1545	1030
6	600	1199	1823	3349	3162	2941	1655	1023
7	658	1283	1884	3351	3104	2857	1594	1021
8	649	1274	1875	3342	3095	2848	1585	1012
9	666	1263	1842	3307	3078	2859	1618	1047
10	728	1293	1780	3277	3140	2889	1556	1017
11	683	1315	1794	3236	3185	2867	1542	1058
12	756	1242	1867	3163	3258	2794	1615	985
13	711	1264	1881	3122	3303	2772	1601	1026
14	773	1294	1819	3092	3365	2802	1539	996
15	790	1283	1786	3057	3348	2813	1572	1031
16	781	1274	1777	3048	3339	2804	1563	1022
17	839	1358	1838	3050	3281	2720	1502	1020
18	729	1365	1948	3043	3171	2727	1612	1013
19	797	1376	1865	3150	3103	2716	1695	906
20	638	1535	1706	3309	2944	2875	1536	1065
21	649	1512	1728	3301	2933	2898	1514	1073
22	830	1447	1547	3366	3114	2833	1333	1138
23	-530	588	1692	4430	4474	3692	1188	74

Table A.8: Summed intensities for case number 2 (in mV).

$\phi =$	0°	45°	90°	135°	180°	225°	270°	315°
m								
0	2438	2438	2438	2438	2438	2438	2438	2438
1	1260	1989	2980	3655	3616	2887	1896	1221
2	1669	1745	2571	3899	4025	2643	1487	1465
3	1601	1862	2474	3920	4093	2526	1584	1444
4	1697	1766	2570	3824	4189	2430	1680	1348
5	1624	1836	2543	3792	4262	2360	1707	1380
6	1595	1883	2572	3745	4233	2407	1736	1333
7	1576	1887	2597	3776	4252	2403	1711	1302
8	1451	1762	2472	3651	4127	2278	1586	1177
9	1534	1860	2528	3632	4044	2180	1530	1196
10	1442	1821	2620	3671	3952	2141	1622	1235
11	1521	1726	2676	3687	3873	2236	1566	1219
12	1512	1735	2667	3696	3864	2245	1557	1228
13	1506	1815	2561	3767	3870	2165	1663	1157
14	1519	1768	2548	3814	3883	2118	1650	1204
15	1481	1754	2566	3853	3921	2132	1632	1165
16	1494	1767	2579	3866	3934	2145	1645	1178
17	1488	1745	2554	3853	3940	2167	1670	1191
18	1529	1718	2513	3880	3981	2140	1629	1218
19	1543	1681	2551	3863	3967	2177	1591	1235
20	1608	1616	2616	3798	4032	2112	1656	1170
21	1622	1579	2654	3781	4018	2149	1618	1187
22	1663	1552	2613	3808	4059	2122	1577	1214
23	1657	1530	2588	3795	4065	2144	1602	1227
24	1670	1543	2601	3808	4078	2157	1615	1240
25	1632	1529	2619	3847	4116	2171	1597	1201
26	1645	1482	2606	3894	4129	2124	1584	1248
27	1639	1562	2500	3965	4135	2044	1690	1177
28	1630	1571	2491	3974	4126	2053	1681	1186
29	1709	1476	2547	3990	4047	2148	1625	1170
30	1617	1437	2639	4029	3955	2109	1717	1209
31	1700	1535	2695	4010	3872	2011	1661	1228
32	1575	1410	2570	3885	3747	1886	1536	1103
33	1556	1414	2595	3916	3766	1882	1511	1072
34	1527	1461	2624	3869	3737	1929	1540	1025
35	1454	1531	2597	3837	3810	1859	1567	1057
36	1550	1435	2693	3741	3906	1763	1663	961
37	1482	1552	2596	3762	3974	1646	1760	940
38	1891	1308	2187	4006	4383	1402	1351	1184
39	713	859	2729	5223	5561	1851	809	-33

Table A.9: Summed intensities for case number 3 (in mV).

$\phi =$	0°	45°	90°	135°	180°	225°	270°	315°
m								
0	2876	2876	2876	2876	2876	2876	2876	2876
1	2110	2324	2862	3408	3642	3428	2890	2344
2	2437	1909	2535	3823	3969	3013	2563	2759
3	2470	1723	2765	3684	3936	3199	2333	2898
4	2354	1839	2649	3800	3820	3315	2217	3014
5	2248	1963	2580	3774	3926	3191	2286	3040
6	2251	2019	2577	3718	3929	3247	2283	2984
7	2100	1898	2557	3811	4080	3368	2303	2891
8	2215	2013	2672	3926	4195	3483	2418	3006
9	2205	2003	2668	3930	4205	3493	2422	3002
10	2168	1921	2705	4012	4168	3411	2459	3084
11	2253	1885	2671	4096	4083	3447	2493	3000
12	2263	1875	2681	4086	4093	3437	2503	2990
13	2288	1828	2722	4075	4068	3484	2462	3001
14	2306	1773	2704	4130	4086	3429	2444	3056
15	2312	1810	2750	4158	4080	3392	2398	3028
16	2291	1789	2729	4137	4059	3371	2377	3007
17	2250	1770	2743	4176	4100	3390	2363	2968
18	2227	1709	2766	4237	4077	3329	2386	3029
19	2273	1717	2709	4310	4031	3321	2443	2956
20	2215	1775	2651	4368	3973	3379	2385	3016
21	2261	1783	2594	4441	3927	3371	2442	2941
22	2238	1722	2617	4502	3904	3310	2465	3002
23	2197	1703	2631	4541	3945	3329	2451	2963
24	2176	1682	2610	4520	3924	3308	2430	2942
25	2182	1719	2656	4548	3918	3271	2384	2914
26	2200	1664	2638	4603	3936	3216	2366	2969
27	2225	1617	2679	4592	3911	3263	2325	2980
28	2235	1607	2689	4582	3921	3253	2335	2970
29	2320	1571	2655	4666	3836	3289	2369	2886
30	2283	1489	2692	4748	3799	3207	2406	2968
31	2273	1479	2688	4752	3809	3217	2410	2964
32	2388	1594	2803	4867	3924	3332	2525	3079
33	2237	1473	2783	4960	4075	3453	2545	2986
34	2240	1529	2780	4904	4078	3509	2542	2930
35	2134	1653	2711	4878	4184	3385	2611	2956
36	2018	1769	2595	4994	4068	3501	2495	3072
37	2051	1583	2825	4855	4035	3687	2265	3211
38	2378	1168	2498	5270	4362	3272	1938	3626
39	1612	616	2484	5802	5128	3824	1952	3094

Table A.10: Summed intensities for case number 4 (in mV).

$\phi =$	0°	45°	90°	135°	180°	225°	270°	315°
m								
0	2872	2872	2872	2872	2872	2872	2872	2872
1	2160	2224	2667	3231	3584	3520	3077	2513
2	2289	1973	2538	3482	3713	3269	2948	2764
3	2168	2002	2618	3340	3834	3240	2868	2908
4	2200	1970	2650	3308	3866	3208	2900	2874
5	2145	2025	2627	3285	3921	3153	2923	2897
6	2088	2128	2684	3182	3864	3256	2980	2794
7	2181	2205	2700	3128	3771	3179	2964	2848
8	2269	2293	2788	3216	3859	3267	3052	2936
9	2254	2293	2802	3237	3874	3267	3038	2915
10	2263	2353	2793	3177	3883	3327	3029	2855
11	2277	2359	2771	3202	3869	3321	3051	2830
12	2138	2498	2632	3341	3730	3460	2912	2969
13	2152	2504	2610	3366	3716	3454	2934	2944
14	2161	2564	2601	3306	3725	3514	2925	2884
15	2146	2564	2615	3327	3740	3514	2911	2863
16	2234	2652	2703	3415	3828	3602	2999	2951
17	2327	2729	2719	3361	3735	3525	2983	3005
18	2270	2832	2776	3258	3678	3628	3040	2902
19	2215	2887	2753	3235	3733	3573	3063	2925
20	2247	2855	2785	3203	3765	3541	3095	2893
21	2126	2884	2865	3061	3886	3512	3015	3035
22	2255	2633	2736	3312	4015	3261	2886	3286
23	1543	1985	2531	3671	4727	3909	3091	2927

Table A.11: Summed intensities for case number 5 (in mV).

$\phi =$	0°	45°	90°	135°	180°	225°	270°	315°
m								
0	2858	2858	2858	2858	2858	2858	2858	2858
1	2291	2381	2750	3183	3425	3335	2966	2533
2	2219	2219	2822	3345	3353	3173	3038	2695
3	2024	2228	3004	3078	3548	3164	2856	2962
4	2236	2016	3216	2866	3760	2952	3068	2750
5	2174	2068	3204	2831	3822	2900	3080	2785
6	2200	2043	3178	2856	3848	2875	3054	2810
7	2322	2102	3139	2742	3726	2816	3093	2924
8	2144	1924	2961	2564	3548	2638	2915	2746
9	2266	1983	2922	2450	3426	2579	2954	2860
10	2292	1958	2896	2475	3452	2554	2928	2885
11	2230	2010	2884	2440	3514	2502	2940	2920
12	2442	1798	3096	2228	3726	2290	3152	2708
13	2247	1807	3278	1961	3921	2281	2970	2975
14	2175	1645	3350	2123	3849	2119	3042	3137
15	1608	1168	3242	2448	4416	2596	3150	2812

Table A.12: Summed intensities for case number 6 (in mV).

$\phi =$	0°	45°	90°	135°	180°	225°	270°	315°
m								
0	2585	2585	2585	2585	2585	2585	2585	2585
1	2648	2631	2587	2542	2522	2539	2583	2628
2	2692	2590	2543	2583	2566	2498	2539	2669
3	2506	2716	2551	2446	2752	2372	2531	2806
4	2437	2785	2482	2515	2683	2441	2462	2875
5	2350	2827	2510	2434	2770	2399	2434	2956
6	2331	2912	2529	2349	2751	2484	2453	2871
7	2310	2945	2596	2411	2772	2451	2386	2809
8	2265	2900	2551	2366	2727	2406	2341	2764
9	2291	2930	2568	2360	2701	2376	2324	2770
10	2346	2936	2513	2354	2756	2382	2269	2764
11	2389	2871	2561	2351	2713	2447	2221	2767
12	2408	2852	2580	2332	2732	2428	2240	2748
13	2451	2787	2628	2329	2689	2493	2192	2751
14	2506	2793	2573	2323	2744	2499	2137	2745
15	2532	2823	2590	2317	2718	2469	2120	2751
16	2487	2778	2545	2272	2673	2424	2075	2706
17	2466	2811	2612	2334	2694	2391	2008	2644
18	2447	2896	2631	2249	2675	2476	2027	2559
19	2360	2938	2659	2168	2762	2434	1999	2640
20	2291	3007	2590	2237	2693	2503	1930	2709
21	2105	3133	2598	2100	2879	2377	1922	2846
22	2149	3092	2554	2141	2923	2336	1878	2887
23	2212	3138	2556	2098	2860	2290	1876	2930

Table A.13: Summed intensities for case number 7 (in mV).

$\phi =$	0°	45°	90°	135°	180°	225°	270°	315°
m								
0	1906	1906	1906	1906	1906	1906	1906	1906
1	2586	2407	1935	1445	1226	1405	1877	2367
2	2970	2004	1551	1848	1610	1002	1493	2770
3	3000	1953	1594	1839	1580	1053	1450	2779
4	3072	1881	1666	1767	1652	981	1522	2707
5	3052	1879	1689	1736	1672	983	1499	2738
6	2956	1932	1785	1683	1576	1036	1595	2685
7	2978	1950	1788	1669	1554	1018	1592	2699
8	2862	1834	1672	1553	1438	902	1476	2583
9	2859	1841	1685	1564	1441	895	1463	2572
10	2827	1877	1717	1528	1409	931	1495	2536
11	2813	1868	1743	1500	1423	940	1469	2564
12	2868	1813	1798	1445	1478	885	1524	2509
13	2902	1806	1774	1486	1444	892	1548	2468
14	2911	1780	1765	1512	1453	866	1539	2494
15	2907	1770	1755	1508	1457	876	1549	2498
16	2946	1809	1794	1547	1496	915	1588	2537
17	2953	1808	1785	1535	1489	916	1597	2549
18	2978	1767	1760	1576	1514	875	1572	2590
19	2945	1780	1775	1542	1547	862	1557	2624
20	2867	1858	1697	1620	1469	940	1479	2702
21	2834	1871	1712	1586	1502	927	1464	2736
22	2859	1830	1687	1627	1527	886	1439	2777
23	2866	1829	1678	1615	1520	887	1448	2789
24	2905	1868	1717	1654	1559	926	1487	2828
25	2901	1858	1707	1650	1563	936	1497	2832
26	2910	1832	1698	1676	1572	910	1488	2858
27	2944	1825	1674	1717	1538	917	1512	2817
28	2999	1770	1729	1662	1593	862	1567	2762
29	2985	1761	1755	1634	1607	871	1541	2790
30	2953	1797	1787	1598	1575	907	1573	2754
31	2950	1804	1800	1609	1578	900	1560	2743
32	2834	1688	1684	1493	1462	784	1444	2627
33	2856	1706	1687	1479	1440	766	1441	2641
34	2760	1759	1783	1426	1344	819	1537	2588
35	2740	1757	1806	1395	1364	821	1514	2619
36	2812	1685	1878	1323	1436	749	1586	2547
37	2842	1634	1921	1314	1406	800	1543	2556
38	3226	1231	1537	1717	1790	397	1159	2959
39	3906	1732	1566	1256	1110	-104	1130	3420

Table A.14: Summed intensities for case number 8 (in mV).

$\phi =$	0°	45°	90°	135°	180°	225°	270°	315°
m								
0	2480	2480	2480	2480	2480	2480	2480	2480
1	3060	3255	2997	2436	1900	1705	1963	2524
2	3394	2895	2663	2796	2234	1345	1629	2884
3	3510	2856	2602	2921	2118	1384	1690	2759
4	3548	2818	2640	2883	2156	1346	1728	2721
5	3604	2833	2562	2978	2100	1331	1806	2626
6	3586	2895	2580	2916	2082	1393	1824	2564
7	3538	2885	2614	2974	2130	1403	1790	2506
8	3410	2757	2486	2846	2002	1275	1662	2378
9	3319	2727	2535	2945	2093	1305	1613	2279
10	3190	2722	2664	2950	1964	1300	1742	2284
11	3133	2721	2723	2869	2021	1301	1683	2365
12	3097	2757	2687	2905	1985	1337	1647	2401
13	3108	2825	2580	2988	1974	1269	1754	2318
14	3122	2832	2566	2981	1988	1276	1740	2311
15	3130	2848	2581	2986	1980	1260	1725	2306
16	3143	2861	2594	2999	1993	1273	1738	2319
17	3142	2863	2598	3002	1994	1271	1734	2316
18	3194	2835	2546	3030	2046	1243	1682	2344
19	3234	2800	2556	3051	2006	1278	1672	2323
20	3326	2708	2648	2959	2098	1186	1764	2231
21	3366	2673	2658	2980	2058	1221	1754	2210
22	3418	2645	2606	3008	2110	1193	1702	2238
23	3417	2647	2610	3011	2111	1191	1698	2235
24	3430	2660	2623	3024	2124	1204	1711	2248
25	3438	2676	2638	3029	2116	1188	1696	2243
26	3452	2683	2624	3022	2130	1195	1682	2236
27	3463	2751	2517	3105	2119	1127	1789	2153
28	3427	2787	2481	3141	2083	1163	1753	2189
29	3370	2786	2540	3060	2140	1164	1694	2270
30	3241	2781	2669	3065	2011	1159	1823	2275
31	3150	2751	2718	3164	2102	1189	1774	2176
32	3022	2623	2590	3036	1974	1061	1646	2048
33	2974	2613	2624	3094	2022	1071	1612	1990
34	2956	2675	2642	3032	2004	1133	1630	1928
35	3012	2690	2564	3127	1948	1118	1708	1833
36	3050	2652	2602	3089	1986	1080	1746	1795
37	3166	2613	2541	3214	1870	1119	1807	1670
38	3500	2253	2207	3574	2204	759	1473	2030
39	4080	3028	2724	3530	1624	-16	956	2074

Table A.15: Summed intensities for case number 9 (in mV).

$\phi =$	0°	45°	90°	135°	180°	225°	270°	315°
m								
0	2387	2387	2387	2387	2387	2387	2387	2387
1	3497	3169	2383	1599	1277	1605	2391	3175
2	3663	2994	2217	1774	1443	1430	2225	3350
3	3580	3049	2222	1712	1526	1375	2220	3412
4	3481	3148	2123	1811	1427	1474	2121	3511
5	3407	3226	2087	1784	1501	1396	2157	3538
6	3346	3271	2148	1739	1440	1441	2218	3493
7	3278	3254	2192	1818	1508	1458	2174	3414
8	3274	3250	2188	1814	1504	1454	2170	3410
9	3257	3212	2151	1800	1521	1492	2207	3424
10	3286	3210	2122	1802	1550	1490	2178	3426
11	3342	3160	2138	1830	1494	1540	2162	3398
12	3382	3120	2178	1790	1534	1500	2202	3358
13	3438	3070	2194	1818	1478	1550	2186	3330
14	3467	3068	2165	1820	1507	1548	2157	3332
15	3450	3030	2128	1806	1524	1586	2194	3346
16	3446	3026	2124	1802	1520	1582	2190	3342
17	3378	3009	2168	1881	1588	1599	2146	3263
18	3317	3054	2229	1836	1527	1644	2207	3218
19	3243	3132	2193	1809	1601	1566	2243	3245
20	3144	3231	2094	1908	1502	1665	2144	3344
21	3061	3286	2099	1846	1585	1610	2139	3406
22	3227	3111	1933	2021	1751	1435	1973	3581
23	4337	3893	1929	1233	641	653	1977	4369

Table A.16: Summed intensities for case number 10 (in mV).

$\phi =$	0°	45°	90°	135°	180°	225°	270°	315°
m								
0	2295	2295	2295	2295	2295	2295	2295	2295
1	1113	1585	2472	3256	3477	3005	2118	1334
2	1184	1622	2401	3219	3548	3042	2047	1297
3	1121	1619	2469	3126	3611	3045	1979	1390
4	934	1806	2282	3313	3424	3232	1792	1577
5	921	1937	2109	3426	3437	3101	1965	1464
6	874	1899	2156	3464	3390	3063	2012	1502
7	845	1917	2210	3522	3419	3045	1958	1444
8	837	1909	2202	3514	3411	3037	1950	1436
9	849	1877	2145	3466	3399	3069	2007	1484
10	876	1864	2118	3479	3426	3056	1980	1497
11	925	1854	2083	3539	3377	3066	2015	1437
12	921	1858	2079	3543	3373	3070	2011	1441
13	970	1848	2044	3603	3324	3080	2046	1381
14	997	1835	2017	3616	3351	3067	2019	1394
15	1009	1803	1960	3568	3339	3099	2076	1442
16	1001	1795	1952	3560	3331	3091	2068	1434
17	972	1813	2006	3618	3360	3073	2014	1376
18	925	1775	2053	3656	3313	3035	2061	1414
19	912	1906	1880	3769	3326	2904	2234	1301
20	725	2093	1693	3956	3139	3091	2047	1488
21	662	2090	1761	3863	3202	3094	1979	1581
22	733	2127	1690	3826	3273	3131	1908	1544
23	-449	1417	1867	4787	4455	3841	1731	583

Table A.17: Summed intensities for case number 11 (in mV).

$\phi =$	0°	45°	90°	135°	180°	225°	270°	315°
m								
0	1632	1632	1632	1632	1632	1632	1632	1632
1	1226	1474	1815	2048	2038	1790	1449	1216
2	1284	1423	1757	2099	2096	1739	1391	1267
3	1350	1368	1769	2137	2030	1794	1379	1229
4	1562	1156	1981	1925	2242	1582	1591	1017
5	1455	1206	2018	1823	2349	1532	1554	1119
6	1457	1290	2016	1739	2351	1616	1552	1035
7	1480	1247	1933	1664	2328	1659	1635	1110
8	1456	1223	1909	1640	2304	1635	1611	1086
9	1498	1291	1962	1648	2262	1567	1558	1078
10	1490	1344	1970	1595	2254	1620	1566	1025
11	1506	1259	2074	1533	2238	1705	1462	1087
12	1480	1285	2048	1559	2212	1731	1436	1113
13	1490	1273	2055	1561	2202	1743	1429	1111
14	1509	1325	2036	1509	2221	1795	1410	1059
15	1485	1281	1998	1499	2245	1839	1448	1069
16	1438	1234	1951	1452	2198	1792	1401	1022
17	1487	1265	1945	1413	2149	1761	1407	1061
18	1429	1292	2003	1386	2091	1788	1465	1034
19	1429	1327	1954	1421	2091	1753	1514	999
20	1487	1269	2012	1363	2149	1695	1572	941
21	1438	1308	2006	1332	2198	1656	1578	972
22	1485	1327	1959	1313	2245	1675	1531	953
23	1509	1317	1921	1269	2221	1685	1569	992
24	1489	1297	1901	1249	2201	1665	1549	977
25	1479	1295	1908	1261	2211	1667	1542	965
26	1505	1304	1882	1252	2237	1676	1516	956
27	1489	1242	1986	1167	2253	1738	1412	1041
28	1497	1234	1994	1159	2261	1730	1420	1033
29	1455	1226	2047	1092	2303	1738	1367	1100
30	1479	1291	2023	1027	2327	1803	1343	1035
31	1456	1216	1940	984	2350	1878	1426	1078
32	1454	1214	1938	982	2348	1876	1424	1076
33	1561	1316	1975	932	2241	1774	1387	1126
34	1349	1219	2187	1029	2029	1677	1599	1223
35	1283	1257	2199	974	2095	1639	1587	1278
36	1226	1314	2142	1031	2038	1696	1530	1335
37	1632	898	2324	1189	1632	2112	1348	1177

Table A.18: Summed intensities for case number 12 (in mV).

$\phi =$	0°	45°	90°	135°	180°	225°	270°	315°
m								
0	2780	2780	2780	2780	2780	2780	2780	2780
1	2216	2312	2681	3109	3344	3248	2879	2451
2	1959	2559	2938	2862	3087	3495	3136	2204
3	1819	2342	3385	2447	3227	3712	2689	2619
4	2037	2124	3603	2229	3445	3494	2907	2401
5	1935	2196	3602	2158	3547	3422	2908	2472
6	2014	2221	3523	2133	3626	3447	2829	2447
7	2061	2107	3314	1952	3579	3561	3038	2628
8	1892	1938	3145	1783	3410	3392	2869	2459
9	1943	1995	3175	1768	3359	3335	2839	2474
10	1878	1928	3240	1835	3294	3268	2904	2541
11	1897	1877	3293	1811	3275	3319	2851	2565
12	1948	1826	3344	1760	3326	3268	2902	2514
13	1967	1775	3397	1736	3307	3319	2849	2538
14	1902	1708	3462	1803	3242	3252	2914	2605
15	1953	1765	3492	1788	3191	3195	2884	2620
16	1784	1596	3323	1619	3022	3026	2715	2451
17	1831	1482	3114	1438	2975	3140	2924	2632
18	1910	1507	3035	1413	3054	3165	2845	2607
19	1808	1579	3034	1342	3156	3093	2846	2678
20	2026	1361	3252	1124	3374	2875	3064	2460
21	1886	1144	3699	709	3514	3092	2617	2875
22	1629	1391	3956	462	3257	3339	2874	2628
23	1065	923	3857	791	3821	3807	2973	2299

Table A.19: Summed intensities for case number 13 (in mV).

$\phi =$	0°	45°	90°	135°	180°	225°	270°	315°
m								
0	1834	1834	1834	1834	1834	1834	1834	1834
1	1922	1925	1874	1800	1746	1743	1794	1868
2	2332	1466	1464	2259	2156	1284	1384	2327
3	2285	1467	1509	2194	2203	1283	1339	2392
4	2366	1386	1590	2113	2284	1202	1420	2311
5	2395	1329	1641	2097	2255	1259	1369	2327
6	2320	1388	1716	2038	2180	1318	1444	2268
7	2343	1394	1701	2011	2157	1312	1459	2295
8	2224	1275	1582	1892	2038	1193	1340	2176
9	2263	1300	1578	1861	1999	1168	1344	2207
10	2289	1350	1552	1811	2025	1218	1318	2157
11	2308	1331	1559	1820	2006	1237	1311	2148
12	2362	1277	1613	1766	2060	1183	1365	2094
13	2372	1279	1599	1783	2050	1181	1379	2077
14	2390	1264	1581	1798	2068	1166	1361	2092
15	2405	1279	1588	1792	2053	1151	1354	2098
16	2424	1298	1607	1811	2072	1170	1373	2117
17	2411	1280	1595	1811	2085	1188	1385	2117
18	2408	1241	1598	1850	2082	1149	1388	2156
19	2372	1264	1602	1822	2118	1126	1384	2184
20	2313	1323	1543	1881	2059	1185	1325	2243
21	2277	1346	1547	1853	2095	1162	1321	2271
22	2274	1307	1550	1892	2092	1123	1324	2310
23	2261	1289	1538	1892	2105	1141	1336	2310
24	2280	1308	1557	1911	2124	1160	1355	2329
25	2295	1323	1564	1905	2109	1145	1348	2335
26	2313	1308	1546	1920	2127	1130	1330	2350
27	2323	1310	1532	1937	2117	1128	1344	2333
28	2377	1256	1586	1883	2171	1074	1398	2279
29	2396	1237	1593	1892	2152	1093	1391	2270
30	2422	1287	1567	1842	2178	1143	1365	2220
31	2461	1312	1563	1811	2139	1118	1369	2251
32	2342	1193	1444	1692	2020	999	1250	2132
33	2365	1199	1429	1665	1997	993	1265	2159
34	2290	1258	1504	1606	1922	1052	1340	2100
35	2319	1201	1555	1590	1893	1109	1289	2116
36	2400	1120	1636	1509	1974	1028	1370	2035
37	2353	1121	1681	1444	2021	1027	1325	2100
38	2763	662	1271	1903	2431	568	915	2559
39	2851	753	1311	1869	2343	477	875	2593

Table A.20: Summed intensities for case number 14 (in mV).

$\phi =$	0°	45°	90°	135°	180°	225°	270°	315°
m								
0	1440	1440	1440	1440	1440	1440	1440	1440
1	2235	1922	1327	798	645	958	1553	2082
2	2481	1949	1081	771	891	985	1307	2055
3	2545	1903	1082	815	827	1031	1306	2011
4	2732	1716	1269	628	1014	844	1493	1824
5	2753	1593	1423	534	993	967	1339	1918
6	2833	1564	1343	563	1073	938	1259	1947
7	2811	1424	1167	454	1095	1078	1435	2056
8	2771	1384	1127	414	1055	1038	1395	2016
9	2769	1417	1175	449	1057	1005	1347	1981
10	2685	1415	1259	451	973	1003	1431	1983
11	2669	1415	1275	428	989	1003	1415	2006
12	2587	1497	1193	510	907	1085	1333	2088
13	2571	1497	1209	487	923	1085	1317	2111
14	2487	1495	1293	489	839	1083	1401	2113
15	2485	1528	1341	524	841	1050	1353	2078
16	2445	1488	1301	484	801	1010	1313	2038
17	2423	1348	1125	375	823	1150	1489	2147
18	2503	1319	1045	404	903	1121	1409	2176
19	2524	1196	1199	310	882	1244	1255	2270
20	2711	1009	1386	123	1069	1057	1442	2083
21	2775	963	1387	167	1005	1103	1441	2039
22	3021	990	1141	140	1251	1130	1195	2012
23	3816	1472	1028	-502	456	648	1308	2654

Table A.21: Summed intensities for case number 15 (in mV).

$\phi =$	0°	45°	90°	135°	180°	225°	270°	315°
m								
0	1411	1411	1411	1411	1411	1411	1411	1411
1	2117	1790	1241	791	705	1032	1581	2031
2	2298	1721	1060	860	886	963	1400	2100
3	2182	1789	1079	764	1002	895	1381	2196
4	2203	1768	1100	743	1023	874	1402	2175
5	2220	1686	1198	686	1006	956	1304	2232
6	2271	1698	1147	674	1057	968	1253	2220
7	2323	1730	1140	632	1005	936	1260	2262
8	2381	1788	1198	690	1063	994	1318	2320
9	2393	1841	1260	725	1051	941	1256	2285
10	2353	1849	1300	717	1011	949	1296	2277
11	2309	1857	1333	662	1055	941	1263	2332
12	2262	1904	1286	709	1008	988	1216	2379
13	2218	1912	1319	654	1052	980	1183	2434
14	2178	1920	1359	646	1012	988	1223	2426
15	2190	1973	1421	681	1000	935	1161	2391
16	2248	2031	1479	739	1058	993	1219	2449
17	2300	2063	1472	697	1006	961	1226	2491
18	2351	2075	1421	685	1057	973	1175	2479
19	2368	1993	1519	628	1040	1055	1077	2536
20	2389	1972	1540	607	1061	1034	1098	2515
21	2273	2040	1559	511	1177	966	1079	2611
22	2454	1971	1378	580	1358	897	898	2680
23	3160	2350	1208	-40	652	518	1068	3300

Table A.22: Summed intensities for case number 16 (in mV).

$\phi =$	0°	45°	90°	135°	180°	225°	270°	315°
m								
0	1424	1424	1424	1424	1424	1424	1424	1424
1	2466	2250	1550	777	382	598	1298	2071
2	2706	2434	1310	593	622	782	1058	1887
3	2857	2278	1379	651	471	938	989	1829
4	2980	2155	1502	528	594	815	1112	1706
5	3019	2019	1656	447	555	951	958	1787
6	3167	1983	1508	483	703	915	810	1823
7	3292	1973	1369	296	578	925	949	2010
8	3385	2066	1462	389	671	1018	1042	2103
9	3409	2177	1595	466	647	907	909	2026
10	3317	2278	1687	365	555	1008	1001	1925
11	3215	2331	1713	275	657	955	975	2015
12	3172	2374	1670	318	614	998	932	2058
13	3212	2383	1618	383	574	989	984	1993
14	3177	2403	1653	363	539	1009	1019	1973
15	3169	2392	1645	363	547	1020	1027	1973
16	3088	2311	1564	282	466	939	946	1892
17	3080	2288	1539	270	474	962	971	1904
18	3079	2294	1540	264	473	968	972	1898
19	3079	2294	1540	264	473	968	972	1898
20	3080	2293	1541	263	474	967	973	1897
21	3088	2305	1516	286	466	955	998	1874
22	3169	2305	1435	286	547	955	917	1874
23	3177	2305	1427	275	539	955	925	1885
24	3212	2340	1462	310	574	990	960	1920
25	3172	2275	1410	301	614	1055	1012	1929
26	3215	2205	1367	371	657	985	969	1999
27	3316	2115	1393	424	556	1075	943	1946
28	3408	2023	1485	332	648	983	1035	1854
29	3384	1945	1619	221	672	1061	901	1965
30	3291	1876	1712	290	579	992	994	2034
31	3166	1689	1573	280	704	1179	1133	2044
32	3018	1541	1425	132	556	1031	985	1896
33	2979	1622	1579	268	595	950	831	1760
34	2856	1701	1702	189	472	1029	954	1681
35	2705	1759	1771	33	623	971	885	1837
36	2465	1999	1531	273	383	1211	645	2077
37	1423	2646	1657	-553	1425	564	519	2903

Table A.23: Λ values as a function of m for cases 1–8.

case:	1	2	3	4	5	6	7	8
m								
0	.576	.438	.249	.139	.145	.077	.326	.290
1	.100	.154	.150	.049	.113	.075	.216	.162
2	.072	.085	.075	.058	.093	.073	.079	.085
3	.074	.080	.052	.042	.082	.042	.082	.065
4	.060	.061	.048	.041	.038	.039	.056	.063
5	.034	.067	.054	.044	.041	.037	.056	.057
6	.048	.067	.056	.038	.036	.030	.053	.064
7	.028	.061	.053	.030	.033	.027	.050	.057
8	.029	.047	.045	.028	.033	.019	.023	.034
9	.029	.040	.046	.026	.036	.020	.024	.026
10	.017	.036	.041	.024	.041	.016	.033	.024
11	.024	.035	.029	.024	.038	.000	.035	.035
12	.024	.038	.029	.024	.082	.000	.030	.042
13	.017	.034	.028	.024	.093	.016	.030	.025
14	.029	.023	.023	.026	.113	.020	.030	.024
15	.029	.025	.023	.028	.145	.019	.029	.021
16	.028	.023	.019	.030		.027	.024	.022
17	.048	.024	.018	.038		.030	.025	.021
18	.034	.017	.017	.044		.037	.021	.018
19	.060	.017	.011	.041		.039	.024	.021
20	.074	.017	.011	.042		.042	.024	.021
21	.072	.017	.017	.058		.073	.021	.018
22	.100	.024	.018	.049		.075	.025	.021
23	.576	.023	.019	.139		.077	.024	.022
24		.025	.023				.029	.021
25		.023	.023				.030	.024
26		.034	.028				.030	.025
27		.038	.029				.030	.042
28		.035	.029				.035	.035
29		.036	.041				.033	.024
30		.040	.046				.024	.026
31		.047	.045				.023	.034
32		.061	.053				.050	.057
33		.067	.056				.053	.064
34		.067	.054				.056	.057
35		.061	.048				.056	.063
36		.080	.052				.082	.065
37		.085	.075				.079	.085
38		.154	.150				.216	.162
39		.438	.249				.326	.290

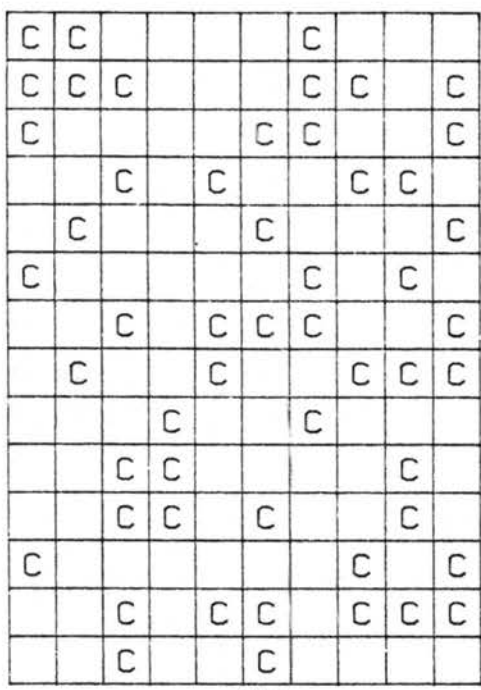
Table A.24: Λ values as a function of m for cases 9–16.

case:	9	10	11	12	13	14	15	16
m								
0	.311	.436		.264	.256	.493	.392	
1	.080	.100		.175	.255	.225	.141	
2	.040	.104		.183	.081	.166	.114	
3	.038	.097		.119	.081	.176	.084	
4	.026	.059		.089	.057	.131	.081	
5	.030	.020		.080	.057	.081	.045	
6	.030	.023		.088	.069	.101	.043	
7	.018	.029		.070	.066	.052	.052	
8	.018	.030		.027	.022	.057	.040	
9	.014	.023		.026	.014	.047	.031	
10	.016	.021		.017	.030	.031	.027	
11	.010	.000		.000	.010	.030	.037	
12	.010	.000		.010	.024	.037	.019	
13	.016	.021		.017	.025	.031	.027	
14	.014	.023		.026	.020	.047	.031	
15	.018	.030		.027	.019	.057	.040	
16	.018	.029		.070	.020	.052	.052	
17	.030	.023		.088	.021	.101	.043	
18	.030	.020		.080	.018	.081	.045	
19	.026	.059		.089	.018	.131	.081	
20	.038	.097		.119	.018	.176	.084	
21	.040	.104		.183	.018	.166	.114	
22	.080	.100		.175	.021	.225	.141	
23	.311	.436		.264	.020	.493	.392	
24					.019			
25					.020			
26					.025			
27					.024			
28					.030			
29					.030			
30					.014			
31					.022			
32					.066			
33					.069			
34					.057			
35					.057			
36					.081			
37					.081			
38					.255			
39					.256			

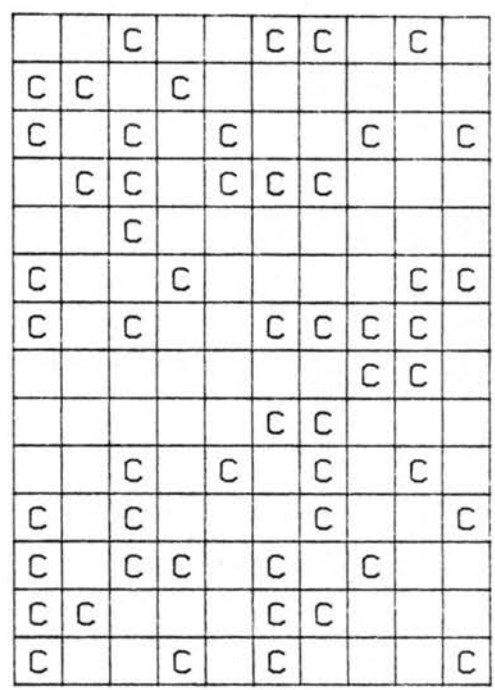
Appendix B

RANDOMLY ORIENTED CLOUD FIELDS USED IN STUDY

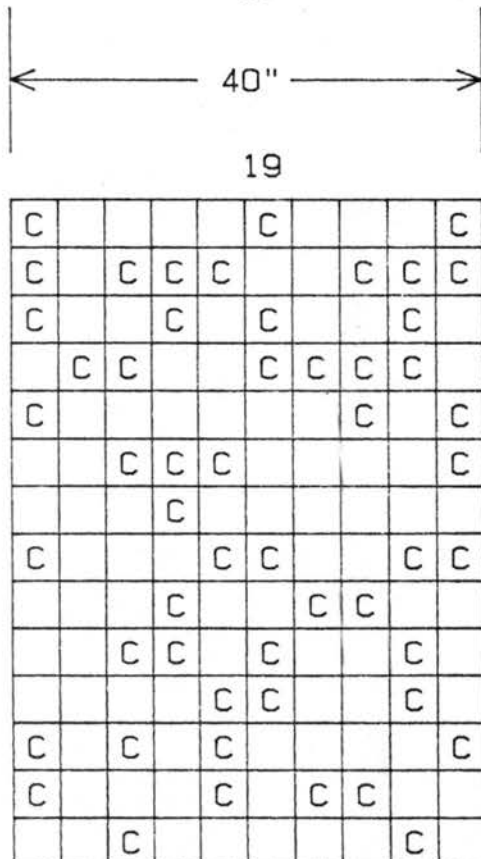
This appendix contains diagrams which depict the 20 cloud fields used in this study. Random cloud fields were generated using a computer routine which chose 54 random coordinates which correspond cloud placement locations. A "C" denotes a grid square upon which a cloud was placed. A blank square denotes a "clear" area. Dimensions of the cloud field grid are also shown. The number above or below the field (from 1 to 20) denotes cloud field number.



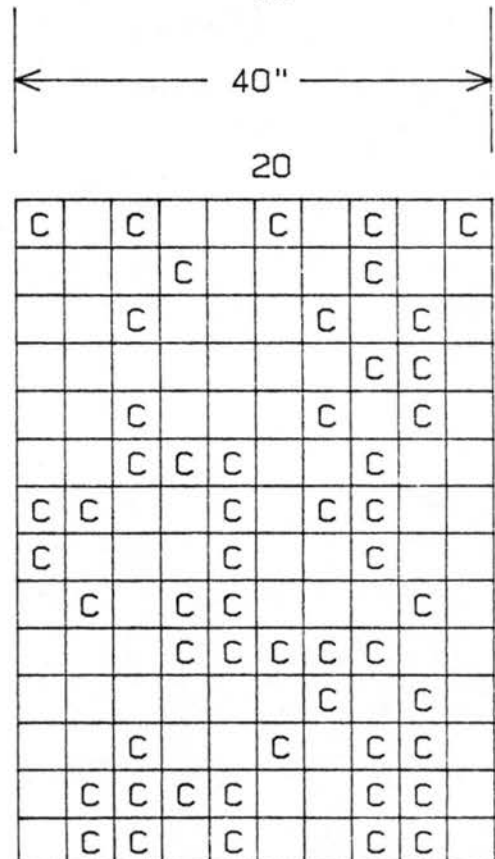
17



18



19



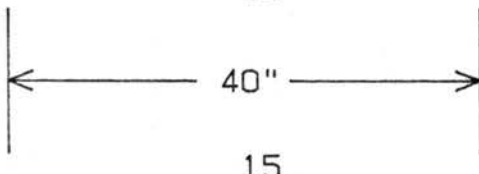
	C	C	C	C	C	C
C		C				
	C	C	C	C	C	
C		C	C	C		
	C	C	C	C	C	C
C	C			C		
C	C	C	C	C	C	
	C	C	C			
C	C		C	C		
C	C	C	C	C	C	
	C					
C	C	C	C	C	C	
	C					
C	C		C	C	C	

13

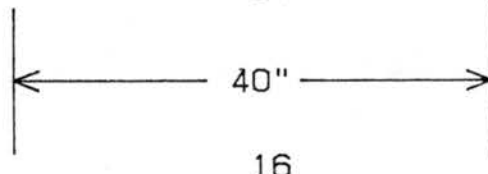
56"

			C	C		
C	C	C	C			C
	C	C	C	C	C	
C	C	C	C			
	C	C	C	C	C	C
C	C	C	C	C	C	C
	C	C	C	C	C	C
C	C	C	C	C	C	C
	C	C	C	C	C	C
C	C	C	C	C	C	C
	C	C	C	C	C	C
C	C	C	C	C	C	C

14



15



16

C		C	C	C		
C	C	C	C	C		
C	C	C	C		C	
C	C	C	C	C	C	
	C	C	C			
	C	C	C	C	C	
	C		C			
C	C	C	C			
	C	C	C	C		
C	C	C		C	C	
C	C	C	C	C	C	
	C		C	C	C	
C	C	C	C	C	C	

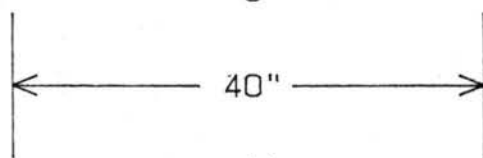
56"

C		C	C	C	C	C
C	C		C	C	C	
			C	C	C	C
C	C		C	C	C	C
			C	C	C	C
C	C		C	C	C	C
			C	C	C	C
C	C		C	C	C	C
C	C		C	C	C	C
C	C		C	C	C	C
	C	C	C	C	C	C
C	C		C	C	C	C

56"

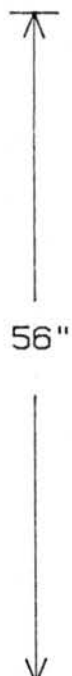
	C	C		C		C	C
C	C		C	C	C	C	
C		C				C	
C					C	C	
	C				C	C	C
		C			C	C	C
C	C	C		C			
		C	C		C	C	C
C	C	C	C				
		C	C		C	C	C
C	C	C	C				
C	C		C				
C	C		C				
C	C		C				
C	C		C				

9



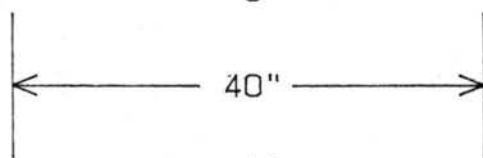
11

			C				
C		C	C		C	C	
		C			C		
C	C		C	C	C		
	C				C		
				C	C		
		C	C	C	C	C	C
C		C	C	C	C	C	C
	C	C	C	C	C	C	C
C	C	C	C	C	C	C	C
C	C	C	C	C	C	C	C
C	C	C	C	C	C	C	C
C	C	C	C	C	C	C	C
C	C	C	C	C	C	C	C
C	C	C	C	C	C	C	C
C	C	C	C	C	C	C	C
C	C	C	C	C	C	C	C



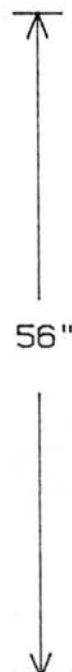
10

			C	C			
C	C	C	C	C	C	C	
	C	C					
C	C	C	C	C	C	C	
C		C			C		
	C	C	C	C	C	C	C
C	C	C	C	C	C	C	C
C	C	C	C	C	C	C	C
C	C	C	C	C	C	C	C
C	C	C	C	C	C	C	C
C	C	C	C	C	C	C	C
C	C	C	C	C	C	C	C
C	C	C	C	C	C	C	C
C	C	C	C	C	C	C	C
C	C	C	C	C	C	C	C



12

			C	C			
C	C	C	C	C	C	C	
	C	C					
C	C	C	C	C	C	C	
C		C			C		
	C	C	C	C	C	C	C
C	C	C	C	C	C	C	C
C	C	C	C	C	C	C	C
C	C	C	C	C	C	C	C
C	C	C	C	C	C	C	C
C	C	C	C	C	C	C	C
C	C	C	C	C	C	C	C
C	C	C	C	C	C	C	C
C	C	C	C	C	C	C	C
C	C	C	C	C	C	C	C
C	C	C	C	C	C	C	C
C	C	C	C	C	C	C	C

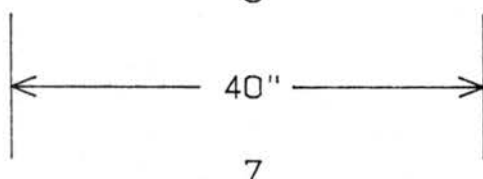


C	C	C	C			C	C	C
C		C	C			C		
C	C	C		C		C	C	C
C	C		C			C		
			C					
			C		C			
C	C	C				C		
C		C				C		
		C	C	C	C	C	C	C

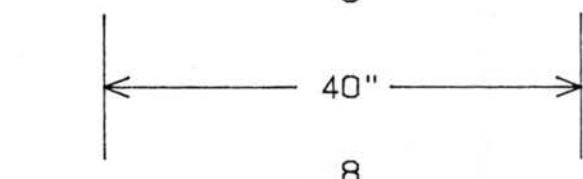
5

			C			C	C	C
C	C			C	C	C	C	C
	C	C	C	C	C	C	C	C
C	C	C		C		C	C	C
C	C	C				C		
C	C		C			C		
C	C	C	C	C	C	C	C	C
C	C	C		C		C	C	C
	C	C	C	C	C	C	C	C

6



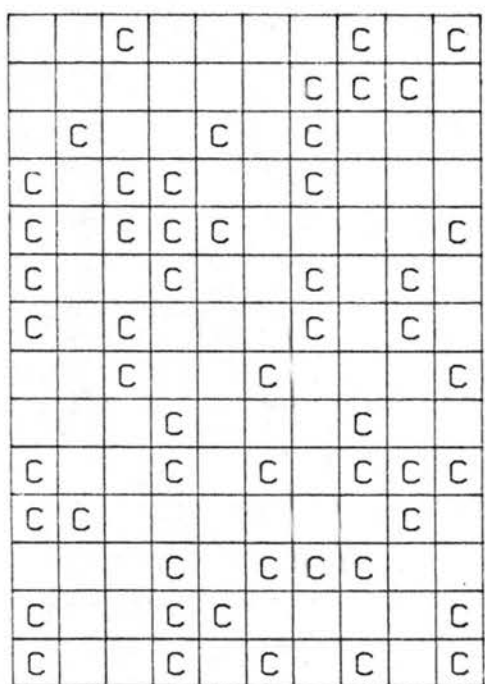
7



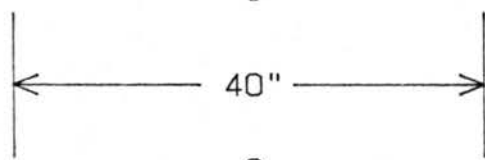
8

			C	C	C	C		C	C
C	C	C			C				
	C	C	C	C					
C	C		C	C	C				
	C		C	C	C				
C	C	C		C	C				
C	C	C	C	C	C				
C	C	C		C	C				
C	C	C	C	C	C				
	C	C	C	C	C				

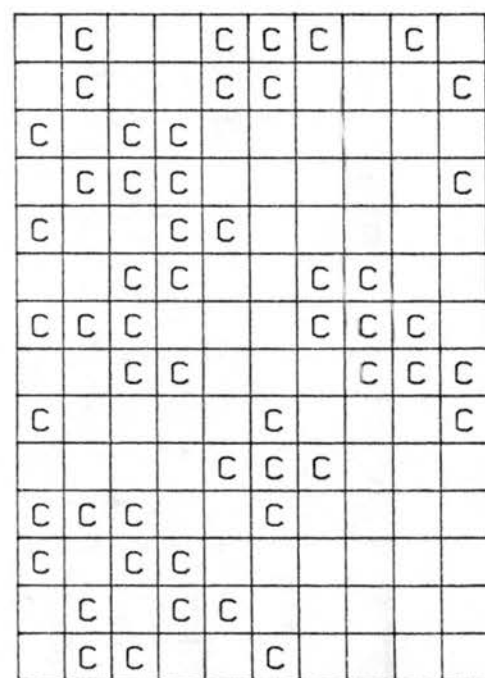
			C	C	C	C		C	C
C	C			C					
	C	C	C	C	C	C		C	C
C	C	C	C	C	C	C		C	C
C	C	C		C	C	C		C	C
C	C	C		C	C	C		C	C
C	C	C	C	C	C	C		C	C
C	C	C		C	C	C		C	C
C	C	C	C	C	C	C		C	C
C	C	C		C	C	C		C	C



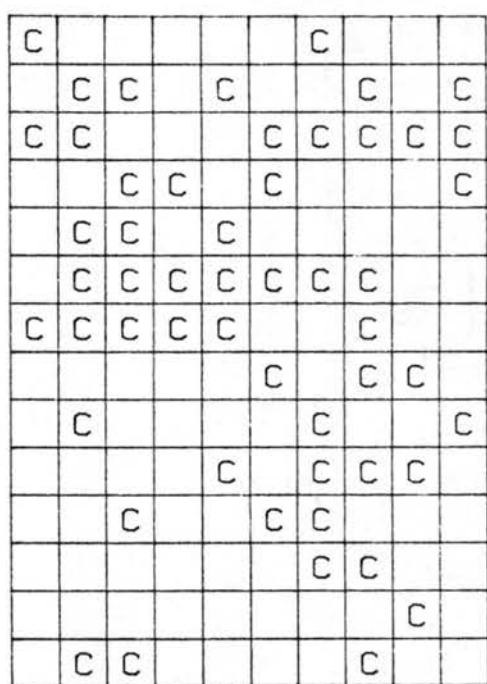
1



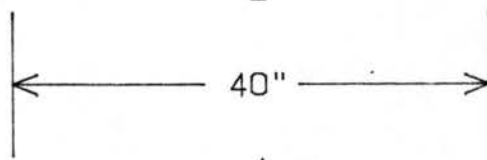
3



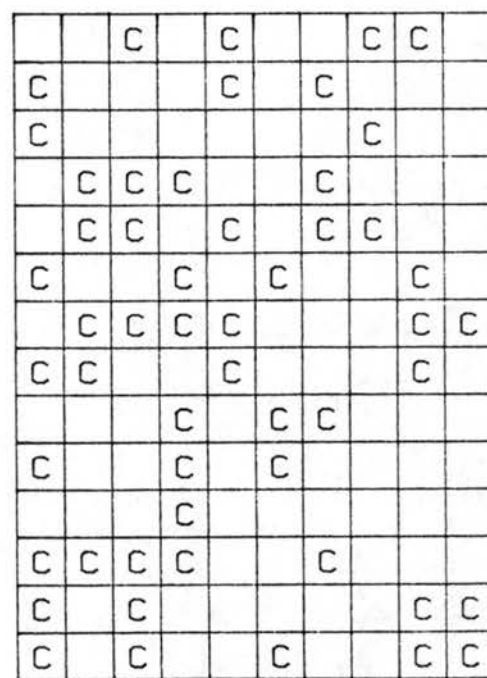
56"



2



4



Appendix C

RELATIVE IRRADIANCES AS A FUNCTION OF Θ_0 FOR 20 CLOUD FIELDS

The table shown in this appendix contains irradiances for each source zenith angle measured in each cloud field. Irradiances shown are relative to the irradiance calculated for a source zenith angle of $\Theta_0 = 0^\circ$ in each field. Columns represent source zenith angles and rows correspond to the cloud field number. Irradiances have been normalized to isolate the geometric dependence of cloud field on irradiances. Normalization procedures are discussed in detail in chapter four.

Table C.1: Irradiances relative to irradiances at $\Theta_0 = 0^\circ$.

$\Theta_0:$	-60°	-40°	-20°	0°	-20°	-40°	-60°
$\Phi:$	Φ_0				$\Phi_0 + 180^\circ$		
Field							
1	1.37	1.03	0.92	1.00	0.86	0.91	1.30
2	1.67	1.29	1.07	1.00	1.12	1.26	1.55
3	1.63	1.25	0.98	1.00	0.99	1.28	1.45
4	1.51	1.18	0.99	1.00	1.04	1.16	1.54
5	1.64	1.20	0.99	1.00	1.12	1.28	1.65
6	1.63	1.29	1.02	1.00	1.10	1.37	1.73
7	1.74	1.33	1.14	1.00	1.07	1.29	1.64
8	1.99	1.46	1.14	1.00	1.18	1.29	2.20
9	1.92	1.62	1.16	1.00	1.18	1.25	1.75
10	1.75	1.31	1.07	1.00	1.08	1.35	1.80
11	1.42	1.24	1.09	1.00	1.08	1.23	1.46
12	1.78	1.36	1.09	1.00	1.08	1.33	1.71
13	1.65	1.34	1.10	1.00	1.07	1.25	1.67
14	1.67	1.17	1.02	1.00	1.10	1.26	1.45
15	1.78	1.30	1.02	1.00	1.14	1.32	1.73
16	1.87	1.34	1.13	1.00	1.11	1.33	1.88
17	1.62	1.29	1.07	1.00	1.11	1.20	1.64
18	1.48	1.28	1.00	1.00	1.00	1.22	1.58
19	1.63	1.29	1.08	1.00	1.08	1.22	1.57
20	1.59	1.31	1.01	1.00	1.06	1.22	1.59
All	1.65	1.29	1.05	1.00	1.08	1.25	1.63

Appendix D

LOCATIONS OF ANISOTROPIC REFLECTANCE FACTORS FOR EACH CASE STUDY

This appendix contains tables representing frequencies of occurrence of anisotropic reflectance factors at location j,k for each source zenith angle and for each range of anisotropic reflectance factors studied. Each table represents one source zenith angle and one range of Γ . These are denoted at the top of each table. The values of Γ are calculated using equation (3.12). The values shown are the values of Γ expressed as percentages of the entire field. The letters j and k denote the detector arc scan number (refer to table 3.2) and photodiode number (table 3.1) respectively. One horizontal row corresponds to one photodiode and one vertical column corresponds to one detector arc scan.

Table D.1: $\Theta_0 = -60^\circ, \Phi = \Phi_0, \Gamma < -40\%$

j:	1	2	3	4	5	6	7	8	9	10	11	12	13
k													
1	0.00	0.00	0.00	0.00	0.20	0.20	0.20	0.59	0.59	0.59	0.79	0.39	0.20
2	0.00	0.00	0.00	0.20	0.20	0.20	0.20	0.59	0.79	0.79	0.79	0.79	0.20
3	0.00	0.00	0.00	0.00	0.20	0.39	0.79	0.99	1.78	1.58	1.78	1.38	0.39
4	0.00	0.00	0.00	0.00	0.20	0.20	0.39	0.59	1.18	1.58	1.38	1.18	0.79
5	0.00	0.00	0.00	0.00	0.20	0.39	0.79	1.38	1.58	1.97	1.58	0.99	0.59
6	0.00	0.00	0.00	0.00	0.20	0.39	0.59	1.78	2.17	1.97	1.58	1.38	1.18
7	0.00	0.00	0.00	0.00	0.20	0.39	0.79	1.38	1.97	1.78	1.78	1.97	1.38
8	0.00	0.00	0.00	0.00	0.00	0.39	0.99	1.58	1.97	1.97	2.17	1.97	1.97
9	0.00	0.00	0.00	0.00	0.20	0.79	0.99	1.18	1.58	1.97	1.38	0.99	0.59
10	0.00	0.00	0.00	0.20	0.59	0.59	0.79	0.99	1.18	0.99	0.79	0.39	0.39
11	0.00	0.00	0.00	0.00	0.00	0.20	0.59	0.59	0.99	0.99	1.18	0.79	0.59
12	0.00	0.00	0.00	0.00	0.00	0.00	0.00	0.59	0.39	0.79	0.99	0.79	0.39
13	0.00	0.00	0.00	0.00	0.00	0.20	0.39	0.59	0.59	0.39	0.39	0.39	0.00

Table D.2: $\Theta_0 = -60^\circ, \Phi = \Phi_0, -40\% \leq \Gamma < -20\%$

j:	1	2	3	4	5	6	7	8	9	10	11	12	13
k													
1	0.00	0.13	0.13	0.13	0.13	0.63	0.76	0.76	0.63	0.38	0.00	0.25	0.38
2	0.00	0.00	0.13	0.00	0.00	0.51	0.88	0.88	1.14	1.01	0.76	0.38	0.51
3	0.00	0.00	0.00	0.13	0.38	0.51	0.88	1.39	0.88	0.88	0.76	0.88	1.26
4	0.00	0.00	0.00	0.13	0.00	0.63	1.64	1.64	1.39	1.26	1.26	1.01	0.88
5	0.00	0.00	0.00	0.13	0.25	0.76	1.14	1.52	1.39	1.14	1.39	1.52	1.14
6	0.00	0.00	0.00	0.13	0.13	0.88	1.64	1.14	1.01	1.14	1.52	1.26	0.88
7	0.00	0.00	0.00	0.00	0.13	0.88	1.39	1.39	1.26	1.39	1.39	1.01	0.88
8	0.00	0.00	0.00	0.00	0.25	0.63	1.01	1.01	1.01	1.14	0.88	0.76	0.51
9	0.00	0.13	0.25	0.51	0.76	0.76	0.76	1.39	1.14	0.88	1.39	1.64	1.26
10	0.13	0.13	0.13	0.25	0.13	0.38	0.88	0.88	1.01	1.26	1.52	1.39	1.01
11	0.00	0.00	0.00	0.25	0.38	0.25	0.38	1.01	0.88	0.88	0.88	1.26	1.14
12	0.00	0.00	0.00	0.00	0.00	0.13	0.51	0.13	0.38	0.38	0.51	0.88	1.01
13	0.00	0.00	0.00	0.13	0.25	0.51	0.38	0.25	0.25	0.51	0.38	0.38	0.38

Table D.3: $\Theta_0 = -60^\circ, \Phi = \Phi_0, -20\% \leq \Gamma < 0\%$

j:	1	2	3	4	5	6	7	8	9	10	11	12	13
k													
1	0.16	0.00	0.33	0.65	0.98	0.65	0.65	0.33	0.65	0.98	1.31	0.65	0.00
2	0.00	0.16	0.16	0.82	1.31	1.14	1.31	0.98	0.65	0.82	1.14	1.31	1.14
3	0.00	0.00	0.00	0.65	0.98	1.63	1.14	0.65	0.65	0.82	0.65	0.82	0.82
4	0.00	0.00	0.00	0.00	1.47	1.80	0.82	0.65	0.49	0.33	0.49	0.82	1.14
5	0.00	0.00	0.00	0.33	0.65	1.63	1.14	0.16	0.16	0.16	0.16	0.33	0.98
6	0.00	0.00	0.16	0.33	1.31	1.47	0.65	0.33	0.16	0.16	0.00	0.33	0.98
7	0.00	0.00	0.00	0.16	0.82	1.47	0.82	0.33	0.00	0.00	0.00	0.16	0.65
8	0.00	0.00	0.00	0.00	0.98	1.31	0.98	0.65	0.33	0.16	0.33	0.65	0.49
9	0.33	0.16	0.16	0.49	0.49	0.82	0.98	0.33	0.49	0.49	0.33	0.33	0.82
10	0.16	0.00	0.16	0.49	0.98	1.14	1.14	1.14	0.98	0.82	0.65	1.14	0.98
11	0.00	0.00	0.16	0.49	0.82	1.47	1.63	0.98	0.82	0.98	0.82	0.65	0.82
12	0.00	0.00	0.00	0.00	0.65	1.14	0.98	1.14	1.47	1.47	1.14	0.98	1.14
13	0.00	0.00	0.33	0.33	0.49	0.00	0.16	0.65	0.65	0.65	1.31	1.31	1.31

Table D.4: $\Theta_0 = -60^\circ, \Phi = \Phi_0, 0\% \leq \Gamma < 20\%$

j:	1	2	3	4	5	6	7	8	9	10	11	12	13
k													
1	0.23	0.47	0.70	0.70	0.70	0.47	0.93	1.40	1.17	1.40	1.40	1.87	1.64
2	0.47	0.47	1.40	0.93	0.93	1.17	0.47	0.47	0.47	0.47	0.47	0.93	1.64
3	0.00	0.00	1.40	0.70	1.87	0.93	0.47	0.00	0.00	0.00	0.23	0.23	0.70
4	0.00	0.00	0.70	1.87	2.34	0.70	0.00	0.00	0.00	0.00	0.00	0.23	0.23
5	0.23	0.00	1.17	1.40	2.34	0.47	0.00	0.00	0.00	0.00	0.00	0.23	0.23
6	0.00	0.00	0.70	1.40	2.10	0.47	0.00	0.00	0.00	0.00	0.00	0.23	0.00
7	0.00	0.00	0.00	1.87	2.57	0.47	0.00	0.00	0.00	0.00	0.00	0.23	0.23
8	0.00	0.00	0.23	1.87	1.40	1.17	0.23	0.00	0.00	0.00	0.00	0.00	0.47
9	0.00	0.00	0.93	0.23	1.17	0.93	0.70	0.23	0.00	0.00	0.00	0.00	0.47
10	0.23	0.70	1.17	0.70	0.70	1.64	0.47	0.23	0.00	0.00	0.00	0.00	0.93
11	0.47	0.70	0.93	1.17	1.40	1.40	0.70	0.70	0.47	0.23	0.23	0.23	0.47
12	0.00	0.00	0.47	1.17	1.17	1.17	1.40	1.64	0.93	0.47	0.47	0.47	0.23
13	0.00	0.70	0.23	0.93	0.70	1.40	2.10	1.40	1.64	1.40	0.47	0.47	0.70

Table D.5: $\Theta_0 = -60^\circ, \Phi = \Phi_0, 20\% \leq \Gamma < 40\%$

j:	1	2	3	4	5	6	7	8	9	10	11	12	13
k													
1	0.58	0.87	0.58	1.45	1.16	1.74	0.87	0.58	0.58	0.29	0.00	0.58	1.45
2	0.58	1.16	0.29	1.45	1.45	0.58	0.58	0.58	0.29	0.29	0.29	0.29	0.29
3	1.16	1.45	0.87	3.19	0.58	0.00	0.00	0.00	0.00	0.00	0.00	0.00	0.00
4	1.16	0.58	2.32	3.19	0.00	0.00	0.00	0.00	0.00	0.00	0.00	0.00	0.29
5	0.58	1.16	1.16	2.32	0.87	0.00	0.00	0.00	0.00	0.00	0.00	0.00	0.00
6	0.29	1.16	1.16	3.19	0.29	0.00	0.00	0.00	0.00	0.00	0.00	0.00	0.00
7	0.29	0.00	2.61	3.19	0.58	0.00	0.00	0.00	0.00	0.00	0.00	0.00	0.00
8	0.29	0.29	1.74	2.03	1.45	0.00	0.00	0.00	0.00	0.00	0.00	0.00	0.29
9	0.29	1.16	0.58	1.74	1.16	0.29	0.00	0.00	0.00	0.00	0.00	0.00	0.00
10	0.58	0.29	0.29	1.45	2.03	0.00	0.00	0.00	0.00	0.00	0.00	0.00	0.00
11	0.29	0.87	0.58	1.45	1.45	0.58	0.29	0.00	0.29	0.29	0.29	0.29	0.29
12	0.58	0.58	1.74	1.74	2.32	2.03	1.16	0.29	0.29	0.29	0.29	0.00	0.58
13	0.87	0.58	1.74	1.45	2.03	1.45	0.58	0.87	0.58	0.58	0.87	0.58	0.58

Table D.6: $\Theta_0 = -60^\circ, \Phi = \Phi_0, 40\% \leq \Gamma < 60\%$

j:	1	2	3	4	5	6	7	8	9	10	11	12	13
k													
1	1.50	0.38	1.88	1.50	0.75	0.38	0.75	0.38	0.38	0.38	0.75	0.75	1.50
2	2.26	1.50	1.88	0.75	0.75	0.38	0.00	0.00	0.00	0.00	0.00	0.00	0.00
3	1.13	1.13	2.63	0.38	0.00	0.00	0.00	0.00	0.00	0.00	0.00	0.00	0.00
4	0.38	2.63	2.26	0.00	0.00	0.00	0.00	0.00	0.00	0.00	0.00	0.00	0.00
5	0.75	1.13	1.88	1.13	0.00	0.00	0.00	0.00	0.00	0.00	0.00	0.00	0.38
6	1.50	1.88	3.38	0.00	0.00	0.00	0.00	0.00	0.00	0.00	0.00	0.00	0.38
7	0.00	2.26	3.76	0.00	0.00	0.00	0.00	0.00	0.00	0.00	0.00	0.00	0.38
8	0.38	1.13	3.38	1.88	0.38	0.00	0.00	0.00	0.00	0.00	0.00	0.00	0.00
9	0.38	1.13	1.13	1.50	0.38	0.00	0.00	0.00	0.00	0.00	0.00	0.00	0.00
10	1.13	2.26	2.63	2.26	0.00	0.00	0.00	0.00	0.00	0.00	0.00	0.00	0.00
11	1.88	0.75	3.38	1.13	0.38	0.00	0.00	0.00	0.00	0.00	0.00	0.00	0.00
12	1.50	3.01	3.01	3.01	1.13	0.00	0.00	0.38	0.38	0.38	0.00	0.00	0.00
13	1.88	1.88	1.50	1.13	1.13	0.75	0.75	0.38	0.38	0.38	0.38	0.38	0.75

Table D.7: $\Theta_0 = -60^\circ, \Phi = \Phi_0, \Gamma > 60\%$

j:	1	2	3	4	5	6	7	8	9	10	11	12	13
k													
1	2.78	3.02	1.62	0.70	0.70	0.23	0.00	0.00	0.00	0.00	0.00	0.00	0.00
2	2.32	2.09	1.39	0.70	0.00	0.00	0.00	0.00	0.00	0.00	0.00	0.00	0.00
3	3.02	2.78	0.93	0.00	0.00	0.00	0.00	0.00	0.00	0.00	0.00	0.00	0.00
4	3.48	2.55	0.70	0.00	0.00	0.00	0.00	0.00	0.00	0.00	0.00	0.00	0.00
5	3.48	3.02	1.39	0.00	0.00	0.00	0.00	0.00	0.00	0.00	0.00	0.00	0.00
6	3.48	2.55	0.70	0.00	0.00	0.00	0.00	0.00	0.00	0.00	0.00	0.00	0.00
7	4.41	3.25	0.23	0.00	0.00	0.00	0.00	0.00	0.00	0.00	0.00	0.00	0.00
8	4.18	3.71	0.93	0.00	0.00	0.00	0.00	0.00	0.00	0.00	0.00	0.00	0.00
9	3.71	2.55	1.86	0.46	0.00	0.00	0.00	0.00	0.00	0.00	0.00	0.00	0.00
10	2.78	2.09	1.16	0.00	0.00	0.00	0.00	0.00	0.00	0.00	0.00	0.00	0.00
11	2.78	2.78	0.93	0.46	0.00	0.00	0.00	0.00	0.00	0.00	0.00	0.00	0.00
12	3.25	2.32	0.93	0.23	0.00	0.00	0.00	0.00	0.00	0.00	0.23	0.23	0.00
13	2.78	2.32	1.62	1.16	0.46	0.46	0.23	0.23	0.23	0.23	0.23	0.46	0.46

Table D.8: $\Theta_0 = -60^\circ, \Phi = \Phi_0, -5\% \leq \Gamma \leq 5\%$

j:	1	2	3	4	5	6	7	8	9	10	11	12	13
k													
1	0.76	0.00	0.00	0.00	1.52	0.76	1.52	0.00	0.76	0.00	0.00	0.00	0.00
2	1.52	0.00	0.00	1.52	1.52	0.00	0.76	0.00	0.00	1.52	0.76	0.76	0.00
3	0.76	0.00	0.00	0.00	0.76	3.03	0.76	1.52	0.00	0.76	1.52	1.52	0.76
4	1.52	0.00	0.00	0.00	0.00	0.00	1.52	2.27	0.00	0.00	0.76	0.00	0.00
5	0.76	0.00	0.00	0.00	1.52	1.52	0.76	1.52	0.00	0.76	1.52	1.52	0.76
6	0.00	0.00	0.00	2.27	1.52	0.00	0.00	0.00	0.00	0.00	0.00	0.00	0.00
7	0.00	0.00	0.00	0.76	3.03	0.76	0.00	2.27	1.52	0.76	1.52	1.52	1.52
8	0.00	0.00	0.00	0.76	1.52	0.00	0.76	0.00	0.00	0.00	0.00	0.00	0.00
9	0.76	0.76	0.00	0.00	2.27	0.76	0.00	0.00	0.00	0.00	0.00	0.00	0.00
10	0.00	0.00	0.00	0.76	2.27	1.52	0.00	0.76	0.76	0.76	0.76	1.52	0.00
11	0.76	0.76	0.76	0.76	3.79	0.76	0.76	0.76	0.76	0.76	0.76	0.00	0.76
12	0.00	0.00	0.76	0.00	1.52	1.52	1.52	0.00	0.00	0.00	0.00	0.00	0.76
13	0.00	0.00	0.76	0.76	1.52	0.76	0.00	0.76	0.76	0.00	0.00	0.00	0.76

Table D.9: $\Theta_0 = -60^\circ, \Phi = \Phi_0, -10\% \leq \Gamma \leq 10\%$

j:	1	2	3	4	5	6	7	8	9	10	11	12	13
k													
1	0.38	0.00	0.00	0.38	0.76	0.76	1.53	0.76	0.38	0.38	0.00	0.00	0.00
2	0.76	0.38	0.00	1.15	1.15	0.38	1.15	0.38	0.76	0.76	0.76	0.76	0.38
3	0.76	0.00	0.00	0.00	0.38	2.29	0.76	0.76	0.76	1.15	1.15	1.15	1.15
4	0.76	0.00	0.00	0.38	0.00	0.76	2.29	1.53	1.15	1.15	0.38	0.00	0.76
5	0.38	0.38	0.00	0.38	1.53	1.15	0.76	0.76	1.15	0.76	0.76	0.76	0.38
6	0.38	0.00	0.00	1.15	2.29	0.76	0.00	0.38	0.00	0.38	0.38	0.00	0.00
7	0.00	0.00	0.00	0.76	1.53	0.38	0.00	1.15	1.15	1.53	1.15	1.15	1.15
8	0.00	0.00	0.00	0.76	1.15	1.15	0.38	0.38	0.00	0.00	0.00	0.00	0.38
9	0.38	0.38	0.38	0.38	1.53	0.76	0.00	0.38	0.00	0.00	0.00	0.76	0.38
10	0.00	0.00	0.00	0.76	2.67	0.76	0.38	0.38	0.38	0.38	0.38	1.15	0.38
11	0.38	0.38	0.38	0.76	2.67	1.91	0.38	0.38	0.38	0.38	0.38	0.38	1.15
12	0.00	0.00	0.38	0.76	1.53	1.53	1.15	0.38	0.00	0.00	0.38	0.38	1.15
13	0.00	0.00	0.38	0.76	1.53	1.53	1.15	0.38	0.38	0.38	0.00	0.00	0.38

Table D.10: $\Theta_0 = -40^\circ, \Phi = \Phi_0, \Gamma < -40\%$

j:	1	2	3	4	5	6	7	8	9	10	11	12	13
k													
1	0.00	0.00	0.00	0.00	0.00	0.00	0.00	0.00	0.00	0.70	0.70	0.00	0.00
2	0.00	0.00	0.00	0.00	0.00	0.00	0.70	0.70	1.40	2.10	2.10	0.70	0.70
3	0.00	0.00	0.00	0.00	0.00	0.00	0.70	0.70	2.10	2.10	2.10	2.10	1.40
4	0.00	0.00	0.00	0.00	0.00	0.00	0.00	0.70	0.00	0.70	0.70	0.70	0.70
5	0.00	0.00	0.00	0.00	0.00	0.00	0.70	0.70	0.70	0.70	0.00	1.40	1.40
6	0.00	0.00	0.00	0.00	0.00	0.00	0.70	0.70	2.10	2.10	2.10	2.80	2.10
7	0.00	0.00	0.00	0.00	0.00	0.00	0.00	2.80	3.50	3.50	4.20	2.80	2.80
8	0.00	0.00	0.00	0.00	0.00	0.00	0.70	2.10	2.80	2.10	4.20	4.20	2.10
9	0.00	0.00	0.00	0.00	0.00	0.00	1.40	2.10	2.10	2.10	0.70	0.00	0.00
10	0.00	0.00	0.70	0.00	0.70	1.40	1.40	2.10	0.00	0.00	0.00	0.00	0.70
11	0.00	0.00	0.00	0.00	0.00	0.00	0.00	0.00	0.00	0.00	0.00	1.40	0.70
12	0.00	0.00	0.00	0.00	0.00	0.00	0.00	0.00	0.00	0.70	0.70	0.70	0.00
13	0.00	0.00	0.00	0.00	0.00	0.00	0.00	0.00	0.00	0.00	0.00	0.00	0.00

Table D.11: $\Theta_0 = -40^\circ, \Phi = \Phi_0, -40\% \leq \Gamma < -20\%$

j:	1	2	3	4	5	6	7	8	9	10	11	12	13
k													
1	0.00	0.00	0.20	0.00	0.00	0.20	0.59	0.59	0.59	0.39	0.39	0.59	0.39
2	0.00	0.00	0.00	0.20	0.20	0.20	0.59	0.79	0.79	0.79	0.39	0.59	0.39
3	0.00	0.00	0.00	0.00	0.00	0.59	0.99	1.58	1.18	1.38	1.58	0.99	0.59
4	0.00	0.00	0.00	0.00	0.00	0.20	0.79	1.38	1.78	1.78	1.58	1.38	1.18
5	0.00	0.00	0.00	0.00	0.00	0.20	0.39	1.58	2.17	2.17	2.17	0.79	0.59
6	0.00	0.00	0.00	0.00	0.20	0.39	0.79	1.58	1.58	1.97	1.58	0.79	0.79
7	0.00	0.00	0.00	0.00	0.00	0.00	1.18	1.38	1.18	1.38	0.99	1.38	0.99
8	0.00	0.00	0.00	0.00	0.00	0.39	0.59	1.18	1.18	1.97	1.38	0.99	1.18
9	0.00	0.00	0.39	0.39	0.79	1.18	0.99	0.99	1.18	1.78	1.78	1.38	0.99
10	0.00	0.20	0.00	0.39	0.20	0.00	0.59	0.79	1.58	1.38	1.18	0.59	0.39
11	0.00	0.00	0.00	0.00	0.20	0.39	0.59	0.99	1.38	1.18	1.18	0.59	0.59
12	0.00	0.00	0.00	0.00	0.00	0.00	0.00	0.59	0.79	0.39	0.79	0.59	0.59
13	0.00	0.00	0.00	0.00	0.20	0.20	0.59	0.79	0.79	0.79	0.99	0.59	0.20

Table D.12: $\Theta_0 = -40^\circ, \Phi = \Phi_0, -20\% \leq \Gamma < 0\%$

j:	1	2	3	4	5	6	7	8	9	10	11	12	13
k													
1	0.00	0.14	0.29	0.57	0.57	0.71	0.57	0.86	0.71	0.57	0.43	0.14	0.14
2	0.00	0.00	0.29	0.14	0.29	1.14	1.28	1.14	0.86	0.57	0.86	0.86	0.14
3	0.00	0.00	0.14	0.14	0.57	1.00	1.00	0.86	0.86	0.57	0.29	0.71	0.86
4	0.00	0.00	0.00	0.00	0.43	1.00	1.28	1.00	1.00	0.86	1.00	0.57	0.71
5	0.00	0.00	0.29	0.29	0.57	0.86	1.14	1.14	1.14	1.00	1.00	1.57	0.71
6	0.00	0.00	0.14	0.14	0.43	1.00	1.43	1.43	1.28	1.00	0.86	1.28	0.86
7	0.00	0.00	0.00	0.00	0.14	1.14	1.00	1.00	1.28	1.14	1.00	0.86	0.57
8	0.00	0.00	0.00	0.00	0.29	0.57	1.14	1.14	1.00	0.71	0.57	0.86	0.71
9	0.14	0.29	0.29	0.43	0.43	0.43	0.57	1.14	1.14	0.71	1.14	1.71	1.00
10	0.14	0.00	0.29	0.14	0.29	0.57	0.86	0.71	0.86	1.00	1.43	1.57	0.86
11	0.00	0.00	0.57	0.29	0.43	0.71	1.00	1.14	0.86	1.14	1.28	1.14	1.00
12	0.00	0.00	0.14	0.00	0.14	0.43	0.71	0.29	0.29	0.57	0.57	1.14	1.00
13	0.00	0.00	0.00	0.29	0.43	0.43	0.43	0.29	0.43	0.57	0.29	0.57	0.57

Table D.13: $\Theta_0 = -40^\circ, \Phi = \Phi_0, 0\% \leq \Gamma < 20\%$

j:	1	2	3	4	5	6	7	8	9	10	11	12	13
k													
1	0.33	0.33	0.33	0.16	0.66	0.66	0.49	0.66	0.82	0.99	0.99	0.33	0.33
2	0.00	0.33	0.66	0.82	1.15	0.66	0.16	0.33	0.66	0.82	0.66	0.49	0.99
3	0.00	0.00	0.66	0.33	0.99	1.15	0.82	0.66	0.66	0.66	0.82	0.49	0.82
4	0.00	0.00	0.66	0.66	1.32	1.48	1.15	0.82	0.66	0.66	0.49	0.99	0.66
5	0.16	0.33	0.66	0.66	0.82	1.32	1.48	0.49	0.00	0.16	0.33	0.33	1.15
6	0.00	0.16	0.33	0.49	0.82	1.48	0.82	0.16	0.00	0.00	0.49	0.33	0.82
7	0.00	0.00	0.16	0.33	1.81	1.64	1.15	0.33	0.00	0.00	0.33	0.49	0.66
8	0.00	0.00	0.16	0.33	1.48	1.15	1.15	0.49	0.49	0.33	0.49	0.49	0.49
9	0.16	0.00	0.33	0.33	0.33	0.66	0.99	0.33	0.33	0.33	0.16	0.16	1.15
10	0.16	0.49	0.49	0.16	0.82	1.15	0.82	1.15	0.99	0.99	0.66	0.82	1.48
11	0.00	0.16	0.33	0.49	0.66	0.66	1.15	0.66	0.82	0.66	0.33	0.82	0.99
12	0.00	0.00	0.16	0.33	0.66	0.66	0.66	1.64	1.48	1.32	0.99	0.49	0.82
13	0.00	0.16	0.99	0.49	0.49	0.66	0.66	0.82	0.66	0.33	0.49	0.66	0.99

Table D.14: $\Theta_0 = -40^\circ, \Phi = \Phi_0, 20\% \leq \Gamma < 40\%$

j:	1	2	3	4	5	6	7	8	9	10	11	12	13
k													
1	0.22	0.22	0.22	0.65	0.43	0.65	0.87	0.22	0.65	0.65	0.65	1.52	0.22
2	0.43	0.65	0.65	0.65	1.09	0.65	0.65	0.65	0.43	0.43	0.65	1.09	1.74
3	0.00	0.43	0.87	1.96	1.74	0.43	0.22	0.22	0.22	0.43	0.43	0.65	0.43
4	0.22	0.43	1.09	2.17	1.74	0.65	0.00	0.00	0.00	0.00	0.22	0.22	0.43
5	0.00	0.22	0.87	1.30	1.74	1.09	0.00	0.00	0.00	0.00	0.00	0.22	0.22
6	0.00	0.22	1.74	1.30	2.17	0.43	0.00	0.00	0.00	0.00	0.00	0.22	0.00
7	0.00	0.00	1.96	2.39	1.30	0.43	0.00	0.00	0.00	0.00	0.00	0.00	0.43
8	0.00	0.00	1.74	1.96	1.09	1.52	0.22	0.00	0.00	0.00	0.00	0.00	0.65
9	0.22	0.65	0.65	0.65	1.09	1.09	0.22	0.43	0.22	0.22	0.22	0.00	0.22
10	0.22	0.22	0.65	1.52	1.30	0.87	0.87	0.22	0.00	0.00	0.00	0.22	0.22
11	0.43	1.09	0.87	0.87	1.52	1.30	0.43	0.43	0.43	0.22	0.43	0.00	0.22
12	0.00	0.43	1.09	1.09	0.87	1.96	1.74	0.65	0.65	0.65	0.65	0.65	0.43
13	0.43	1.09	0.87	1.09	0.65	0.65	0.87	0.87	0.87	1.30	1.30	0.65	0.43

Table D.15: $\Theta_0 = -40^\circ, \Phi = \Phi_0, 40\% \leq \Gamma < 60\%$

j:	1	2	3	4	5	6	7	8	9	10	11	12	13
k													
1	0.30	0.30	1.19	1.49	1.49	0.89	0.89	1.19	0.60	0.60	0.89	1.19	2.38
2	0.89	0.30	1.19	1.49	0.60	0.30	0.60	0.30	0.60	0.60	0.60	0.60	0.30
3	0.89	1.79	2.38	1.79	0.30	0.30	0.30	0.00	0.00	0.00	0.00	0.30	0.60
4	0.30	1.19	2.08	1.49	0.30	0.00	0.00	0.00	0.00	0.00	0.00	0.30	0.30
5	0.60	1.49	1.49	1.19	0.89	0.00	0.00	0.00	0.00	0.00	0.00	0.00	0.30
6	0.60	1.19	1.79	2.68	0.30	0.00	0.00	0.00	0.00	0.00	0.00	0.00	0.30
7	0.00	0.89	1.49	1.79	0.60	0.00	0.00	0.00	0.00	0.00	0.00	0.00	0.30
8	0.00	0.89	1.49	2.08	1.19	0.00	0.00	0.00	0.00	0.00	0.00	0.00	0.00
9	0.00	0.60	1.49	1.49	1.19	0.60	0.60	0.00	0.00	0.00	0.00	0.00	0.00
10	0.30	0.89	0.89	1.49	0.60	0.89	0.00	0.00	0.00	0.00	0.00	0.00	0.30
11	0.60	0.00	0.30	0.89	0.30	0.89	0.30	0.30	0.00	0.30	0.30	0.30	0.60
12	0.89	1.19	1.79	2.68	3.27	1.19	0.89	0.60	0.30	0.00	0.00	0.00	0.60
13	1.49	0.89	0.30	0.30	1.19	1.49	0.60	1.19	1.19	0.60	0.30	0.89	0.00

Table D.16: $\Theta_0 = -40^\circ, \Phi = \Phi_0, \Gamma > 60\%$

j:	1	2	3	4	5	6	7	8	9	10	11	12	13
k													
1	2.56	2.40	1.60	1.12	0.80	0.64	0.48	0.32	0.32	0.32	0.32	0.48	0.96
2	2.40	2.24	1.12	0.80	0.48	0.48	0.16	0.16	0.00	0.00	0.00	0.00	0.16
3	2.72	1.92	0.48	0.32	0.16	0.00	0.00	0.00	0.00	0.00	0.00	0.00	0.00
4	2.88	2.24	0.64	0.16	0.00	0.00	0.00	0.00	0.00	0.00	0.00	0.00	0.16
5	2.72	1.92	0.80	0.64	0.00	0.00	0.00	0.00	0.00	0.00	0.00	0.00	0.16
6	2.88	2.24	0.48	0.16	0.00	0.00	0.00	0.00	0.00	0.00	0.00	0.00	0.16
7	3.20	2.72	0.80	0.16	0.00	0.00	0.00	0.00	0.00	0.00	0.00	0.00	0.00
8	3.20	2.72	0.96	0.32	0.00	0.00	0.00	0.00	0.00	0.00	0.00	0.00	0.00
9	2.72	2.08	0.96	0.80	0.32	0.00	0.00	0.00	0.00	0.00	0.00	0.00	0.00
10	2.56	1.92	1.28	0.64	0.48	0.00	0.00	0.00	0.00	0.00	0.00	0.00	0.00
11	2.56	2.24	1.44	1.28	0.64	0.00	0.00	0.00	0.00	0.00	0.00	0.16	0.00
12	2.72	2.24	1.12	0.64	0.00	0.00	0.00	0.00	0.16	0.32	0.32	0.32	0.16
13	2.08	1.76	1.44	1.44	0.96	0.64	0.64	0.16	0.16	0.32	0.48	0.48	1.12

Table D.17: $\Theta_0 = -40^\circ, \Phi = \Phi_0, -5\% \leq \Gamma \leq 5\%$

j:	1	2	3	4	5	6	7	8	9	10	11	12	13
k													
1	0.00	0.00	0.00	0.54	1.09	0.54	1.09	1.09	1.09	1.09	0.54	0.54	1.09
2	1.09	0.00	0.00	0.54	1.09	1.09	0.54	0.54	0.00	0.00	0.00	0.00	1.09
3	0.54	0.00	0.00	0.00	0.00	0.54	0.54	2.17	1.63	0.54	0.54	0.00	0.54
4	0.00	0.00	0.00	0.00	0.00	0.00	0.00	0.00	1.09	0.54	0.54	1.09	1.09
5	1.63	0.54	0.00	0.00	0.54	0.00	0.54	0.00	0.54	0.54	1.09	0.54	1.09
6	0.54	0.00	0.00	1.09	0.54	1.09	1.09	1.63	1.09	0.54	0.54	0.54	0.54
7	0.54	0.00	0.00	0.00	0.54	1.63	2.17	0.54	1.09	1.09	1.09	1.09	0.00
8	0.00	0.00	0.00	0.00	0.54	1.63	0.00	0.00	0.00	0.54	0.00	0.00	0.00
9	0.00	0.54	0.54	0.00	0.54	1.09	1.63	0.00	0.54	1.09	0.54	0.54	1.09
10	0.00	0.00	0.00	0.00	0.54	1.09	1.63	1.09	1.09	1.09	0.54	0.54	0.54
11	0.00	0.00	0.00	0.00	0.00	1.09	1.09	0.54	1.09	0.54	1.09	1.63	1.09
12	0.00	0.00	0.00	0.54	0.00	0.00	2.72	1.09	1.09	1.09	1.09	1.09	1.09
13	0.00	0.00	0.00	0.54	0.00	1.09	2.17	1.63	1.09	0.54	0.54	1.09	2.17

Table D.18: $\Theta_0 = -40^\circ$, $\Phi = \Phi_0$, $-10\% \leq \Gamma \leq 10\%$

j:	1	2	3	4	5	6	7	8	9	10	11	12	13
k													
1	0.85	0.00	0.00	0.28	0.57	0.28	1.42	0.85	1.14	0.57	0.57	0.85	0.57
2	0.85	0.00	0.00	0.57	0.85	0.57	0.85	0.85	0.57	0.28	0.28	0.57	0.85
3	0.28	0.00	0.00	0.28	0.28	0.28	0.85	1.42	1.14	0.57	0.57	0.85	0.85
4	0.00	0.00	0.00	0.28	0.00	0.28	0.28	0.28	1.14	1.42	0.57	0.85	0.57
5	0.85	0.28	0.00	0.28	0.28	0.57	0.57	0.57	0.28	0.57	0.57	0.57	1.14
6	1.14	0.00	0.00	0.57	0.57	0.85	0.85	0.85	1.14	0.85	0.57	0.57	0.85
7	0.28	0.00	0.00	0.28	0.28	1.14	1.42	0.85	1.14	1.71	1.14	0.57	0.57
8	0.28	0.00	0.00	0.00	0.57	1.14	0.28	0.57	0.28	0.28	0.28	0.00	0.28
9	0.28	0.28	0.28	0.28	0.85	0.57	0.85	0.57	0.57	0.57	0.28	0.28	0.85
10	0.28	0.00	0.00	0.28	0.85	1.42	1.42	0.85	0.85	0.85	0.57	0.28	0.57
11	0.00	0.00	0.00	0.00	0.00	1.14	1.42	1.14	1.14	0.85	1.42	1.42	0.57
12	0.00	0.00	0.28	0.28	0.28	0.57	1.71	1.14	1.14	1.42	0.85	0.85	0.57
13	0.00	0.00	0.00	0.28	0.28	1.14	1.71	1.71	1.14	0.85	0.57	1.14	1.14

Table D.19: $\Theta_0 = -20^\circ, \Phi = \Phi_0, \Gamma < -40\%$

j:	1	2	3	4	5	6	7	8	9	10	11	12	13
k													
1	0.00	0.00	0.00	0.00	0.00	0.00	0.00	0.00	0.00	0.00	0.00	0.00	0.00
2	0.00	0.00	0.00	0.00	0.00	0.00	0.00	0.00	0.00	0.00	2.22	0.00	0.00
3	0.00	0.00	0.00	0.00	0.00	0.00	0.00	2.22	2.22	0.00	2.22	4.44	2.22
4	0.00	0.00	0.00	0.00	0.00	0.00	0.00	0.00	0.00	0.00	0.00	2.22	0.00
5	0.00	0.00	0.00	0.00	0.00	0.00	0.00	0.00	0.00	0.00	0.00	0.00	0.00
6	0.00	0.00	0.00	0.00	0.00	0.00	2.22	2.22	0.00	0.00	0.00	0.00	4.44
7	0.00	0.00	0.00	0.00	0.00	0.00	0.00	0.00	0.00	0.00	2.22	2.22	4.44
8	0.00	0.00	0.00	0.00	0.00	0.00	0.00	0.00	2.22	4.44	2.22	6.67	6.67
9	0.00	0.00	2.22	2.22	2.22	0.00	0.00	0.00	0.00	0.00	0.00	0.00	0.00
10	0.00	2.22	2.22	4.44	4.44	4.44	2.22	4.44	4.44	0.00	0.00	0.00	0.00
11	0.00	0.00	0.00	0.00	0.00	0.00	0.00	0.00	0.00	0.00	0.00	0.00	2.22
12	0.00	0.00	0.00	0.00	0.00	0.00	0.00	0.00	0.00	0.00	2.22	2.22	0.00
13	0.00	0.00	0.00	0.00	0.00	0.00	0.00	0.00	0.00	0.00	0.00	0.00	0.00

Table D.20: $\Theta_0 = -20^\circ, \Phi = \Phi_0, -40\% \leq \Gamma < -20\%$

j:	1	2	3	4	5	6	7	8	9	10	11	12	13
k													
1	0.33	0.33	0.33	0.33	0.98	0.33	0.33	0.00	0.33	0.66	0.33	0.00	0.00
2	0.00	0.00	0.00	0.00	0.66	0.66	0.66	0.66	1.97	1.64	0.66	0.98	0.33
3	0.00	0.00	0.00	0.00	0.98	0.98	0.98	0.66	1.64	1.64	0.98	0.66	0.33
4	0.00	0.00	0.00	0.00	0.66	0.66	0.66	0.66	1.31	0.98	0.66	0.66	0.98
5	0.00	0.00	0.00	0.66	0.98	0.98	0.66	0.66	0.66	0.98	0.66	0.66	0.98
6	0.00	0.00	0.00	0.66	0.66	0.66	0.33	0.66	1.31	1.97	1.31	1.31	0.66
7	0.00	0.00	0.00	0.00	0.00	0.00	0.33	1.31	1.31	1.97	1.64	1.64	0.98
8	0.00	0.00	0.00	0.00	0.00	0.33	0.66	0.98	0.98	1.64	2.95	2.30	0.98
9	0.33	0.33	0.00	0.33	0.98	0.98	1.31	1.97	2.30	2.62	1.31	0.98	0.66
10	0.33	0.00	0.33	0.00	0.98	0.33	0.98	0.66	0.66	1.31	0.66	0.33	0.33
11	0.00	0.00	0.00	0.00	0.98	0.00	0.66	0.66	0.66	0.33	0.98	0.98	0.66
12	0.00	0.00	0.00	0.00	0.00	0.00	0.00	0.00	0.66	0.66	0.33	0.66	0.66
13	0.00	0.00	0.00	0.00	0.33	0.33	0.66	0.98	0.66	0.66	0.66	0.33	0.33

Table D.21: $\Theta_0 = -20^\circ, \Phi = \Phi_0, -20\% \leq \Gamma < 0\%$

j:	1	2	3	4	5	6	7	8	9	10	11	12	13
k													
1	0.00	0.17	0.51	0.68	0.51	0.68	1.18	1.52	1.02	0.51	0.51	0.51	0.51
2	0.00	0.17	0.51	0.68	0.68	0.51	1.02	1.02	0.51	0.85	0.85	0.17	0.51
3	0.00	0.00	0.00	0.34	0.17	0.17	0.34	1.35	1.02	1.02	1.35	0.68	0.85
4	0.00	0.00	0.17	0.34	0.51	0.17	0.68	1.18	1.18	1.52	1.52	1.02	0.34
5	0.00	0.00	0.34	0.17	0.68	0.17	0.68	0.68	1.18	1.86	1.86	0.85	0.34
6	0.00	0.00	0.17	0.51	0.34	0.34	0.51	1.02	1.69	1.52	1.18	0.68	0.68
7	0.00	0.00	0.00	0.00	0.51	0.68	0.85	1.02	1.18	1.35	1.18	1.02	0.68
8	0.00	0.00	0.00	0.00	1.02	0.68	0.68	1.18	1.52	1.18	0.34	0.34	1.02
9	0.17	0.17	0.34	0.51	0.68	0.85	0.85	0.68	0.51	0.85	1.52	1.52	0.85
10	0.00	0.00	0.34	0.34	0.34	0.51	0.34	0.68	0.85	0.85	1.18	1.35	0.68
11	0.00	0.34	0.34	0.51	0.68	0.51	0.51	1.02	1.18	1.35	1.18	0.68	0.34
12	0.00	0.00	0.00	0.00	0.51	0.00	0.34	0.51	0.34	0.51	0.85	0.68	0.51
13	0.00	0.17	0.17	0.51	0.68	0.51	0.34	0.17	0.34	0.34	0.68	0.51	0.34

Table D.22: $\Theta_0 = -20^\circ, \Phi = \Phi_0, 0\% \leq \Gamma < 20\%$

j:	1	2	3	4	5	6	7	8	9	10	11	12	13
k													
1	0.25	0.25	0.12	0.12	0.12	0.62	0.25	0.25	0.62	0.87	0.50	0.25	0.12
2	0.12	0.25	0.37	0.37	0.50	0.99	0.62	0.74	0.74	0.37	0.37	0.74	0.25
3	0.00	0.25	0.50	0.37	1.49	1.36	1.24	0.74	0.74	0.74	0.37	0.74	0.62
4	0.00	0.25	0.37	0.62	1.24	1.61	1.36	1.24	0.99	0.62	0.50	0.50	0.74
5	0.12	0.37	0.74	0.74	0.50	0.99	1.11	1.49	1.24	0.74	0.74	1.11	0.74
6	0.00	0.12	0.37	0.62	1.49	1.36	1.49	1.11	0.74	0.62	0.87	0.99	0.74
7	0.00	0.00	0.25	0.50	1.24	1.24	1.11	0.99	0.99	0.50	0.50	0.50	0.62
8	0.00	0.00	0.00	0.50	0.62	0.74	1.24	0.74	0.50	0.37	0.50	0.25	0.12
9	0.00	0.25	0.25	0.37	0.50	0.25	0.50	0.74	0.87	0.50	0.74	0.62	0.87
10	0.25	0.37	0.12	0.50	0.37	0.25	0.62	0.62	0.74	0.87	0.99	0.62	1.11
11	0.25	0.37	0.50	0.50	0.37	0.74	0.87	0.87	0.99	0.87	0.62	0.74	0.87
12	0.00	0.00	0.37	0.37	0.37	0.87	0.74	0.99	0.87	0.99	0.62	0.37	0.87
13	0.12	0.12	0.25	0.37	0.50	0.50	0.62	0.62	0.62	0.25	0.37	0.12	

Table D.23: $\Theta_0 = -20^\circ, \Phi = \Phi_0, 20\% \leq \Gamma < 40\%$

j:	1	2	3	4	5	6	7	8	9	10	11	12	13
k													
1	0.00	0.00	0.00	0.17	1.04	0.17	0.17	0.35	0.17	0.17	0.52	0.52	0.35
2	0.52	0.35	0.17	0.69	1.04	0.52	0.87	0.69	0.52	0.87	0.69	0.69	0.69
3	0.69	0.69	0.52	1.22	0.52	0.69	0.69	0.52	0.35	0.35	0.69	0.52	0.69
4	0.52	0.69	1.04	0.87	0.69	0.52	0.52	0.17	0.17	0.52	0.69	0.69	0.69
5	0.69	0.87	0.17	0.17	1.22	1.22	0.87	0.35	0.17	0.00	0.17	0.52	1.04
6	0.52	1.04	0.87	0.87	0.52	0.52	0.52	0.35	0.00	0.00	0.35	0.52	0.35
7	0.00	0.69	1.04	1.91	1.04	0.87	0.69	0.35	0.17	0.35	0.52	0.35	0.52
8	0.17	0.35	1.04	1.04	1.39	1.39	0.52	0.52	0.52	0.52	0.69	0.87	0.69
9	0.35	0.35	0.69	0.52	0.35	0.69	0.69	0.35	0.35	0.35	0.00	0.35	0.69
10	0.17	0.52	0.35	0.35	1.04	1.22	1.04	1.04	0.87	0.69	0.52	0.87	0.17
11	0.17	0.17	0.17	0.35	0.69	0.87	0.87	0.69	0.35	0.52	0.52	0.69	0.52
12	0.17	0.69	0.35	1.04	1.56	1.39	1.39	1.04	1.22	0.69	0.87	1.22	0.52
13	0.35	0.35	0.87	0.52	0.35	0.17	0.17	0.35	0.35	0.35	0.69	0.87	1.22

Table D.24: $\Theta_0 = -20^\circ, \Phi = \Phi_0, 40\% \leq \Gamma < 60\%$

j:	1	2	3	4	5	6	7	8	9	10	11	12	13
k													
1	0.00	0.48	1.20	0.96	0.96	0.96	1.68	1.20	0.96	0.96	1.20	0.72	0.24
2	0.24	0.72	0.96	1.44	0.48	0.48	0.00	0.00	0.00	0.00	0.96	0.72	1.44
3	1.20	1.20	1.44	1.68	0.00	0.00	0.24	0.00	0.00	0.24	0.00	0.48	0.24
4	0.72	0.96	0.72	1.44	0.24	0.24	0.00	0.00	0.00	0.00	0.24	0.24	0.72
5	0.24	0.24	0.96	1.68	0.48	0.24	0.00	0.00	0.00	0.00	0.00	0.24	0.24
6	0.96	0.72	1.20	1.44	0.24	0.48	0.00	0.00	0.00	0.00	0.00	0.24	0.24
7	1.44	1.68	1.68	0.96	0.24	0.24	0.24	0.00	0.00	0.00	0.00	0.48	0.24
8	0.72	1.44	2.40	2.16	0.00	0.00	0.24	0.24	0.00	0.00	0.00	0.24	0.24
9	0.24	0.48	0.72	0.72	0.96	0.96	0.48	0.24	0.00	0.00	0.24	0.24	0.24
10	1.68	0.96	1.44	1.20	0.72	0.72	0.72	0.24	0.00	0.00	0.00	0.24	0.96
11	0.72	0.72	1.20	0.72	0.96	0.72	0.48	0.00	0.00	0.00	0.48	0.48	0.96
12	0.48	0.96	1.92	1.44	1.20	1.20	0.96	0.72	0.48	0.48	0.24	0.00	0.24
13	0.72	1.20	0.48	0.72	0.96	1.20	1.20	0.96	1.20	1.44	0.72	0.72	0.48

Table D.25: $\Theta_0 = -20^\circ, \Phi = \Phi_0, \Gamma > 60\%$

j:	1	2	3	4	5	6	7	8	9	10	11	12	13
k													
1	2.66	2.19	1.57	1.41	0.47	0.78	0.31	0.31	0.47	0.47	0.63	1.41	2.04
2	2.35	1.88	1.41	0.47	0.31	0.31	0.31	0.31	0.31	0.31	0.16	0.47	0.63
3	1.72	1.41	1.10	0.16	0.16	0.16	0.00	0.00	0.00	0.00	0.16	0.16	0.47
4	2.19	1.57	1.10	0.31	0.00	0.00	0.00	0.00	0.00	0.00	0.00	0.31	0.31
5	2.19	1.72	1.10	0.47	0.00	0.00	0.00	0.00	0.00	0.00	0.00	0.00	0.31
6	2.04	1.57	0.94	0.16	0.00	0.00	0.00	0.00	0.00	0.00	0.00	0.00	0.47
7	2.19	1.41	0.78	0.16	0.00	0.00	0.00	0.00	0.00	0.00	0.00	0.00	0.31
8	2.51	1.88	0.63	0.16	0.16	0.16	0.00	0.00	0.00	0.00	0.00	0.00	0.31
9	2.35	1.88	1.25	0.94	0.31	0.31	0.16	0.16	0.16	0.16	0.00	0.00	0.16
10	1.41	1.41	1.10	0.78	0.16	0.31	0.00	0.00	0.00	0.00	0.00	0.00	0.16
11	2.19	1.72	1.25	1.25	0.31	0.47	0.16	0.16	0.16	0.16	0.00	0.16	0.16
12	2.66	1.88	1.10	0.78	0.00	0.00	0.00	0.00	0.00	0.16	0.31	0.47	0.63
13	2.19	1.72	1.57	1.25	0.78	0.94	0.78	0.78	0.63	0.47	0.78	0.78	1.10

Table D.26: $\Theta_0 = -20^\circ, \Phi = \Phi_0, -5\% \leq \Gamma \leq 5\%$

j:	1	2	3	4	5	6	7	8	9	10	11	12	13
k													
1	1.35	0.00	0.00	0.90	0.45	0.00	0.45	0.00	0.90	0.45	0.00	1.35	0.90
2	0.45	0.00	0.00	0.90	0.45	0.45	0.90	0.45	0.45	0.90	1.35	0.90	0.45
3	0.00	0.00	0.00	0.00	0.00	1.35	0.45	0.45	0.90	1.80	1.35	1.35	0.00
4	0.45	0.00	0.45	0.00	0.00	0.45	0.45	0.00	0.45	0.90	1.35	0.90	1.80
5	0.45	0.00	0.00	0.00	0.00	0.00	0.45	0.45	0.90	0.90	1.35	0.45	0.45
6	0.00	0.00	0.00	0.45	1.35	0.00	0.45	0.45	0.00	1.35	0.00	0.90	1.35
7	0.00	0.00	0.45	0.00	0.90	0.45	0.45	1.35	1.35	1.80	1.35	0.90	1.35
8	0.00	0.00	0.00	0.45	0.45	0.00	0.90	0.90	0.90	0.45	0.45	0.45	1.35
9	0.00	0.00	0.00	0.00	0.45	0.45	0.45	2.25	1.35	0.90	0.90	0.45	0.45
10	0.45	0.45	0.45	0.90	0.45	0.90	2.25	0.90	1.35	1.35	1.35	1.35	0.90
11	0.00	0.00	0.00	0.00	0.45	0.45	0.90	0.45	0.90	1.35	1.35	0.45	0.90
12	0.00	0.00	0.00	0.00	0.00	0.00	0.90	2.25	1.80	1.80	0.90	0.45	0.00
13	0.00	0.00	0.00	0.90	0.45	0.90	0.90	0.90	0.45	0.45	0.00	0.90	0.45

Table D.27: $\Theta_0 = -20^\circ, \Phi = \Phi_0, -10\% \leq \Gamma \leq 10\%$

j:	1	2	3	4	5	6	7	8	9	10	11	12	13
k													
1	1.01	0.00	0.00	0.51	0.25	0.51	0.25	0.51	0.76	0.76	1.01	1.26	0.51
2	0.76	0.00	0.25	0.51	0.51	0.51	0.51	0.51	0.25	0.76	1.26	1.26	1.01
3	0.00	0.00	0.25	0.00	0.25	0.76	0.25	0.76	0.76	1.52	1.01	0.76	0.51
4	0.76	0.00	0.25	0.00	0.00	0.25	0.25	0.51	0.51	0.76	0.76	1.01	1.26
5	0.25	0.00	0.00	0.25	0.25	0.25	0.51	0.25	1.01	1.01	1.26	0.76	0.51
6	0.25	0.25	0.25	0.51	0.76	0.51	0.51	0.51	0.76	0.76	0.51	0.76	0.76
7	0.00	0.00	0.25	0.00	0.51	0.51	0.51	1.26	1.26	1.26	0.76	1.01	0.76
8	0.00	0.00	0.00	0.51	0.51	0.00	0.76	1.01	0.76	0.76	0.51	0.51	1.52
9	0.00	0.00	0.00	0.00	0.76	0.25	1.01	1.77	1.26	0.76	0.76	0.76	0.25
10	0.25	0.25	0.51	0.51	1.01	1.01	1.52	1.52	1.01	1.01	1.01	0.76	0.51
11	0.00	0.00	0.00	0.00	0.76	0.76	1.01	0.76	1.01	1.26	1.01	0.76	0.51
12	0.00	0.00	0.00	0.00	0.51	0.25	1.01	1.52	2.02	1.52	1.26	0.51	0.00
13	0.00	0.00	0.00	0.51	0.76	1.01	1.26	1.01	1.01	1.01	0.25	0.76	0.76

Table C.28: $\Theta_0 = 0^\circ$, $\Gamma < -40\%$

j:	1	2	3	4	5	6	7	8	9	10	11	12	13
k													
1	4.00	4.00	4.00	0.00	0.00	0.00	0.00	0.00	0.00	0.00	0.00	0.00	0.00
2	0.00	0.00	0.00	0.00	0.00	0.00	0.00	0.00	0.00	0.00	0.00	0.00	0.00
3	0.00	0.00	0.00	0.00	0.00	0.00	0.00	0.00	0.00	0.00	0.00	0.00	0.00
4	0.00	0.00	0.00	0.00	0.00	0.00	0.00	0.00	0.00	0.00	0.00	0.00	0.00
5	0.00	0.00	0.00	0.00	0.00	0.00	0.00	0.00	0.00	0.00	0.00	0.00	0.00
6	0.00	0.00	0.00	0.00	0.00	0.00	0.00	0.00	0.00	0.00	0.00	0.00	0.00
7	0.00	0.00	0.00	0.00	0.00	0.00	0.00	0.00	0.00	0.00	0.00	0.00	0.00
8	0.00	0.00	0.00	0.00	0.00	0.00	0.00	0.00	0.00	0.00	0.00	4.00	0.00
9	8.00	8.00	4.00	4.00	4.00	0.00	0.00	0.00	0.00	0.00	0.00	0.00	0.00
10	4.00	4.00	4.00	8.00	8.00	8.00	8.00	0.00	0.00	0.00	0.00	0.00	0.00
11	0.00	0.00	4.00	0.00	0.00	0.00	0.00	0.00	0.00	0.00	0.00	0.00	0.00
12	0.00	0.00	0.00	0.00	0.00	0.00	0.00	0.00	0.00	0.00	4.00	4.00	0.00
13	0.00	0.00	0.00	0.00	0.00	0.00	0.00	0.00	0.00	0.00	0.00	0.00	0.00

Table C.29: $\Theta_0 = 0^\circ$, $-40\% \leq \Gamma < -20\%$

j:	1	2	3	4	5	6	7	8	9	10	11	12	13
k													
1	0.00	0.45	0.45	0.90	0.90	0.90	1.35	0.00	0.00	0.00	0.00	0.00	0.00
2	0.45	0.90	0.90	0.45	0.90	0.90	1.35	0.90	0.90	0.90	0.90	0.45	0.00
3	0.00	0.00	0.45	0.00	0.90	0.90	1.35	1.35	0.00	0.90	0.90	0.90	0.45
4	0.00	0.00	0.00	0.45	0.90	0.90	1.35	0.00	0.00	0.00	0.45	0.45	0.45
5	0.45	0.90	1.35	1.35	1.35	1.35	1.35	0.45	0.00	0.00	0.00	0.00	0.00
6	0.45	0.45	0.45	0.90	0.90	1.35	1.35	0.45	0.00	0.00	0.00	0.45	0.90
7	0.00	0.00	0.00	0.00	0.00	0.00	0.90	0.00	0.00	0.45	0.45	0.90	0.90
8	0.00	0.00	0.00	0.00	0.00	0.45	1.35	1.35	1.35	0.45	0.45	0.90	1.79
9	0.45	0.45	1.35	2.24	2.24	2.69	2.69	1.79	0.90	0.00	0.00	0.00	0.00
10	0.45	0.90	1.35	0.90	0.45	0.90	1.35	1.79	0.00	0.00	0.00	0.00	0.00
11	0.00	1.79	1.35	1.79	1.35	0.90	1.35	0.00	0.00	0.00	0.45	0.45	0.45
12	0.00	0.00	0.00	0.00	0.00	0.00	0.00	0.00	0.90	0.90	0.00	0.00	0.45
13	0.00	0.45	0.45	0.90	1.79	1.79	1.79	0.90	0.45	0.00	0.45	0.45	0.00

Table C.30: $\Theta_0 = 0^\circ$, $-20\% \leq \Gamma < 0\%$

j:	1	2	3	4	5	6	7	8	9	10	11	12	13
k													
1	0.16	0.16	0.16	0.65	0.81	0.81	0.97	1.45	0.97	0.97	0.48	0.48	0.00
2	0.16	0.16	0.65	0.97	0.97	1.29	1.29	0.81	0.81	0.81	0.32	0.48	0.16
3	0.00	0.32	0.81	0.81	0.48	0.65	1.61	0.97	1.13	0.81	0.48	0.32	0.16
4	0.32	0.81	0.81	0.48	0.32	0.81	1.45	1.13	1.13	0.81	0.48	0.32	0.32
5	0.16	0.65	0.81	0.65	0.81	0.97	1.29	0.97	0.65	0.00	0.16	0.48	0.48
6	0.16	0.65	0.65	0.81	0.97	0.81	1.13	0.65	0.97	0.48	0.65	0.48	0.32
7	0.16	0.48	0.32	0.48	0.81	0.81	1.45	1.13	1.29	1.13	0.81	0.65	0.65
8	0.00	0.16	0.00	0.32	0.81	0.81	1.29	0.97	0.65	1.13	1.45	0.97	0.16
9	0.00	0.65	0.48	0.16	0.32	0.32	0.65	0.81	1.13	0.97	0.48	0.32	0.16
10	0.32	0.32	0.16	0.16	0.81	0.65	0.97	0.48	0.97	0.65	0.48	0.32	0.16
11	0.48	0.32	0.48	0.48	0.48	0.65	1.13	0.32	0.65	0.97	0.65	0.32	0.32
12	0.00	0.48	0.48	0.32	0.32	0.48	0.97	0.65	0.32	0.32	0.65	0.48	0.32
13	0.16	0.00	0.32	0.32	0.00	0.00	0.48	0.48	0.65	0.81	0.32	0.00	0.16

Table C.31: $\Theta_0 = 0^\circ$, $0\% \leq \Gamma < 20\%$

j:	1	2	3	4	5	6	7	8	9	10	11	12	13
k													
1	0.11	0.11	0.43	0.22	0.22	0.33	0.33	0.11	0.43	0.11	0.43	0.11	0.43
2	0.33	0.33	0.33	0.11	0.43	0.43	0.54	0.76	0.76	0.54	0.65	0.11	0.22
3	0.65	0.87	0.76	0.87	0.98	1.08	0.65	0.87	0.98	0.76	0.87	0.43	0.43
4	0.33	0.33	0.54	0.98	1.08	1.08	0.87	1.08	0.98	0.98	0.98	0.54	0.43
5	0.65	0.33	0.22	0.43	0.43	0.65	0.87	0.98	1.30	1.41	0.98	0.33	0.11
6	0.54	0.43	0.43	0.54	0.65	0.98	0.98	1.19	1.08	1.19	0.87	0.54	0.22
7	0.76	0.54	0.98	1.41	1.19	1.30	0.65	0.98	0.76	0.87	0.65	0.54	0.22
8	0.43	0.76	1.19	1.19	1.08	1.08	0.76	0.76	0.87	0.54	0.22	0.43	0.54
9	0.54	0.22	0.43	0.43	0.43	0.33	0.76	0.33	0.54	0.76	1.08	0.76	0.54
10	0.54	0.43	0.43	0.43	0.33	0.43	0.43	0.54	0.54	0.54	0.76	0.76	0.33
11	0.33	0.11	0.22	0.43	0.33	0.43	0.65	1.08	0.87	0.87	0.43	0.65	0.33
12	0.43	0.22	0.33	0.54	0.65	0.76	0.98	0.65	0.54	0.54	0.43	0.43	0.33
13	0.33	0.65	0.33	0.43	0.54	0.54	0.22	0.22	0.11	0.11	0.43	0.54	0.22

Table C.32: $\Theta_0 = 0^\circ$, $20\% \leq \Gamma < 40\%$

j:	1	2	3	4	5	6	7	8	9	10	11	12	13
k													
1	0.14	0.14	0.42	0.28	0.28	0.28	0.56	0.70	0.70	0.98	0.28	0.14	0.00
2	0.14	0.42	0.28	0.98	0.56	0.42	0.28	0.56	0.42	0.56	0.42	0.98	0.14
3	0.56	0.14	0.28	0.56	0.70	0.42	0.14	0.28	0.14	0.42	0.14	0.84	0.84
4	0.56	0.56	0.56	0.70	0.84	0.42	0.00	0.42	0.56	0.56	0.84	0.56	0.14
5	0.28	0.56	0.56	0.84	0.98	0.56	0.14	0.56	0.56	0.98	0.84	1.26	0.70
6	0.42	0.70	0.98	0.98	0.70	0.42	0.14	0.56	0.56	0.70	0.84	1.12	0.56
7	0.70	1.40	1.12	0.42	0.42	0.42	0.42	0.56	0.56	0.42	0.70	0.56	0.56
8	0.98	1.26	1.12	0.70	0.42	0.28	0.14	0.42	0.56	0.56	0.42	0.14	0.42
9	0.70	0.70	0.42	0.56	0.56	0.98	0.14	0.84	0.56	0.84	0.56	0.98	0.84
10	0.56	0.42	0.56	1.12	0.84	0.70	0.70	0.56	0.70	0.84	0.84	0.70	0.84
11	0.42	0.42	0.56	0.28	0.56	0.84	0.42	0.84	0.84	0.28	0.98	0.56	0.70
12	0.28	0.56	0.84	1.26	1.40	1.26	0.56	1.12	1.12	0.84	0.56	0.70	0.84
13	0.56	0.14	0.70	0.56	0.28	0.42	0.56	0.56	0.70	0.70	0.42	0.56	0.28

Table C.33: $\Theta_0 = 0^\circ$, $40\% \leq \Gamma < 60\%$

j:	1	2	3	4	5	6	7	8	9	10	11	12	13
k													
1	0.25	0.99	0.49	0.99	1.23	1.23	0.49	0.25	0.25	0.49	1.48	0.99	0.25
2	0.74	0.74	1.23	0.49	0.74	0.49	0.25	0.25	0.25	0.49	0.99	0.49	1.48
3	0.00	0.74	0.99	0.49	0.00	0.25	0.00	0.25	0.74	0.49	1.23	0.49	0.49
4	0.74	0.74	1.48	0.49	0.00	0.00	0.00	0.00	0.00	0.49	0.74	0.99	1.48
5	0.74	0.25	1.23	0.74	0.25	0.25	0.00	0.00	0.00	0.00	0.99	0.74	1.72
6	0.99	0.74	0.74	0.25	0.25	0.00	0.00	0.00	0.00	0.25	0.49	0.00	1.48
7	0.25	0.00	0.25	0.25	0.25	0.00	0.00	0.00	0.25	0.25	0.49	0.49	0.99
8	0.74	0.49	0.00	0.49	0.49	0.49	0.25	0.25	0.00	0.49	0.99	0.99	0.25
9	0.99	0.74	0.74	0.49	0.74	0.25	0.49	0.25	0.25	0.00	0.49	0.49	0.49
10	0.49	0.99	1.48	0.49	0.49	0.49	0.00	0.99	0.99	0.74	0.99	1.48	0.74
11	0.74	0.99	0.49	1.23	1.23	0.74	0.25	0.25	0.25	0.74	0.25	0.99	0.74
12	1.23	0.99	1.23	0.99	0.49	0.25	0.25	0.25	0.49	0.74	0.99	0.49	0.74
13	0.49	0.99	0.49	0.99	1.23	1.23	1.48	1.48	1.23	0.49	0.49	0.74	1.23

Table C.34: $\Theta_0 = 0^\circ$, $\Gamma > 60\%$

j:	1	2	3	4	5	6	7	8	9	10	11	12	13
k													
1	3.19	2.34	1.70	1.28	0.85	0.64	0.43	0.85	0.85	0.85	1.06	2.34	3.19
2	2.34	1.70	0.85	0.64	0.21	0.21	0.21	0.21	0.43	0.43	0.64	1.28	2.13
3	2.13	1.28	0.21	0.21	0.21	0.00	0.00	0.00	0.00	0.21	0.21	0.85	1.28
4	1.70	1.06	0.00	0.00	0.00	0.00	0.00	0.00	0.00	0.00	0.43	0.64	1.28
5	1.49	1.28	0.21	0.00	0.00	0.00	0.00	0.00	0.00	0.00	0.00	0.43	0.85
6	1.28	0.64	0.21	0.00	0.00	0.00	0.00	0.00	0.00	0.00	0.00	0.64	0.85
7	1.28	0.43	0.00	0.00	0.00	0.00	0.00	0.00	0.00	0.00	0.21	0.64	0.85
8	1.28	0.21	0.21	0.00	0.00	0.00	0.00	0.00	0.21	0.21	0.21	0.43	1.28
9	0.64	0.64	0.64	0.64	0.21	0.21	0.00	0.21	0.21	0.21	0.21	0.43	1.28
10	1.06	0.85	0.21	0.21	0.21	0.21	0.00	0.00	0.00	0.00	0.00	0.21	1.49
11	1.70	1.28	1.06	0.43	0.43	0.21	0.00	0.21	0.21	0.21	0.64	0.64	1.28
12	1.91	1.49	0.64	0.00	0.00	0.00	0.00	0.21	0.21	0.43	0.64	1.06	1.06
13	2.13	1.70	1.49	0.85	0.85	0.64	0.21	0.64	0.85	1.49	1.70	1.49	2.13

Table C.35: $\Theta_0 = 0^\circ$, $-5\% \leq \Gamma \leq 5\%$

j:	1	2	3	4	5	6	7	8	9	10	11	12	13
k													
1	0.00	0.00	0.00	0.49	0.49	0.97	0.49	2.43	0.49	0.49	0.97	0.49	0.49
2	0.00	0.49	0.00	0.00	0.49	0.49	0.49	0.49	0.00	1.46	0.49	0.49	0.49
3	0.00	0.00	0.49	0.97	1.46	0.49	0.49	1.46	0.00	0.00	0.00	0.00	0.49
4	0.00	0.00	0.00	0.00	0.00	0.00	0.00	0.49	0.49	0.49	0.49	0.00	0.49
5	0.00	0.00	0.49	0.49	0.49	1.46	0.00	0.49	0.00	0.49	0.00	0.00	0.49
6	0.00	0.49	0.49	0.49	0.00	0.49	0.97	0.49	0.49	0.49	0.00	0.97	0.49
7	0.00	0.97	0.97	1.46	0.49	0.49	0.49	0.49	0.49	2.43	2.43	0.97	0.00
8	0.00	0.49	0.97	0.00	0.97	0.97	1.46	1.46	0.97	0.97	0.97	0.49	0.97
9	0.49	0.97	1.46	0.97	1.46	1.94	1.46	0.97	0.49	0.97	0.97	0.00	0.00
10	0.00	0.00	0.00	0.49	0.97	0.49	0.00	1.46	0.97	1.46	0.49	0.00	0.49
11	1.46	0.49	1.46	1.46	1.46	1.46	0.49	0.97	0.00	0.00	0.97	0.00	0.49
12	0.49	0.97	0.49	0.97	0.49	0.49	2.91	0.49	0.49	0.00	0.00	0.00	0.49
13	0.00	0.97	0.49	0.49	0.49	0.97	0.49	0.49	0.49	0.97	0.97	0.97	0.49

Table C.36: $\Theta_0 = 0^\circ$, $-10\% \leq \Gamma \leq 10\%$

j:	1	2	3	4	5	6	7	8	9	10	11	12	13
k													
1	0.49	0.00	0.25	0.25	0.25	0.49	0.99	1.23	0.74	0.49	0.74	0.74	0.25
2	0.25	0.49	0.25	0.25	0.49	0.74	0.49	0.49	0.49	0.74	0.49	0.49	0.49
3	0.25	0.25	0.74	0.49	0.74	0.49	0.49	0.74	0.00	0.25	0.25	0.00	0.25
4	0.00	0.25	0.00	0.00	0.00	0.00	0.49	0.49	0.25	0.49	0.49	0.25	0.25
5	0.00	0.00	0.25	0.25	0.49	0.74	0.74	0.49	0.25	0.74	0.25	0.25	0.25
6	0.00	0.25	0.49	0.49	0.25	0.49	1.23	0.25	0.49	0.74	0.49	0.74	0.25
7	0.00	0.49	0.49	0.74	0.74	0.49	0.74	0.74	1.23	1.23	1.23	0.99	0.25
8	0.25	0.74	0.99	0.74	0.74	0.74	1.23	0.99	0.74	0.99	1.23	0.99	0.49
9	0.49	0.74	0.74	0.74	1.48	1.48	0.99	1.23	0.99	0.49	0.49	0.25	0.25
10	0.00	0.49	0.25	0.99	1.23	1.23	0.74	0.99	0.99	1.23	0.49	0.25	0.25
11	0.74	0.99	0.74	1.23	0.99	1.23	0.74	0.49	0.49	0.49	0.49	0.00	0.25
12	0.49	0.99	0.74	0.99	1.48	1.23	1.72	0.99	0.74	0.49	0.25	0.25	0.74
13	0.49	0.74	0.49	0.74	0.49	0.74	0.99	0.74	0.49	0.99	0.74	0.74	0.25

Table D.37: $\Theta_0 = -20^\circ, \Phi = \Phi_0 + 180^\circ, \Gamma < -40\%$

j:	1	2	3	4	5	6	7	8	9	10	11	12	13
k													
1	2.38	2.38	2.38	1.19	1.19	0.00	0.00	0.00	0.00	0.00	0.00	0.00	0.00
2	1.19	2.38	1.19	0.00	0.00	0.00	0.00	0.00	0.00	0.00	0.00	0.00	0.00
3	0.00	0.00	0.00	1.19	1.19	1.19	0.00	0.00	0.00	0.00	0.00	0.00	0.00
4	0.00	0.00	0.00	1.19	0.00	0.00	0.00	0.00	0.00	0.00	0.00	0.00	0.00
5	1.19	1.19	3.57	2.38	2.38	1.19	1.19	0.00	0.00	0.00	0.00	0.00	0.00
6	1.19	1.19	2.38	2.38	1.19	1.19	1.19	0.00	0.00	0.00	0.00	0.00	0.00
7	0.00	0.00	0.00	0.00	0.00	0.00	0.00	0.00	0.00	0.00	0.00	0.00	0.00
8	0.00	0.00	0.00	0.00	0.00	0.00	0.00	0.00	0.00	0.00	0.00	0.00	0.00
9	3.57	4.76	4.76	4.76	4.76	1.19	0.00	0.00	0.00	0.00	0.00	0.00	0.00
10	3.57	2.38	3.57	3.57	2.38	1.19	1.19	0.00	0.00	0.00	0.00	0.00	0.00
11	1.19	3.57	3.57	3.57	2.38	0.00	0.00	0.00	0.00	0.00	0.00	0.00	0.00
12	0.00	0.00	0.00	0.00	0.00	0.00	0.00	0.00	0.00	0.00	0.00	0.00	0.00
13	0.00	0.00	0.00	0.00	1.19	0.00	0.00	0.00	0.00	0.00	0.00	0.00	0.00

Table D.38: $\Theta_0 = -20^\circ, \Phi = \Phi_0 + 180^\circ, -40\% \leq \Gamma < -20\%$

j:	1	2	3	4	5	6	7	8	9	10	11	12	13
k													
1	0.00	0.36	0.36	0.73	0.36	0.36	0.00	0.00	0.00	0.00	0.00	0.00	0.00
2	0.36	0.36	1.09	1.82	1.09	0.73	0.73	0.36	0.36	0.00	0.00	0.00	0.00
3	0.36	0.73	1.82	1.46	1.46	0.00	0.36	0.36	0.00	0.00	0.00	0.00	0.00
4	0.36	1.46	1.82	1.46	0.73	0.73	0.36	0.00	0.00	0.00	0.00	0.00	0.00
5	1.09	1.46	1.82	2.19	1.09	0.73	0.36	0.36	0.36	0.00	0.00	0.00	0.00
6	1.46	1.82	1.46	1.46	1.09	0.73	0.36	0.73	0.73	0.00	0.00	0.00	0.00
7	1.09	1.09	1.82	1.82	0.73	1.09	1.09	0.36	0.73	0.00	0.00	0.00	0.00
8	0.36	0.73	1.46	1.46	1.09	1.46	1.09	1.09	1.09	0.73	0.36	0.36	0.00
9	0.36	1.09	1.46	1.82	1.46	2.19	1.46	0.36	0.36	0.00	0.00	0.00	0.00
10	0.00	1.46	0.73	1.09	1.46	1.82	1.09	0.73	1.09	0.00	0.00	0.00	0.00
11	1.46	1.09	1.09	0.73	1.09	1.09	0.00	0.00	0.00	0.00	0.00	0.00	0.00
12	0.36	0.36	0.36	0.36	0.36	0.00	0.00	0.00	0.36	0.36	0.36	0.36	0.00
13	0.36	0.36	0.73	1.09	0.73	1.09	1.09	0.73	0.73	0.00	0.00	0.00	0.00

Table D.39: $\Theta_0 = -20^\circ, \Phi = \Phi_0 + 180^\circ, -20\% \leq \Gamma < 0\%$

j:	1	2	3	4	5	6	7	8	9	10	11	12	13
k													
1	0.30	0.15	0.15	0.30	1.04	1.19	1.19	0.74	0.89	0.00	0.00	0.00	0.00
2	0.44	0.44	0.30	0.74	1.04	1.33	1.04	1.19	1.19	0.44	0.30	0.15	0.00
3	1.04	1.04	1.04	1.04	1.33	1.19	1.04	0.59	1.04	0.15	0.15	0.15	0.00
4	1.04	1.04	0.89	1.33	1.78	1.63	1.04	1.04	0.89	0.30	0.44	0.44	0.30
5	0.59	0.89	0.44	0.59	0.89	1.04	1.19	0.74	0.89	0.00	0.00	0.00	0.00
6	0.30	0.89	1.19	1.19	1.33	1.48	1.19	0.59	0.59	0.15	0.15	0.15	0.15
7	0.89	1.48	1.48	1.63	1.93	1.48	0.74	0.74	0.89	0.44	0.30	0.30	0.30
8	0.89	1.63	1.78	1.93	0.89	0.59	0.74	0.59	0.74	0.30	0.30	0.15	0.30
9	0.74	0.44	0.30	0.15	0.30	0.44	0.89	0.89	1.19	0.00	0.00	0.00	0.00
10	0.74	0.30	0.74	0.59	0.89	0.44	0.59	0.74	0.59	0.15	0.15	0.00	0.00
11	0.15	0.15	0.44	0.74	0.89	0.89	0.59	0.15	0.30	0.15	0.15	0.15	0.15
12	0.30	0.44	0.59	0.59	0.15	0.74	0.44	0.44	0.15	0.15	0.00	0.00	0.00
13	0.44	0.44	0.44	0.44	0.30	0.15	0.15	0.30	0.30	0.15	0.00	0.00	0.00

Table D.40: $\Theta_0 = -20^\circ, \Phi = \Phi_0 + 180^\circ, 0\% \leq \Gamma < 20\%$

j:	1	2	3	4	5	6	7	8	9	10	11	12	13
k													
1	0.00	0.13	0.51	0.63	0.25	0.25	0.51	0.76	0.63	0.89	0.51	0.25	0.00
2	0.25	0.25	0.76	0.51	0.76	0.51	0.76	0.76	0.51	1.02	0.38	0.13	0.25
3	0.25	0.63	0.76	0.76	0.63	1.14	1.14	1.40	1.27	0.76	0.51	0.25	0.25
4	0.25	0.13	0.63	0.63	0.63	0.63	1.27	1.14	1.02	0.38	0.00	0.00	0.13
5	0.63	0.38	0.51	0.89	1.02	1.02	1.02	1.27	1.14	0.51	0.25	0.25	0.25
6	0.63	0.51	0.63	0.63	0.76	0.63	0.89	1.27	1.14	0.89	0.25	0.25	0.25
7	0.51	0.51	0.51	0.38	0.51	0.63	1.27	1.02	0.51	0.63	0.38	0.13	0.13
8	0.89	0.76	0.38	0.25	1.14	1.14	0.76	0.63	0.76	0.51	0.63	0.38	0.25
9	0.76	0.63	0.63	0.76	0.76	0.63	0.76	1.14	1.02	0.89	0.25	0.13	0.00
10	0.76	0.63	0.38	0.51	0.25	0.51	0.63	0.63	0.76	0.63	0.13	0.13	0.13
11	0.51	0.51	0.51	0.38	0.63	0.89	1.27	1.02	1.52	0.13	0.13	0.13	0.00
12	0.38	0.51	0.76	1.27	2.03	1.27	0.89	0.63	1.02	0.38	0.51	0.38	0.25
13	0.51	0.63	0.63	0.51	0.51	0.76	0.51	0.13	0.13	0.38	0.51	0.13	0.00

Table D.41: $\Theta_0 = -20^\circ, \Phi = \Phi_0 + 180^\circ, 20\% \leq \Gamma < 40\%$

j:	1	2	3	4	5	6	7	8	9	10	11	12	13
k													
1	0.35	0.71	0.53	0.71	0.71	0.71	0.53	0.71	0.89	0.53	0.53	0.53	0.35
2	0.18	1.06	0.89	0.71	0.53	0.53	0.53	0.35	0.71	0.35	1.24	0.71	0.00
3	0.35	0.71	0.18	0.18	0.18	0.35	0.53	0.35	0.35	1.06	0.18	0.35	0.18
4	0.71	1.06	0.71	0.18	0.18	0.35	0.35	0.71	1.06	1.42	0.89	0.18	0.00
5	0.35	0.71	0.89	0.18	0.18	0.18	0.18	0.53	0.71	1.24	0.71	0.18	0.18
6	0.89	0.53	0.18	0.18	0.18	0.35	0.53	0.53	0.89	0.71	0.89	0.35	0.18
7	0.71	0.35	0.18	0.18	0.18	0.35	0.35	0.89	1.24	0.89	0.89	0.53	0.35
8	0.35	0.00	0.00	0.18	0.18	0.35	0.89	1.06	0.53	0.89	0.53	0.89	0.00
9	0.35	0.35	0.35	0.18	0.35	0.53	0.35	0.18	0.18	1.60	1.42	0.71	0.35
10	0.35	0.53	1.06	0.71	0.71	1.06	0.89	0.71	0.71	1.24	1.42	0.53	0.35
11	0.53	0.71	0.53	0.71	0.35	0.35	0.53	1.42	0.71	1.42	1.24	1.06	0.53
12	0.71	1.06	1.06	0.71	0.18	0.71	1.60	1.42	1.06	1.06	0.71	0.71	0.53
13	0.71	0.71	0.35	0.53	0.71	0.35	0.71	0.89	1.24	0.18	0.18	0.53	0.18

Table D.42: $\Theta_0 = -20^\circ, \Phi = \Phi_0 + 180^\circ, 40\% \leq \Gamma < 60\%$

j:	1	2	3	4	5	6	7	8	9	10	11	12	13
k													
1	0.51	0.51	1.02	0.77	0.51	0.51	0.26	0.26	0.26	1.53	0.77	0.00	0.00
2	1.02	0.51	0.26	0.26	0.00	0.26	0.26	0.26	0.26	1.02	0.77	1.02	0.51
3	1.28	0.26	0.26	0.26	0.00	0.00	0.00	0.51	0.26	1.28	1.79	1.79	1.02
4	1.28	0.51	0.00	0.00	0.00	0.00	0.00	0.00	0.00	1.02	1.28	1.28	1.02
5	0.51	0.51	0.00	0.00	0.00	0.26	0.26	0.26	0.00	1.79	1.79	1.02	0.51
6	0.26	0.26	0.00	0.00	0.00	0.00	0.00	0.26	0.00	1.79	1.28	1.02	0.51
7	0.51	0.26	0.00	0.00	0.00	0.00	0.00	0.26	0.26	1.53	0.77	1.28	0.51
8	1.02	0.26	0.26	0.00	0.26	0.26	0.26	0.51	0.77	1.02	0.26	0.26	1.02
9	0.26	0.51	0.77	0.77	0.51	0.26	0.26	0.51	0.26	0.26	1.28	1.53	1.28
10	0.51	0.51	0.00	0.26	0.51	0.26	0.51	1.02	0.77	0.51	1.28	1.28	0.77
11	1.02	1.02	0.77	0.77	0.51	0.26	0.51	0.51	0.26	1.79	0.77	0.26	0.77
12	1.02	1.28	0.77	0.26	0.26	0.26	0.26	1.02	0.77	0.51	1.02	0.77	0.77
13	0.77	1.02	1.02	1.28	1.28	1.02	1.02	0.77	1.28	0.77	1.02	0.77	

Table D.43: $\Theta_0 = -20^\circ, \Phi = \Phi_0 + 180^\circ, \Gamma > 60\%$

j:	1	2	3	4	5	6	7	8	9	10	11	12	13
k													
1	1.99	1.49	0.83	0.50	0.50	0.50	0.66	0.66	0.50	0.66	1.66	2.49	2.99
2	1.33	0.66	0.33	0.17	0.17	0.17	0.17	0.33	0.33	0.50	0.83	1.66	2.65
3	0.50	0.17	0.00	0.00	0.00	0.00	0.00	0.00	0.00	0.33	1.16	1.33	2.16
4	0.17	0.00	0.00	0.00	0.00	0.00	0.00	0.00	0.00	0.50	1.16	1.82	2.16
5	0.50	0.00	0.00	0.00	0.00	0.00	0.00	0.00	0.00	0.33	1.16	2.16	2.49
6	0.33	0.00	0.00	0.00	0.00	0.00	0.00	0.00	0.00	0.17	1.16	1.82	2.32
7	0.17	0.00	0.00	0.00	0.00	0.00	0.00	0.00	0.00	0.17	1.16	1.49	2.16
8	0.00	0.00	0.00	0.00	0.00	0.00	0.00	0.00	0.00	0.50	1.33	1.49	1.99
9	0.33	0.17	0.00	0.00	0.00	0.17	0.17	0.17	0.17	0.50	0.83	1.49	2.16
10	0.33	0.33	0.17	0.17	0.00	0.00	0.00	0.00	0.00	0.83	0.83	1.82	2.32
11	0.50	0.17	0.17	0.00	0.00	0.17	0.17	0.17	0.17	0.50	1.33	1.82	2.16
12	1.00	0.17	0.00	0.00	0.00	0.00	0.00	0.00	0.17	1.16	1.16	1.49	1.99
13	0.83	0.50	0.66	0.33	0.33	0.50	0.66	1.00	0.83	1.49	1.82	1.99	2.65

Table D.44: $\Theta_0 = -20^\circ, \Phi = \Phi_0 + 180^\circ, -5\% \leq \Gamma \leq 5\%$

j:	1	2	3	4	5	6	7	8	9	10	11	12	13
k													
1	0.49	0.49	0.98	0.98	0.49	0.98	1.47	0.49	0.49	0.98	0.00	0.00	0.00
2	0.00	0.00	0.00	0.00	0.49	0.98	0.00	0.00	1.47	0.98	0.00	0.00	0.00
3	0.49	1.47	0.49	0.98	0.49	0.49	1.47	1.47	0.49	0.49	0.00	0.00	0.00
4	0.00	0.98	1.47	0.49	0.00	0.00	0.00	0.00	0.49	0.49	0.49	0.00	0.00
5	0.00	0.00	0.49	0.00	0.49	0.98	0.49	0.49	1.96	0.98	0.00	0.00	0.00
6	0.49	0.00	0.00	0.49	0.49	1.96	0.98	0.49	0.98	0.00	0.49	0.00	0.49
7	0.00	0.00	0.49	0.98	1.47	0.49	1.47	0.49	1.47	0.49	0.00	0.00	0.00
8	0.49	0.49	0.49	0.49	1.96	1.47	1.47	0.49	0.98	0.00	0.98	0.49	0.49
9	0.00	0.49	0.49	0.00	0.98	1.96	1.96	0.98	0.98	0.00	0.00	0.49	0.00
10	0.49	0.00	0.98	1.47	1.47	0.49	0.98	0.98	0.98	0.49	0.00	0.00	0.00
11	0.98	0.00	0.49	1.96	1.47	0.49	0.98	0.98	0.00	0.98	0.00	0.00	0.00
12	0.49	0.49	0.98	0.98	0.98	1.47	2.94	0.98	0.98	0.00	0.00	0.00	0.00
13	1.47	1.96	0.49	0.98	1.47	1.47	1.47	0.49	0.00	0.00	0.00	0.00	0.00

Table D.45: $\Theta_0 = -20^\circ$, $\Phi = \Phi_0 + 180^\circ$, $-10\% \leq \Gamma \leq 10\%$

j:	1	2	3	4	5	6	7	8	9	10	11	12	13
k													
1	0.26	0.26	0.79	1.05	0.52	0.79	0.79	0.26	0.52	1.31	0.00	0.00	0.00
2	0.00	0.00	0.00	0.52	0.26	0.52	0.52	0.52	1.05	0.79	0.00	0.00	0.00
3	0.26	0.79	0.52	0.52	0.79	0.79	1.31	1.05	0.52	0.52	0.00	0.00	0.26
4	0.00	1.05	1.05	1.05	1.05	0.52	0.26	0.00	0.26	0.26	0.26	0.00	0.00
5	0.00	0.52	0.52	0.00	0.26	1.05	1.05	0.52	1.05	0.52	0.26	0.26	0.00
6	0.26	0.00	0.26	0.26	0.52	1.31	1.31	1.31	0.79	0.52	0.52	0.52	0.26
7	0.00	0.26	0.26	0.52	1.05	1.31	0.79	1.05	1.05	0.79	0.52	0.26	0.26
8	0.26	0.52	0.79	1.31	1.05	1.57	0.79	0.79	0.52	0.79	0.79	0.52	0.26
9	0.52	0.52	0.79	0.52	1.31	1.31	1.31	1.05	0.79	0.00	0.00	0.26	0.00
10	0.26	0.52	0.52	1.05	1.31	1.05	0.79	0.79	1.05	0.52	0.00	0.00	0.00
11	0.79	0.52	1.05	1.31	1.83	1.05	0.79	0.52	0.26	0.79	0.26	0.00	0.00
12	0.79	0.26	1.05	0.79	1.31	1.83	1.57	0.79	0.79	0.00	0.00	0.00	0.00
13	1.05	1.05	1.05	1.57	1.05	0.79	1.05	0.79	0.26	0.79	0.00	0.00	0.26

Table D.46: $\Theta_0 = -40^\circ, \Phi = \Phi_0 + 180^\circ, \Gamma < -40\%$

j:	1	2	3	4	5	6	7	8	9	10	11	12	13
k													
1	0.85	0.93	0.93	0.71	0.57	0.43	0.00	0.00	0.00	0.00	0.00	0.00	0.00
2	0.93	1.35	1.35	0.85	0.57	0.57	0.28	0.28	0.00	0.00	0.00	0.00	0.00
3	1.35	1.14	1.14	1.28	1.21	1.42	0.64	0.00	0.00	0.00	0.00	0.00	0.00
4	0.28	1.14	1.14	1.42	1.21	1.00	0.28	0.00	0.00	0.00	0.00	0.00	0.00
5	1.14	2.28	2.28	1.99	1.71	1.64	0.28	0.28	0.00	0.00	0.00	0.00	0.00
6	0.57	1.99	1.99	1.78	2.21	1.85	0.28	0.28	0.00	0.00	0.00	0.00	0.00
7	0.64	1.14	1.57	1.92	1.92	1.49	0.50	0.00	0.00	0.00	0.00	0.00	0.00
8	0.36	0.71	1.42	2.42	1.85	1.49	0.36	0.28	0.00	0.00	0.00	0.00	0.00
9	1.28	1.64	1.99	2.14	2.14	1.64	1.35	0.43	0.00	0.00	0.00	0.00	0.00
10	0.85	1.14	1.42	1.42	1.42	1.35	1.14	0.00	0.00	0.00	0.00	0.00	0.00
11	1.35	1.64	1.64	1.42	1.42	0.50	0.50	0.00	0.00	0.00	0.00	0.00	0.00
12	0.00	0.50	0.50	0.36	0.21	0.00	0.00	0.00	0.00	0.00	0.00	0.00	0.00
13	0.28	0.28	0.28	0.78	0.78	0.28	0.00	0.00	0.00	0.00	0.00	0.00	0.00

Table D.47: $\Theta_0 = -40^\circ, \Phi = \Phi_0 + 180^\circ, -40\% \leq \Gamma < -20\%$

j:	1	2	3	4	5	6	7	8	9	10	11	12	13
k													
1	0.27	0.34	0.51	0.93	0.86	0.82	0.89	0.34	0.24	0.00	0.00	0.00	0.00
2	0.38	0.45	0.86	1.23	1.30	1.13	0.93	0.69	0.27	0.14	0.14	0.14	0.00
3	0.55	0.99	1.44	1.54	1.37	1.03	1.13	0.82	0.27	0.14	0.14	0.00	0.00
4	1.10	1.20	1.54	1.54	1.68	1.37	1.27	0.51	0.17	0.00	0.17	0.00	0.00
5	1.27	0.79	0.75	1.17	1.34	0.99	1.06	0.45	0.14	0.00	0.00	0.00	0.00
6	1.34	0.96	1.48	1.68	1.34	1.41	1.23	0.34	0.24	0.00	0.00	0.00	0.00
7	1.44	1.65	1.78	1.61	1.61	1.68	1.17	0.82	0.48	0.00	0.10	0.00	0.00
8	1.30	1.96	1.75	1.37	1.65	1.30	1.10	0.45	0.41	0.27	0.17	0.00	0.00
9	0.89	0.69	0.58	0.69	0.65	0.69	0.69	0.48	0.58	0.00	0.00	0.00	0.00
10	0.62	0.65	0.75	0.93	0.82	0.69	0.58	0.58	0.27	0.00	0.00	0.00	0.00
11	0.21	0.21	0.41	0.75	0.82	0.89	0.69	0.45	0.00	0.00	0.00	0.00	0.00
12	0.65	0.41	0.21	0.58	0.48	0.51	0.41	0.31	0.17	0.14	0.14	0.10	0.00
13	0.75	0.89	0.69	0.38	0.38	0.55	0.51	0.51	0.03	0.00	0.00	0.00	0.00

Table D.48: $\Theta_0 = -40^\circ, \Phi = \Phi_0 + 180^\circ, -20\% \leq \Gamma < 0\%$

j:	1	2	3	4	5	6	7	8	9	10	11	12	13
k													
1	0.10	0.44	0.61	0.44	0.44	0.51	0.55	0.92	0.65	0.55	0.24	0.14	0.00
2	0.31	0.38	0.20	0.20	0.44	0.72	0.79	0.72	1.02	0.89	0.61	0.00	0.14
3	0.65	0.89	0.55	0.38	0.58	0.82	0.82	0.92	0.68	0.41	0.34	0.27	0.14
4	0.85	0.85	0.58	0.44	0.41	0.82	1.13	1.64	0.99	0.44	0.27	0.27	0.14
5	0.34	0.51	0.82	0.55	0.51	0.89	1.33	1.61	1.26	0.48	0.10	0.00	0.00
6	0.68	0.75	0.24	0.14	0.27	0.38	1.26	1.74	0.92	0.75	0.38	0.00	0.00
7	0.58	0.48	0.14	0.14	0.14	0.27	1.26	1.40	0.82	0.96	0.51	0.14	0.00
8	1.13	0.38	0.24	0.14	0.14	0.65	1.16	1.30	1.02	0.85	0.82	0.27	0.10
9	0.75	0.79	0.99	0.68	0.72	0.89	0.79	0.96	0.58	0.48	0.20	0.00	0.00
10	1.23	1.06	0.96	0.72	0.75	0.99	0.85	1.09	0.68	0.44	0.31	0.00	0.00
11	0.99	0.99	0.89	0.55	0.58	1.02	1.06	1.02	0.55	0.03	0.27	0.03	0.00
12	0.51	1.16	1.54	1.30	1.43	1.33	1.02	0.65	0.41	0.27	0.38	0.03	0.00
13	0.55	0.41	0.68	0.82	0.72	0.65	0.55	0.14	0.51	0.41	0.38	0.00	0.00

Table D.49: $\Theta_0 = -40^\circ, \Phi = \Phi_0 + 180^\circ, 0\% \leq \Gamma < 20\%$

j:	1	2	3	4	5	6	7	8	9	10	11	12	13
k													
1	0.45	0.49	0.31	0.13	0.49	0.71	0.71	0.58	0.89	0.76	1.07	0.09	0.18
2	0.80	0.85	0.54	0.62	0.49	0.36	0.71	1.12	0.58	0.40	0.58	0.49	0.00
3	0.54	0.27	0.18	0.18	0.18	0.18	0.54	0.94	1.69	1.07	0.98	0.27	0.18
4	0.71	0.09	0.00	0.00	0.00	0.00	0.18	0.67	1.61	1.52	1.07	0.18	0.18
5	0.27	0.36	0.00	0.00	0.00	0.00	0.18	0.62	1.47	1.83	1.25	0.18	0.13
6	0.45	0.00	0.00	0.00	0.00	0.00	0.04	0.58	1.65	1.03	1.12	0.54	0.36
7	0.45	0.00	0.00	0.00	0.00	0.00	0.00	0.58	1.61	0.71	0.89	0.36	0.36
8	0.09	0.00	0.00	0.00	0.00	0.00	0.31	0.94	1.29	0.67	0.67	0.22	0.31
9	0.36	0.54	0.18	0.36	0.36	0.40	0.71	0.98	1.43	1.47	1.16	0.04	0.00
10	0.36	0.27	0.22	0.45	0.54	0.45	0.89	0.98	1.52	1.52	1.52	0.18	0.00
11	0.67	0.58	0.76	0.80	0.76	0.67	0.89	1.20	1.38	1.38	1.25	0.13	0.18
12	1.12	0.76	0.71	0.80	0.85	1.07	1.61	1.69	1.96	1.07	0.85	0.40	0.27
13	0.71	1.07	1.29	1.07	1.03	1.20	0.94	0.85	0.62	0.54	0.40	0.31	0.00

Table D.50: $\Theta_0 = -40^\circ$, $\Phi = \Phi_0 + 180^\circ$, $20\% \leq \Gamma < 40\%$

j:	1	2	3	4	5	6	7	8	9	10	11	12	13
k													
1	1.16	0.71	0.58	0.71	0.83	0.58	0.58	1.03	0.83	1.03	0.71	0.90	0.19
2	1.22	0.51	0.96	0.64	0.51	0.26	0.26	0.00	1.22	1.73	1.67	0.96	0.26
3	0.77	0.06	0.00	0.00	0.00	0.00	0.00	0.39	0.51	1.86	1.48	0.90	0.96
4	0.06	0.00	0.00	0.00	0.00	0.00	0.00	0.00	0.51	1.54	1.48	1.41	0.51
5	0.58	0.00	0.00	0.00	0.00	0.00	0.00	0.00	0.26	1.41	2.63	0.83	0.58
6	0.06	0.00	0.00	0.00	0.00	0.00	0.00	0.00	0.45	2.12	2.25	0.58	0.26
7	0.00	0.00	0.00	0.00	0.00	0.00	0.00	0.00	0.26	2.18	1.48	1.09	0.71
8	0.00	0.00	0.00	0.00	0.00	0.00	0.00	0.13	0.45	1.41	1.28	1.73	0.32
9	0.26	0.00	0.00	0.00	0.00	0.00	0.00	0.51	0.77	1.48	2.50	1.16	0.26
10	0.19	0.39	0.19	0.00	0.00	0.00	0.00	0.45	1.03	1.80	1.41	1.16	0.26
11	0.58	0.45	0.00	0.13	0.00	0.00	0.00	0.51	1.99	1.99	1.80	1.28	0.51
12	1.22	0.51	0.26	0.00	0.00	0.00	0.00	0.77	0.71	2.18	1.73	1.35	0.71
13	0.77	0.77	0.32	0.51	0.77	0.77	1.35	2.12	1.80	0.90	1.41	0.51	0.00

Table D.51: $\Theta_0 = -40^\circ$, $\Phi = \Phi_0 + 180^\circ$, $40\% \leq \Gamma < 60\%$

j:	1	2	3	4	5	6	7	8	9	10	11	12	13
k													
1	1.78	1.42	1.18	1.54	0.95	0.95	0.36	0.47	1.30	2.72	3.79	2.60	0.95
2	0.00	0.59	0.12	0.00	0.00	0.47	0.47	0.95	0.59	0.95	1.18	3.79	2.01
3	0.00	0.00	0.00	0.00	0.00	0.00	0.00	0.00	0.47	0.59	1.30	3.08	0.12
4	0.00	0.00	0.00	0.00	0.00	0.00	0.00	0.00	0.00	0.83	1.42	0.83	2.01
5	0.00	0.00	0.00	0.00	0.00	0.00	0.00	0.00	0.00	0.12	0.71	2.49	0.71
6	0.00	0.00	0.00	0.00	0.00	0.00	0.00	0.00	0.00	0.00	0.83	2.49	1.30
7	0.00	0.00	0.00	0.00	0.00	0.00	0.00	0.00	0.00	0.00	2.01	2.60	0.59
8	0.00	0.00	0.00	0.00	0.00	0.00	0.00	0.00	0.00	0.47	0.71	1.66	1.18
9	0.00	0.00	0.00	0.00	0.00	0.00	0.00	0.00	0.00	0.95	0.83	2.96	1.42
10	0.12	0.00	0.00	0.00	0.00	0.00	0.00	0.00	0.00	0.36	1.42	2.60	1.78
11	0.00	0.00	0.00	0.00	0.00	0.00	0.00	0.00	0.00	1.78	1.66	2.60	1.07
12	0.00	0.00	0.00	0.00	0.00	0.00	0.00	0.00	0.71	0.47	1.42	2.13	2.49
13	0.83	0.00	0.00	0.00	0.00	0.00	0.59	0.36	1.89	2.72	1.89	3.20	2.13

Table D.52: $\Theta_0 = -40^\circ$, $\Phi = \Phi_0 + 180^\circ$, $\Gamma > 60\%$

j:	1	2	3	4	5	6	7	8	9	10	11	12	13
k													
1	0.93	0.62	0.47	0.08	0.00	0.00	0.62	0.62	0.62	0.47	0.31	2.79	4.89
2	0.62	0.23	0.00	0.00	0.00	0.00	0.00	0.00	0.23	0.31	0.54	1.24	4.11
3	0.00	0.00	0.00	0.00	0.00	0.00	0.00	0.00	0.00	0.31	0.62	1.86	4.19
4	0.00	0.00	0.00	0.00	0.00	0.00	0.00	0.00	0.00	0.00	0.47	2.87	3.49
5	0.00	0.00	0.00	0.00	0.00	0.00	0.00	0.00	0.00	0.00	0.00	3.10	4.65
6	0.00	0.00	0.00	0.00	0.00	0.00	0.00	0.00	0.00	0.00	0.00	2.79	4.27
7	0.00	0.00	0.00	0.00	0.00	0.00	0.00	0.00	0.00	0.00	0.00	2.09	4.19
8	0.00	0.00	0.00	0.00	0.00	0.00	0.00	0.00	0.00	0.31	0.62	1.86	4.11
9	0.00	0.00	0.00	0.00	0.00	0.00	0.00	0.00	0.00	0.00	0.00	2.64	4.81
10	0.00	0.00	0.00	0.00	0.00	0.00	0.00	0.00	0.00	0.00	0.08	2.64	4.58
11	0.00	0.00	0.00	0.00	0.00	0.00	0.00	0.00	0.00	0.00	0.00	2.48	4.42
12	0.00	0.00	0.00	0.00	0.00	0.00	0.00	0.00	0.00	0.31	0.39	2.02	3.10
13	0.08	0.00	0.00	0.00	0.00	0.00	0.00	0.31	0.31	1.32	1.55	2.79	4.65

Table D.53: $\Theta_0 = -40^\circ$, $\Phi = \Phi_0 + 180^\circ$, $-5\% \leq \Gamma \leq 5\%$

j:	1	2	3	4	5	6	7	8	9	10	11	12	13
k													
1	0.61	0.15	0.30	0.08	0.61	0.68	0.76	0.38	0.38	1.29	0.91	0.15	0.30
2	0.30	0.30	0.46	0.61	0.99	0.38	0.61	0.68	0.38	0.53	0.91	0.00	0.00
3	0.91	0.61	0.00	0.00	0.00	0.08	0.84	0.84	1.06	0.38	0.61	0.23	0.23
4	0.61	0.91	0.00	0.00	0.00	0.08	0.53	0.99	2.20	0.68	0.53	0.15	0.46
5	0.30	0.99	0.00	0.00	0.00	0.00	0.61	1.75	1.59	1.14	0.84	0.00	0.00
6	0.00	0.08	0.00	0.00	0.00	0.00	0.53	0.53	1.67	0.99	0.99	0.30	0.00
7	0.68	0.00	0.00	0.00	0.00	0.00	0.38	1.75	0.84	1.67	0.68	0.23	0.30
8	0.53	0.00	0.00	0.00	0.00	0.00	0.61	1.82	0.30	1.29	1.21	0.15	0.53
9	0.46	0.91	1.14	0.61	0.61	0.30	1.06	1.37	1.21	0.99	1.14	0.00	0.00
10	0.38	0.08	0.91	0.91	1.44	1.59	1.67	1.06	0.99	0.91	0.68	0.00	0.00
11	0.38	0.00	0.46	0.61	0.68	0.76	1.29	1.90	1.75	0.30	0.61	0.30	0.08
12	1.21	0.84	0.84	1.06	1.29	1.44	1.67	1.21	0.76	0.30	0.76	0.00	0.00
13	0.46	0.61	1.21	0.84	0.84	0.91	1.14	0.76	0.53	0.38	0.46	0.00	0.00

Table D.54: $\Theta_0 = -40^\circ$, $\Phi = \Phi_0 + 180^\circ$, $-10\% \leq \Gamma \leq 10\%$

j:	1	2	3	4	5	6	7	8	9	10	11	12	13
k													
1	0.35	0.42	0.38	0.23	0.38	0.46	0.61	1.00	0.81	0.84	0.69	0.15	0.15
2	0.46	0.58	0.54	0.46	0.77	0.61	0.46	0.65	0.42	0.84	0.77	0.00	0.04
3	0.61	0.65	0.15	0.08	0.15	0.54	1.00	1.19	0.92	0.65	0.61	0.23	0.15
4	0.73	0.61	0.15	0.00	0.00	0.15	0.58	1.04	1.69	0.61	0.50	0.31	0.31
5	0.38	0.84	0.04	0.00	0.00	0.15	0.73	1.42	1.96	1.04	0.77	0.04	0.00
6	0.15	0.38	0.12	0.00	0.00	0.00	0.54	1.23	1.73	1.27	0.84	0.31	0.00
7	0.65	0.15	0.12	0.00	0.00	0.00	0.42	1.31	1.15	1.27	0.81	0.23	0.31
8	0.58	0.15	0.15	0.00	0.00	0.00	0.88	1.00	0.77	1.07	1.07	0.23	0.31
9	0.54	0.92	0.65	0.50	0.50	0.65	1.00	0.88	1.15	0.92	0.73	0.00	0.00
10	0.31	0.46	0.92	0.81	0.92	1.07	1.19	1.23	1.04	0.77	0.77	0.15	0.00
11	0.58	0.31	0.54	0.65	0.69	0.81	1.04	1.42	1.31	0.38	0.58	0.15	0.15
12	0.92	1.46	0.96	1.27	1.15	1.54	1.27	1.34	0.54	0.31	0.77	0.00	0.00
13	0.92	0.77	1.07	1.07	1.00	0.73	0.77	0.61	0.58	0.54	0.46	0.00	0.00

Table D.55: $\Theta_0 = -60^\circ, \Phi = \Phi_0 + 180^\circ, \Gamma < -40\%$

j:	1	2	3	4	5	6	7	8	9	10	11	12	13
k													
1	0.60	1.01	0.81	0.81	0.81	0.40	0.00	0.00	0.00	0.00	0.00	0.00	0.00
2	0.81	1.01	1.01	1.21	0.81	0.60	0.20	0.20	0.00	0.00	0.00	0.00	0.00
3	1.21	1.41	1.41	1.41	1.01	1.01	0.60	0.20	0.00	0.00	0.00	0.00	0.00
4	1.41	1.41	1.61	1.41	1.41	0.40	0.20	0.00	0.00	0.00	0.00	0.00	0.00
5	1.61	1.81	2.22	1.81	2.02	1.01	0.60	0.20	0.00	0.00	0.00	0.00	0.00
6	1.61	2.22	2.22	2.22	2.22	1.61	0.40	0.20	0.00	0.00	0.00	0.00	0.00
7	0.81	1.41	2.22	2.22	2.02	1.61	0.81	0.00	0.00	0.00	0.00	0.00	0.00
8	0.60	1.21	1.81	2.02	2.02	1.01	0.81	0.60	0.20	0.00	0.00	0.00	0.00
9	1.21	1.41	1.61	1.81	1.81	1.41	1.01	0.40	0.00	0.00	0.00	0.00	0.00
10	0.81	1.01	1.01	1.41	1.01	0.81	0.60	0.40	0.00	0.00	0.00	0.00	0.00
11	1.21	1.21	1.21	1.21	1.01	0.81	0.40	0.00	0.00	0.00	0.00	0.00	0.00
12	0.20	0.40	0.40	0.20	0.00	0.00	0.00	0.00	0.00	0.00	0.00	0.00	0.00
13	0.20	0.40	0.60	0.40	0.40	0.20	0.00	0.00	0.00	0.00	0.00	0.00	0.00

Table D.56: $\Theta_0 = -60^\circ, \Phi = \Phi_0 + 180^\circ, -40\% \leq \Gamma < -20\%$

j:	1	2	3	4	5	6	7	8	9	10	11	12	13
k													
1	0.28	0.00	0.14	0.71	0.85	0.85	0.71	0.28	0.14	0.00	0.00	0.00	0.00
2	0.43	0.57	0.85	0.85	1.14	0.99	0.57	0.43	0.28	0.14	0.14	0.00	0.00
3	0.43	0.43	0.99	1.56	1.85	1.42	0.85	0.57	0.28	0.00	0.00	0.00	0.00
4	0.57	0.99	1.28	1.70	1.70	1.85	1.70	0.57	0.00	0.00	0.00	0.00	0.00
5	0.57	0.71	0.85	1.42	1.28	1.85	1.42	0.28	0.14	0.00	0.00	0.00	0.00
6	0.85	0.85	1.28	1.28	1.28	1.56	1.99	0.99	0.14	0.00	0.00	0.00	0.00
7	1.56	1.70	1.28	1.28	1.42	1.42	1.85	0.99	0.28	0.14	0.00	0.00	0.00
8	1.70	1.85	1.56	1.28	1.28	1.85	1.42	0.57	0.28	0.28	0.00	0.00	0.00
9	1.14	0.85	0.85	0.85	0.85	0.71	0.85	0.57	0.28	0.00	0.00	0.00	0.00
10	1.42	0.99	1.14	1.14	1.28	0.71	0.57	0.43	0.43	0.00	0.00	0.00	0.00
11	0.57	0.71	0.85	0.85	0.85	0.71	0.85	0.43	0.00	0.00	0.00	0.00	0.00
12	0.57	0.43	0.71	0.85	0.71	0.43	0.00	0.00	0.00	0.00	0.00	0.00	0.00
13	0.43	0.57	0.43	0.57	0.43	0.43	0.43	0.28	0.00	0.00	0.00	0.00	0.00

Table D.57: $\Theta_0 = -60^\circ, \Phi = \Phi_0 + 180^\circ, -20\% \leq \Gamma < 0\%$

j:	1	2	3	4	5	6	7	8	9	10	11	12	13
k													
1	0.17	0.50	1.16	0.50	0.17	0.50	0.83	0.99	0.83	0.50	0.17	0.00	0.00
2	0.50	0.83	0.83	0.50	0.50	0.83	1.65	1.32	0.99	0.50	0.00	0.17	0.00
3	0.99	1.16	0.83	0.17	0.17	0.66	1.49	1.49	0.99	0.50	0.17	0.00	0.00
4	0.66	0.83	0.33	0.00	0.17	0.83	0.99	1.98	1.16	0.33	0.17	0.17	0.00
5	0.50	0.66	0.50	0.17	0.17	0.33	1.16	2.48	0.66	0.00	0.00	0.00	0.00
6	0.33	0.50	0.00	0.00	0.00	0.17	0.66	1.65	1.16	0.33	0.00	0.00	0.00
7	0.50	0.17	0.00	0.00	0.00	0.33	0.50	1.65	1.16	0.17	0.17	0.17	0.00
8	0.66	0.17	0.00	0.17	0.17	0.33	0.83	1.65	0.66	0.17	0.33	0.17	0.00
9	0.83	1.16	0.99	0.83	0.83	1.16	0.99	1.16	0.83	0.50	0.00	0.00	0.00
10	0.66	0.99	0.99	0.66	0.83	1.32	1.32	0.83	0.83	0.33	0.00	0.00	0.00
11	0.66	0.33	0.99	1.16	1.16	1.32	1.16	0.99	0.83	0.00	0.00	0.00	0.00
12	0.99	1.32	1.32	1.65	2.15	1.98	1.65	0.66	0.33	0.33	0.17	0.17	0.00
13	1.49	1.16	0.83	0.83	0.83	0.83	0.50	0.33	0.66	0.17	0.00	0.00	0.00

Table D.58: $\Theta_0 = -60^\circ, \Phi = \Phi_0 + 180^\circ, 0\% \leq \Gamma < 20\%$

j:	1	2	3	4	5	6	7	8	9	10	11	12	13
k													
1	0.63	1.46	0.63	0.63	0.63	0.63	0.84	1.04	0.84	0.84	0.42	0.21	0.21
2	1.25	0.63	0.21	0.42	0.84	0.63	0.42	1.04	1.46	1.04	1.04	0.21	0.21
3	0.21	0.42	0.00	0.00	0.00	0.00	0.21	0.84	1.46	0.84	0.63	0.42	0.21
4	0.84	0.21	0.21	0.21	0.00	0.00	0.21	0.63	1.88	1.25	0.42	0.21	0.42
5	0.84	0.42	0.00	0.00	0.00	0.00	0.00	0.42	2.51	1.46	0.21	0.21	0.21
6	0.84	0.00	0.00	0.00	0.00	0.00	0.00	0.42	1.88	1.88	0.21	0.21	0.21
7	0.42	0.00	0.00	0.00	0.00	0.00	0.00	0.63	1.67	1.25	0.63	0.00	0.21
8	0.21	0.00	0.00	0.00	0.00	0.00	0.21	0.63	1.88	1.25	0.42	0.21	0.42
9	0.21	0.00	0.00	0.00	0.00	0.21	0.63	1.46	1.88	0.63	0.63	0.00	0.00
10	0.42	0.42	0.21	0.21	0.21	0.63	1.04	1.67	1.04	1.67	0.63	0.00	0.00
11	1.25	0.84	0.42	0.21	0.42	0.63	1.04	2.30	1.88	1.46	0.21	0.00	0.00
12	1.25	1.46	1.04	0.63	0.42	1.04	2.09	2.51	1.25	0.63	0.42	0.00	0.00
13	0.63	0.84	1.46	1.46	1.46	1.25	1.46	1.25	0.21	0.63	0.21	0.00	0.00

Table D.59: $\Theta_0 = -60^\circ, \Phi = \Phi_0 + 180^\circ, 20\% \leq \Gamma < 40\%$

j:	1	2	3	4	5	6	7	8	9	10	11	12	13
k													
1	1.22	0.61	0.61	0.61	1.22	0.92	0.92	1.22	1.53	1.83	1.53	0.61	0.31
2	0.31	0.00	0.00	0.61	0.00	0.31	0.61	0.31	0.61	1.83	1.83	0.61	0.31
3	0.31	0.31	0.31	0.31	0.31	0.31	0.31	0.61	1.22	2.45	1.22	1.22	0.92
4	0.31	0.00	0.00	0.00	0.00	0.00	0.00	0.31	0.92	2.14	1.83	0.31	0.31
5	0.31	0.00	0.00	0.00	0.00	0.00	0.00	0.00	0.92	2.75	2.45	0.61	0.31
6	0.00	0.00	0.00	0.00	0.00	0.00	0.00	0.00	0.61	1.53	1.83	0.61	0.61
7	0.00	0.00	0.00	0.00	0.00	0.00	0.00	0.00	0.61	2.75	0.92	0.92	0.61
8	0.00	0.00	0.00	0.00	0.00	0.00	0.00	0.00	0.61	1.83	1.53	0.92	0.61
9	0.00	0.00	0.00	0.00	0.00	0.00	0.00	0.00	1.22	2.45	1.53	0.61	0.00
10	0.00	0.00	0.00	0.00	0.00	0.00	0.00	0.61	2.14	0.92	1.53	0.92	0.31
11	0.00	0.00	0.00	0.00	0.00	0.00	0.00	0.00	1.83	2.45	1.83	0.31	1.22
12	0.92	0.00	0.00	0.00	0.00	0.00	0.00	1.22	3.36	1.53	1.53	0.92	0.92
13	0.31	0.31	0.31	0.61	0.61	0.92	1.53	1.22	1.53	0.92	0.92	0.31	0.00

Table D.60: $\Theta_0 = -60^\circ, \Phi = \Phi_0 + 180^\circ, 40\% \leq \Gamma < 60\%$

j:	1	2	3	4	5	6	7	8	9	10	11	12	13
k													
1	1.85	0.37	0.00	0.37	0.37	0.74	0.37	0.37	0.74	1.11	1.85	1.85	1.11
2	0.37	0.37	1.11	0.37	0.37	0.37	0.37	0.37	0.74	0.74	0.74	2.58	1.85
3	1.11	0.00	0.00	0.00	0.00	0.00	0.00	0.00	0.37	1.48	1.85	1.11	1.11
4	0.00	0.00	0.00	0.00	0.00	0.00	0.00	0.00	0.37	1.48	1.48	1.48	1.48
5	0.00	0.00	0.00	0.00	0.00	0.00	0.00	0.00	0.00	1.48	1.48	1.48	1.48
6	0.00	0.00	0.00	0.00	0.00	0.00	0.00	0.00	0.37	1.11	2.21	0.74	0.74
7	0.00	0.00	0.00	0.00	0.00	0.00	0.00	0.00	0.37	0.74	3.32	0.74	0.74
8	0.00	0.00	0.00	0.00	0.00	0.00	0.00	0.00	0.74	1.11	2.58	1.11	0.37
9	0.00	0.00	0.00	0.00	0.00	0.00	0.00	0.00	0.00	2.21	2.21	1.48	1.11
10	0.00	0.00	0.00	0.00	0.00	0.00	0.00	0.00	0.00	1.85	2.21	1.48	1.48
11	0.00	0.00	0.00	0.00	0.00	0.00	0.00	0.00	0.00	1.85	1.85	2.21	0.37
12	0.00	0.00	0.00	0.00	0.00	0.00	0.00	0.00	0.37	2.21	1.48	1.85	1.85
13	0.37	0.74	0.37	0.00	0.37	0.74	0.37	1.85	2.58	1.85	2.58	1.11	1.48

Table D.61: $\Theta_0 = -60^\circ, \Phi = \Phi_0 + 180^\circ, \Gamma > 60\%$

j:	1	2	3	4	5	6	7	8	9	10	11	12	13
k													
1	0.40	0.40	0.60	0.40	0.20	0.20	0.40	0.40	0.60	0.80	1.41	2.41	3.01
2	0.40	0.40	0.00	0.00	0.00	0.00	0.00	0.20	0.20	0.60	1.20	1.81	2.61
3	0.00	0.00	0.00	0.00	0.00	0.00	0.00	0.00	0.00	0.20	1.41	2.21	2.61
4	0.00	0.00	0.00	0.00	0.00	0.00	0.00	0.00	0.00	0.20	1.41	2.61	2.61
5	0.00	0.00	0.00	0.00	0.00	0.00	0.00	0.00	0.00	0.00	1.41	2.61	2.81
6	0.00	0.00	0.00	0.00	0.00	0.00	0.00	0.00	0.00	0.20	1.41	3.01	3.01
7	0.00	0.00	0.00	0.00	0.00	0.00	0.00	0.00	0.00	0.20	0.80	2.81	3.01
8	0.00	0.00	0.00	0.00	0.00	0.00	0.00	0.00	0.00	0.40	0.80	2.41	3.01
9	0.00	0.00	0.00	0.00	0.00	0.00	0.00	0.00	0.00	0.00	1.20	2.81	3.41
10	0.00	0.00	0.00	0.00	0.00	0.00	0.00	0.00	0.00	0.40	1.20	2.61	3.01
11	0.00	0.00	0.00	0.00	0.00	0.00	0.00	0.00	0.00	0.00	1.61	2.61	3.01
12	0.00	0.00	0.00	0.00	0.00	0.00	0.00	0.00	0.00	0.80	1.61	2.21	2.41
13	0.40	0.00	0.00	0.00	0.00	0.00	0.20	0.20	0.60	1.61	1.81	3.21	3.21

Table D.62: $\Theta_0 = -60^\circ, \Phi = \Phi_0 + 180^\circ, -5\% \leq \Gamma \leq 5\%$

j:	1	2	3	4	5	6	7	8	9	10	11	12	13
k													
1	0.00	0.74	0.00	0.00	0.74	0.74	0.00	0.74	2.21	1.47	0.74	0.00	0.00
2	0.00	0.74	0.74	0.00	0.00	0.74	0.74	0.74	0.74	0.74	0.00	0.00	0.00
3	0.00	1.47	1.47	0.74	0.74	0.74	0.00	0.74	2.21	0.74	0.00	0.00	0.00
4	0.74	1.47	1.47	1.47	1.47	1.47	1.47	0.00	0.00	0.00	0.00	0.00	0.00
5	0.00	0.74	2.21	1.47	0.74	0.00	0.74	2.94	1.47	0.74	0.00	0.74	0.00
6	0.00	0.74	0.74	0.00	0.74	0.00	0.00	0.74	2.94	0.00	0.00	0.74	0.00
7	1.47	2.21	0.74	0.74	0.74	0.74	0.74	0.00	1.47	0.74	0.00	0.00	0.00
8	0.00	0.74	0.00	0.74	0.74	0.74	1.47	1.47	2.21	1.47	0.74	0.00	0.00
9	0.00	0.00	0.74	0.74	0.00	0.00	0.00	0.74	1.47	0.00	0.74	0.74	0.00
10	0.00	0.74	0.00	0.00	0.74	0.00	0.74	1.47	1.47	2.21	0.00	0.00	0.74
11	1.47	0.00	0.00	0.00	0.00	0.74	0.74	1.47	0.00	0.74	0.74	0.00	0.00
12	0.74	0.74	0.00	0.00	0.00	0.74	1.47	1.47	2.21	0.00	0.00	0.00	0.00
13	0.00	0.00	0.00	0.00	0.00	0.74	0.00	1.47	1.47	0.74	0.00	0.00	0.00

Table D.63: $\Theta_0 = -60^\circ, \Phi = \Phi_0 + 180^\circ, -10\% \leq \Gamma \leq 10\%$

j:	1	2	3	4	5	6	7	8	9	10	11	12	13
k													
1	0.00	0.79	0.00	0.00	0.39	0.39	0.00	1.18	1.57	1.18	0.39	0.00	0.00
2	0.00	0.79	0.79	0.79	0.79	0.39	0.39	0.39	0.79	1.57	0.39	0.00	0.00
3	0.00	0.79	0.79	0.39	0.39	0.39	0.39	0.79	1.18	0.79	0.39	0.00	0.00
4	0.39	0.79	0.79	0.79	1.18	1.57	1.57	0.79	0.39	0.00	0.39	0.00	0.00
5	0.00	1.18	1.57	0.79	1.18	0.79	1.18	2.36	1.18	0.39	0.00	0.39	0.00
6	0.39	0.79	0.79	0.79	0.39	0.39	0.00	1.97	2.36	0.39	1.18	0.39	0.39
7	0.79	1.18	0.39	0.39	0.79	0.79	1.18	1.18	1.57	0.79	0.39	0.00	0.00
8	0.39	0.79	0.79	0.39	0.39	0.39	1.18	1.57	1.97	1.97	0.39	0.00	0.00
9	0.39	0.39	0.79	0.79	0.39	0.00	0.39	1.18	0.79	0.39	0.39	0.39	0.00
10	0.00	0.79	0.00	0.39	0.39	0.00	0.39	0.79	1.18	1.18	0.00	0.39	0.39
11	1.18	0.00	0.00	0.00	0.39	0.39	1.18	0.79	1.18	0.39	0.39	0.00	0.00
12	0.39	0.39	0.00	0.39	0.39	0.39	1.18	1.18	1.97	0.00	0.00	0.00	0.00
13	0.39	0.00	0.00	0.00	0.39	0.39	1.18	1.97	1.57	0.39	0.39	0.00	0.00

Table D.64: Entire data set, $\Gamma < -40\%$

j:	1	2	3	4	5	6	7	8	9	10	11	12	13
k													
1	0.55	0.69	0.62	0.48	0.48	0.21	0.07	0.21	0.21	0.27	0.34	0.14	0.07
2	0.48	0.62	0.55	0.55	0.41	0.34	0.21	0.34	0.41	0.48	0.55	0.34	0.14
3	0.48	0.55	0.62	0.76	0.62	0.62	0.62	0.55	0.89	0.76	0.89	0.82	0.34
4	0.55	0.55	0.69	0.62	0.62	0.27	0.21	0.27	0.41	0.62	0.55	0.55	0.34
5	0.76	0.82	1.24	1.10	1.17	0.69	0.62	0.62	0.62	0.76	0.55	0.48	0.34
6	0.69	1.03	1.17	1.17	1.03	0.89	0.62	0.82	0.96	0.89	0.76	0.76	0.76
7	0.27	0.48	0.76	0.89	0.89	0.82	0.55	0.76	1.03	0.96	1.10	1.03	0.89
8	0.21	0.41	0.62	0.76	0.89	0.69	0.69	0.96	1.10	1.03	1.24	1.37	1.10
9	1.03	1.17	1.37	1.51	1.51	1.17	0.89	0.76	0.76	0.89	0.55	0.34	0.21
10	0.76	0.82	1.03	1.24	1.24	1.10	0.89	0.82	0.55	0.34	0.27	0.14	0.21
11	0.69	1.03	0.96	0.82	0.62	0.41	0.34	0.21	0.34	0.34	0.41	0.41	0.34
12	0.07	0.14	0.14	0.07	0.00	0.00	0.00	0.21	0.14	0.34	0.55	0.48	0.14
13	0.07	0.14	0.21	0.14	0.27	0.14	0.14	0.21	0.21	0.14	0.14	0.14	0.00

Table D.65: Entire data set, $-40\% \leq \Gamma < -20\%$

j:	1	2	3	4	5	6	7	8	9	10	11	12	13
k													
1	0.12	0.22	0.25	0.40	0.47	0.56	0.56	0.34	0.31	0.22	0.09	0.16	0.16
2	0.25	0.34	0.50	0.56	0.65	0.65	0.68	0.62	0.78	0.62	0.40	0.31	0.22
3	0.31	0.34	0.59	0.68	0.93	0.81	0.90	0.90	0.62	0.65	0.59	0.50	0.47
4	0.31	0.59	0.65	0.81	0.75	0.93	1.18	0.81	0.75	0.68	0.65	0.56	0.53
5	0.37	0.62	0.59	0.78	0.75	1.06	0.93	0.84	0.81	0.72	0.75	0.56	0.47
6	0.56	0.59	0.59	0.68	0.84	1.00	1.18	0.93	0.72	0.78	0.75	0.59	0.47
7	0.56	0.72	0.81	0.81	0.78	0.84	1.24	0.96	0.75	0.81	0.68	0.68	0.53
8	0.47	0.72	0.84	0.78	0.68	1.00	1.03	0.93	0.81	0.90	0.78	0.65	0.53
9	0.40	0.53	0.65	0.78	0.96	1.09	1.12	1.06	0.84	0.75	0.75	0.72	0.53
10	0.44	0.53	0.50	0.59	0.68	0.62	0.84	0.78	0.75	0.65	0.62	0.47	0.34
11	0.34	0.37	0.44	0.56	0.75	0.56	0.59	0.59	0.50	0.44	0.53	0.53	0.47
12	0.22	0.22	0.28	0.28	0.25	0.12	0.12	0.12	0.37	0.31	0.34	0.40	0.44
13	0.16	0.25	0.31	0.47	0.50	0.59	0.59	0.47	0.34	0.31	0.34	0.25	0.16

Table D.66: Entire data set, $-20\% \leq \Gamma < 0\%$

j:	1	2	3	4	5	6	7	8	9	10	11	12	13
k													
1	0.16	0.20	0.43	0.61	0.72	0.76	0.92	0.94	0.76	0.49	0.40	0.25	0.09
2	0.18	0.31	0.52	0.65	0.81	1.06	1.28	1.03	0.79	0.58	0.52	0.47	0.27
3	0.34	0.45	0.56	0.63	0.76	1.01	1.08	0.97	0.85	0.56	0.45	0.38	0.38
4	0.38	0.47	0.49	0.49	0.90	1.12	1.10	1.10	0.88	0.58	0.63	0.47	0.40
5	0.36	0.36	0.45	0.52	0.72	0.88	1.10	0.99	0.70	0.43	0.45	0.47	0.36
6	0.22	0.38	0.54	0.63	0.81	0.99	1.01	0.92	0.88	0.52	0.40	0.43	0.43
7	0.43	0.52	0.43	0.45	0.72	1.06	0.94	0.99	0.88	0.63	0.52	0.45	0.40
8	0.45	0.49	0.43	0.49	0.76	0.81	0.94	0.97	0.76	0.58	0.52	0.47	0.38
9	0.47	0.49	0.43	0.47	0.54	0.65	0.79	0.81	0.83	0.49	0.49	0.56	0.40
10	0.45	0.36	0.54	0.52	0.74	0.79	0.85	0.72	0.81	0.56	0.58	0.63	0.38
11	0.20	0.31	0.56	0.63	0.74	0.92	0.99	0.74	0.65	0.65	0.61	0.43	0.38
12	0.25	0.34	0.40	0.49	0.67	0.79	0.81	0.58	0.45	0.49	0.47	0.52	0.43
13	0.45	0.38	0.36	0.40	0.43	0.31	0.36	0.40	0.47	0.40	0.38	0.34	0.34

Table D.67: Entire data set, $0\% \leq \Gamma < 20\%$

j:	1	2	3	4	5	6	7	8	9	10	11	12	13
k													
1	0.22	0.35	0.48	0.37	0.37	0.52	0.50	0.60	0.67	0.76	0.58	0.35	0.32
2	0.35	0.35	0.52	0.50	0.69	0.69	0.56	0.78	0.73	0.71	0.58	0.35	0.45
3	0.28	0.50	0.67	0.52	0.91	0.95	0.86	0.84	0.91	0.65	0.60	0.41	0.43
4	0.30	0.24	0.50	0.76	0.99	0.95	0.95	1.02	0.97	0.67	0.32	0.43	0.39
5	0.43	0.35	0.58	0.65	0.76	0.80	0.91	0.97	1.12	0.73	0.48	0.39	0.39
6	0.39	0.32	0.41	0.54	0.84	0.84	0.89	0.93	0.89	0.78	0.50	0.43	0.35
7	0.37	0.26	0.37	0.67	1.04	0.89	0.86	0.80	0.73	0.58	0.43	0.35	0.35
8	0.37	0.32	0.37	0.60	0.86	0.84	0.86	0.67	0.76	0.50	0.45	0.30	0.37
9	0.37	0.26	0.43	0.43	0.54	0.54	0.76	0.73	0.80	0.58	0.52	0.30	0.45
10	0.48	0.56	0.48	0.43	0.41	0.65	0.67	0.76	0.67	0.80	0.54	0.37	0.56
11	0.52	0.43	0.45	0.52	0.58	0.78	0.97	1.04	1.02	0.63	0.35	0.43	0.41
12	0.39	0.45	0.63	0.80	0.97	0.97	1.02	1.12	0.89	0.65	0.54	0.32	0.39
13	0.32	0.50	0.60	0.67	0.65	0.73	0.76	0.54	0.45	0.50	0.39	0.32	0.26

Table D.68: Entire data set, $20\% \leq \Gamma < 40\%$

j:	1	2	3	4	5	6	7	8	9	10	11	12	13
k													
1	0.34	0.43	0.34	0.54	0.74	0.60	0.66	0.63	0.77	0.68	0.60	0.54	0.34
2	0.43	0.63	0.46	0.80	0.74	0.51	0.57	0.54	0.63	0.66	0.77	0.68	0.43
3	0.49	0.54	0.40	0.94	0.57	0.37	0.31	0.43	0.49	0.74	0.40	0.63	0.49
4	0.57	0.60	0.80	0.91	0.54	0.31	0.17	0.40	0.63	0.80	0.74	0.34	0.34
5	0.31	0.63	0.51	0.63	0.74	0.49	0.26	0.40	0.54	0.91	0.68	0.51	0.43
6	0.37	0.57	0.71	0.86	0.57	0.29	0.20	0.37	0.49	0.57	0.68	0.49	0.31
7	0.37	0.46	0.94	1.06	0.51	0.34	0.26	0.46	0.63	0.68	0.60	0.34	0.37
8	0.40	0.37	0.80	0.80	0.63	0.54	0.34	0.49	0.54	0.68	0.54	0.46	0.40
9	0.37	0.57	0.51	0.54	0.54	0.63	0.29	0.46	0.54	0.88	0.66	0.46	0.37
10	0.34	0.34	0.51	0.83	0.97	0.77	0.74	0.66	0.80	0.71	0.80	0.51	0.31
11	0.34	0.54	0.49	0.57	0.71	0.63	0.49	0.80	0.83	0.74	0.88	0.46	0.49
12	0.51	0.66	0.86	0.91	1.00	1.28	1.23	1.08	1.23	0.86	0.74	0.68	0.63
13	0.54	0.60	0.83	0.77	0.74	0.66	0.68	0.83	0.80	0.60	0.68	0.54	0.40

Table D.69: Entire data set, $40\% \leq \Gamma < 60\%$

j:	1	2	3	4	5	6	7	8	9	10	11	12	13
k													
1	0.61	0.53	0.93	0.97	0.85	0.85	0.69	0.65	0.65	0.89	1.18	0.81	0.69
2	0.85	0.65	0.89	0.73	0.45	0.36	0.24	0.20	0.36	0.69	0.85	0.89	0.81
3	0.89	0.77	1.09	0.73	0.08	0.08	0.12	0.24	0.36	0.77	0.97	0.61	0.61
4	0.57	0.81	0.89	0.53	0.08	0.04	0.00	0.00	0.16	0.69	0.81	0.65	0.73
5	0.53	0.49	0.77	0.69	0.24	0.12	0.04	0.04	0.12	0.73	0.89	0.53	0.69
6	0.65	0.65	0.93	0.65	0.12	0.08	0.00	0.04	0.24	0.81	0.89	0.36	0.57
7	0.36	0.69	0.93	0.45	0.16	0.04	0.04	0.04	0.24	0.65	0.77	0.61	0.53
8	0.45	0.61	1.01	0.93	0.32	0.12	0.12	0.20	0.28	0.53	0.61	0.53	0.32
9	0.32	0.49	0.69	0.69	0.57	0.32	0.36	0.20	0.16	0.61	0.85	0.61	0.49
10	0.65	0.81	0.93	0.81	0.36	0.36	0.20	0.53	0.49	0.65	0.81	0.73	0.65
11	0.85	0.65	0.89	0.73	0.57	0.49	0.32	0.24	0.41	1.05	0.65	0.69	0.61
12	0.89	1.13	1.26	1.18	0.89	0.45	0.41	0.61	0.73	0.81	0.77	0.61	0.57
13	0.85	1.05	0.69	0.73	1.01	1.18	1.05	1.05	1.26	1.01	0.81	0.85	0.65

Table D.70: Entire data set, $\Gamma > 60\%$

j:	1	2	3	4	5	6	7	8	9	10	11	12	13
k													
1	2.13	1.78	1.19	0.84	0.56	0.48	0.43	0.46	0.48	0.66	0.94	1.70	2.18
2	1.65	1.32	0.79	0.41	0.20	0.20	0.15	0.23	0.23	0.36	0.53	1.07	1.60
3	1.42	1.02	0.38	0.10	0.08	0.03	0.00	0.00	0.03	0.20	0.56	0.99	1.30
4	1.45	1.02	0.36	0.08	0.00	0.00	0.00	0.00	0.00	0.18	0.56	1.14	1.32
5	1.45	1.07	0.48	0.18	0.00	0.00	0.00	0.00	0.00	0.08	0.51	1.14	1.37
6	1.40	0.96	0.33	0.05	0.00	0.00	0.00	0.00	0.00	0.08	0.46	1.14	1.37
7	1.52	1.07	0.28	0.05	0.00	0.00	0.00	0.00	0.00	0.13	0.48	1.02	1.27
8	1.52	1.17	0.38	0.08	0.03	0.03	0.00	0.00	0.08	0.25	0.48	0.89	1.30
9	1.35	1.02	0.63	0.41	0.13	0.10	0.05	0.10	0.13	0.20	0.46	1.07	1.42
10	1.14	0.94	0.56	0.28	0.13	0.08	0.00	0.00	0.03	0.28	0.43	1.07	1.42
11	1.35	1.12	0.69	0.51	0.20	0.13	0.05	0.08	0.10	0.28	0.69	1.14	1.32
12	1.60	1.12	0.53	0.25	0.00	0.00	0.00	0.05	0.10	0.58	0.76	1.09	1.30
13	1.50	1.09	0.94	0.74	0.51	0.48	0.46	0.61	0.63	1.04	1.22	1.52	1.98